Wetting and non-aqueous phase liquid saturations in homogeneous porous media.

by

Mike Wei

Submitted in partial fulfillment of
the requirements for the degree of
Master of Science in Hydrology

New Mexico Institute of Mining and Technology
Socorro, New Mexico

January, 1991

Abstract

Organosilanes were used to alter wettability of glass beads and etched glass micromodels to study the influence of wetting on the behavior of non-aqueous phase liquids (NAPL) resulting from groundwater contamination. Wettability and stability of the silane treatment were characterized by contact angle measurements on treated glass slides stored in a variety of fluids. All treated surfaces displayed contact angle hysteresis. The silane-treated surfaces remained stable in air and organic liquids but deteriorated in water. Deterioration was indicated by a decrease in advancing and receding angles and an increase in contact angle hysteresis and critical surface tension. Receding angle and contact angle hysteresis were the most sensitive indicators of deterioration.

GlassClad® 18 (GC18) and t-Butyldimethylchlorosilane (tBDM) remained the most stable in water and were used to treat uniform glass beads and micromodels. The advancing and receding water-Soltrol® contact angles for GC18 was $151.4° \pm 6.8°$ and $119.8° \pm 5.0°$, respectively. For tBDM, the values were $108.0° \pm 2.7°$ and $81.8° \pm 7.8°$, respectively. Upon exposure to water, the receding angle on tBDM-treated slides decreased from 81.8° to 37.2°. By comparison, the advancing and receding water-Soltrol® contact angles for untreated glass were $68.8° \pm 9.1°$ and $40.7° \pm 7.7°$, respectively.

Residual saturations and capillary pressure-saturation data were obtained from 5-cm long glass bead packed column experiments. In the experiments, Soltrol® displaced water in the initially water-saturated columns until irreducible water saturation (IWS) was reached. Water then displaced Soltrol® out of the column until residual oil saturation (ROS) was reached. The displacement sequence simulated NAPL migration into a homogeneous sand aquifer; the NAPL was then partially removed by ambient groundwater flow.

The amount of residual oil trapped after Soltrol® displacement by water was greater in untreated beads ($ROS = 17.6 \pm 1.8\%$) than in GC18-treated beads ($ROS = 10.1 \pm 0.7\%$). The ROS for tBDM-treated beads was about 18.4%, but this estimate was unreliable due to poor reproducibility. Wettability did not appear to have much affect on the IWS for contact angles ranging between 41° and 120°.Values for IWS were similar for untreated ($7.5 \pm 2.0\%$), GC18-treated ($6.6 \pm 4.3\%$), and tBDM-treated ($10.1 \pm 3.3\%$) beads.

Capillary pressure-saturation data showed that, in GC18-treated beads, intermediate-wet conditions prevailed during water displacement by Soltrol® and oil-wet

conditions prevailed during Soltrol® displacement by water. This was consistent with the contact angles measured on GC18–treated slides. In the tBDM–treated beads, water–wet conditions prevailed during water displacement by Soltrol®. This was expected from the low receding angle of tBDM–treated slides stored in water (37°). Wetting conditions during Soltrol® displacement by water were inconsistent, ranging from water–wet to intermediate–wet. The discrepancy in wetting behavior could not be pinpointed but may have been that silane treatment or stability was inconsistent.

Observations from the GC18–treated micromodel showed that Soltrol® at ROS occupied the smaller pore throats and formed thin wedges and possibly thin films along pore walls. Wedges and films permitted Soltrol® trapped behind the displacement front to drain. In contrast, residual Soltrol® in the untreated model occupied the larger cavity of the pores forming 'blobs'. These 'blobs' were disconnected from each other and could not drain. The preference for smaller pores and the continuous nature of the Soltrol® under oil–wet conditions support the low value of ROS measured in the GC18–treated beads. The micromodel experiments also showed that ROS in the untreated beads was a result of trapping of Soltrol® while ROS in the GC18–treated case was a result of drainage and isolation of Soltrol®.

The use of interfacial tension and grain size to scale capillary pressures in glass beads appeared valid. The use of cosine of the contact angle to scale capillary pressures from strongly water–wet to strongly oil–wet (or vise versa) also appeared valid. Scaling by cosine of the contact angle to not strongly wetted conditions could not be confirmed with the results from the tBDM–treated beads.

The average bulk wettability calculated by the USBM and Amott methods confirmed that untreated beads were strongly water–wet and GC18–treated beads were strongly oil–wet. Wettability of tBDM–treated beads was calculated to be as strongly water–wet as the untreated beads. The USBM and Amott–Harvey indexes combined the wetting behavior from both the water and Soltrol® displacements and therefore ignored the effect of contact angle hysteresis.

The results of this thesis indicated that wettability could influence the mechanism of NAPL trapping, ROS, and location of NAPL in uniformly wetted, homogeneous aquifer materials beneath hazardous waste sites. Wettability could, therefore, affect hazardous waste site characterization and remediation design.

Table of contents

List of figures

List of tables

Acknowledgements

I thank the Lord for the opportunity to study here in New Mexico and for him persevering with me.

Many thanks to my advisors, Rob Bowman, John Wilson, and Norman Morrow for their wisdom and support. Paul Hoffman, Roger Huddleston, Robert Mace, Bill Mason, Wendy Soll, and Jiamin Wan gave useful input, healthy criticisms, and helped show the way in the lab. Anil Bagri, Peter Burck, and Paul Hoffman helped with data acquisition. Paul Hoffman made the micromodel, H6C, for the experiments done here.

I am grateful to have worked on this project funded by USGS and New Mexico Water Resources Institute under USGS grant number 14–08–0001–G1657. Equipment and supplies bought from funding by Environmental Protection Agency Cooperative Agreement number CR–813571 and Department of Energy project–Small scale laboratory studies of flow and transport phenomena in pores and fractures–are also appreciated.

Mike Hiskey, Dr. Hatch, Dr. Oxley, and staff of the Chemistry Department, Tom Kieft of the Biology Department, Lynn Branvold in the Bureau of Mines, and Jill Buckley in the Petroleum Research Recovery Center provided suggestions and use of their facilities. Mike Aimes and the staff at the Computing Center were also very helpful. Advice from Dave Baehr of Regis Chromatography and from Hulls America Petrarch is greatly appreciated.

Thanks to all the Hydros past and present for their friendship. No research in this program could ever have succeeded without them. I am grateful for the unending love and support of my parents and my sister through the years. A special thanks to Ann Stark for her love, patience, and belief in me.

1. Introduction

There is growing awareness among earth scientists about the role of hydrophobic geologic materials and the application of wettability in environmental, engineering, and agricultural problems today. The usual assumption has been that geologic materials including soils, aquifers, and oil reservoirs are hydrophilic or water–wet; that is, they have an affinity for water in the presence of other fluids. This assumption is not always valid.

Naturally occurring hydrophobic soils have been documented (Letey et al, 1975; DeBano and Letey, 1969). Problems with hydrophobic soils are associated with agricultural management as well as erosion, flooding, and decreased recharge in burned areas (Wilson, 1988). Most hydrophobic soils, however, only extend to a few centimeters' depth into the ground.

Hydrophobic conditions can also prevail over a significant portion of the thickness and area of an oil reservoir. Field experience and laboratory studies over the last 50 years in the petroleum industry have led researchers to conclude that most oil reservoirs are not hydrophilic (Cuiec, 1991; Morrow, 1991; Treiber et al 1972). Laboratory studies suggest that reservoir rocks acquire their hydrophobic character from adsorption of polar organic compounds associated with the heavier fractions of crude oils such as resins and asphaltenes (Anderson, 1986a).

The fact that wettability of cleaned reservoir rocks can be altered by aging in crude oil at room temperature and pressure is leading contaminant hydrologists to speculate that wettability of aquifer materials may be altered by adsorption of similar polar organic constituents in non–aqueous phase liquid (NAPL) contaminants. The hypothesis of wettability alteration of the vadose zone and aquifer beneath disposal sites contaminated with NAPL provided the impetus for this research project (Bowman and Wilson, 1988). The overall goal is to document the existence and mechanisms of wettability

alteration in the subsurface contaminated by NAPL's and to understand how wettability affects capillary trapping, distribution, and relative mobility of NAPL in groundwater. These issues have implications in site investigation and characterization as well as remedial action design.

Wettability is defined here as the relative affinity of different immiscible fluids to a solid surface. For example, in a water/oil/solid system (eg. in an aquifer contaminated with NAPL), if water preferentially adheres to the solid surface in the presence of the oil, the system is *hydrophilic* or *water–wet*. Water is the *wetting* liquid and oil is the *non–wetting* liquid. If oil preferentially adheres, the system is *hydrophobic* or *oil–wet*. Oil then becomes the wetting liquid and water becomes the non–wetting liquid. If neither liquid shows a preference to adhere, the system is *neutral–* or *intermediate–wet*. The definition of wetting and non–wetting liquid loses meaning in this special case.

1.1 Thesis objectives

This thesis investigated the hypothesis that wettability affects capillary trapping and residual saturations of NAPL's in aquifers. The motivation for this study was to see how wettability affects capillary trapping in an unconsolidated, homogeneous porous medium of uniform wettability. Although natural systems are heterogeneous and wettability variation is the norm, the study of the most simplest system (homogeneous porous medium and uniform wettability) was a necessary first step in understanding the role of wettability in capillary trapping.

The objectives of this thesis were:

- alter the wetting of homogeneous porous media and characterize the change in wettability

- measure residual oil saturations (ROS) and capillary pressures for various degrees of uniformly wetted, homogeneous porous media
- determine the mechanism(s) that cause the difference in ROS between one degree of wettability and another
- develop laboratory techniques to quantify the above effects.

1.2 General approach

The general approach was to alter the wettability of glass with organosilanes. Glass was used as an analogue for the aquifer material. Different degrees of wettability could be achieved either by changing the silane concentration or by using different silanes. Several silanes were investigated. The hydrophobic nature of the silane-treated surfaces were first characterized by measuring contact angles on flat, smooth treated glass slides. The contact angle is the simplest quantitative measure of wettability (Anderson, 1986b). Contact angles were also periodically measured over time to quantify the stability of the treated surface for slides stored in a variety of fluids which would be used in laboratory experiments later on. Surface stability in these fluids needed to be checked before the experiments could proceed. If the surface was not stable and surface properties changed, the wettability would change during the experiments. This change in wettability would be undesirable because it could not be controlled. Once the wettability and stability of the silane treatments were adequately understood, the most suitable silanes were employed to treat glass porous media. A suitable silane was one which gave a hydrophobic surface that remained stable long enough for the experiments to be carried out.

Experiments involving displacement of water and oil in treated and untreated glass beads (representing various degrees of wettability) were performed. The beads were packed in 5- to 6-cm long by 5-cm diameter glass columns. These columns, called

short columns, permitted measurement of ROS and water saturation–capillary pressure (S_w–ψ) data. Bulk wettability indexes of the glass beads could also be calculated from the S_w–ψ data.

The mechanism of NAPL trapping was inferred from visual observations of micromodel experiments. Micromodels are etched glass plate models of a 2–dimensional pore network. Water–oil displacement experiments were also performed on the treated and untreated model to observe how wettability affected residual saturations. The same micromodel was used for all experiments so that pore geometry could be fixed.

1.3 Background

1.3.1 Altering wettability of glass with organosilanes

Organosilanes have been used in the petroleum industry to alter wettability of glass and sand since the 1950's (see for example, Jennings, 1957; Gatenby and Marsden, 1957; Coley et al, 1956; Newcombe et al, 1955; Bethel and Calhoun, 1953). Most of these early experiments focused on how sand, glass beads, or fritted glass cores treated with silane (altered wettability) affected oil recovery of initially oil–saturated columns. Gatenby and Marsden (1957) studied how silane treatment affected the capillary pressure–saturation behavior of treated fritted glass cores. Organosilanes have recently been used to study sorption kinetics of silane–treated silica in groundwater hydrology (Szecsody, 1988). Organosilanes have also been used in chemical engineering, for example in particle separation applications (see Menawat et al, 1984).

An organosilane is an organic molecule containing a silicon atom and a hydrolyzable group. The general chemical formula of an organosilane is:

$$R_nSiX_{(4-n)} \tag{1.1}$$

The X is the hydrolyzable group and is involved in the reaction with the silica surface (Arkles, 1987). Chlorine and alkoxy are common hydrolyzable groups. In the reaction,

X is hydrolyzed and the silane forms an Si–O–Si covalent bond with the silica surface. *R* is the functional organic group which imparts the hydrophobic character to the treated silica surface. The *n* is a number between 1 and 3 depending on the number of hydrolyzable groups in the silane. Monofunctional silanes ($n=3$) have one hydrolyzable group while di- ($n=2$) and trifunctional ($n=1$) silanes have two and three hydrolyzable groups respectively. Multifunctional silanes have the opportunity to form multiple Si–O–Si bonds on the glass surface (Singhal and Dranchuk, 1973). Figure 1.1 shows an example reaction of a monofunctional organochlorosilane with glass.

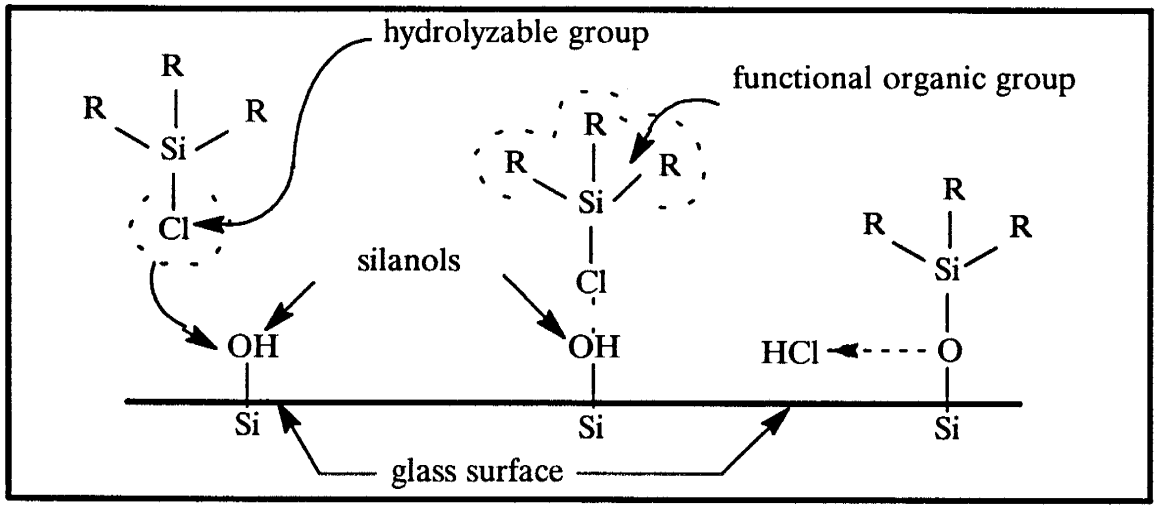

Figure 1.1. General reaction for monofunctional organochlorosilane.

The use of organosilanes to alter wettability of glass seemed, at first, to offer great advantages:

- the covalent bond between the organosilane and the glass surface would appear to be quite stable
- theoretically, the concentration of the silane used for reaction could be varied so that different degrees of wettability could be achieved. Maximum hydrophobicity would result if enough silane was added to react with all the silanol sites on the glass surface

- different functional organic groups of the different silanes could impart different wettability, hysteretic, and adsorption properties to the glass surface
- silane treatment would not affect visualization of micromodels
- the density, size, and grain shape of the glass beads used for column experiments would be identical for treated and untreated beads.

Unfortunately, silanes had not been adequately characterized in the early studies in the petroleum industry. In some cases, it was even assumed that the treatment would be permanent (Bethel and Calhoun, 1953). Only recently have the issues of silane treatment of glass, stability of the treated surface in different aqueous and organic liquids, and hysteresis been systematically studied (Takach et al, 1989; Takach et al, 1988; Menawat et al, 1984). Although expertise exists in silylation chemistry in the field of chromatography, much of the information regarding treatment is proprietary and silane characterization is for altogether different applications (Berendsen and de Galan, 1978).

It was recognized early in the project that treatment, stability, and wettability characteristics of a silane must be adequately understood and characterized before it can be used with confidence in subsequent experiments. Silylation of glass, which was initially believed to be a straightforward process, thus became a major part of the initial research.

1.3.2 Characterizing wettability of the silane-treated slides

Previous researchers in the petroleum industry seemed to regard organosilane treatment as a relatively straight-forward process and that an understanding of silane chemistry was secondary. Characterization of treated surfaces in these early studies usually involved measuring a contact angle on a treated glass slide (Newcombe et al, 1955), calculating an effective contact angle from measuring the capillary rise in

treated capillary tubes (Bethel and Calhoun, 1953), or measuring imbibition rates in treated uniform bead packs. Although each of these methods were valid, their application in characterizing silane–treated surfaces was very limited. For example, contact angles of the treated surfaces were seldom measured beyond a day after silylation; stability of the treated surface (exposed to air, water, brine, or oil) beyond one day was also seldom measured. Contact angle hysteresis and wettability for various liquids were not addressed; permanency of the treated surface was often assumed (Bethel and Calhoun, 1953).

Only recently has silane treatment in petroleum and groundwater applications been critically studied. Takach et al (1989) and Takach et al (1988) found that solution–phase silylation of silica slides with dimethyldichlorosilane produced treated surfaces which lasted only a few days when stored in water. In experiments where the treated surface came in contact with water for a few days or more, the wettability would change. This would be unacceptable in experiments where a system of constant wettability was desired.

Takach et al (1989) and Takach et al (1988) had greater success with vapor–phase silylation with bis(dimethylamino)dimethylsilane (BDMADMS) which produced surfaces that remained stable in water for up to 13 weeks. Their studies showed that silylated glass surfaces indeed had limited stability and that the silylation procedure, among other factors, could greatly determine the stability of the treated surface. It was, therefore, imperative that the issues of silylation, types of organosilanes to be used, and their wettability and stability characteristics including hysteresis be understood before silane treatment could be usefully applied to petroleum and groundwater studies.

There are 3 standard methods for quantifying wettability (Anderson, 1986b):

- 1) contact angle method

- 2) Amott method
- 3) USBM method.

The contact angle method measures the angle of the interface of two immiscible fluids at the solid surface. Water and air, organic liquid and air, or water and organic liquid are the most common fluids employed. A simple method of measuring a contact angle is by the use of a sessile drop on a flat, homogeneous, solid surface (Figure 1.2).

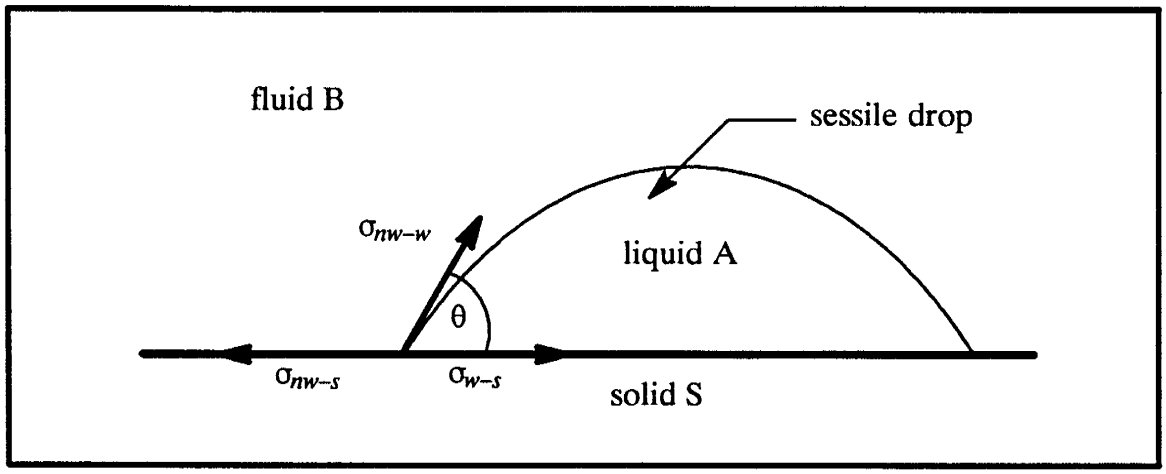

Figure 1.2. Contact angle measurement using the sessile drop method.

Commonly, contact angles are measured by placing a water sessile drop on the solid surface. The contact angle in this case is referred to as a *water–air contact angle*. By convention, the displacing fluid (the sessile drop) appears first in the prefix. The *organic liquid–air contact angle* and *water–organic liquid contact angle* are similarly defined.

In Figure 1.2, if the contact angle, θ, is less than 90° measured through the sessile drop, liquid A preferentially wets the solid surface compared to fluid B; liquid A is the *wetting phase*. If θ is greater than 90°, liquid A is the *non–wetting phase*. Under equilibrium, the contact angle is defined by Young's equation (see Bear, 1972):

$$\sigma_{nw-w} \cos\theta = \sigma_{nw-s} - \sigma_{w-s}\,; \qquad \cos\theta = (\sigma_{nw-s} - \sigma_{w-s}) / \sigma_{nw-w} \qquad (1.2)$$

where σ is the interfacial energy and the subscripts *w*, *nw*, and *s* stand for wetting phase, non–wetting phase, and solid phase, respectively. Equation 1.2 shows that the cosine of the contact angle equals the ratio of the difference in interfacial tension between fluid B and the solid and liquid A and the solid, $(\sigma_{nw-s} - \sigma_{w-s})$, to the interfacial tension between fluid B and liquid A, (σ_{nw-w}). In the special case where the term σ_{nw-w} cos θ in equation 1.2 is zero ($\theta = 90°$), both liquid A and fluid B have an equal affinity for the surface (Bear, 1972).

Equation 1.2 also shows that wetting depends on the surface energy of the solid and the fluids. It is important to remember that the wettability of a treated surface is defined for a given pair of fluids (such as oil and water) and that wettability has only a relative meaning. Anderson (1986b) described the following wettability classification for a water/oil/solid system defined by the contact angle (Table 1.1).

Table 1.1. Wettability classification using contact angles (Anderson, 1986b).

	Wettability		
Contact angle	***Water–wet***	***Neutral–wet***	***Oil–wet***
minimum	0°	60–75°	105–120°
maximum	60–75°	105–120°	180°

Interfacial energy is different when a fluid–fluid interface is advancing or receding on the solid surface. This is manifested in hysteresis of the contact angle. Contact angle hysteresis is attributed to three factors (Johnson and Dettre, 1969; Adamson, 1982):

- surface roughness
- surface heterogeneities
- surface immobility on a macromolecular scale.

Where the actual or true contact angle, θ_t, is less than 90°, surface roughness decreases the apparent contact angle, θ_a. Where the true contact angle is greater than 90°, surface roughness increases the apparent angle (Anderson, 1987). This phenome-

non is shown schematically in Figure 1.3. Wenzel's equation empirically accounts for the effect of surface roughness on the contact angle (Anderson, 1987):

$$\cos \theta_a = (A/A') \cos \theta_t \tag{1.3}$$

where A is the true surface area of the solid accounting for the peaks and valleys and A' is the projected flat surface area.

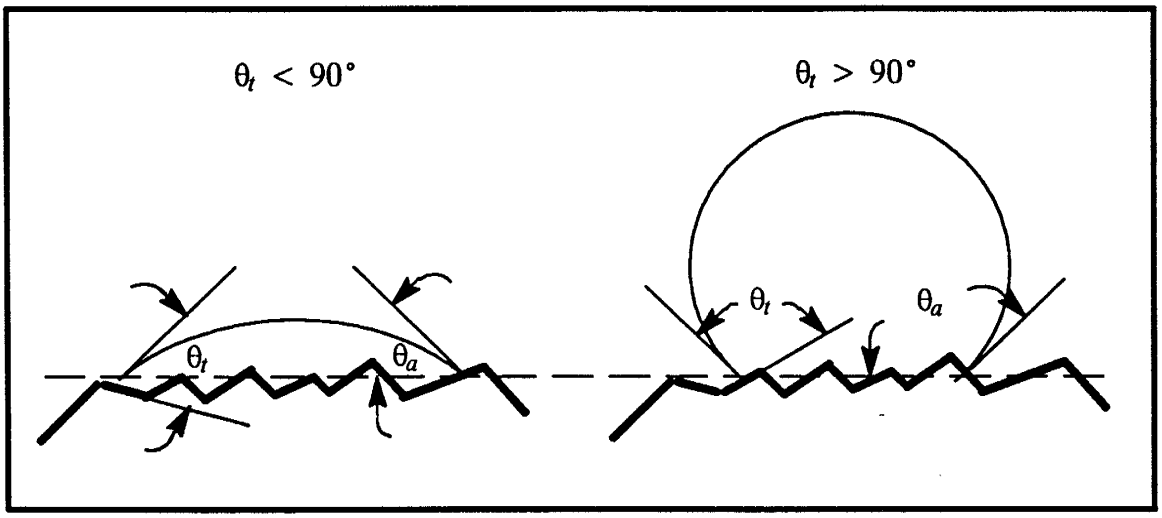

Figure 1.3. Effects of surface roughness on apparent contact angles.

Surface heterogeneities resulting in contact angle hysteresis include contamination of the liquid drop or the solid surface. Suppose, for example, a water drop was placed on a solid surface contaminated with a thin water soluble coating. The coating underneath the water drop will dissolve and the advancing angle measured as the water drop advances over the contaminated surface may be different (higher) than the receding angle measured where the water contacts the freshly exposed surface after the coating had been dissolved.

According to Adamson (1982), surface immobility caused by drag forces on the solid surface can also cause hysteresis by providing a barrier to motion which prevents the contact angle to reach its equilibrium value. It is conceivable that different organosilanes, with different organic moieties, can impart different drag forces on the treated glass surface.

The Amott and USBM methods were developed for measuring the average, bulk wettability of consolidated cores. Since our main objective in treating glass slides was to characterize the wettability of the treated surface without any affects from pore network, heterogeneities, and surface roughness inherent in porous media, these methods were not appropriate. The Amott and USBM methods will be discussed in section 4.

In our study, the silane-treated glass surfaces were characterized in three ways:

- stability of the treated surface with time
- wettability for liquids with various surface tensions
- wettability for the oil-water system to be used in the laboratory experiments.

The stability and character of the hydrophobic surface of the treated glass slides exposed to different environments such as water, air, and various organic liquids were measured at regular time intervals over a period of up to 6 weeks. This was done to ensure that the organosilane used to treat porous media later on for short column experiments would be reliable in maintaining an essentially stable and uniform surface because the treated porous media could be exposed to water, organic liquids (Soltrol® and other liquids), and air for up to several weeks. The question of whether the wettability would change over the course of each experiment had to be adequately answered before any results could be properly interpreted. Therefore, the variation of the contact angle with time was observed to see if any deterioration of the treated surface occurred. Wettability was characterized by measuring contact angles of drops of water placed on the slides (see sections 2.6 and 2.7).

Contact angles were also measured using other drops of liquids besides water to more thoroughly characterize the wettability for a whole spectrum of liquid surface tensions. Liquids with a lower surface tension form drops with lower contact angles.

As the liquid surface tension decreases to the value where the contact angle approaches zero, the *critical surface tension* (σ_c) is reached where any liquid with a surface tension below this critical value spreads on the surface (Fox and Zisman, 1950). The surface tension–contact angle relationship (commonly called Zisman plots – see section 2.8), which is unique for any given solid material, is a more thorough characterization of wettability (Morrow, 1989, pers. comm.).

Finally, some contact angles of water drops on treated slides immersed in organic liquids were also measured to observe the wettability and contact angles in the actual two–phase liquid system to be used in the experiments later on.

1.3.3 Short column experiments

Short column experiments provided quantitative data on residual liquid saturations and S_w–ψ relationships for displacement of immiscible liquids in porous media. Identical short columns were used by Wilson et al (1990) and Hagan (1989) to measure residual saturations of various NAPL in Sevietta sand and by Mace (1990) to measure residual saturations of Soltrol® 130 for Sevietta sand containing different percentages of clay. Lenhard and Parker (1987) used similar short columns to measure S_w–ψ relationships for soils using different pairs of immiscible liquids. In the experiments for this study, uniform glass beads were used to simulate a homogeneous aquifer. Wettability of the system was varied by using untreated and treated beads. Soltrol® 130, a mixture of C_8 to C_{13} isoparaffins with negligible solubility in water, was used as the organic liquid. Soltrol® was found by Wilson et al (1990) and Hagan (1989) to be an ideal, non–toxic, generic NAPL. Water with 1000mg/L sodium azide (NaN_3) as a bacteriacide was used as the aqueous liquid.

A short column is a 5–cm diameter and 5–cm to 6–cm long glass chromatographic column. Glass beads, soil, or other granular materials are packed into the column and contained in the column by endcaps which are threaded into the column at both ends.

In our experiments, the lighter liquid (Soltrol®) entered and left the column through the top endcap only. Water entered and left through the bottom endcap. The column was kept short so that liquid saturations (and capillary pressures) could remain uniform along the whole length of the column. Liquid saturations were determined gravimetrically by knowing the change in mass of the column during the experiment and the density difference between the liquids. Pressures were calculated by measuring the level of the Soltrol® and water in the burets connected to the top and bottom of the endcaps. The column and set-up are described in greater detail in section 2.

The short column allowed S_w–ψ data to be measured. This was done by letting displacement occur incrementally and measuring the capillary pressure and saturation at the end of each incremental displacement. The hanging column is an analogous apparatus used in soil physics to measure S_w–ψ relationships in soils. Similar procedures in petroleum engineering involve the use of centrifuge (Donaldson et al, 1969) or some modified pressure plate method (Bethel and Calhoun, 1953; Killins et al, 1953). Morrow and Mungan (1971) used a capillary pressure cell which allowed capillary pressure–saturation data to be measured during continuous displacement at very slow rates.

In the experiments, Soltrol® was introduced into an originally water–saturated column packed with glass beads. The invasion of Soltrol® into the column displaced water out of the pores. This process, called the *primary water displacement by oil (oil flood)*, was continued until *irreducible water saturation (IWS)* was reached where no more water could be displaced out of the column. After IWS, water was then introduced into the column to displace the Soltrol®. This process, called the *primary oil displacement by water (water flood)*, proceeded until *residual oil saturation (ROS)* was attained. At ROS, further displacement of oil or Soltrol® out of the column was not practical. In some experiments, secondary displacements were performed.

The above displacement sequence simulated NAPL contamination into an aquifer. The initial water displacement by Soltrol® represented a leak or spill of NAPL percolating into the aquifer. The aquifer was homogeneous and had uniform wettability. The hydrophobic character of the aquifer was a result of adsorption of organics in the dissolved part of the plume onto the aquifer matrix. The NAPL was, in turn, displaced by ambient groundwater flow (the water flood). Not all the hydrocarbon would be completely removed by groundwater flow, however. Some NAPL would be trapped in the pores, leaving behind a residual organic liquid saturation which became a long-term source of contamination.

In column studies of immiscible displacement, it is conventional to saturate the column with the *wetting phase* and then drain it by introducing the *non-wetting phase* into the column. A reason for this practice may be that it is much easier to saturate the column with the wetting liquid than with the non-wetting liquid. This convention was followed by many in the petroleum industry (eg. Morrow and McCaffery, 1978; Gatenby and Marsden, 1957; Coley et al, 1956; Newcombe et al, 1955; Bethel and Calhoun, 1953; Killins et al, 1953). This convention applied in our experiments only for the untreated (water-wet) beads where Soltrol® (non-wetting liquid) displaced water (wetting liquid) from the water-saturated column in the initial displacement. In the oil-wet case, the beads were saturated with the non-wetting liquid (water). During the initial displacement, Soltrol® (the wetting liquid) displaced water (the non-wetting liquid) out of the column. Even though the wetting liquid had changed, the sequence of liquid displacement had not. The sequence of Soltrol® displacing into an originally water-saturated bead pack followed by water displacement kept the NAPL contamination scenario consistent at the expense of convention. For the case of intermediate wettability, the convention loses meaning.

Capillarity, or the difference in pressure between the immiscible fluids, is the main factor governing displacement, trapping, and fluid distribution in porous media:

$$P_c = P_{nw} - P_w = \sigma_{nw/w} (1/r_1 + 1/r_2) \quad (1.4)$$

where P_c is the capillary pressure, P_{nw} and P_w are the pressure in the non–wetting and wetting phase respectively, $\sigma_{nw/w}$ is the interfacial tension between the fluids, and r_1 and r_2 are the principal radii of curvature of the interface (Hillel, 1980). For the capillary model of a bundle of capillary tubes representing porous media, equation (1.4) becomes:

$$P_c = 2\sigma_{nw/w} \cos \theta / r_t \quad (1.5)$$

where θ is the contact angle and r_t is a representative tube radius. For porous media represented by this model, r_t is commonly assumed to be the median grain size. This simple model shows that the magnitude of capillarity increases with increasing σ and cosine θ or decreasing r_t. The approach here was to keep $\sigma_{nw/w}$ and r_t constant by using the same liquids and same size glass beads throughout all of the short column experiments and to treat the beads to achieve various values of cosine θ. This changed capillarity which, in turn, would affect the mechanisms and amount of residual NAPL trapping. Although this model shows that wettability (represented by cos θ) affects P_c, it does not reveal anything about how wettability affects residual saturations in real porous media.

In actual porous media where pores are not tubular but irregularly shaped, the larger the value of P_c, the greater the propensity for capillary trapping of the non–wetting phase. Snap–off in individual pores and by–passing along non–uniform pore networks are two examples of such trapping mechanisms (Wilson et al, 1990; Chatzis and Dullien, 1983; Wardlaw, 1982). Trapping depends on the actual pore geometry of the medium and the amount of trapping must be directly measured in experiments.

1.3.4 Micromodel experiments

Micromodels are glass plate models of a 2–dimensional pore network. The models were made by etching the pore network pattern onto two glass plates and then fusing

the plates together. A typical micromodel consists of the pore network and end reservoirs. The end reservoirs have holes drilled into them where fluids can enter and leave the model. The greatest advantage in using micromodels is that we could observe how immiscible fluids displace one another and their distributions in the pores. It was hoped that micromodel experiments could give us visual insights on the trapping and displacement mechanisms operative in the short column experiments.

Micromodels have been used extensively in petroleum and chemical engineering to study the physical behavior of immiscible flow (Buckley, 1991; Chatzis and Dullien, 1983; Wardlaw, 1982; Mattax and Kyte, 1961). Micromodels have also been used to observe the behavior of NAPL trapping in groundwater contamination (Mace, 1990; Wilson et al, 1990; Mason, 1989) and colloidal transport (Wan and Wilson, 1990).

Despite their popularity, micromodel experiments have largely remained a qualitative tool for visualizing physical phenomena on the pore level scale. The 2–dimensionality of the pore network (although the pores themselves are 3–dimensional), capillary end effects, inability to measure pore pressures in the model, and the cost of equipment for quantitative visual analyses have limited the use of micromodels for quantitative analysis. For the above reasons, micromodels were used strictly as a visual analogue for the short column experiments in order to observe interfacial curvatures, displacement processes, and liquid distributions in a qualitative sense.

2. Procedures and methods

In this section, procedures and methods are presented for silylating glass, measuring contact angles, packing and running short columns, and running micromodel experiments. After each topic has been presented, a discussion follows which explains some of the reasoning behind the procedures, limitations of the technique, and possible sources of error.

2.1 Finding a suitable organosilane

In searching for a suitable silane, we included organochlorosilanes which had been used in previous studies so that our results could be compared with published results. A suitable silane was one which gave a hydrophobic surface that remained stable in water and organic liquid for five to six weeks. This was enough time to run the short column experiments. Organochlorosilanes were also widely available. Furthermore, the reaction could occur in alcohol or hydrocarbon solutions where the silane concentration could easily be controlled for achieving a wide spectrum of wettability (for silylating procedures, see sections 2.2 to 2.4). An alkoxysilane was also used to examine silylation by an alternate method. The list of silanes investigated in detail is shown in Table 2.1. All silanes were purchased from Petrarch Systems Silanes and Silicones (Bristol, PA).

Table 2.1. List of silanes investigated.

Silane	Formula	M.W.	Abbrev.
Trimethylchlorosilane	C_3H_9ClSi	108.64	TMCS
t–Butyldimethylchlorosilane	$C_6H_{15}ClSi$	150.72	tBDM
t–Butyldiphenylchlorosilane	$C_{16}H_{19}ClSi$	274.84	tBDP
n–Octadecyltrichlorosilane	$C_{18}H_{37}Cl_3Si$	387.93	OtS
GlassClad® 18	N/A[1]	N/A[1]	GC18

1. A 20% active octadecylsilane derivative in a solution of t–butanol and diacetone alcohol; chemical formula proprietary and unavailable.

Contact angle measurements were used to characterize the silane-treated glass surfaces. The wettability and stability of treated glass slides stored in different liquids over a period of time were of critical interest. Once a suitable silane was found, it would be used to treat glass beads and glass micromodels for laboratory experiments.

2.2 Silylating glass slides using organochlorosilanes and GlassClad® 18

Corning Plain Micro Slides 2947 (sodalime glass) were used as the substrate. Polished quartz and fused silica slides from Heraeus Amersil (Buford, GA) were also used to examine if purer substrates would affect the wettability and stability of the treated surface. The chemical composition of the slides are shown in Appendix A1. All the slides had dimensions of 76mm x 25mm (3" x 1") x 1mm.

2.2.1 Procedures for cleaning slides

The slides were cleaned following the procedures outlined in Menawat et al (1984). Prior to cleaning, the slides were cut into approximately 38mm x 25mm (1.5" x 1") pieces, inserted into slots machined into a Teflon® block, and put into a glass mason jar. The slides were first cleaned with 2-butanone and then with hot nitric (70%) acid. About 20 minutes were allowed for each cleaning process. A sonicator was used to enhance the cleaning action. The 2-butanone removed any organic contaminants from the glass. Nitric acid removed inorganic contaminants and oxidized organics not removed by the 2-butanone.

After cleaning with 2-butanone, the slides were rinsed three to four times with deionized water before the nitric acid was added. The slides were again rinsed three to four times with deionized water after acid treatment. After cleaning, the slides were placed in a drying oven for at least one day at $110° \pm 5°C$ and then cooled in a dessicator. A water-soluble coating commonly appeared on the slides after drying for several hours. The coating was rinsed away with deionized water.

2.2.2 Preparing the chlorosilane solution

The chlorosilane solution was prepared by adding silane to redistilled toluene in a 500mL glass graduated cylinder. The solution was stirred using a Teflon® coated magnetic stir bar until all the silane had dissolved and/or had been thoroughly mixed. The solution was then poured into the jar containing the cleaned, dried slides. The jar was covered with a screw–on lid to minimize toluene evaporation. The set–up is shown in Figure 2.1. Two glass tubes inserted through the lid and filled with Drierite® ($CaSO_4$) pellets helped maintain dry atmospheric conditions.

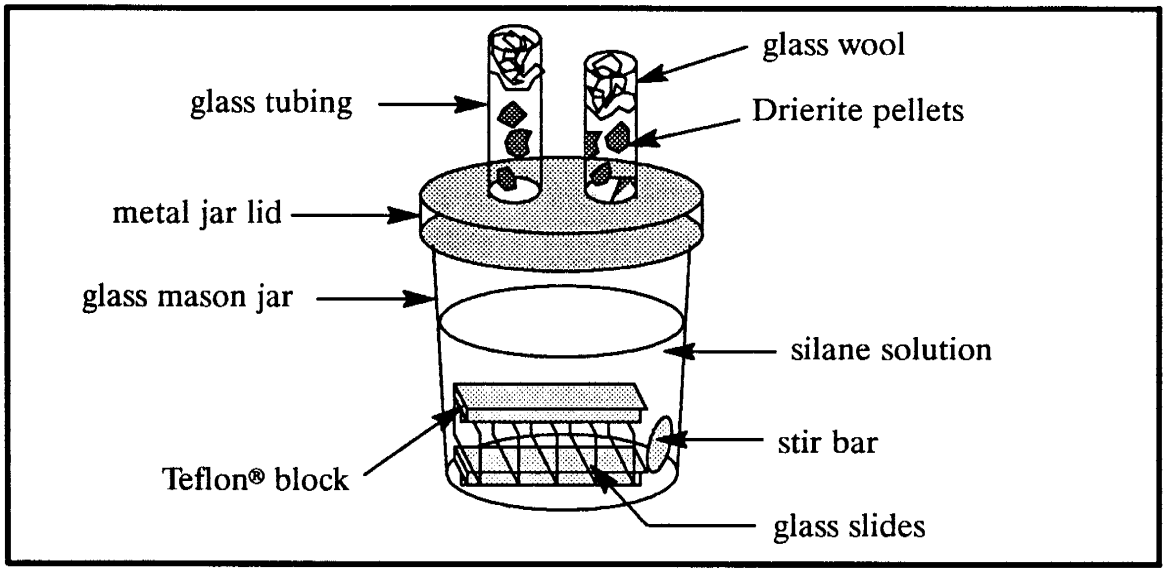

Figure 2.1. Set–up for treating glass slides with organochlorosilane.

Dry conditions were essential for minimizing bulk deposition of silanes from the toluene solution. Water in the system readily displaces the chlorine from the silane molecules. The silane molecules then form silanols and condense to form dimers (monofunctional silanes) or polymers (multifunctional silanes). This process of hydrolysis occurs very fast and can not be controlled. Early *bulk deposition* by dimerization and polymerization eliminates silanes from the reaction with the silica surface.

All glassware such as pipettes, graduated cylinders, and reaction jars plus Teflon® coated magnetic stir bars, were oven–dried for about one–half hour at 105°C to re-

move any adsorbed water and rinsed with distilled toluene prior to preparation of the chlorosilane solution. Nitrogen gas was used to purge the silane storage bottles to displace any moist air before the bottles were stored away.

2.2.3 Reaction procedures for chlorosilanes

The solution was heated on a hot plate to about 70°C to 80°C and stirred with a Teflon® coated magnetic stir bar. Reaction time was 24 to 48 hours for the lighter chlorosilanes (TMS, tBDM, and tBDP) and one week for the longer–chained, heavier chlorosilanes (OtS) as recommended by Berendsen and de Galan (1978).

In reactions involving OtS, and in later experiments with tBDM and tBDP, pyridine, in amounts (10.0 mL) greater than the silane concentration, was added to the solution one day before the end of reaction to neutralize the HCl by–product of the reaction and help drive the reaction forward (Berendsen and de Galan, 1978).

After the reaction, the excess silane was washed off with redistilled toluene. In the OtS, and later tBDM and tBDP experiments, additional rinsing with methanol, 50:50 methanol:deionized water, and methanol again was done (Berendsen and de Galan, 1978). Finally, the treated slides were cured in the oven at 110° ± 5°C for 4 hours and then stored in a dessicator before testing.

2.2.4 Procedures for treating glass slides with GlassClad® 18

The procedures recommended in Silicone Compounds Register and Review (Petrarch Systems Silanes & Silicones, 1987) for treating glass using GlassClad® 18 (GC18) were modified. A 1% by volume of aqueous silane solution was prepared by mixing with deionized water. The solution was poured into the Mason jar containing the cleaned slides and the jar was then immersed in a sonicator for 1½ to 2 minutes to allow the reaction to occur. After the reaction, the solution was poured out and any excess silane was then rinsed away with deionized water. The glass slides were cured

in the oven for 3–5 minutes at 110° ± 5° C. This procedure was repeated six to seven times. The treated slides were then stored in a dessicator before testing.

2.3 Silylating glass beads using organochlorosilanes and GlassClad® 18

Sodalime glass beads from Cataphote, Inc. (Jackson, MS) were used. The chemical composition of the glass beads was very similar to the composition of the glass slides used in characterizing the silanes. The chemical composition is shown in Appendix A1. The glass beads used were Class V Closed Sized Uni–Spheres. The particle density of the beads was 2.471 ± 0.009 g/cm^3. The particle size was specified by the manufacturer to be 90% within the range of 250 – 297μm.

2.3.1 Procedures for cleaning glass beads

The cleaning procedures for glass beads were modified from the procedures for cleaning glass slides in section 2.2.1. Approximately 180g of glass beads were slowly poured into a 1000mL Erlenmeyer flask containing about 250mL of 2–butanone and a 64mm– or 76mm– (2½" or 3") long Teflon® coated magnetic stir bar. The beads were stirred on a stir plate for approximately 20 to 30 minutes. After cleaning, the 2–butanone was poured away into a waste bottle and the beads were thoroughly rinsed with deionized water. The beads were stirred for several minutes during rinsing. About five rinses were generally required to thoroughly remove the 2–butanone (Figure 2.2).

Next, about 250mL of nitric (70%) acid was poured into the flask with the beads and heated to about 70° C for roughly 20 to 30 minutes. The acid was then poured into another waste bottle and the glass beads were again rinsed thoroughly with deionized water. The glass beads were transferred into a beaker or Mason jar and dried in the oven at 110° ± 5° C for a minimum of 24 hours. After several hours of drying, the beads were rinsed again with deionized water to remove any of the water–soluble coating observed previously in the glass slides. The beads were then stored in a dessicator until time for treatment.

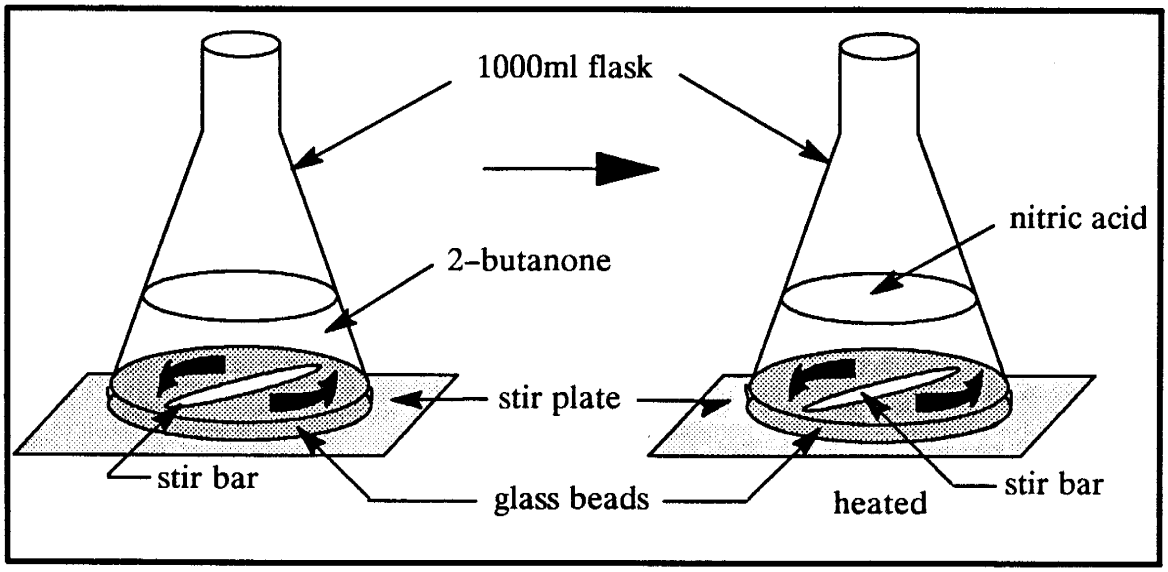

Figure 2.2. Set-up for cleaning glass beads.

2.3.2 Reaction procedures for chlorosilanes

The chlorosilane solution was prepared as described in section 2.2.2. The solution was poured into a 1000mL Erlenmeyer flask containing a 64mm- to 76mm- (2½" to 3") Teflon® coated stir bar. About 180g of clean, dried beads were then poured into the flask. The mouth of the flask was joined to a drying tube to keep the atmosphere inside the flask as dry as possible. Figure 2.3 shows the experimental set-up. Any moist air in the flask, which may promote early deposition of the chlorosilane, was initially displaced by blowing nitrogen gas into the flask through the drying tube. The flask was then heated to about 70°C to 80°C and stirred on a hot plate during the reaction. As described in section 2.2.3, the reaction time was 48 hours for the lighter chlorosilanes and up to 1 week for the heavier chlorosilanes.

One day before the end of the reaction, the drying tube was temporarily removed and pyridine, in amounts (10.0 mL) greater than the silane concentration, was added to the solution. After the reaction, the silane solution was poured into a waste bottle. Any excess silane left in the flask was rinsed away with about 100 - 200 mL of redistilled toluene. The toluene rinse was repeated. The treated beads were then rinsed

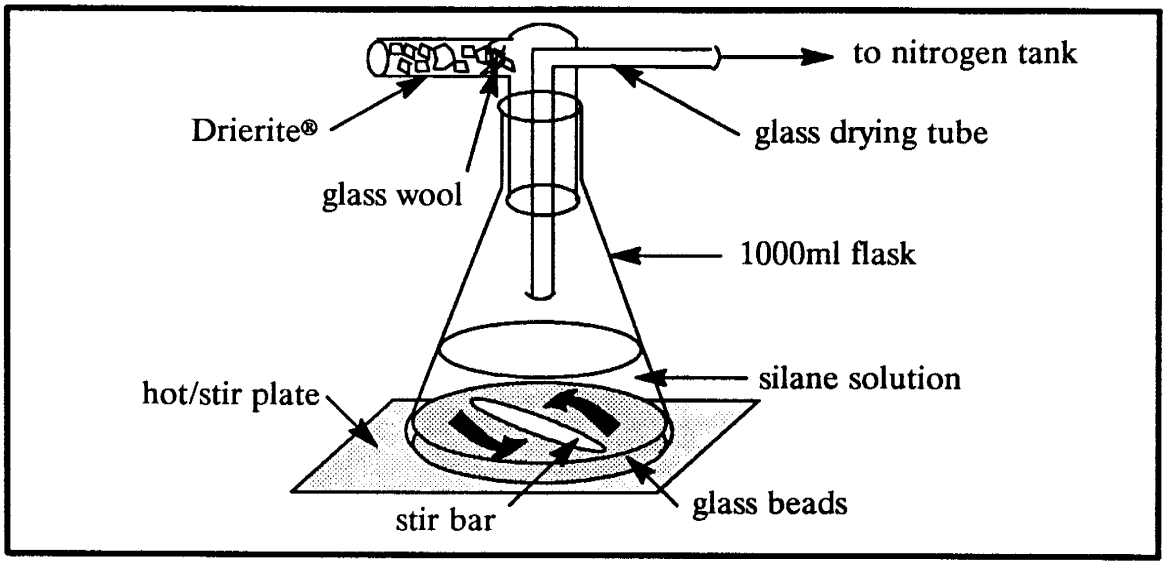

Figure 2.3. Set–up for treating glass beads with organochlorosilanes.

with methanol, 50:50 methanol:deionized water, and methanol again as with the case for treating glass slides in section 2.2.3. The beads were then poured into a Buchner funnel, drained by vacuum (Figure 2.4), and finally, cured in the oven at 110° ±5°C for about 4 hours. The treated beads were then transferred to a beaker and stored in a dessicator until use.

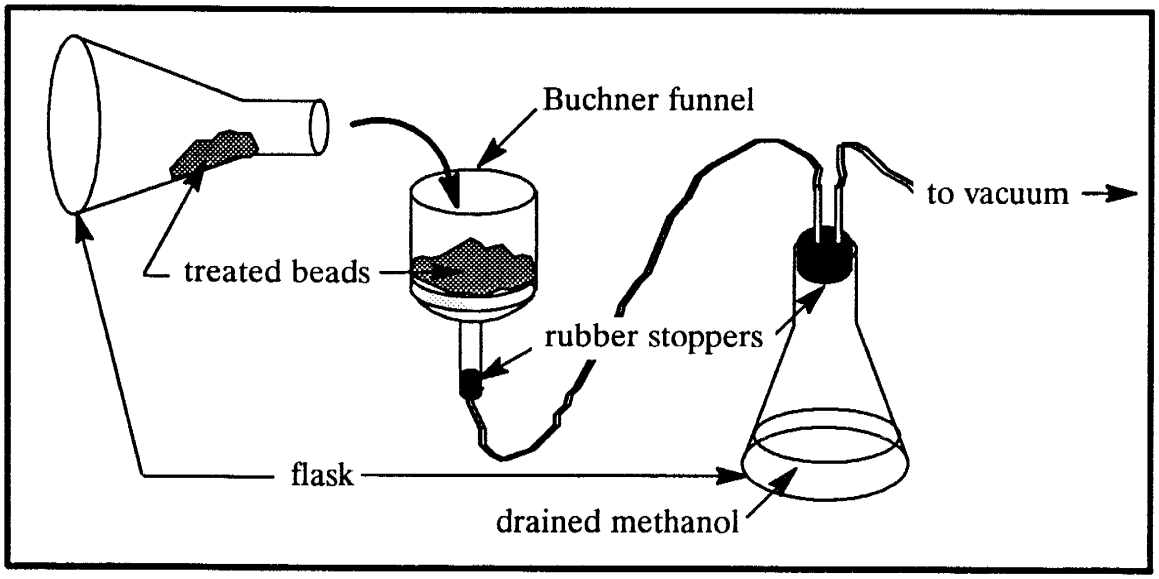

Figure 2.4. Draining wet glass beads treated with organochlorosilanes prior to curing.

2.3.3 Procedures for treating glass beads with GlassClad® 18

Treatment of glass beads with GC18 was also carried out in a flask. A 1% by volume solution of GlassClad® 18 in water was prepared in a glass beaker using 200mL of deionized water and 2.0mL silane as described in section 2.2.4. The solution was stirred and then gently poured into a 1000mL Erlenmeyer flask containing the Teflon® coated stir bar. About 180g of cleaned, dried glass beads were poured into the flask for reaction. The beads were stirred on a stirring plate for about 2½ minutes. The beads were then sonicated for another 2½ minutes.

After reaction, the silane solution was poured away and any excess silane was rinsed away with deionized water. The wet beads in the flask were drained by pouring them into a porcelain funnel. The mouth of the funnel was attached to an Erlenmeyer flask. A vacuum was applied to the funnel through the side nozzle on the flask which was connected to the vacuum line (Figure 2.5). The base of the funnel was lined with a polypropylene filter. The filter size was large enough to allow water but not the beads to be pulled through thereby draining the beads. The drained beads were then transferred to a Pyrex pan, cured in the oven for up to 30 minutes at 110° ± 5°C, and stored in a dessicator until use.

2.4 Silylating glass micromodels using organochlorosilanes and GlassClad® 18

The same micromodel, H6C, was used for all the experiments. Procedures for model construction are presented in section 2.14. The model was cleaned by thoroughly rinsing with acetone. During cleaning, acetone was injected into the model through one end reservoir and sucked out through the other end reservoir connected to the vacuum line. The model was then dried in the oven at 110° ± 5°C for 24 hours prior to treatment. The Willard mirrors (O' Malley Glass, Albuquerque, NM) used for the micromodel were very similar in chemical composition to the glass slides and glass beads (Appendix A1).

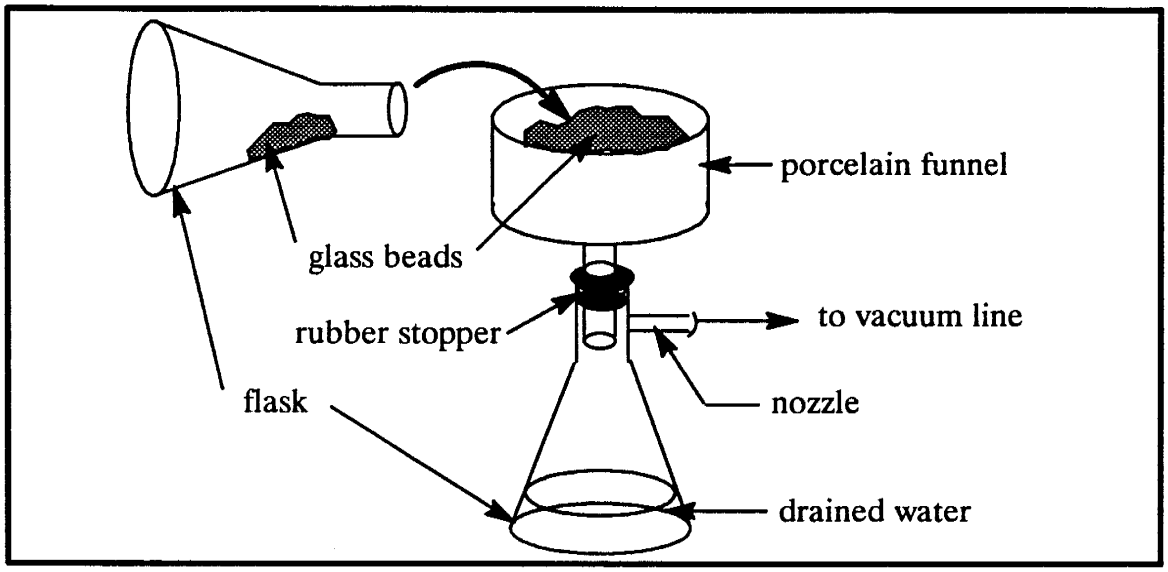

Figure 2.5. Draining wet glass beads treated with GlassClad® 18 prior to curing.

2.4.1 Silylating the micromodel using organochlorosilanes

The model was treated under the ventilation hood in the laboratory (Figure 2.6). Chlorosilane was added to 100 mL of distilled toluene and stirred with a Teflon® stir bar in a clean, dry glass beaker. The solution was then transferred to a 100 cc glass syringe. Teflon® tubing connected the syringe to the micromodel. Another Teflon® tube was connected to the outlet reservoir.

The solution was injected into the model at a slow rate (about 10 mL/hr) with a Sage syringe pump and discharge from the outlet reservoir of the model into a waste beaker. The injection took about ten hours to complete. Once the silane solution had been injected, the syringe was refilled with pure toluene which was flushed through the model to remove the excess silane. The model was then rinsed by injecting methanol through the model. The toluene and methanol rinses were done at high flow rates (about 60 mL/min) and took less time. The excess methanol in the model was removed by suction with a vacuum line. The set-up did not allow the reaction to occur in a heated environment such as an oven. After treatment, the model was disconnected and left in the oven to dry and cure for 4 hours at $110° \pm 5°C$.

2.4.2 Silylating micromodels using GlassClad® 18

A 50 mL, 1% silane solution was prepared following procedures outlined in section 2.2.4. The solution was transferred to a 50 mL polypropylene syringe and injected through the model at about 10 mL/min with the syringe pump (Figure 2.7). Teflon® tubing and Teflon®/nylon fittings were used.

Afterwards, deionized water from another syringe was injected through the model to remove the excess silane. The excess water inside the model was removed by vacuum. The model was then dried and cured in the oven at 110° ±5°C for ½ hour.

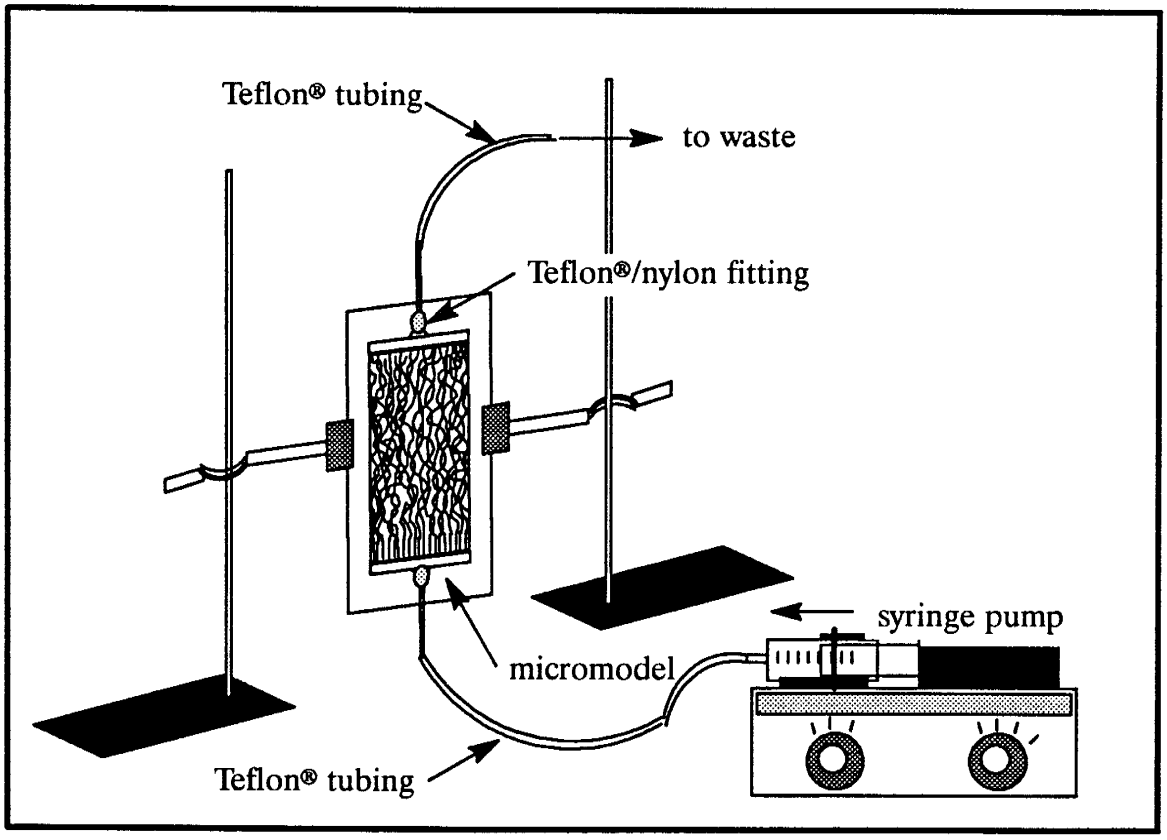

Figure 2.6. Set-up for treating micromodel with organochlorosilanes.

The silylation procedure was repeated 10 times to ensure that the model was fully silylated. The silane solution was injected into the model through both end reservoirs during repeated treatments so that none of the pores would be missed.

2.4.3 Removing the silane treatment

It was necessary to remove the previous treatment before the model could be cleaned and retreated with another silane for another experiment. The treatment was removed by heating the model in the furnace at 300° – 325°C for 1 hour. A temperature of 300°C or greater was required to destroy the silane surface and render the glass water–wet (Appendix A2). Temperatures higher than 350°C were not recommended as sodalime glass softens at that temperature. The purged model was then cooled overnight in the furnace before it was taken out for cleaning and retreatment.

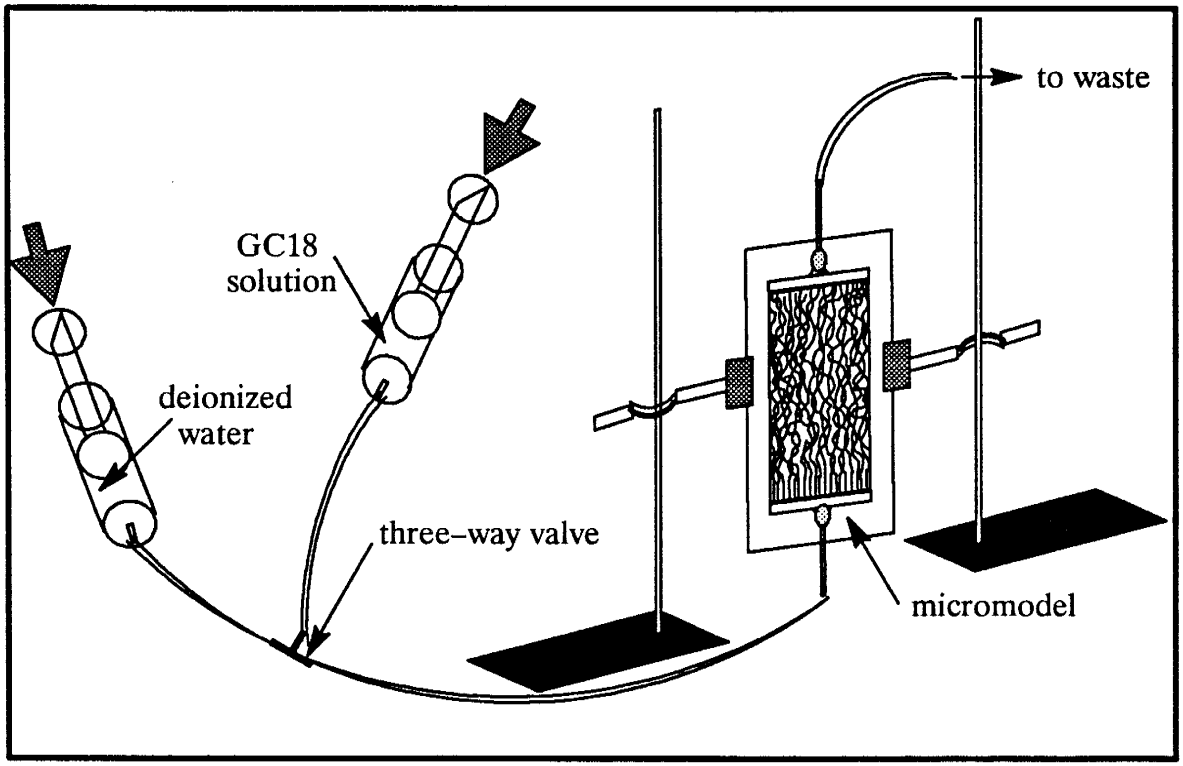

Figure 2.7. Set–up for treating micromodels with GC18.

2.5 Discussion of silylation procedures

Treatment with organochlorosilanes involved a direct nucleophilic displacement of the silane chlorines by the surface silanols on the glass. The chlorines of the silane

molecule reacted with the silanol hydrogens on the glass surface. An Si–O–Si bond was formed between the silane and the glass. HCl was produced as a by–product of the reaction. The presence of any adsorbed water, however, caused early bulk deposition of the chlorosilane molecules to occur. Bulk deposition by dimerization or polymerization eliminated silanes from the reaction with the glass surface. This was minimized by using water–free redistilled toluene boiled in sodium and by adding an excess amount of silane to off–set any early bulk deposition. Furthermore, any moist air in the reaction flask was initially displaced with nitrogen gas.

The amount of silane required for complete reaction was estimated based on the following empirical equation (Petrarch Systems Silanes & Silicones, 1987):

$$M = (m_s \, a_m) / ws \qquad (2.1)$$

where M is the number of grams of silane required, m_s is the mass of the substrate in grams, a_m is the specific surface area of the substrate in m^2/g, and ws is the wetting surface (m^2/g) of the silane. The wetting surface can be estimated from the molecular weight of the silane (Figure 2.8). Knowing the surface area and mass of the substrate (for example, glass slides or glass beads), the amount of silanes required can easily be calculated using equation 2.1. Figure 2.8, which was compiled from the Petrarch catalogue, shows that wetting surface decreases as molecular weight of the silane increases. This implies that for a given reaction, a greater amount of heavier silanes than lighter silanes is required because heavier silanes are less reactive. That is also the reason for the longer reaction time when silylating with OtS.

The amount of silane used in the reaction rather than the silane concentration may be the more important criterion in achieving varying degrees of wettability. For example, to achieve complete coverage with chlorosilanes, enough silane must be added in the toluene solution to react with all of silanol sites on the glass surface. If enough silane is present, complete coverage should result even if the silane is mixed with a

large volume of toluene to form a low concentration solution. On the other hand, if only half the amount of silane was used, only 50% coverage could be achieved even if the silane was mixed with a much smaller volume of toluene to form a higher concentration solution. Up to three orders of magnitude excess silane was added in silylation with organochlorosilanes (see section 3).

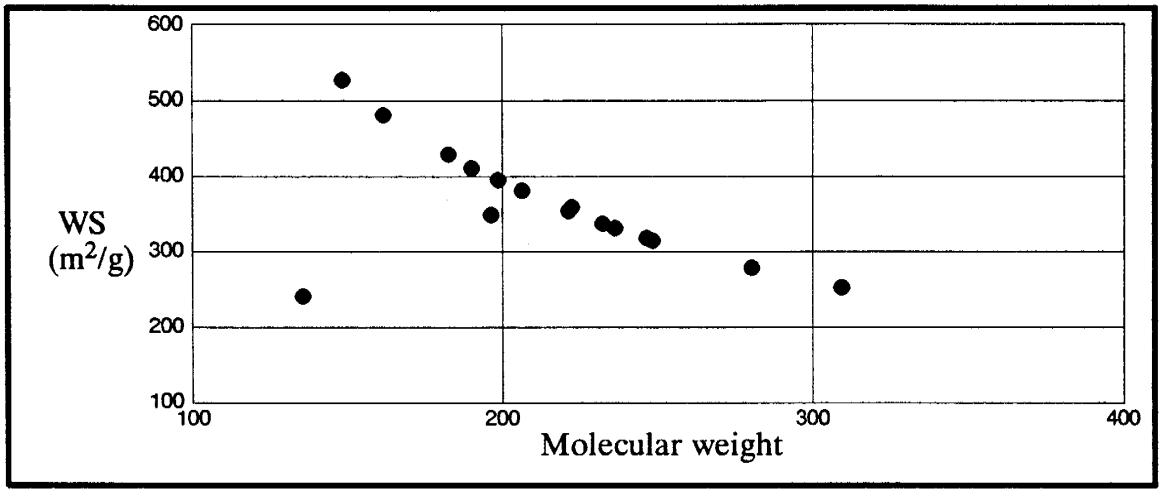

Figure 2.8. Silane wetting surface as a function of molecular weight (Petrarch Systems Silanes & Silicones, 1987).

The silylation procedures evolved for glass slides. In the earlier experiments with TMS, tBDM, and tBDP, the procedures were still being refined. In later experiments, reaction time for the lighter silanes was extended from 24 hours to 48 hours when pyridine was added one day prior to the end of reaction. The methanol rinse was also applied after the reaction and prior to curing. In reactions with organochlorosilanes, pyridine was added to neutralize the HCl by–product of the reaction by forming pyridine–hydrochloride salt. Removal of the HCl helped drive the reaction forward. Pyridine was not added to the chlorosilane solution for treating the micromodel because the pyridine–hydrochloride tended to settle in the syringe and impeded the injection process. According to D. Baehr of Regis Chromatograhy (Morton Grove, IL), the methanol rinse after the reaction converted the reacted chlorosilanes to a more stable

derivative which is apparently much less susceptible to hydrolysis by water (D. Baehr, 1990, personal communication). The preceding methanol:water rinse dissolved the pyridine–hydrochloride which was insoluble in toluene.

Monofunctional silanes yield a more uniform, hydrophobic surface than multifunctional silanes (D. Baehr, 1990, personal communication; Menawat et al, 1984). Multifunctional silanes tend to form a multimolecular layer on the glass surface instead of a monomolecular layer. The thickness of the multimolecular layer varies from one reaction to the next. Consequently, wetting characteristics (for example, contact angle and contact angle hysteresis) of surfaces treated with multifunctional silanes are apt to be more non–uniform. Typically, only one or two of the chlorines of multifunctional chlorosilane molecule adhere to a silanol site on the glass surface. The remaining chlorines remain very active. The methanol rinse also converts these highly active groups to esters that are much less reactive (D. Baehr, 1990, personal communication). Multifunctional silanes offer greater hydrolytic stability than monofunctional silanes, however.

The most complete treatment was likely achieved with glass slides. The pore networks in the micromodel were very inaccessible and deadend pores and pore networks so oriented in the "shadow" of the advancing silane solution may not have been fully treated. The shorter time for tBDM treatment of the micromodel, however, should not result in a less thorough treatment compared to tBDM treatment of glass slides and glass beads. Usually, complete treatment can be realized in as little as 4 hours (Berendsen et al, 1980); reaction time for tBDM in all cases was greater than that. The affect on the durability of the treated surface from the stirring action during glass bead treatment was also unknown. Finally, the limited surface area of the substrates used here did not permit the use of any visual indicator, such as methyl red color pH indicator, to check the effectiveness of our cleaning and silylating procedures. Comparison of the uniformity of experimental results provided the only check on the procedures.

2.6 Procedures for measuring contact angles with the sessile drop method

2.6.1 Procedures for storing and handling the treated glass slides

After curing, the freshly silylated slides were immediately divided up (there were about 24 slides in each batch). Slides stored in aqueous solution (deionized water, 3000mg/L $CaCl_2$ solution, and/or deionized water containing 1000mg/L sodium azide (NaN_3) as a bacteriacide) or air were put in plastic containers with removeable tops. Slides stored in organic liquids such as Soltrol®130, xylene, ethanol, etc. were placed in clean glass Mason jars with lids. Care was taken to not have any of the slides overlap each other so that the top surface of all the slides was wholly exposed to the aqueous or organic liquid in which they were stored.

When a slide was used for contact angle measurements, it was taken out of its container with clean Teflon® tweezers, rinsed thoroughly, oven dried at low temperatures (60°–80°C) for about 15 minutes, and then air cooled. Slides stored in aqueous solution or alcohol (ethanol and methanol) were rinsed with deionized water; slides stored in other organic liquids were rinsed with acetone to remove the organic liquid and then with deionized water. Prior to contact angle measurements, the slides were allowed to equilibrate with the atmosphere or with the (organic) liquid in which the measurements were to take place (Mungan, 1981; Fox and Zisman, 1950). After measurement, the slide was air dried and then replaced into its original container. Slides immersed in organic liquid for water–Soltrol® contact angle measurements were once again rinsed with acetone, then rinsed with deionized water, and oven dried at low temperatures before being returned to their storage containers. Care was taken to always return the slide with its top side faced upright.

2.6.2 Measuring advancing contact angles from a static sessile drop

In the early stages of the project, the laboratory was equipped only to measure contact angles from a sessile drop placed on glass slides (Figure 2.9). The angles measured

were advancing angles. There was no way to contract the drops for measuring receding angles and determining contact angle hysteresis. However, the static sessile drop method was still useful for comparing advancing angles of the different silane–treated surfaces.

Contact angles were measured following procedures specified by ASTM C813–75 (ASTM, 1986). The slide was placed on a level, adjustable lab jack which was secured onto the table. A 5 mL microburet was used to form drops having a volume of about 0.01 mL (Figure 2.9). To measure a contact angle, the lab stand was slowly raised until

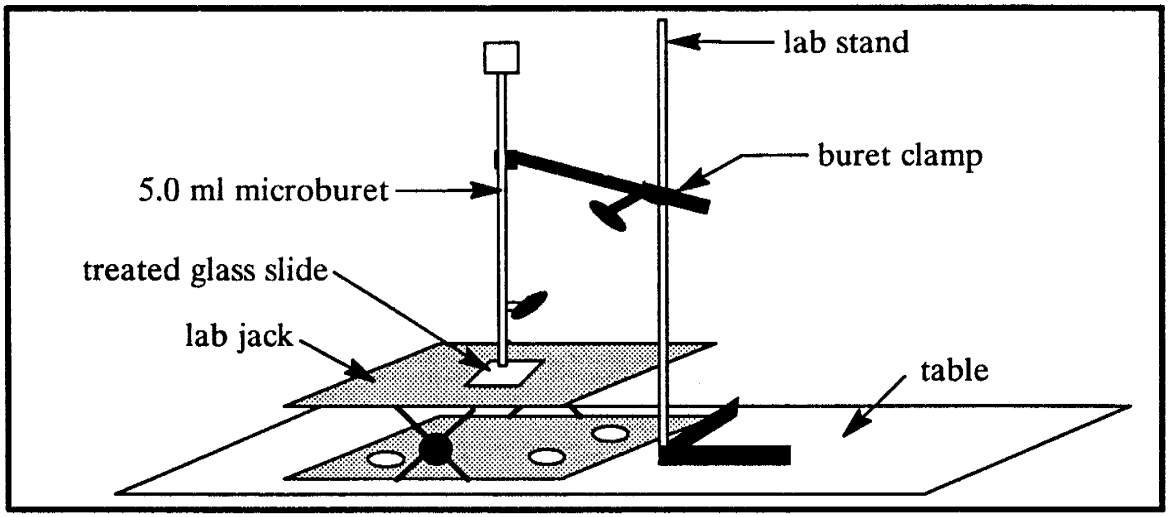

Figure 2.9. Set–up for measuring contact angles using sessile drops.

the drop touched the slide. Then, the lab stand was lowered so that the drop snapped off the buret onto the slide. The contact angle was then calculated by measuring the height and width of the drop with a grid reticule through a microscope (Zeiss 47 50 52 - 9901) and using the following equations:

$$\text{for } \theta < 90^\circ \qquad \theta = 2\,(\tan^{-1}(2h/w)) \tag{2.2}$$

$$\text{for } \theta > 90^\circ \qquad \theta = (\sin^{-1}(2h/w) + 90^\circ) \tag{2.3}$$

where h is the height and w is the width of the drop (Figure 2.10). Equations 2.2 and 2.3 were used to calculate contact angles of small drops where distortion of the spheri-

cal drop shape due to gravity was negligible. Measurements were usually taken within 30 seconds after placing the drop. Contact angles were recorded to 0.1° precision. Three to four angles were measured for each slide to get an average angle and to check the uniformity of the treated surface. Average angles are reported in section 3.

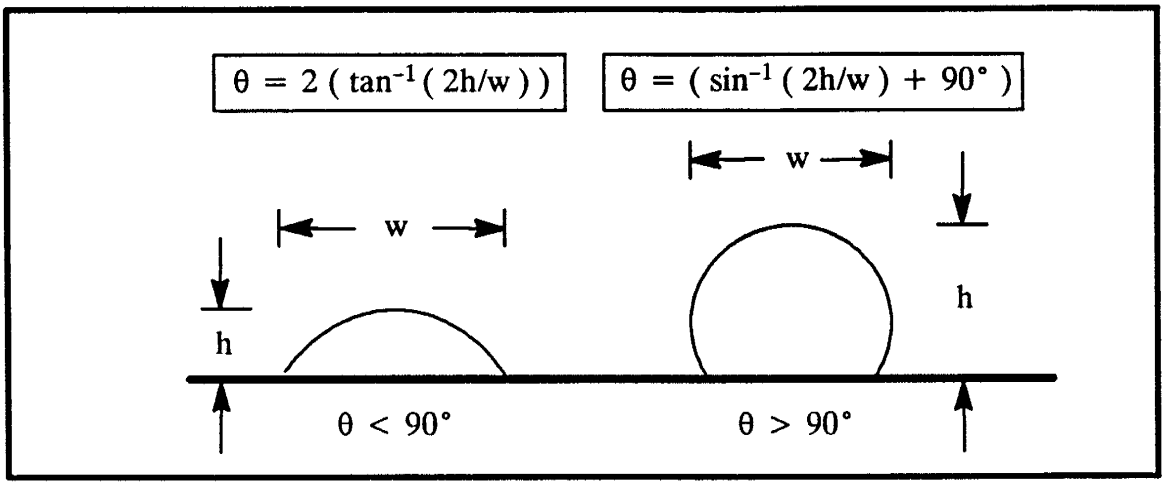

Figure 2.10. Equations for calculating contact angles.

2.6.3 Measuring advancing and receding angles from a dynamic sessile drop

Later on in the project, a Gelmont® 2 mL microburet (Barrington, IL) was purchased and used for expanding and contracting the drop to form advancing and receding angles. A Tiyoda No. 4443 goniometer (Tokyo) for directly measuring contact angles also became available (Figure 2.11).

In the dynamic sessile drop method, the lab jack was raised until it was about 2 mm from the buret tip. The sessile drop was formed by turning the dial at the top of the buret to emit liquid at the buret tip. Once the drop contacted the slide, the drop was expanded slightly so that the liquid/fluid interface advanced on the solid surface. The advancing contact angle of the interface was then measured through the microscope with the goniometer (Figure 2.11). Two measurements were taken for each drop, one of the interface on the left side of the drop and one of the right side. The two measurements, when averaged, offset any differences in the individual angles

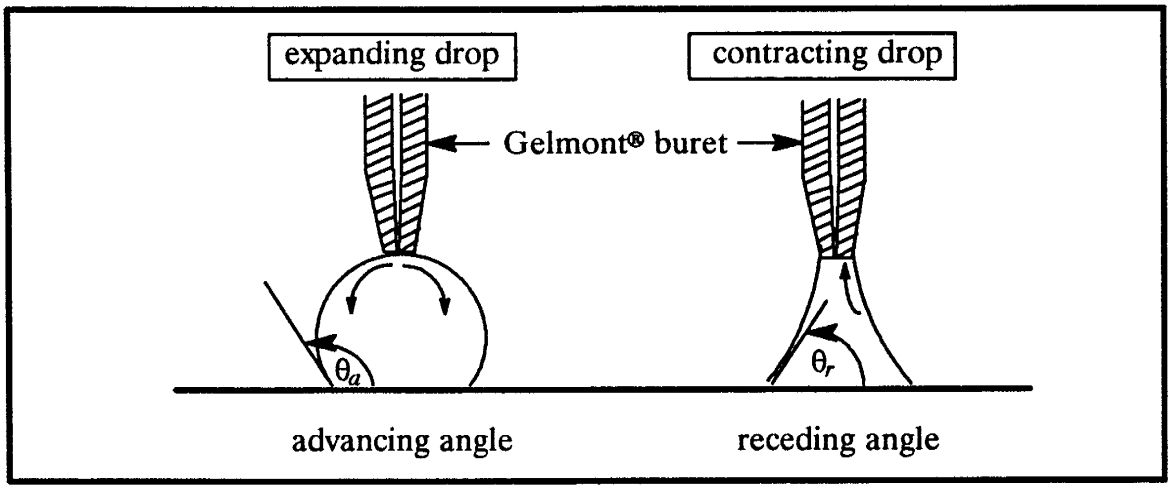

Figure 2.11 Measuring advancing and receding angles on a flat solid surface.

caused by the fact that the surface of the slide is never perfectly level. The averaged angle was taken as the advancing angle for that drop. Once again, the advancing angles were measured generally within 30 seconds of the drop contacting the slide.

To measure the receding angle, the drop was contracted by turning the dial on the buret to withdraw the liquid back up through the tip. As the drop contracted, the liquid/fluid interface receded on the solid surface. The angle of the interface when the interface receded was taken as the receding angle. Measurement on each side of the drop was taken and averaged to obtain the receding angle for that drop. In cases where the interface did not recede and the drop kept contracting until it pinned and snapped off at the buret tip, the minimum angle observed just prior to snap–off was taken as the receding angle (Figure 2.12). In two experiments (Exp.38 & 40A–see section 3), before the arrival of the goniometer, advancing and receding angles were measured from photo enlargements of the drops with a protractor.

Measurements from three to four drops were taken for each glass slide. Once again, the average angles are reported in section 3. Angles could be read off directly with the goniometer to an accuracy of about $\pm 1°$. The room temperature was recorded periodically and varied between 22.0°C and 25.0°C during the period of these experiments.

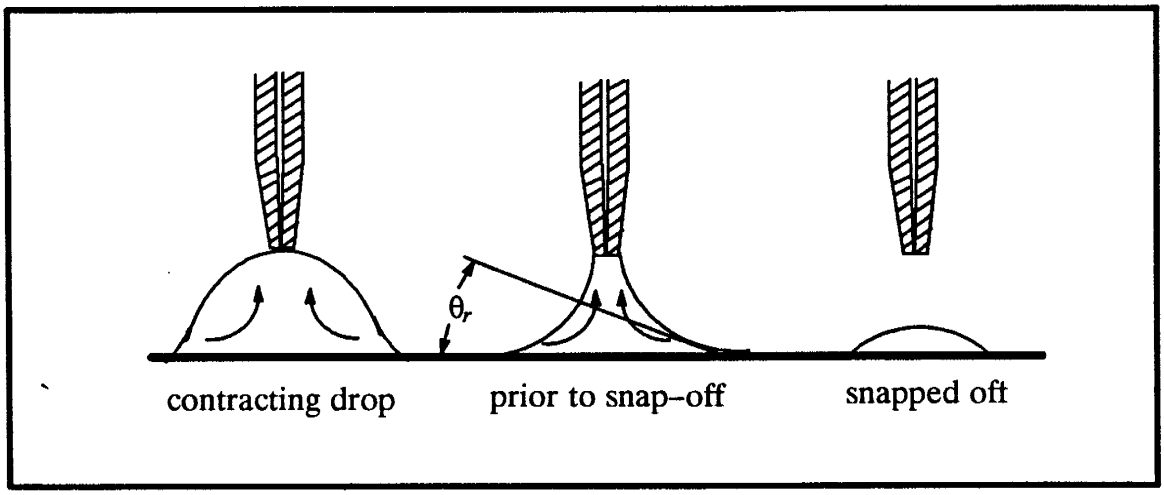

Figure 2.12. Receding contact angle just prior to snap–off.

2.7 Possible sources of error in contact angle measurements

Possible sources of error in contact angle measurements include:

- contamination and mishandling of the slides prior to measurement
- measurement error
- size and placement of the sessile drop
- non–equilibrium between the treated slide and immiscible fluids
- differences in contact angle measurements caused by variations in temperature.

Each of these possible sources of error are discussed briefly in the paragraphs below:

contamination and mishandling of the slides: if slides stored in organic liquid were not thoroughly rinsed, any residual organic liquid occurring as very thin, isolated coatings on the slides could affect (hinder or enhance) the spreading of sessile drops placed over the coating. The contact angle thus measured would not represent the true angle of the interface on the treated slide surface. Natural contaminants in the air and in water (for example, fatty acids, bacteria, organic and inorganic solutes, etc.) could also

adsorb onto the treated glass surface, and if not removed by thorough rinsing prior to measurement, affect the contact angle in a similar way.

Because the treated surface was softer than the untreated glass surface, it could be more easily scratched if mishandled. Scratches increase the heterogeneity and roughness of the surface which, in turn, affect the contact angle.

measurement errors: measuring the height and width of a static sessile drop from a grid reticle required interpolation which is limited by the precision of the reticle. However, based on the limits of interpolation of an average size sessile drop, the measurement error was estimated to be $< \pm 1\frac{1}{2}°$. Measurement error also depended on the contact angle. Error was probably greatest where the contact angle was close to 90°. When the angle of the interface was nearly perpendicular to the slide surface ($\theta = 90°$), it was harder to pick out the base of the drop accurately against the reflection of the drop on the slide.

In the dynamic sessile drop method, measuring the angle of the interface at the point where it contacted the slide was subjective. Depending on the shape of the drop, significant errors could result if the secant of the curved interface rather than the tangent at the slide surface was measured. As mentioned in section 2.6.3, the precision limit of the goniometer was $\pm 1°$.

Another possible source of measurement error was that the slide surface was never perfectly level. This resulted in a slightly greater contact angle on the downslope side and a slightly lesser angle on the upslope side. With dynamic sessile drops, any distortion of the contact angles caused by a slight dip in the platform was cancelled out when the contact angle on both sides were averaged. The line of view of the microscope was also never perpendicular to the drop. The angle thus measured would be an apparent angle instead of a true angle which could be another possible source of measurement error.

Size and placement of the sessile drop: influence of gravity increases as the size of the sessile drop increases. The effect of gravity could cause the drop shape to deviate from a sphere leading to contact angles calculated from equations 2.2 and 2.3 to be less than the true angle. Great care was taken during contact angle measurements to keep the static sessile drops within the volume limit specified by ASTM standards. However, in measuring water–Soltrol® contact angles, slightly larger drops were sometimes required for the water to displace the Soltrol®.

Also, in the method using static sessile drops (section 2.6.2), care was also be exercised to ensure that the drop be placed to ensure an advancing angle. Otherwise, the measured contact angle may be a few degrees lower than the true advancing angle. In the latter experiments, contact angles measured from the static sessile method were checked against the advancing angle from the dynamic sessile method.

Phase disequilibrium: theoretically, air–liquid contact angle measurements should be done in an atmosphere saturated with the vapor of the liquid being measured. For liquids of low vapor pressures such as water, this condition was not as important (Fox and Zisman, 1950). Similarly, when measuring water–Soltrol® contact angles, water and Soltrol® should be equilibrated. Although this was not done, the low solubility of one liquid in another makes any errors, introduced by omitting this step, likely negligible. Greater care was required to quickly measure contact angles of static sessile drops of volatile liquids such as 50:50 ethanol:water and 50:50 methanol:water mixtures because evaporation of these drops caused the interface to recede resulting in a lower angle. Significant evaporation would cause the measured angle to be less than the true advancing angle.

Effects of temperature variations: In general, as the temperature increases, the contact angle decreases. Variation in temperature could, in theory, affect contact angle measurements. According to Adamson (1982) however, the effect of temperature was not

usually very great, typically $-0.1°/K°$. Therefore, any deviation in contact angles due to ambient temperature variation would only be about $\pm 0.2°$.

2.8 Discussion of methods and procedures for contact angle measurements

The importance of drop placement can not be overemphasized. Theoretically, advancing angles measured from the static sessile drop method and the dynamic sessile drop method should be identical. However, procedures in the static sessile drop method could cause the interface to recede slightly when the lab stand was lowered to snap off the drop. The result could be a contact angle less than the true advancing angle. Our experience in developing contact angle measurement techniques showed that drop placement could be one of the most significant sources of error. Results in section 3 bear this out.

The other significant source of error was in measuring contact angles of dynamic sessile drops directly with the goniometer. The method is subjective especially where the interface near the slide surface was curved and in measuring receding angles when the interface at the slide surface remained immobile upon contraction of the drop. In the former case, there is a tendency to measure the secant of the curved interface rather than the tangent at the interface–slide contact. In the latter case, the receding angle was hard to define.

The concept of contact angles may not directly apply to all wettability conditions in porous media. Contact angles as applied here for flat, smooth, homogeneous surfaces are only a measure of the relationship of interfacial energies between the immiscible fluids and the surface energy of the solid surface (equation 1.2). In porous media, other factors such as porous media heterogeneity, pore network and geometry, uniformity of wetting, surface roughness, etc., in addition to the wetting characteristics of the solid surface, would affect the intrinsic contact angle. Contact angles on uniformly treated slides should be applied with caution to similarly treated porous media.

Despite these obvious limitations, contact angles still provided useful insight on the relative wettability and hysteretic behavior of different silane–treated surfaces. Contact angles measured from sessile drops are still the most universal, quantitative method used to characterize wetting on a solid surface and are commonly used to infer wettability in porous media. This was the method used, for example, by Demond (1988), Morrow (1970), Kennedy et al (1955), and Newcombe et al (1955) in 2–phase immiscible displacement studies and by Menawat et al (1984) in particle separation studies in chemical engineering.

2.9. Short column experimental methods

In the following subsections, short column procedures, apparatus, and experimental methods are described in detail. Results for the experiments are presented in section 4.

2.9.1 Description of the porous medium and immiscible liquids

Sodalime glass beads from Cataphote, Inc. were used to construct the porous medium. The bulk chemical composition of the beads is shown in Appendix A1. The beads had a particle diameter between 250 – 297 μm which is typical of a medium sand according to the MIT soils classification (Lambe, 1951). The Sevietta sand, which was the model sand used in other short column experiments at New Mexico Tech, also has a median diameter of about 300 μm. The glass beads, viewed under the microscope, are spherical to sub–spherical in shape. Particle density, measured with pycnometers (Lambe, 1951), was 2.471 ± 0.00 g/cm^3. The saturated hydraulic conductivity of the beads calculated using the Kozeny–Carman equation (Freeze and Cherry, 1979) was 4.7e–3 cm/s.

Hydrophobic beads were treated with GC18. Intermediate wettability was achieved by treating the beads with tBDM. Wettability for untreated, GC18–treated, and tDBM–treated beads was assumed to be uniform.

The aqueous liquid used in all experiments was deionized, de–aired water with 1000 mg/L NaN_3. Sodium azide was added to prevent bacterial growth in the column. The GC18– and tBDM–treated surfaces were not adversely affected by the NaN_3 (see section 3). Soltrol® 130, a C_8 to C_{13} isoparaffin, was used as the organic liquid. The interfacial tension between Soltrol® and water was 40.5 dynes/cm. The density and dynamic viscosity of Soltrol® 130 is 0.753 g/cm^3 and 1.5 cP respectively. Wilson et al (1990) found that, for water–wet Sevietta sand, there was very little difference in residual oil saturations (ROS) when Soltrol®, n–decane, p–xylene, and tetrachloroethylene

were used. The range of interfacial tensions between water and the organic liquids used in that study did not significantly affect the ROS. The negligible solubility and low toxicity of Soltrol®130 made it an ideal representative organic liquid.

2.9.2 Conventional short column apparatus

The conventional column apparatus was almost identical to that developed by Wilson et al (1990). The short column consisted of a glass chromatographic column with Teflon® endcaps from Ace Glass (Vineland, NJ). The dimensions of the glass columns were 5 cm inside diameter and 5cm to 6 cm effective internal length (Figure 2.13).

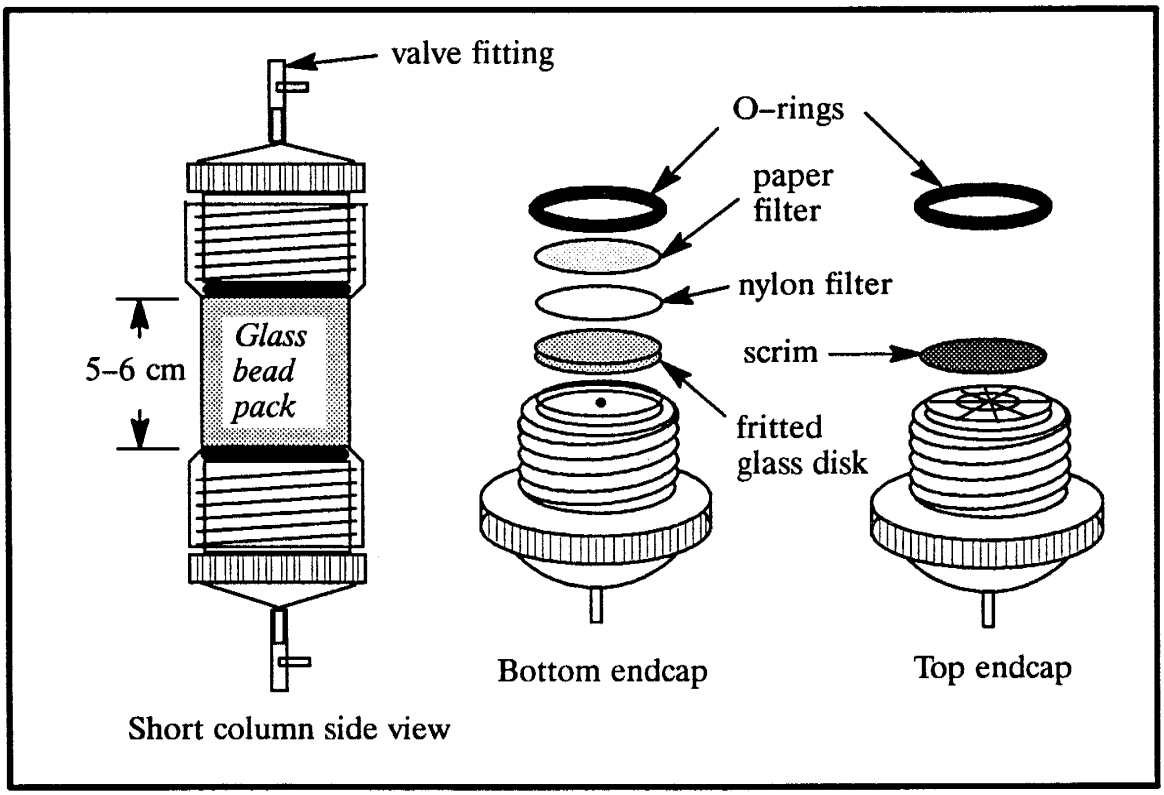

Figure 2.13. Short column apparatus for water–wet and intermediate–wet glass beads.

A glass column treated with GC18 was used when the column was packed with treated beads. The treated column minimized preferential flow of water along the wall of the column during water flood which would normally result in premature breakthrough

of water at the top of the column. The endcaps were screwed into the threaded ends on the glass column and sealed against the column with O-rings. A polypropylene valve fitted onto the nippled outlet on each endcap. The valves allowed liquids to be closed off to the column when the experiment was not running.

The bottom endcap contained a 5 mm thick fritted glass disk (Ace Glass) with a 20 μm average pore diameter. The disk fitted in the taper of the endcap. A water-wet Magna 66 nylon filter (MSI, Westboro, MA) with a 0.22 μm pore diameter was glued along the edges of the fritted glass disk. The nylon filter allowed water but not Soltrol® to leave the column. A paper filter was placed over the nylon filter to protect the nylon from abrasion by the glass beads. Devcon epoxy was used to glue all the filters onto the endcaps.

A network of small channels were machined into the flat face of the top endcap (Figure 2.13). The grooves allowed for a more uniform flow of liquids between the endcap and the bead pack. A polypropylene mesh or scrim from Spetra/Mesh® (Los Angeles, CA) was glued along the edges of the top endcap to prevent the beads from clogging up the small channels.

2.9.2.1 Saturating the bottom endcap and testing the nylon filter

Before assembling the column, the bottom endcap was saturated with water. The integrity of the nylon filter was tested by using an air-entry test (Figure 2.14). To saturate up the bottom endcap, the endcap was put into a beaker of de-aired water with 1000 mg/L NaN_3. The water was pulled through the filter and endcap under suction using a vacuum pump until the filters and fritted disk were saturated and all the air was removed from the tapered void space inside the endcap (Step 1 in Figure 2.14). The suction on the vacuum pump was set at 14 cm Hg, about four times greater than the water suction required to bring the glass bead pack to irreducible water saturation (IWS). After water had been run through the endcap for several minutes, the endcap

was removed from the beaker and held in the air with the vacuum suction continuing (Step 2 in Figure 2.14). No air bubbles in the tubing leading out of the endcap should appear if the filter and glued seal were functioning properly. If bubbles appeared, the filter and glued seal failed the air–entry test and the endcap was not used.

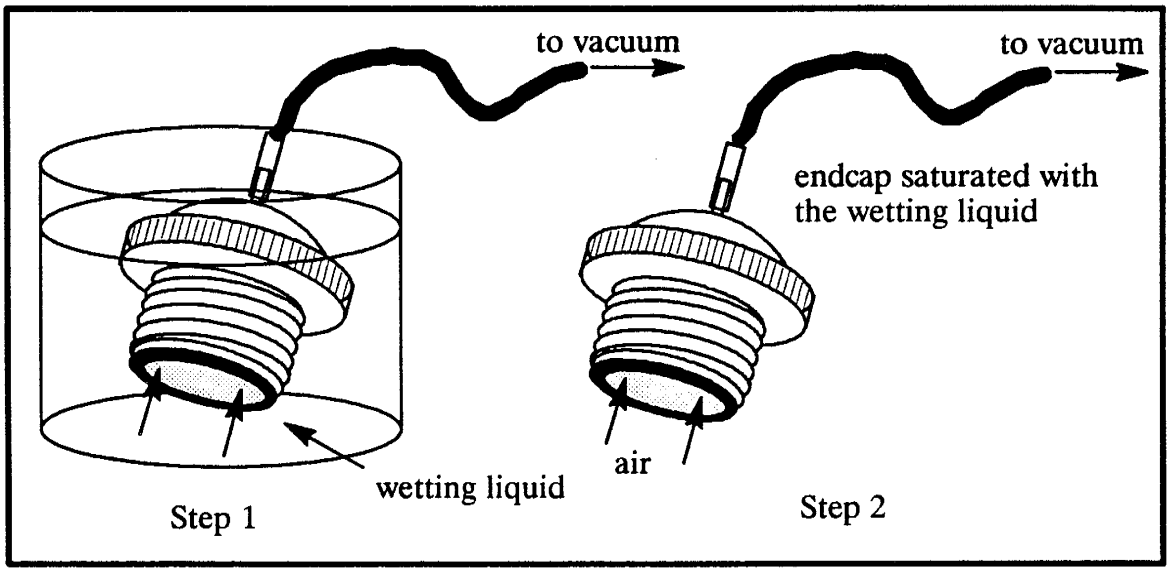

Figure 2.14. Saturating the bottom endcap and testing the filter and seal.

2.9.3 Measuring the volume of the column

The volume of the column was required to calculate the bulk density, porosity, and pore volume of the packed column. To measure the volume of the column, V_c, the column was assembled with the saturated bottom endcap, glass column, and top endcap (with the valve fittings and O–rings) and weighed to determine the dry mass of the column, M_{dry}. The top and bottom endcap were tightened into place. The column was then filled with de–aired, deionized water from a buret connected to the bottom endcap and weighed to determine the saturated mass, M_{sat}. The mass of the column was measured with a Mettler PE1600 balance to a precision of 0.01g.

The water–filled column was left overnight before weighing so that any trapped tiny air bubbles would dissolve away. The polypropylene scrim was not yet glued onto

the top endcap at this point because too much air would have been trapped between the scrim and the endcap face. The volume of the column was calculated by:

$$V_c = (M_{sat} - M_{dry}) / \rho_{water} \quad (2.4)$$

The point to where the top endcap was screwed into the column was marked by a reference mark (Figure 2.15).

The volume of the column calculated from equation 2.4 disregarded three things: 1) the volume of the scrim and glue was not accounted for, 2) the volume of the grooves in the top endcap was included in the volume measurement, and 3) the fact that the top endcap would not be screwed down to the same degree after the beads have been packed in the column. The average volume of the scrim, V_{scrim}, was estimated at 0.44 cm^3. The volume of the grooves, V_{gr}, in the top endcaps had been previously determined and are included in Appendixes C1–C4.

Once the mass of the saturated column had been recorded, the top endcap was unscrewed and left to dry. The dry top endcap and scrim was weighed and then re-weighed after the scrim was glued to the endcap. The difference in weight was the mass of the glue, M_{glue}. The glue mass divided by the density of the glue (1.10 g/cm^3 determined by Wilson et al, 1990) gave the volume of the glue.

Once the column was properly packed with glass beads, the top endcap, with the scrim, was re-screwed into the column. When the O-ring was sealed tightly against the column and the glass beads made good contact with the top endcap, the point to which the top endcap was re-screwed was marked (Figure 2.15). If the column had been over-packed, the endcap would not have screwed down to the original reference mark. If the column was under-packed, the endcap would have screwed down slightly further past the reference mark. The difference in length, L_c, between the final mark and the original mark, measured around the outside circumference of the column, was used to correct empirically for this change in volume.

The final effective volume, V_{ce}, of the column was calculated after the column was packed:

$$V_{ce} = V_c - V_{groove} - V_{scrim} - V_{glue} - C_t L_c \qquad (2.5)$$

where V_{ce}, V_c, V_{groove}, V_{scrim}, V_{glue}, and L_c have been explained above and C_t is the column tightening correction factor.

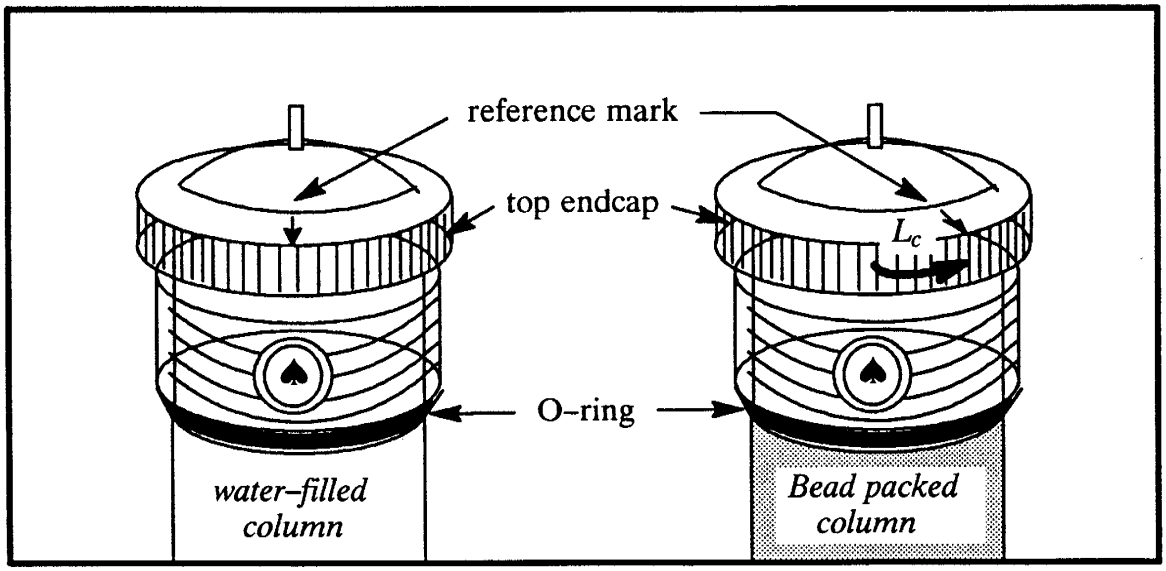

Figure 2.15. The change in volume of the column due to re-screwing in the top endcap after packing.

2.9.4 Packing conventional short columns with glass beads

Untreated glass beads were wet-packed into the columns by hand under 1 to 2 cm of water; treated beads were packed in ethanol. Ethanol has a much lower surface tension than water and wetted the treated beads much better. It was impossible to pack the treated beads in water because a great deal of air would be introduced into the packing and the beads had a tendency to float when they were poured on top of the water.

A previously determined mass of beads were either poured from its beaker into the column or scooped into the column with a small plastic spoon. The column was

gently vibrated with a hand–held vibrator to consolidate the packing after each centimeter depth of beads was added. The beads were packed up to the top end of the column, just to the base of the upper column threads, and then carefully levelled with the spoon before the top endcap was screwed on. After the top endcap was screwed into the column and the O–rings sealed tightly against the column, the difference between the original and final location of the reference mark, L_c, was measured (Figure 2.15).

If too many beads were packed into the column, the excess beads would be pushed up past the O–ring and into the column threads. This prevented the O–ring from sealing properly against the column and the top endcap would have to be unscrewed and the excess beads removed. If the column was under–packed, a cavity would have been evident between the face of the top endcap and the top level of the beads. If the beads did not have good contact with the endcap, by–passing of liquids could occur later on in the experiment. Several attempts were usually required to pack in the right amount of beads and to properly screw on the endcap. The packed column was re–connected to the water–filled buret through the bottom endcap to test the O–ring seal. The valve at the top endcap was closed off and the buret height was raised. If the O–ring did not seal properly against the column, water or ethanol would leak into the threads of the column above the O–ring.

Any beads which were removed were carefully returned to its original beaker with the unused beads. The beads were then dried in the oven overnight and re–weighed. The mass of beads in the column, M_s, was the original mass of beads less the mass of the leftover beads.

During screwing of the top endcap, excess water or ethanol would be displaced into the threads. After packing, the column was held and rotated to work as much of the trapped liquid out as possible. Silicone sealant (Dupont) was placed at the space be-

tween top of the column and the top endcap to prevent evaporation of the trapped liquid in the threads.

2.9.5 Calculating bulk density, pore volume, and porosity of the conventional packed column

The effective column volume, V_{ce}, mass of beads used, M_s, and particle density, ρ_s, were used to calculate the bulk density, ρ_b, pore volume, PV, and porosity, n, from the following equations:

$$\rho_b = M_s / V_{ce} \tag{2.6}$$

$$PV = V_{ce} - (M_s / \rho_s) \tag{2.7}$$

$$n = 1 - (M_s / (\rho_s V_{ce})) \tag{2.8}$$

2.9.6 Water saturating the conventional column

De-aired water with 1000mg/L NaN_3 was flushed through the conventional columns to completely saturate up the column with water. At least 20 pore volumes of water was intermittently flushed through each column over a period of two to three days. This ensured that any air originally trapped in the bead pack was removed or dissolved.

For treated beads packed in ethanol, thorough flushing was also required to completely displace the ethanol from the column. The effluent flushed out of the column was collected periodically, typically during each morning flushing, and the surface tension was measured with a Fisher 20 ring tensiometer to check for any presence of ethanol. Effluent containing negligible ethanol would have a surface tension of close to 72 dynes/cm.

2.10 Dual-filter short column apparatus

Preparation of dual-filter short columns were similar to that for conventional short columns. The main difference was that an oil-wet filter was required in the top endcap

to allow Soltrol® but not water to pass through during the water flood. The procedures in the following subsections were developed, with the available equipment in the laboratory, primarily for short columns packed with treated beads.

The short column apparatus for treated beads is shown in Figure 2.16. The bottom endcap was exactly the same as the one for the conventional column. The top endcap was what was another bottom endcap with a fritted glass disk as a filter support. However, a Teflon® filter with a 0.2 μm pore diameter (Gelman Sciences, Ann Arbor, MI) was used. The side of the Teflon® filter with the polypropylene backing was always placed facing up (into the column) to protect the Teflon® side from abrasion by the glass beads. Epoxy was used to glue the edge of the filter to the disk. The Teflon® filter was designed to allow Soltrol® but not water or air to pass through.

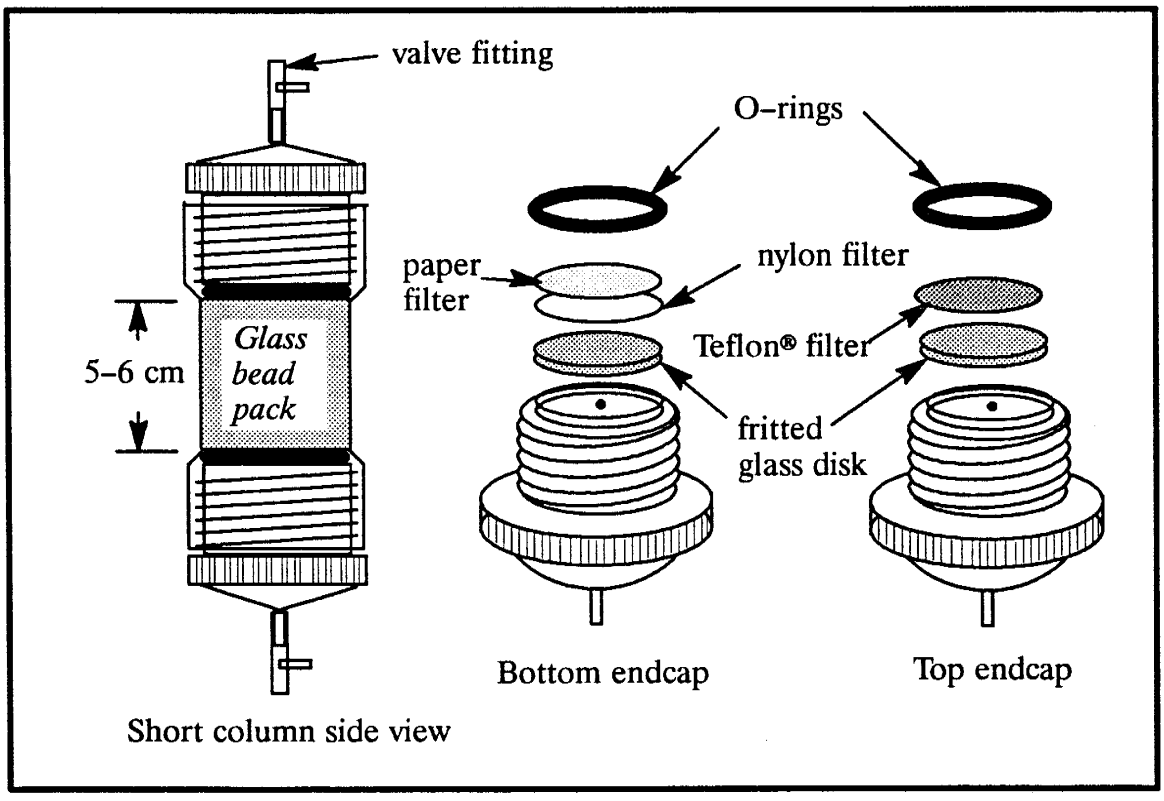

Figure 2.16. Short column apparatus for treated glass beads.

2.10.1 Calculating the volume of the column

The volume of the column was calculated by weighing a water-filled column as in section 2.9.3. However, the top endcap with the Teflon® filter could not be used because air or water could not pass through the filter. A dummy endcap was screwed into the top of the column instead (Figure 2.17). The dummy endcap was matched with the top Teflon® endcap so that both screwed to the same depth in the column. The bottom

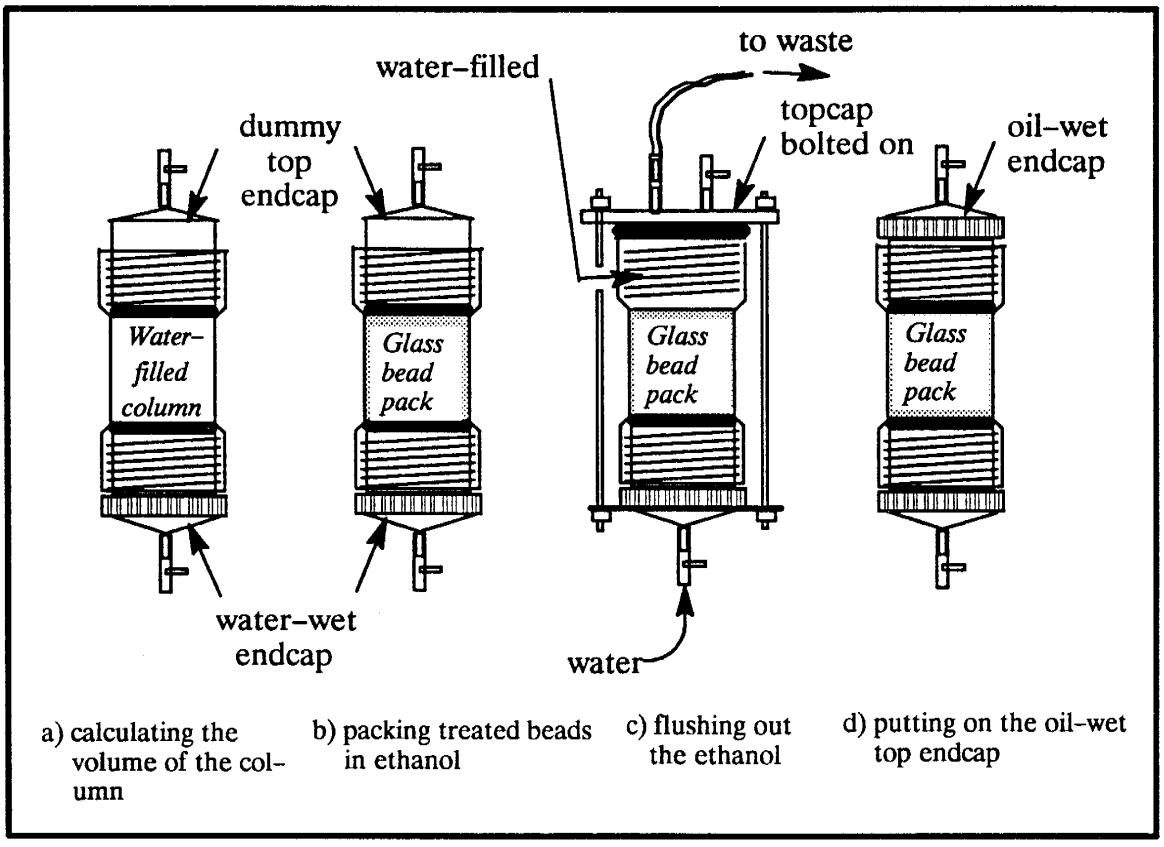

Figure 2.17. Short column preparation for dual filter columns.

endcap was saturated with water and the filter integrity was tested exactly the same as in section 2.9.2 (Figure 2.14). The bottom endcap and top dummy endcap were then screwed into the column and the column assembly was then weighed. The column was filled with water from a buret connected to the bottom endcap and left overnight to allow any trapped air in the column to dissolve. The water-filled column was re-

weighed and the volume was calculated using equation 2.4. The original point to where the dummy endcap was screwed into the column was also marked.

As before, the volume of the grooves in the dummy endcap, the polypropylene scrim, and glue had to be accounted for. The difference in volume from re–screwing the dummy endcap after the beads were packed also had to be accounted for. Equation 2.5 was used to calculate the effective volume of the column, V_{ce}.

2.10.2 Packing the short columns with treated glass beads

After the water–filled column was re–weighed, the dummy endcap was removed and dried overnight. A polypropylene scrim was glued onto the endcap. A previously determined mass of treated beads was then packed into the column in the same manner as in section 2.9.4. Untreated beads were packed in water and treated beads were packed in ethanol. Once the beads were packed to the top of the column, the dummy endcap, with scrim, was rescrewed into the column (Figure 2.17). Several trials were often required before the O–rings sealed tightly against the column and the beads had good contact with the face of the dummy endcap. The distance, L_c, from the original point of the reference mark was measured and the effective volume was calculated from equation 2.5.

The dummy endcap was then removed and the top endcap, without the Teflon® filter, was screwed into the column to check the fit. If the top endcap and dummy endcap were closely matched, the beads would also make good contact with the face of the top endcap and the O–ring would seal tightly against the column. The additional volume of the Teflon® filter and glue should not change the fit significantly. The top endcap was then removed and let dry overnight before the Teflon® filter was glued on. It was important to have the side of the filter with the polypropylene backing facing up. The backing acts as a filter support and protects the Teflon® from abrasion by the

glass beads. Two thin coatings of epoxy were applied to ensure that the filter was properly glued on without any leaks but the amount of epoxy used was minimized.

The unused beads were saved in the original beaker as before (section 2.9.4), dried overnight in the oven, and re-weighed. The mass of beads packed in the column was the difference between the initial mass and the mass of the leftover beads.

2.10.3 Flushing out the ethanol and saturating the short column with water

The ethanol had to be flushed out and the treated glass bead pack saturated with water before the top Teflon® endcap could be screwed on. The packed column was re-connected to the water-filled buret through the bottom endcap. The top of the column was left open or sealed with a Teflon® topcap (Figure 2.17). Water was introduced from the bottom endcap to displace the ethanol which eventually spilled out through the top open end or through the tubing connected to the topcap.

The column was initially flushed with 300 mL of water ($\sim$6 pore volumes) after the beads were properly packed. Thereafter, 100 mL of water ($\sim$2 pore volumes) was flushed each time, in the morning, afternoon, and evening, for three straight days. Columns that were left open during flushing were covered up afterwards with paraffin paper. The first 50 mL of effluent was collected during flushing each morning and the apparent surface tension of the effluent was measured with a Fisher 20 ring tensiometer. If the apparent surface tension was $>$ 72 dynes/cm, it was assumed that all the ethanol had been flushed out. Nearly all of the ethanol was flushed out during the first 100 mL ($\sim$2 pore volumes) of flushing. A total of about 700-1000 mL of water was flushed through each column ($\sim$20 - 35 pore volumes).

2.10.4 Saturating the top Teflon® endcap and testing the Teflon® filter

Before the top Teflon® endcap could be screwed into the column, it had to be saturated with Soltrol®. Procedures for saturating endcaps with Soltrol® were very similar to those for water in section 2.9.2. The top endcap was immersed in a beaker of Sol-

trol® (Figure 2.14). A vacuum pump was used to pull Soltrol® through the column. The vacuum was set at about 11 cm Hg. At higher suction, gas bubbles would come out of solution. After several minutes, the endcap was removed from the beaker and held in the air for a couple of minutes to check if air would breach the filter. If air bubbles could be seen in the tubing leading out of the column, the endcap was not used in the experiment. After the air–entry test, the valve at the top of the endcap was closed and the endcap was placed back into the beaker of Soltrol®. The endcap was left overnight to let any gas bubbles in the endcap to dissolve.

2.10.5 Screwing on the top Teflon® endcap

The top endcap, saturated with Soltrol®, was now ready to be screwed into the column. The column was filled to the brim with water, allowing the face of the endcap to directly contact the water so that no air was trapped. The endcap was then very carefully screwed into the column. The excess water flowed out between the threads. Once the endcap was tightened into the column, it could not be unscrewed without introducing air into the bead pack. The valve on the bottom endcap was left open during screwing to allow some water to drain to release pressure. Once the endcap had been properly screwed on, the O–ring seal was tested by raising the buret height. With the valve on the top endcap closed, any leaks around the O–ring was apparent from water leaking into the threads. If no leaks were detected, the column was left to stand, with the top valve closed, under the raised buret so that any tiny amounts of trapped air in the column could dissolve in the water. The column could not be de–aired by flushing as with the conventional column because of the top Teflon® endcap. Silicon sealant was placed in the space around the outside of the column and the top endcap to prevent further evaporation of the water trapped in the threads.

2.10.6 Calculating bulk density, pore volume, and porosity of the dual filter column

The bulk density, pore volume, and porosity were calculated from equations 2.6 to 2.8 assuming that the bead packing and porosity did not change when the dummy endcap was replaced by the actual top Teflon® endcap.

2.11 Experimental set–up for short column experiments

Once the short column had been properly prepared, Soltrol® was introduced into the column to displace the water until IWS was reached. Process was then reversed with water displacing Soltrol® until ROS was reached. This type of experiment simulated a NAPL contamination event in the saturated zone, beneath the water table. The experiments were all carried out in a constant temperature cabinet. Unfortunately, problems with the temperature regulating system existed. Consequently, the daily temperature in the cabinet commonly fluctuated several degrees Celcius.

2.11.1 Water displacement by Soltrol® (Soltrol® flood)

Before the start of the experiment, the water–saturated column was weighed to determine the initial mass of the column, M_i. The column was then brought to the constant temperature cabinet and hung on the cabinet wall with a 3–finger clamp. A bubble level was used to align the column vertically. The top endcap was connected to a buret filled with Soltrol®. The bottom endcap was connected to a buret filled with de–aired water. The opening at the top of the burets was covered with a rubber stopper and the stoppers were connected by tubing. The tubing arrangement closed the system and minimized evaporation of the liquids.

The experiment began by introducing Soltrol® into the column through the top by lowering the water–filled buret and raising the Soltrol®–filled buret (Figure 2.18). Displacement continued until the equilibrium capillary pressure was reached. The flow rate was controlled by the initial difference in levels of the burets. The greater the ini-

tial difference, the greater the initial flow rate. In experiments with untreated beads, 24 hours was the arbitrary time allowed for capillary pressure and liquid saturation to equilibrate. In experiments with treated beads however, the minimum equilibration time was 8 hours. This was done because if the column was left for an unnecessarily long time the wettability of treated beads could change.

When the capillary pressure equilibrated, the height of the liquid levels in the burets were measured to calculate the average capillary pressure in the column using the following equation:

$$\psi = \gamma_o(h_o - h_c) + (h_c - h_w) \tag{2.9}$$

where ψ is the tension head or capillary pressure head in cm of water, γ_o is the specific weight of Soltrol® (0.753), h_o is the height of the Soltrol® in the buret, h_c is the height of the centerline of the column, and h_w is the height of the water in the buret. The convention in soil physics is employed here; capillary pressure head in the water phase or water tension head is regarded as positive.

The column was also disconnected and weighed. The Soltrol® saturation and water saturation in the column at that capillary pressure was determined by the following:

$$S_o = (M_i - M_{i+1}) / (\Delta\rho \ PV) \tag{2.10}$$

$$S_w = 1 - S_o \tag{2.11}$$

where S_o is the Soltrol® saturation, S_w is the water saturation, $\Delta\rho$ is the density difference between Soltrol® and water (0.247 g/cm^3), M_i is the initial mass of the column, M_{i+1} is the mass of the column after equilibration, and PV is the pore volume. A small correction term was added to equation 2.10 for calculating Soltrol® saturations in the conventional short column:

$$S_o = (M_i - M_{i+1} + \Delta\rho \ V_{gr}) / (\Delta\rho \ PV) \tag{2.12}$$

The term, $\Delta\rho\, V_{gr}$, corrects for the change in density of the liquid in the valve fitting and grooves in the top endcap assuming they were now filled with Soltrol® instead of water.

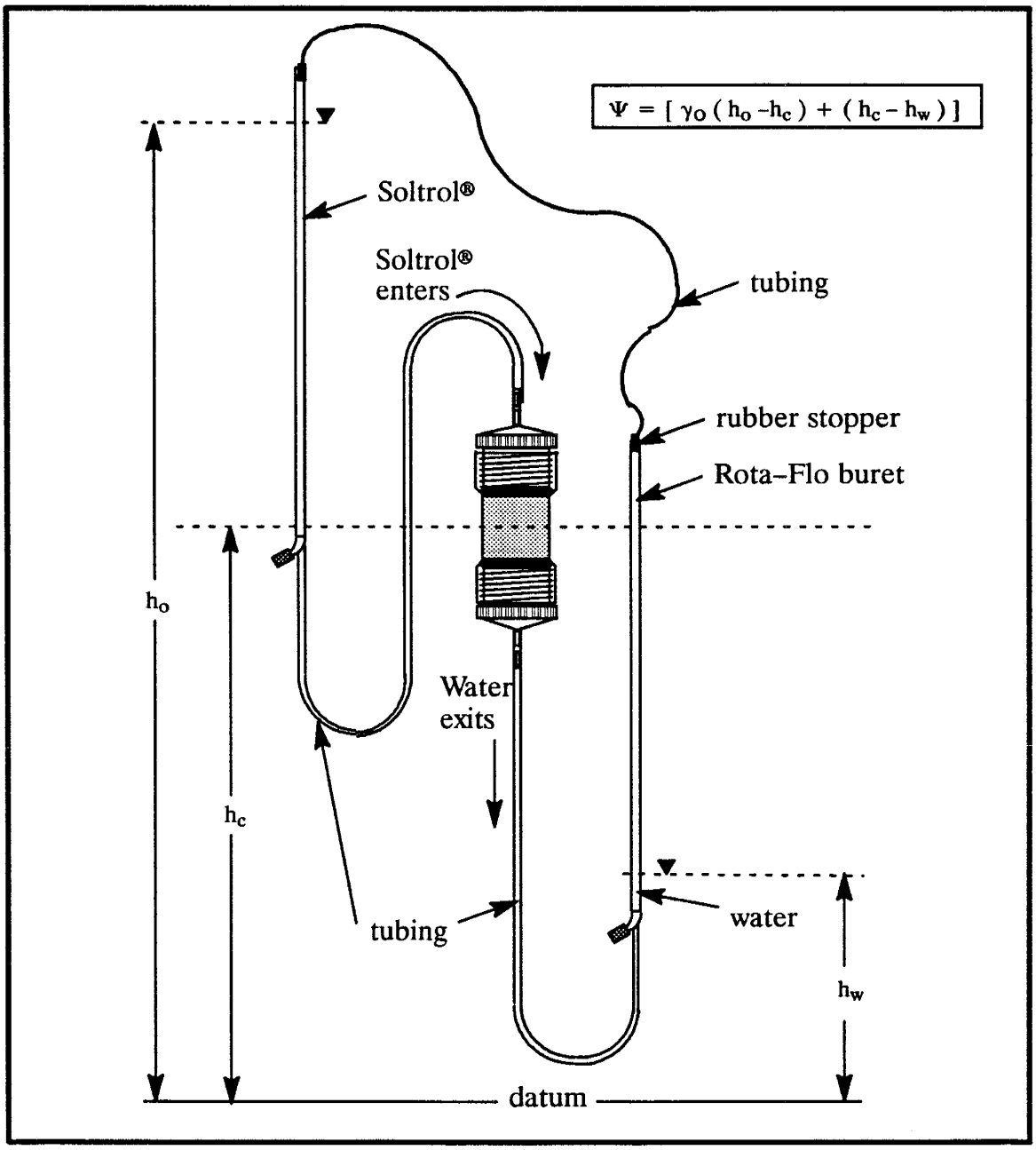

Figure 2.18. Water displacement by Soltrol using burets to measure S_w–ψ data.

The capillary pressure head was increased incrementally until IWS was reached. The capillary head was not increased beyond 50 to 55 cm of water above which Soltrol® could break through the bottom water-wet nylon filter. The S_w at the highest capillary pressure head (water tension head) was taken as the value for IWS although IWS was reached below that pressure head. IWS was reported in percent water saturation (S_w*100%).

If only the IWS was desired and the intermediate saturations and pressures were not required, time was only allowed for equilibration to occur at IWS. The buret levels were changed every few hours to continually extend the Soltrol® flood. The amount of water displaced from the column was monitored. When no more water came out from the column with increasing capillary pressure head, IWS was reached. The capillary pressure head was still increased to 50 to 55 cm of water and the column was allowed to equilibrate for 24 hours before weighing (for both treated and untreated beads).

During displacement, the tubing connected to the bottom endcap was always observed for Soltrol®. The presence of Soltrol® in the tubing signified that the nylon filter or epoxy glue did not maintain its integrity and Soltrol® broke through the bottom endcap.

2.11.2 Soltrol® displacement by water (Water flood)

At IWS, water entered from the bottom of the column to displace Soltrol®. The capillary pressure head was lowered by raising the height of the water-filled buret and lowering the height of the Soltrol®-filled buret (Figure 2.19). As in the Soltrol® flood, 24 hours was allowed for equilibration for untreated beads and a minimum of 8 hours for treated beads. After equilibration, the liquid levels of the burets were measured and the average capillary pressure head in the column was calculated from equation 2.9. The column was temporarily disconnected and weighed to determine liquid satu-

rations (equations 2.10 or 2.12 and 2.11). Equation 2.12 was used to calculate S_o in the conventional column until water broke through the top. At breakthrough, the space in the grooves and valve fitting was assumed to be filled with water and equation 2.10 was used. No correction was necessary for the columns with the top Teflon® end-cap because Soltrol® occupied the space in the valve fitting at all times.

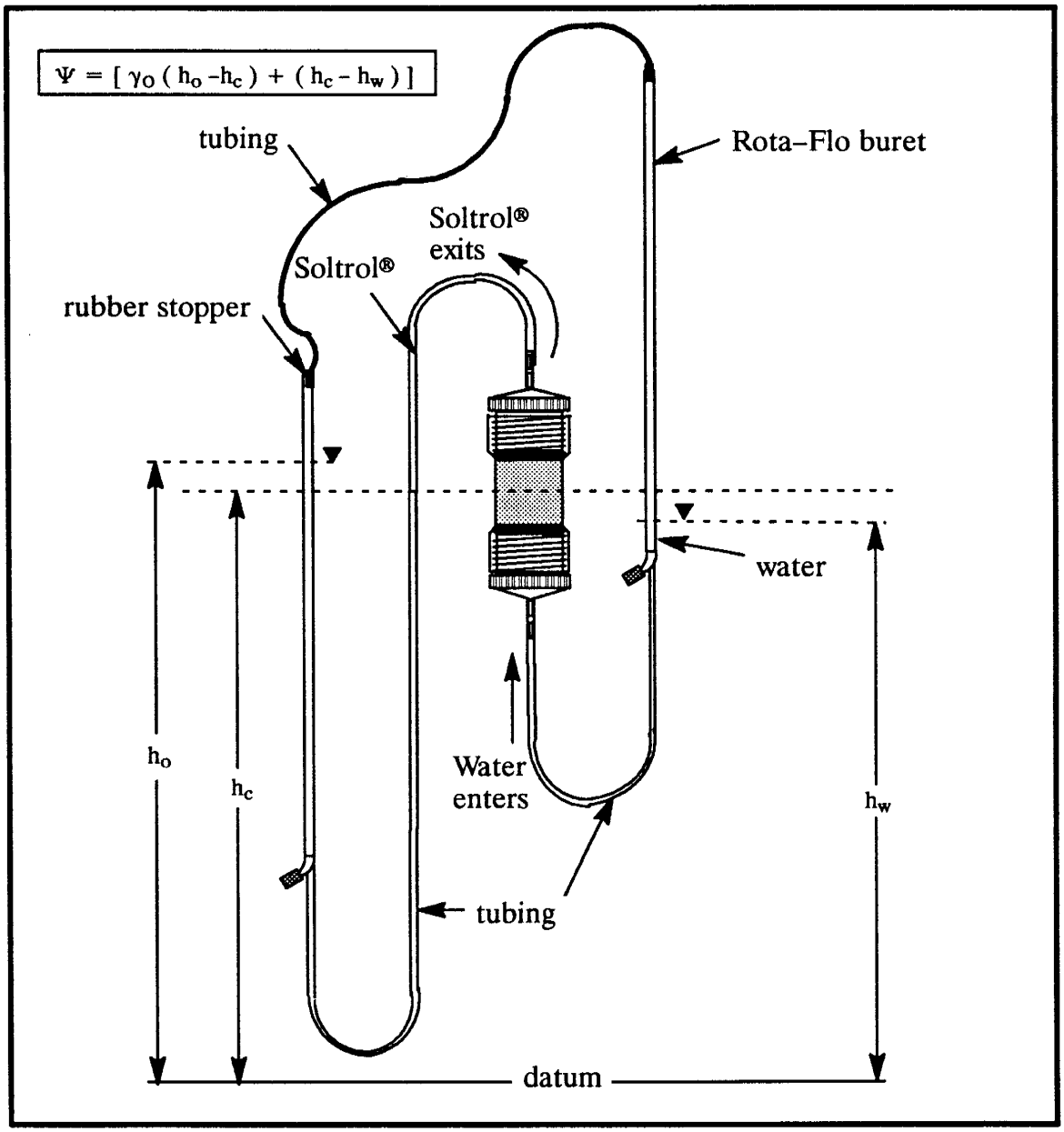

Figure 2.19. Soltrol displacement by water using burets to measure S_w–ψ data.

In experiments with treated bead packs, the capillary pressure was lowered to -50 to -55 cm head of water. ROS in treated bead packs was reached before this pressure head. This pressure head was usually not enough to cause water to breach the Teflon® filter in the top endcap. After the experiment, the column was disassembled and the treated beads were immersed in acetone and sonicated for roughly 20 minutes and dried overnight in the oven. A qualitative drop penetration test was done on the dry treated beads to check if hydrophobicity had decreased significantly as evidenced by infiltration of the water drop into the beads.

For the conventional column where ROS was measured but capillary pressure was not, the water flood was also carried out with a Sage model 351 syringe pump (Figure 2.20). The flow rate was normally set at an arbitrary rate of 0.3 mL/min. The syringe pump permitted a much more uniform and controlled flow rate through the column. The syringe pump could not be used for columns with the top Teflon® endcaps.

In experiments with untreated bead packs in the conventional column, once water broke through the top, the syringe pump was used to flood several more pore volumes of water through the column. The column was then disconnected and weighed to calculate ROS. The beads were stored away after each experiment.

2.12 Possible sources of error

Possible sources of error in short column experiments include:

- trapped gas in the short column
- changes in liquid densities due to temperature fluctuations in the cabinet
- mismatch between the dummy endcap and the top Teflon® endcap
- capillary end effects

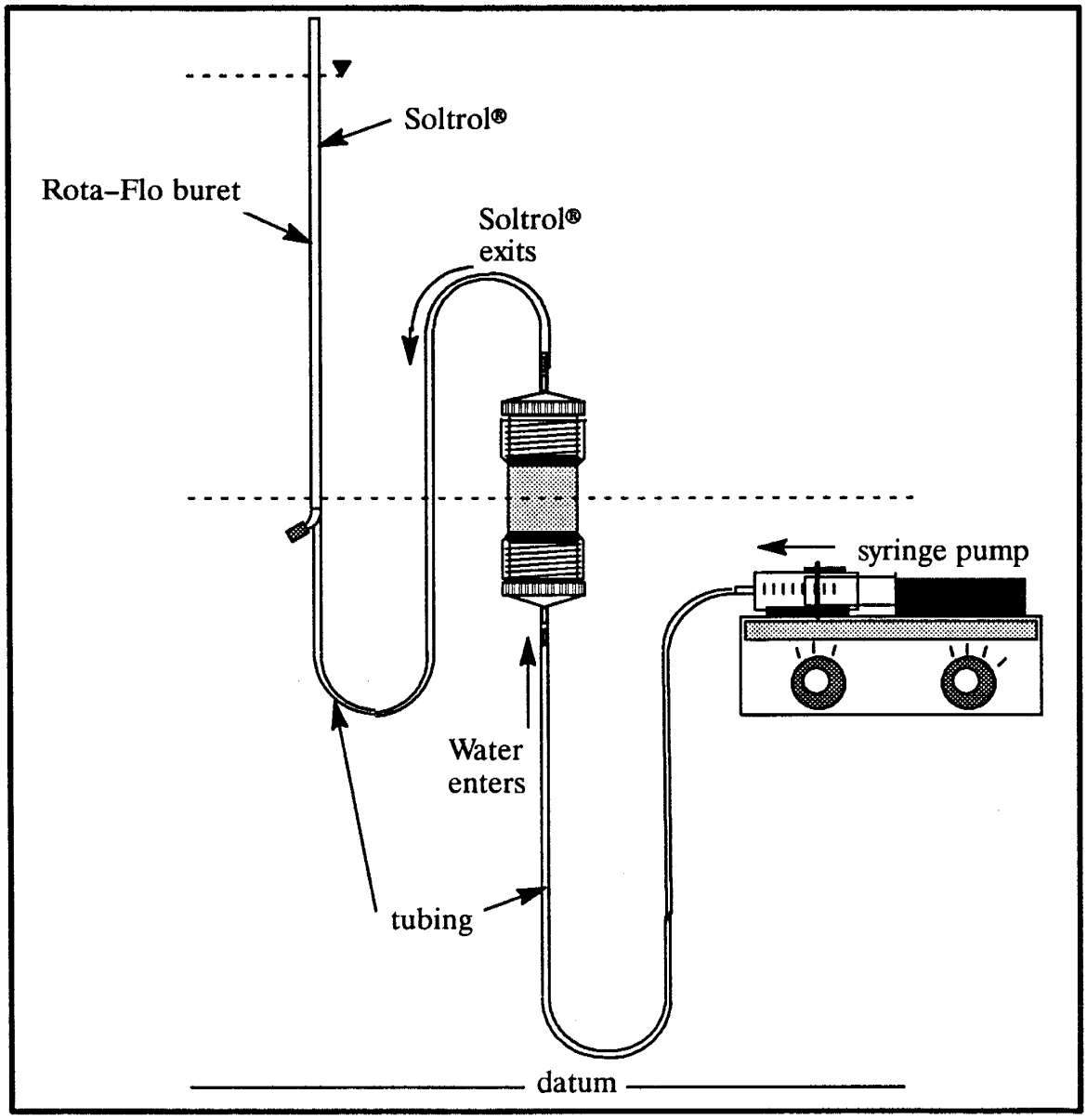

Figure 2.20. Water flood in a conventional short column using syringe pump to provide a constant flow rate.

- space between the polypropylene scrim and top endcap
- loss of filter integrity
- leaky seals in the column leading to leakage and evaporation
- buoyancy effects

- uncontrolled flow rate during flooding of the wetting liquid
- by–passing of the non–wetting phase due to the geometry of the short column
- length of the column
- variability in the glass beads and in packing
- measurement error

Each of these possible sources of error are discussed briefly in the paragraphs below:

trapped gas: Gas was trapped in the pore spaces when the beads were packed into the column and also when the top Teflon® endcap was screwed into the column. Gas bubbles could be present in the endcaps if the endcaps were not totally saturated. Gas bubbles could also appear out of solution in the column if the temperature increased enough and the water was not thoroughly de–aired. The gas saturation in each case would not remain constant throughout the course of the experiment because some gas bubbles could dissolve into solution.

Gases that were trapped during packing were flushed out with de–aired water. The presence of trapped gas inside the endcaps was impossible to check. Soltrol®–saturated endcaps were always left to soak overnight in the beaker so that any trapped gas may have time to dissolve into solution. Any gas trapped inside the endcap which gradually dissolved into solution while the experiment was on–going would increase the calculated value of IWS and decrease the value of ROS. Gas appearing from solution was minimized by using de–aired water and running the experiments in a constant temperature cabinet.

Unfortunately, some gas was always trapped near the top of the treated bead pack when the top Teflon® endcap was screwed into the column. This trapped gas did not readily dissolve into the water and could not be flushed out of the column. In most cases, the volume of trapped gas was equivalent to a few tenths of mL. Nothing could

be done about the trapped gas in this case once the top Teflon® endcap was screwed into the column. The trapped gas effectively reduced the pore volume of the column and caused the water saturation at IWS to be overestimated and the Soltrol® saturation at ROS to be underestimated.

temperature fluctuation during the experiment: temperature variations in the cabinet where the short column was run were at times significant. The temperature typically varied between 23°C to 27°C over the course of a day. Fluctuations in temperature inevitably caused the density of the liquids to change which introduce errors in the gravimetric determinations of the liquid saturations in the column.

The magnitude of error caused by temperature changes was estimated from the following calculation. For a fully water–saturated column, an increase in temperature from 22°C to 27°C would cause a decrease in a typical short column of 0.04g. This, in turn, decreased the calculated water saturation by 0.5%. Errors in liquid saturations at IWS and ROS, caused by temperature fluctuations, could be minimized by scheduling the measurement of IWS and ROS of the experiments at around the same time of day.

mis–match of dummy endcaps and top Teflon® endcaps: the dummy endcap and top Teflon® endcap were matched for each experiment using treated beads. The dummy endcap and top endcap matched if they screwed down to the same depth into the column. This method of matching endcaps was not exact. If the endcaps were mis–matched, errors in the porosity, pore volume, and bulk density of the bead pack could result. Worse, the beads might not have made good contact with the top Teflon® endcap and affect liquid displacement in the experiment.

capillary end effects: Capillary end effects was minimized by using filters which are semi–permeable. End effects during water displacement by Soltrol® were minimized by using a nylon filter on the bottom endcap which let the water but not Soltrol® to leave

the column. End effects at the top of the column during the subsequent water flood were negligible for untreated glass beads. However, end effects persisted for treated beads. This was the sole motivation for using a Teflon® filter at the top endcap. The Teflon® filter allowed Soltrol® but not water to pass through thereby minimizing end effects. A longer column would have also minimized end effects but this advantage was offset by problems with non-uniform pressures and saturations along the column and a larger volume of beads to treat and pack. Capillary end effects could also be minimized by increasing the flow velocity during displacement. This was not feasible for two reasons: 1) S_w–ψ data could not be measured during displacement and 2) the flow velocity would be unrealistic for actual aquifer conditions.

space between the polypropylene scrim and top endcap: although the volume of the epoxy was considered in calculating the effective volume of the conventional column, any space between the polypropylene scrim and the top endcap created by the thickness of the epoxy was not. Any space between the scrim and the endcap would most likely be filled with Soltrol® at IWS. This leads to an underestimate of the IWS (in percent water). This space, caused by the thickness of the epoxy, can not be calculated but should be very minor. The thickness of the epoxy should not affect calculation of IWS in the dual filter column with the Teflon® filter because the filter is permeable only to Soltrol®.

loss of filter integrity: if filter integrity was breached, end effects were not eliminated and the non-wetting liquid could flow into the endcap and out the column. This breakthrough could be seen if the non-wetting liquid leaked out of the endcap into the tubing. Otherwise, breakthrough was very difficult to detect if the non-wetting liquid was only trapped in the endcap. Breakthrough of Soltrol® into the bottom endcap causes IWS to be over estimated. Breakthrough of water in the top Teflon® endcap causes ROS to be under estimated. To minimize breakthrough, the filters were tested before the column was assembled and the capillary pressure was kept well below the entry

pressure of the filters. A paper filter was also used to cover the nylon filter to protect it from abrasion during column packing.

leaky seals in the column leading to leakage and evaporation: the endcaps were sealed against the column with O-rings. The seals were pressure tested before each experiment. The opening between the top endcap and the column was always sealed with silicon gel to prevent the water trapped in the grooves from evaporating during the experiment. Evaporation resulted in higher estimated values of Soltrol® saturations.

buoyancy effects of the immiscible liquids: because the column experiments were run in a vertical position, buoyancy effects on displacement of the non-wetting liquid need to be considered. Buoyancy forces result from the difference in density of the immiscible liquids. Yet it is precisely this density difference which allowed us to measure gravimetric changes in liquid saturations in the columns. For a 2-phase system, the effect of buoyancy forces on the displacement of non-wetting phase liquid can be estimated from the *Bond number,* N_B. The Bond number is a dimensionless ratio of the gravity forces to the capillary forces:

$$N_B = \Delta\rho\, g\, R^2 / \sigma \tag{2.13}$$

where $\Delta\rho$ is the density difference between the two immiscible liquids (g/cm^3), g is the acceleration of gravity (9.81 m/s^2), R^2 is the representative grain radius (mm^2), and σ is the interfacial tension between the liquids (dynes/cm). If the difference in density between the liquids or the bead radius is large or if the interfacial tension is small, this promotes mobilization. Significant buoyant forces in a water-wet bead pack would result in lower values of ROS. For oil-wet bead packs, buoyancy effects are not as important because the wetting liquid, Soltrol®, is advancing downward against the force of gravity.

The size of the glass beads were chosen small enough so that buoyant forces due to liquid density difference would be minimized. For 0.3 mm diameter glass beads in

a water and Soltrol® system where $\Delta\rho$ is 0.247 g/cm, R is 0.14 mm, and σ is 40.5 dynes/cm, the Bond number is 0.0011. Morrow and Songkran (1981) found experimentally that for randomly packed uniform spheres, significant buoyant forces were avoided for Bond numbers of less than 0.005.

uncontrolled flow rate during flooding of the wetting liquid: trapped non-wetting liquid could also be mobilized if the flow rate became so large that the viscous forces were large enough to overcome the capillary forces. The effect of viscous forces and flow rates on mobilization can be estimated from the *Capillary number*, N_C, a dimensionless ratio of viscous to capillary forces:

$$N_C = q_{wetting}\ \mu_{wetting} / \sigma \qquad (2.14)$$

where $q_{wetting}$ is the specific discharge of the wetting liquid (m/s) and $\mu_{wetting}$ (cp) is the viscosity of the wetting liquid. For a given pair of liquids, the greater the flow rate, the greater the Capillary number. For water-wet beads, the Soltrol® displacement by water was more critical (lower ROS) and for oil-wet beads, the initial water displacement by Soltrol® was more critical (lower IWS). With a flow rate of 0.3 mL/min (2.55e-6 m/s), a σ of 40.5 dynes/cm, and a viscosity of 1 or 1.5 cp (water or Soltrol®), the Capillary number was 6.3e-8 or 9.4e-8. These values were 4 orders of magnitude smaller than those required to begin mobilization (Morrow and Songkran, 1981). In each incremental displacement, the initial flow rate in the burets could not be measured. However, the flow rates during the later stages of displacement was less than the critical flow rate required for mobilization.

Both buoyancy and viscous effects could act in combination to mobilize the trapped non-wetting liquid. The effects could be combined in water-wet beads during Soltrol® displacement by water. ROS in water-wet beads would then be most affected by significant viscous and buoyancy effects.

by–passing due to the geometry of the short column: short column experiments of water–wet bead packs run with dyed Soltrol® showed that Soltrol® could be by–passed along the top and bottom rim of the column where there is a flare. Theoretical calculations based on a typical porosity, pore volume, and shape of the flare suggest that the by–passing could increase ROS by 2% (see Appendix E1). By–passing caused by the flare resulted in a zone of negligible flow along the rim. This error could not be remedied with the existing apparatus.

length of the column: the length of the column should affect the pressure–saturation data to some degree. The center of the column was arbitrarily fixed as the datum. However, the average location of the displacement front varied with displacement. This slight difference between the actual average location of the displacement front and the fixed assumed location at the center of the column led to slight misestimates of the capillary pressure. This error could never, in practice, be completely eliminated. However, one motivation for keeping the length of the column short was to minimize this error.

variability in the glass beads and in packing: the variability in the glass bead size and particle density should be minor. Variability in packing may have caused variability in the results but this was unlikely. The consistency of the bulk density and porosity of the bead pack between experiments (section 4) reflected the consistency of packing.

measurement error: random errors due to the precision limit of the apparatus undoubtedly exist. The liquid level in the burets could be read to ± 0.05cm accuracy. The Mettler balance recorded mass to ± 0.01g.

2.13 Discussion of the short column procedures

It was necessary to develop a short column procedure to include a Teflon® filter in the top endcap. It was impossible to measure the S_w–ψ data when water was displacing Soltrol® and the true ROS in oil–wet beads with the conventional column. Prelimi-

nary experiments with oil–wet GC18–treated beads showed that, during the water flood, water preferentially flowed along the column wall and prematurely broke through the top endcap (section 4). Premature breakthrough occurred even when a silylated column was used. The Teflon® filter in the top endcap was designed to prevent water, upon reaching the top endcap, to breakthrough thereby causing a pressure difference along the bead pack, and allowing the Soltrol® to displace water in the glass beads.

The change in volume of water in the buret during incremental displacement could also be used to calculate the water saturation in the column. The obvious advantage is that the column need not be disconnected and weighed after each displacement step. Saturation calculated from water volume measurements were not done however because the volume could only be read to an accuracy of ± 0.05 mL. This was inferior to gravimetric measurements which was accurate to ± 0.01g. Evaporation of water in the buret could also cause volumes to be underestimated.

The existing short column was also only designed for testing unconsolidated repacked and not in–situ samples. The existing filters restrict the capillary pressures to about 100 cm head of water. If the pressure was raised to much greater than this, the filters would likely be breached.

2.14. Micromodel experimental methods

Micromodel experiments were analogous to short column experiments. The model was oriented vertically and initially saturated with water. Soltrol® was introduced into the model from the upper reservoir at a controlled rate. Soltrol® displaced the water in the pore network. Water exited out the bottom end reservoir. Once Soltrol® reached the bottom of the model, water was injected through from the bottom to displace the Soltrol®. This sequence of oil flood followed by water flood simulated NAPL contaminants percolating into the saturated zone and then being partially removed by ambient groundwater flow.

Experiments with the untreated model simulated the water–wet case while experiments after GC18– and tBDM–treatments simulated the oil–wet and neutral–wet cases respectively. The same model was used for all three cases so that differences in pore structure were eliminated. The treated surface was completely destroyed before another treatment with a different silane was employed.

2.14.1 Micromodel construction

Methods for micromodel construction have been presented in detail by Wilson et al (1990) and Mason (1989) and will only be summarized here. Willard mirrors (12.5 cm wide by 20 cm long by 0.3 cm thick) were used for the micromodels. The mirror glass was sodalime glass, the same composition as the glass beads in the short column experiments (Appendix A1). The mirrors were factory coated with silver and copper. The silver and copper backing was protected with an enamel backing.

The enamel backing was stripped off the mirror in a hot NaOH bath to expose the copper backing. The copper surface was then completely coated with a mixture of Kodak Thin Film Resist, an ultraviolet–sensitive resin, and xylene. Once the coating had solidified, the micromodel pattern transparency (see section 2.14.2) was placed on the coated surface. The mirror and transparency was then set under an ultraviolet light

source for exposure. Ultraviolet rays penetrated through the transparency and hardened the resist coating. However, ultraviolet rays could not penetrate through the black micromodel pattern on the transparency to harden the resist underneath. After exposure, the transparency was removed and the coating was rinsed with xylene to wash away the unhardened resist covered by the pattern. The xylene rinse exposed the copper surface underneath.

The mirror was then immersed in HNO_3 for a few seconds to completely remove the exposed copper thereby revealing the glass surface underneath. The edge and the other side of the mirror was then coated with the remaining resist–xylene mixture to protect those areas of the model from being etched in the next step. After drying, the mirror was immersed in HF and the pore network was etched for 17 minutes. After etching, the resist coating was scrubbed off and the residual copper and silver coating was removed by immersing the glass in HNO_3. The result was a piece of clear glass with one half of the pore network pattern and end reservoirs etched on it.

The procedure was repeated for the other side of the micromodel with another mirror, using a mirror–image transparency of the pore network pattern. Holes were then drilled into the reservoirs in one of the two etched glass plates. The two plates were then aligned under the microscope and fused in the furnace at 710° C for 15 minutes. The model was left to cool down in the furnace overnight.

2.14.2 Micromodel pattern design and preparation

The basic network for the model was taken from a Chartpak Matte Acetate 'patio stone' pattern (# PT045). The line patterns represented the network of pore throats. The pore nodes were drawn in manually (Figure 2.21). The model was 9.5 cm wide by 13.0 cm long. A series of thin pore throats were drawn at one end of the pore pattern. These small throats acted as a capillary barrier to the non–wetting liquid to discourage breakthrough of the non–wetting liquid into the end reservoir during the ex-

periments. The capillary barrier innovation was developed by Wilson et al (1990). To decrease the effective size of the thin throats and increase the effectiveness of the capillary barrier, the barrier was cut out of the mirror–image transparency. Thus the barrier was only etched on one mirror and was half as deep as the pore network.

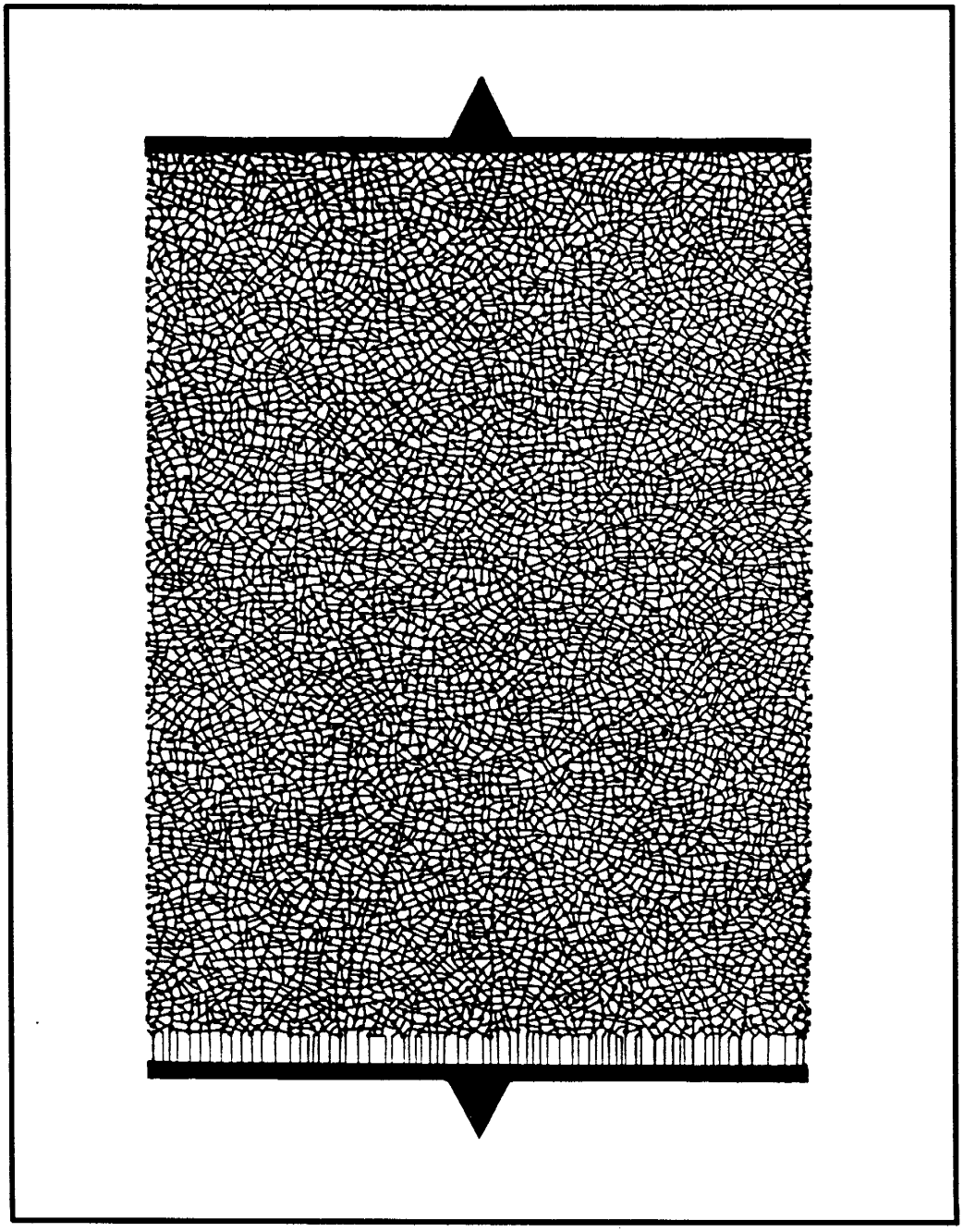

Figure 2.21. Homogeneous micromodel pattern, No. H6C.

Unlike the micromodel designs of Wilson et al (1990) and Mason (1989), lines marking the side boundaries of the model were not drawn in. The sidelines provided a preferred channel for the non-wetting liquid and frequently resulted in premature breakthrough of the non-wetting liquid during experiments. End reservoirs were also drawn at both ends of the model.The model represented a homogeneous porous medium. The height of capillary rise in the model was very similar to that of a medium sand (Bear, 1972).

2.15 Procedures for running micromodel experiments

2.15.1 Liquid preparation

The liquids used in the experiments were water and Soltrol®130. Water was dyed blue by mixing 1 L of de-aired, deionized water with 10 mL of food coloring (Schilling, Baltimore, MD). Sodium azide was not used because experiments were not run long enough to be affected by bacteria growth. The Soltrol® was dyed red with Oil Red O (Polysciences, Inc., Warrington, PA) in proportions of 0.9 g dye to 1 L Soltrol®.

2.15.2 Experimental procedures

Micromodel experiments were designed to simulate the short column experiments. The pattern described in section 2.14.2 represented a homogeneous porous medium. The model was positioned vertically and liquid displacement involved only water and Soltrol®.

The set-up for all the experiments is shown in Figure 2.22. The model was connected to three sets of tubing so that the model could remain connected between the de-airing process and the experiment. An aluminum fitting was mounted over the hole at each reservoir. The fittings were connected to polypropylene tubing which brought the liquids into the model. For the untreated case and tBDM-treated case, the end with the capillary barrier was located at the bottom. For GC18-treated case, the capillary barrier was on top.

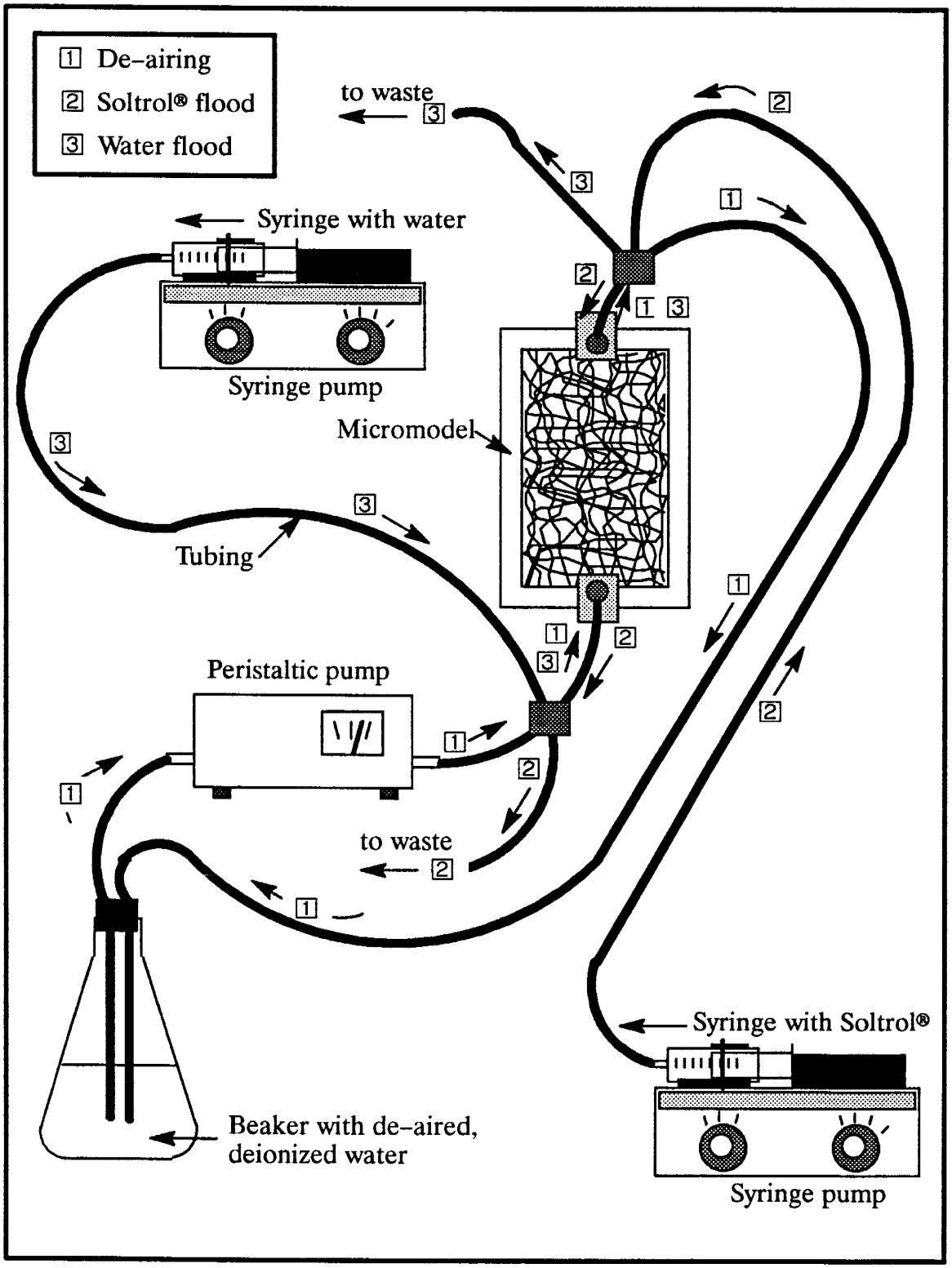

Figure 2.22. Micromodel experimental set-up.

In all cases, the model was initially saturated with water by recirculating de-aired water through the model with a Manostat peristaltic pump (step 1 in Figure 2.23). The de-airing process usually required about one day. Soltrol® was then injected into the model from the top with at a specified rate of 0.1 mL/min with a Sage model 352 syringe pump (step 2). This displacement mimicked the Soltrol® flood in the short column experiments. The Soltrol® flood ended when breakthrough just occurred into the bottom reservoir. Next, water was injected into the model from the bottom to displace the Soltrol® (step 3). The water flood rate was also at 0.1 mL/min. The water flood was analogous to the one in the short columns. Water flood was completed when breakthrough occurred at the top of the model.

Photographs of the model were taken with a macro lens to show the displacement front during the Soltrol® flood and water flood. At the end of each flood, a microscope and camera was brought in to take photographs at the pore scale level. No video recordings of the experiments were made. After every experiment, the model was thoroughly rinsed with acetone and dried for half an hour in the oven at $110° \pm 5°C$.

2.16 Discussion of micromodel experimental procedures

Although the capillary barrier prevented, to some extent, breakthrough of the non-wetting liquid into the end reservoir, it could not be made finer to more closely model the fine filters in the short columns. The other limitation that kept the micromodel from becoming a useful quantitative technique was the inability to measure pressures of the liquids in the model.

The reproducibility of the bulk liquid saturations from one experiment to the next depended a great deal on the ability to control flow rates during liquid displacements. The capillary barrier in the micromodel greatly increased the back pressure against which the syringe pump had to work against. Consequently, the actual flow rate may

have varied from the specified rate. Variability in flow rates could cause the amount of trapping to vary from experiment to experiment.

In observing trapping of the non–wetting liquid in the micromodel, the aspect ratio must be considered. The aspect ratio of the pore body to pore throat, in the plane of the model, appeared larger than 1.5, the value above which snap–off could occur. Snap–off was believed to be a dominant trapping mechanism in glass beads. However, the aspect ratio of the roof–to–floor dimension of the pore body to pore throat must also be considered. Because the pore bodies and pore throats were etched in HF for the same amount of time, the aspect ratio perpendicular to the plane of the model should be close to unity. The effective aspect ratio would then be less than the ratio in the plane of the model. Whether the effective aspect ratio was still large enough for snap–off to occur could only be inferred from the results of the micromodel experiments. The low aspect ratio of the roof–to–floor dimension of the pore body to pore throat could cause trapping in the micromodel and in the glass beads to differ slightly. Because of these limitations, micromodels were used only as a qualitative technique to observe displacement phenomena and help understand the displacement processes which were operative in the short column experiments.

3. Results of silylation of glass slides

It was necessary to silylate glass slides to define how uniform treatment affects the contact angle, independent of surface roughness, pore scale heterogeneity, etc. inherent in porous media. Silylation procedures were presented in detail in section 2. Our work focused especially on the magnitude of the water–air contact angle. Water–air contact angles were used to check the uniformity of the treated surface including contact angle hysteresis, and how the contact angle and hysteresis changed with time for slides stored in different aqueous and organic liquids. Water–Soltrol® contact angles, which were more representative of the liquid/liquid system used in short column and micromodel experiments, were only measured periodically because the treated slides required much more preparation and cleaning prior to measurement.

Summary of the silylation experiments is shown in Tables 3.1 and 3.2. The excess amount of organochlorosilane was estimated by comparing the amount of silane theoretically required to the amount of silane added. The amount required was calculated using equation 2.1 in section 2.5 and knowing the specific surface of the slides (~9e–4 m^2/g), the amount of slides used in each experiment (~55.8g), and estimating the wetting surface of the silane from Figure 2.8. The amount and the amount excess for GC18 could not be calculated because the molecular weight of GC18 was unavailable. Experiments in which the period of observation was limited to only 48 hours or less were not included. Experiments were often repeated to check the reproducibility of the contact angle and stability (Table 3.2).

In general, the batch of slides in each experiment was divided up and stored in different containers filled with air, water, or various organic liquids immediately after treatment. Initial contact angle measurements for each representative slide in the containers were measured prior to storage. The storage and handling of the treated slides were described in section 2.6.1. Periodically, the slides were removed from their con–

Table 3.1 Summary of silylation experiments of glass slides.

Exp. no.	*Silane*	*Amt. (moles)*	*Amt. excess ($x10^{-3}$)*	*Date (mo./yr.)*	*Period of observation (hrs)*	*Comments*
8	tBDM	5.81e–2	96	5/89	530	1
11	TMS	2.44e–1	333	5/89	75	1
13	TMS	2.7e–2	37	5/89	120	1
14	TMS	2.40e–1	328	6/89	60	1
17	TMS	2.53e–1	346	6/89	690	1
18	tBDM	4.86e–2	81	6/89	1000	1
20	tBDP	3e–3	5	7/89	330	1
31A	GC18	N/A	N/A	8/89	1255	
32	OtS	9.8e–3	16	8/89	1030	1
31B	GC18	N/A	N/A	9/89	1780	
34	OtS	2.45e–2	40	9/89	1080	
31C	GC18	N/A	N/A	10/89	955	
37	TMS	1.58e–1	216	10/89	550	1,2
31D	GC18	N/A	N/A	11/89	935	
38	OtS	2.45e–2	40	11/89	935	
39	OtS	2.45e–2	40	1/90	1055	
40A	GC18	N/A	N/A	3/90	1000	
42	tBDM	5.72e–2	95	6/90	1080	
43	tBDP	4e–3	7	8/90	955	

1. no pyridine was added prior to the end of silylation and no methanol rinse was used afterwards.
2. used different siliceous substrates (sodalime, quartz, and fused silica slides).

tainers for contact angle measurements over the period of observation. Three methods of characterizing the treated surface were used:

- measure the water–air and water–Soltrol® contact angles of the treated slides immediately after treatment
- measure the water–air contact angle over time to check the stability of the treated surface stored in different fluids

- measure the advancing contact angle using test liquids of different surface tension to construct a Zisman plot (see section 3.3) and determine the critical surface tension.

The water–air contact angle was always measured. Water–Soltrol® contact angles and contact angles of water:alcohol mixtures for Zisman plots were usually measured only at the beginning and at the end of the experiments.

Table 3.2 Extent of testing.

Exp. no.	***Silane***	***air***	***deionized water***	***$CaCl_2$ water***	***NaN_3 water***	***organic liquid***	***θ_{a-calc} or θ_a***	***θ_r***
8	TMS	✓	✓				✓	
11	TMS	✓	✓			✓	✓	
13	TMS	✓	✓			✓	✓	
14	TMS	✓	✓			✓	✓	
17	TMS	✓	✓				✓	
18	tBDM	✓	✓				✓	
20	tBDP	✓	✓				✓	
31A	GC18	✓	✓			✓	✓	
32	OtS	✓	✓	✓		✓	✓	
31B	GC18		✓	✓			✓	
34	OtS	✓	✓	✓			✓	
31C	GC18		✓			✓	✓	
37	TMS		✓				✓	
31D	GC18				✓		✓	✓
38	OtS		✓		✓		✓	
39	OtS		✓	✓	✓		✓	✓
40A	GC18		✓		✓		✓	✓
42	tBDM	✓	✓		✓	✓	✓	✓
43	tBDP	✓	✓		✓	✓	✓	✓

Although the general methodology outlined above remained the same throughout all the experiments presented below, it was inevitable that, with refinement of the sily-

lation procedures and techniques for measuring contact angles, procedure details evolved from experiment to experiment. For example, treated slides were stored in sodium azide solution only starting in experiment 31D after bacteria on a treated slide surface were discovered through optical microscopy. Similarly, measurement of receding angles and contact angle hysteresis were only possible after experiment 31D when the Gelmont® buret and a goniometer were purchased. The extent of analysis for each experiment is outlined in Table 3.2.

The main objectives of these experiments were to define the contact angle characteristics of organosilane–treated glass surfaces, understand the major mechanisms affecting stability of the treated surface, and how instability could be detected. The experiments were not exhaustive characterization studies but, rather, provided a systematic approach to choosing suitable silanes for treating glass porous media for the experiments later on.

3.1 Wettability of different silane–treated slides

Water–air contact angles and contact angle hysteresis for slides immediately after treatment are shown in Table 3.3. Available data for untreated glass and Teflon® are also included for comparison. The advancing angle, $\theta_{a\ calc.}$, was calculated from the static sessile drop. The advancing angle, θ_a, was measured directly with the goniometer from the dynamic drop.

The advancing contact angle was greatest for OtS–treated slides and least for tBDM– and tBDP–treated slides. When water advanced against air, intermediate–wet conditions prevailed for tBDM–, tBDP–, and GC18–treated slides. The OtS–treated surface had a greater affinity for air than water. The results for advancing contact angles in Table 3.3 also represented the maximum amount achievable in our laboratory for each type of silane. Preliminary experiments with tBDM and tBDP were done at one–tenth to one–hundredth the amount of silane reported above. This resulted in lower advancing angles and less uniformity of surface treatment. Experiments using

larger amounts of silane were impractical because of cost of the silanes. Table 3.1 shows that the amount of organochlorosilanes added for the experiments listed already far exceeds the amount required to completely cover the slides.

Table 3.3. Water–air contact angles and contact angle hysteresis for freshly treated slides.

Silane	$\theta_{a\ calc.}$ *(deg.)*	θ_a *(deg.)*	θ_r *(deg.)*	$\theta_a - \theta_r$ *(deg.)*
TMS	81.1° ±4.3°	N/A	N/A	N/A
tBDM	72.2° ±4.8°	75.3° ±3.7°	57.4° ±5.5°	17.9° ±1.8°
tBDP	64.7° ±5.1°	69.0° ±5.1°	54.0° ±2.2°	15.0° ±2.4°
GC18	91.9° ±2.9°	104.0° ±7.5°	88.2° ±4.6°	15.7° ±3.7°
OtS	108.0° ±6.2°	151.9° ±3.5°	79.7° ±8.1°	72.6° ±6.9°
Untreated	<25°	<25°	N/A	N/A
Teflon©		108°[1]		

1. From Fox and Zisman (1950).

Initial contact angle hysteresis was relatively minor (<20°) for tBDM- , tBDP-, and GC18-treated slides but was significant for OtS-treated slides (Table 3.3). Contact angles show that when water recedes against air, water-wet conditions prevailed for tBDM- and tBDP-treated slides and intermediate-wet conditions prevailed for GC18- and OtS-treated slides (see classification in section 1.3.2). Receding angles for TMS-treated slides were not measured because instability of TMS-treated slides stored in water ruled it out for further study (section 3.3). However, all treated slides displayed contact angle hysteresis with the dynamic sessile drop method.

In a typical oil/water system, such as with Soltrol® and water, tBDM- and tBDP-treated slides have neutral wettability while GC18- and OtS-treated slides were oil-wet for water advancing against Soltrol® (Table 3.4). For GC18- and OtS-treated slides, the static water drop would not adhere to the glass surface; the advancing angles with the static method were arbitrarily defined as 180°. Available data for tBDM-, tBDP-, and GC18-treated slides showed that when water receded against Soltrol®, all three types of treated surface were of neutral wettability (Table 3.4). The wettability

of the treated slides were classified according to Table 1.1. The degree of initial contact angle hysteresis in the water–Soltrol® system ranged between about 15° for tBDP–treated slides to just over 30° for GC18–treated slides. The magnitude of hysteresis was greater in the water–Soltrol® system than in the water–air system for GC18 and tBDM.

Table 3.4 Water–Soltrol contact angles for freshly treated slides.

Silane	$\theta_{w/o\ a\ calc}$ *(deg.)*	$\theta_{w/o\ a}$ *(deg.)*	$\theta_{w/o\ r}$ *(deg.)*	$\theta_{w/o\ a} - \theta_{w/o\ r}$ *(deg.)*
TMS	114.3° ±7.2°	N/A	N/A	N/A
tBDM	107.7° ±5.2°	108.0° ±2.7°	81.8° ±7.8°	26.1° ±7.0°
tBDP	97.8° ±2.8°	98.1° ±3.3°	81.3° ±4.0°	16.8° ±2.9°
GC18	180°[1]	151.4° ±6.8°	119.8° ±5.0°	31.6° ±3.3°
OtS	180°[1]	N/A	N/A	N/A
Untreated	56.6° ±11.0°	68.8° ±9.1°	40.7° ±7.7°	28.1° ±5.1°
Teflon®	N/A	N/A	N/A	N/A

1. Water drop would not adhere to glass surface.

3.2 Stability of silane–treated slides stored in different fluids

3.2.1 Stability in air

Water–air contact angle measurements for treated slides stored in air are shown in Figures 3.1 to 3.8 and Appendix B. The data points in all of the figures showing contact angles are averaged values (Sections 2.6.2 and 2.6.3) and have been connected by straight lines. In the figures, $\theta_{a\ calc}$ refers to the advancing angle using the static sessile drop method and θ_a, θ_r, and θ_a–θ_r refer to the advancing and receding angle, and hysteresis, respectively, from the dynamic method.

In all cases (Figures 3.1, 3.2, 3.4, 3.6, and 3.7), the advancing angle remained essentially constant indicating that the treated glass surfaces were stable over the period of observation. Receding angles were measured in the last two experiments (42 and 43) for tBDM and tBDP. Receding angles and hysteresis did not change (Figures 3.3

and 3.5). Receding angles over time were not measured for slides treated with the other silanes and stored in air.

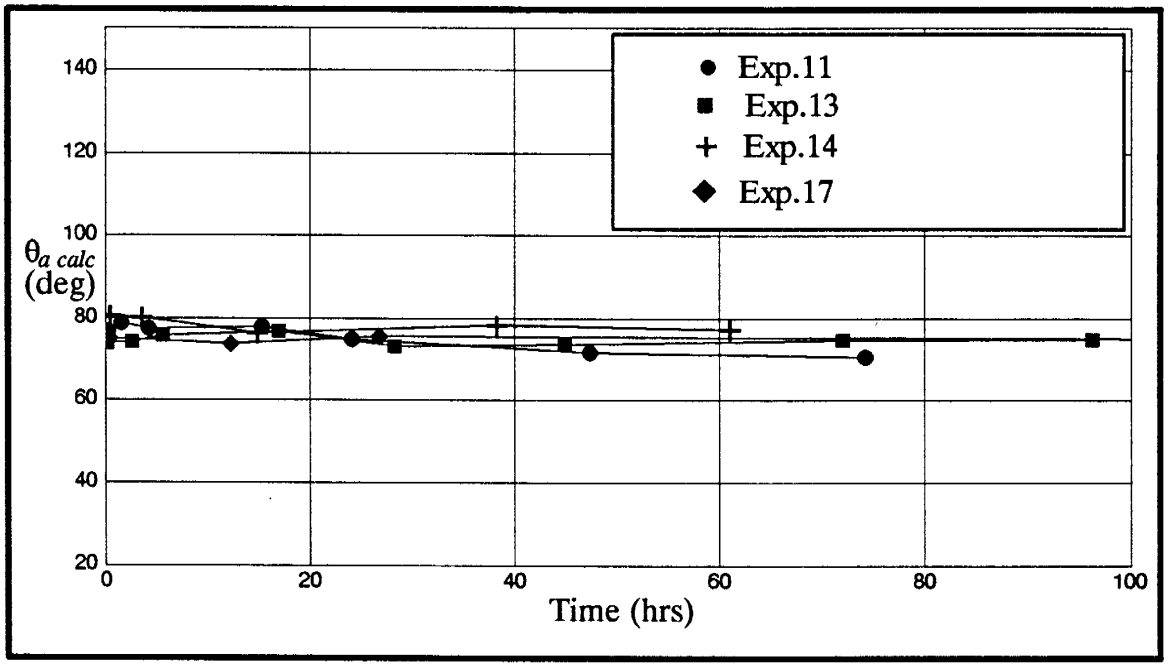

Figure 3.1. Stability of TMS–treated slides stored in air

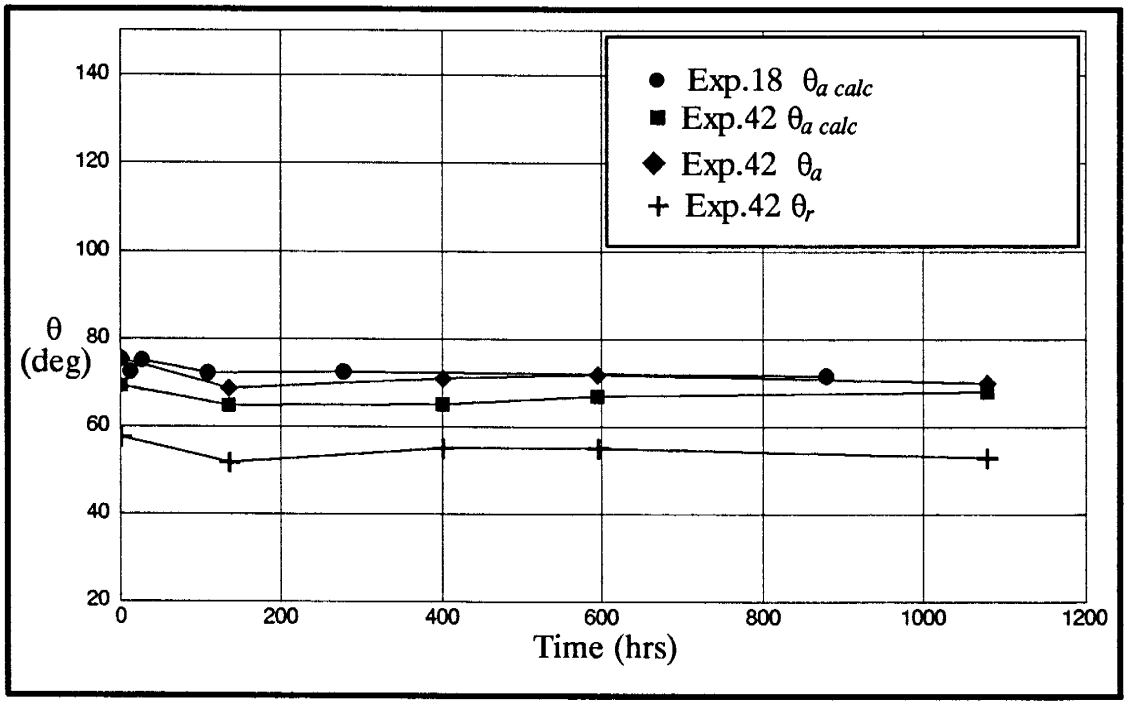

Figure 3.2. Stability of tBDM treated–glass slides stored in air.

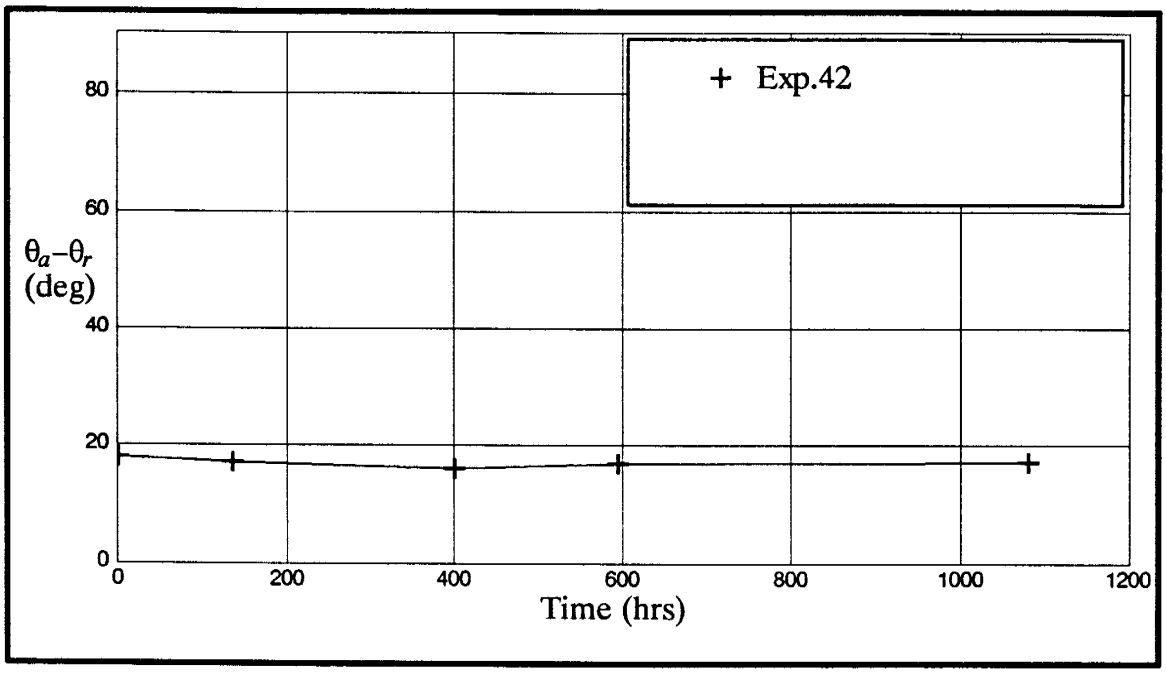

Figure 3.3. Change in contact angle hysteresis with time for tBDM–treated slides stored in air.

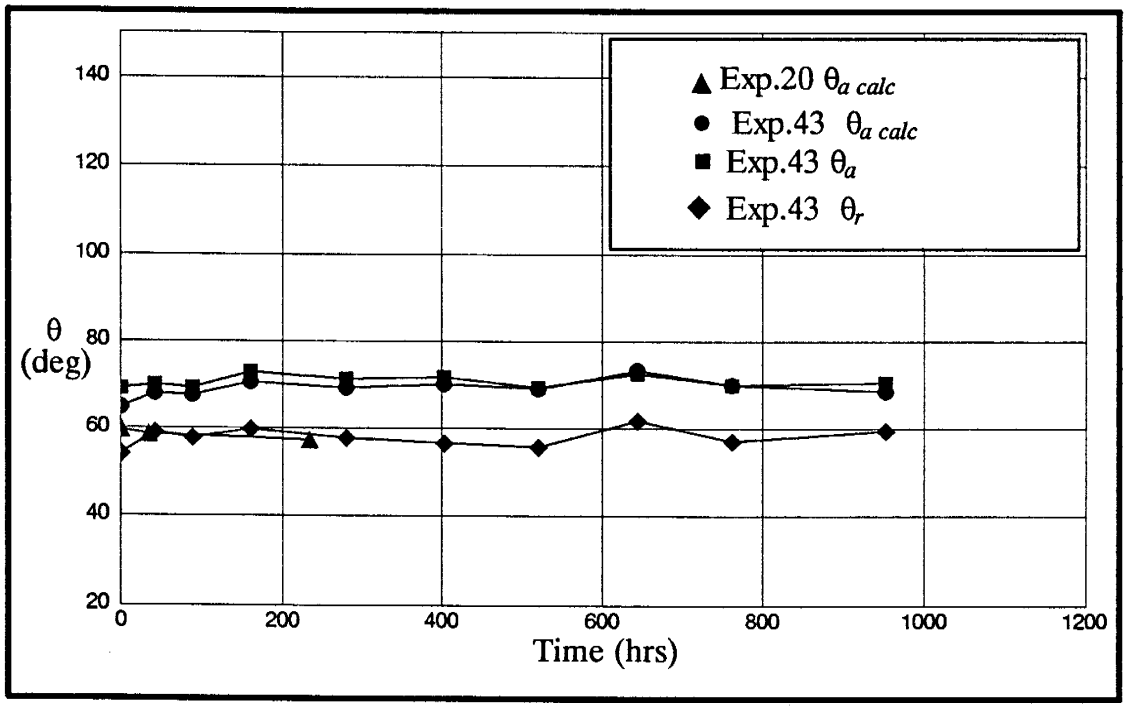

Figure 3.4. Stability of tBDP treated–glass slides stored in air.

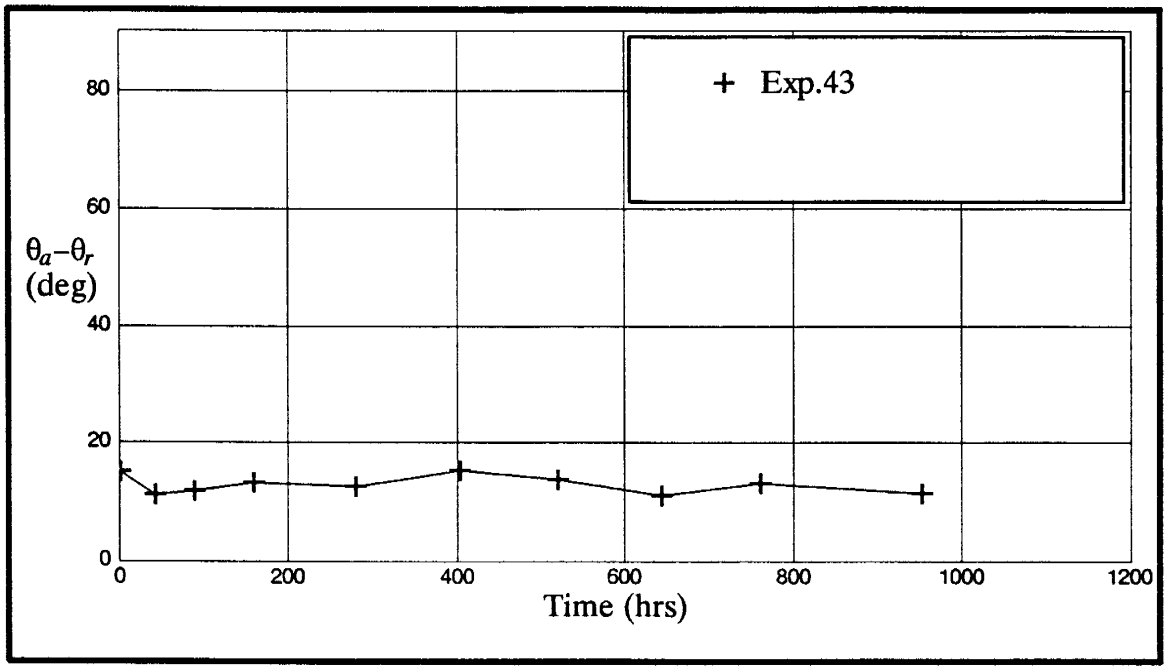

Figure 3.5. Change in contact angle hysteresis with time for tBDP–treated slides stored in air.

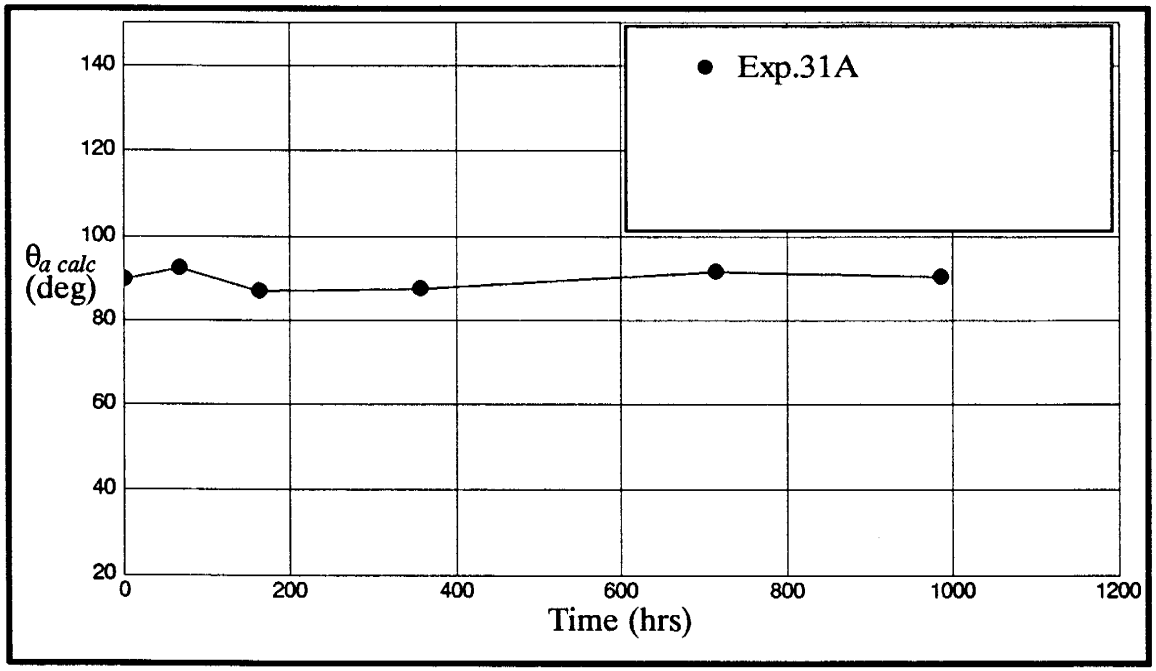

Figure 3.6. Stability of GC18–treated slides stored in air.

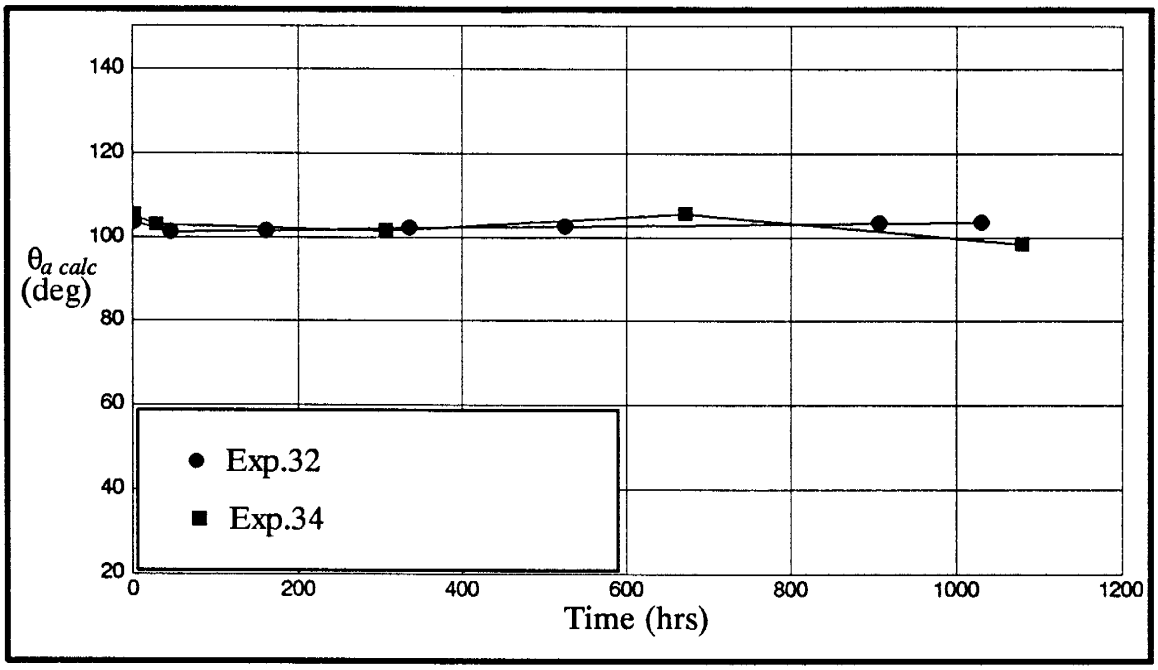

Figure 3.7. Stability of OtS–treated slides stored in air.

For tBDM– and tBDP–treated slides, any change in the advancing angle occurred within the first few days (Figures 3.2 and 3.4). The advancing angle in these cases increased or decreased a few degrees and then remained constant. This phenomenon was not obvious for slides treated with the other silanes.

Although the advancing angle remained essentially constant with time, the variability frequently increased with time. Variability is defined here as the range in measured contact angle values for each period of measurement. A model example is shown in Figure 3.8 for GC18–treated slides where the advancing angle remained constant (Figure 3.6) but the variability, ξ, increased from $\sim 0°$ at the start to $\sim 7°$ after 1000 hours.

Figures 3.1, 3.2, 3.4, and 3.7 show that both the initial contact angle and contact angle behavior with time could be duplicated. Once stability and reproducibility for slides stored in air were confirmed, work focused on treated slides stored in organic and aqueous liquids.

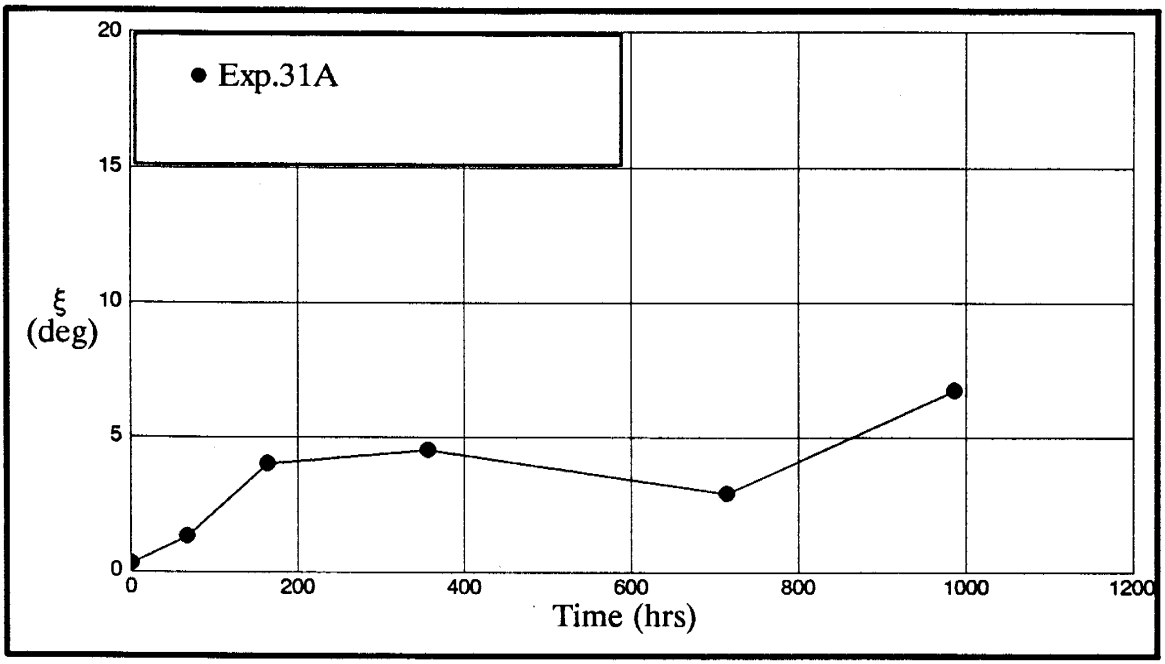

Figure 3.8. Variation in measured advancing contact angles for GC18 treated slides stored in air.

3.2.2 Stability in organic liquids

Contact angles over time for treated slides stored in various organic liquids are shown in Figures 3.9 to 3.19 and in Appendix B. In the earlier experiments with TMS, the slides were stored only in xylene. In later experiments, however, slides were also stored in other organic liquids such as Soltrol® and alcohol. Soltrol® was used as the oil phase in the short column and micromodel experiments; alcohol (ethanol) was used to pack the treated beads in the short columns. Stability in both these kinds of organic liquids were checked. Data for treated slides coated with Soltrol® and stored in deionized water have also been included here in this section (Figures 3.12, 3.16, and 3.19). The slides were coated to check how a Soltrol® film could protect the treated surface in water.

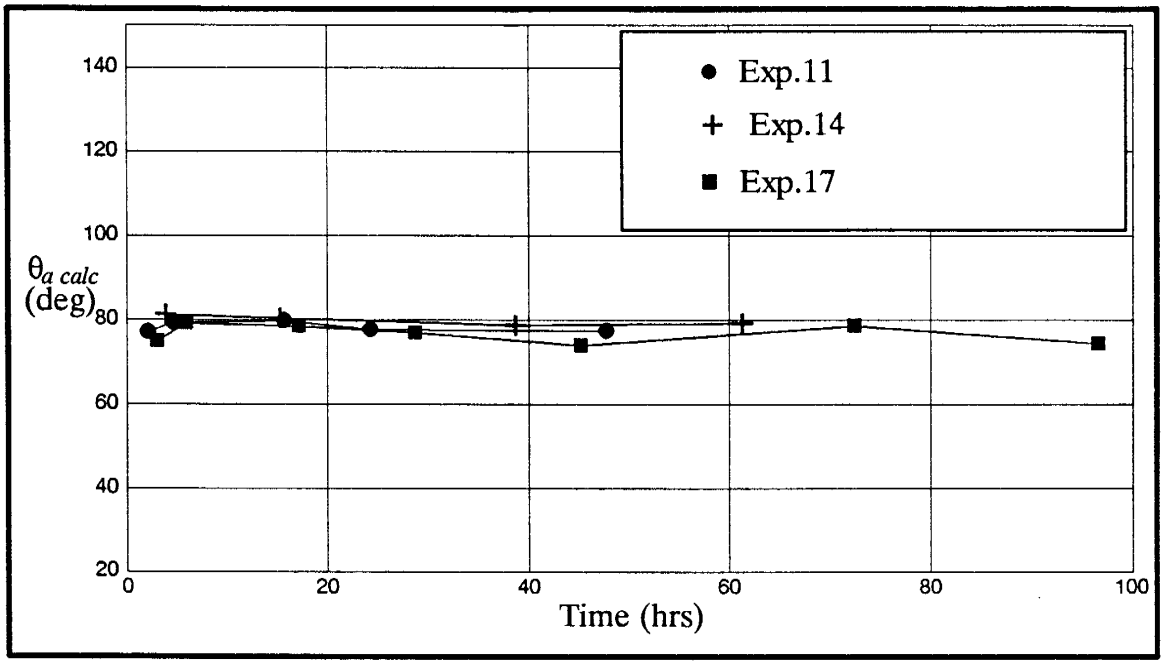

Figure 3.9. Stability of TMS–treated slides stored in xylene.

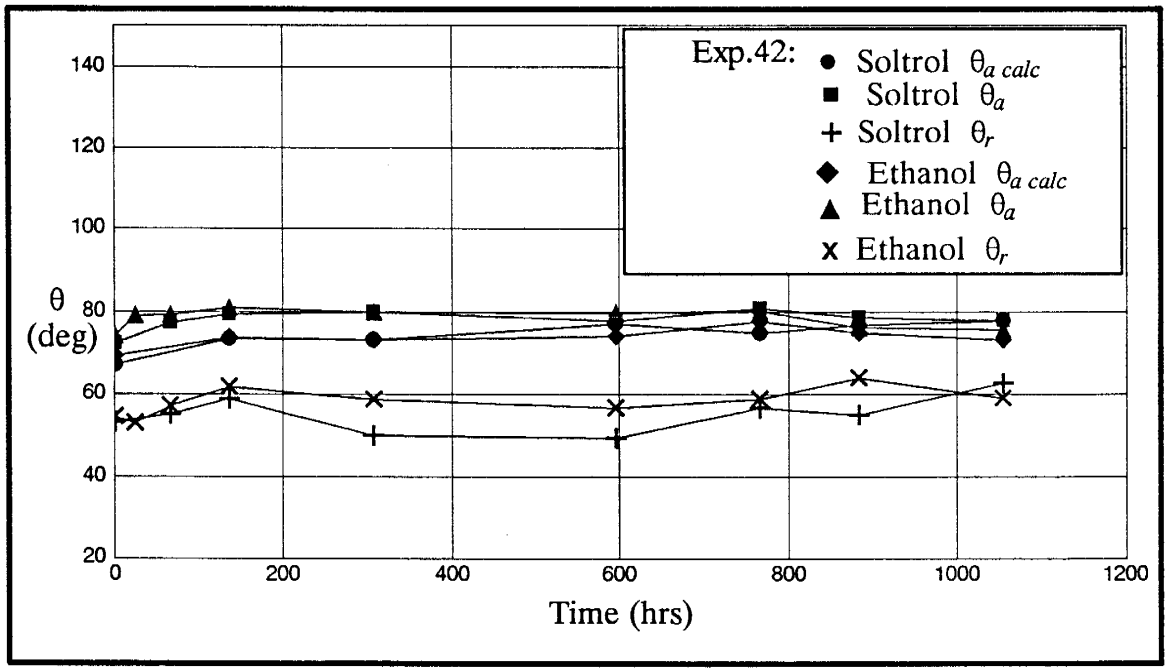

Figure 3.10. Stability of tBDM–treated slides stored in Soltrol and ethanol.

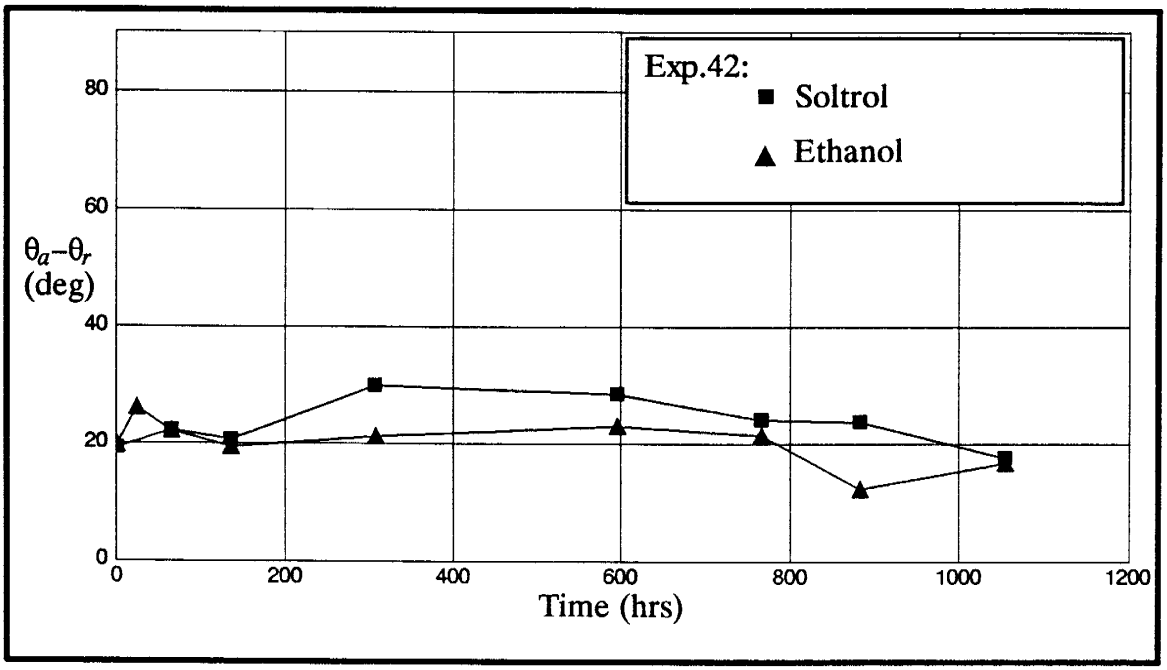

Figure 3.11. Contact angle hysteresis for tBDM–treated slides stored in Soltrol and ethanol.

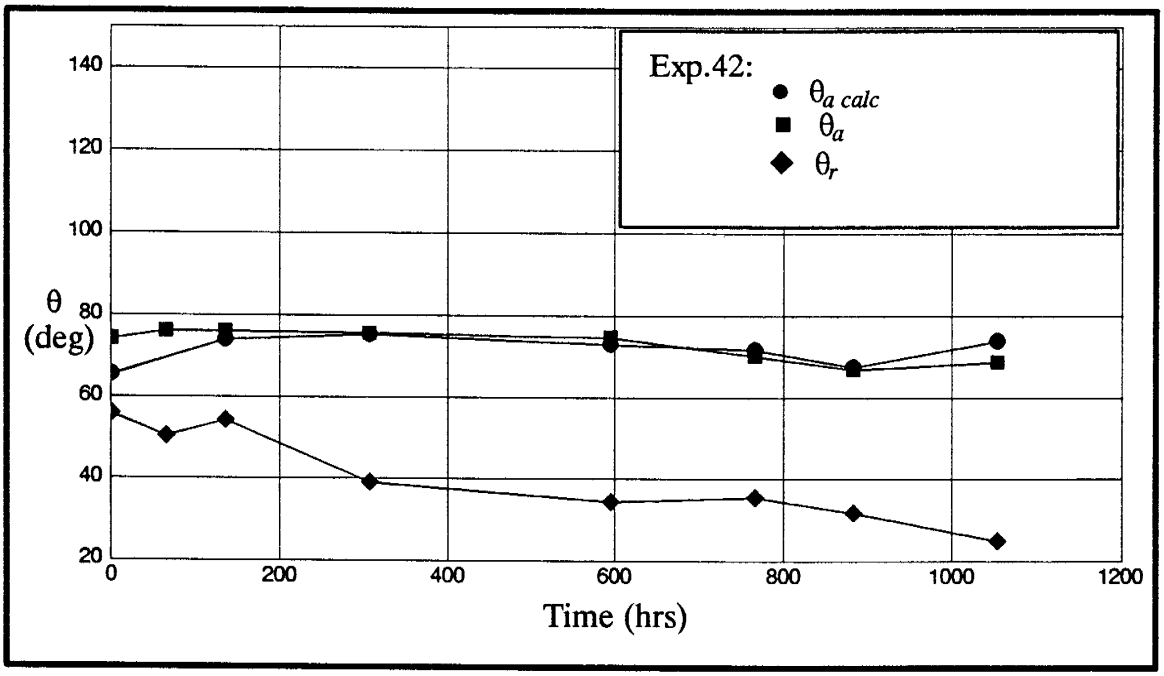

Figure 3.12. Stability of tBDM–treated slides coated in Soltrol and stored in deionized water.

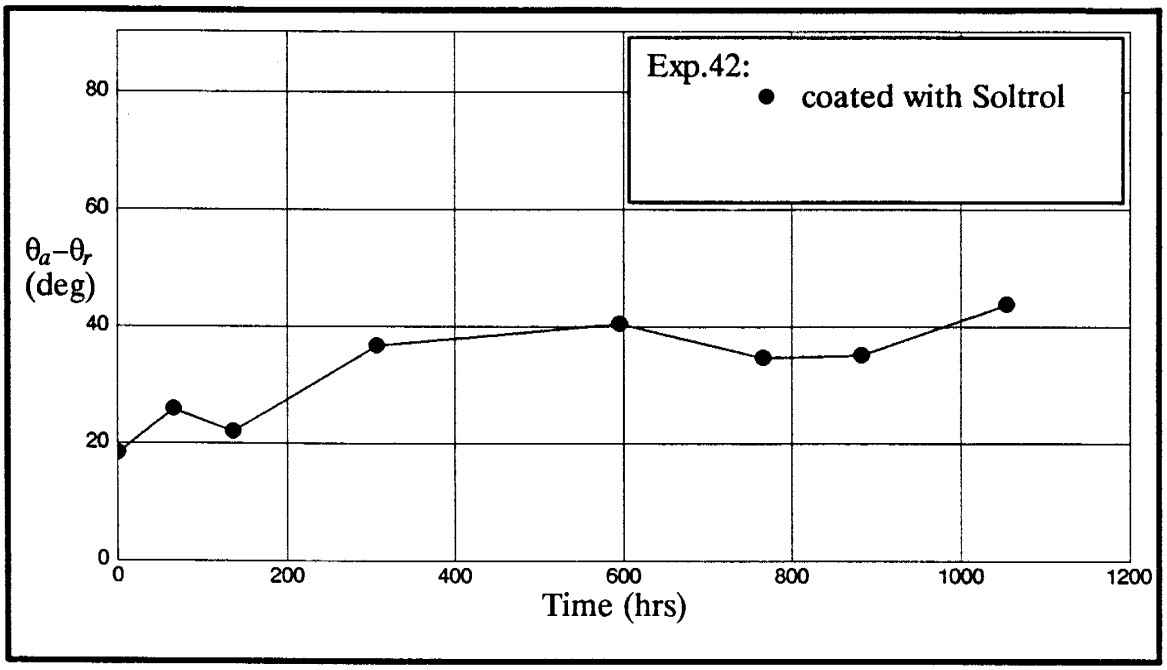

Figure 3.13. Contact angle hysteresis for tBDM–treated slides coated in Soltrol and stored in deionized water.

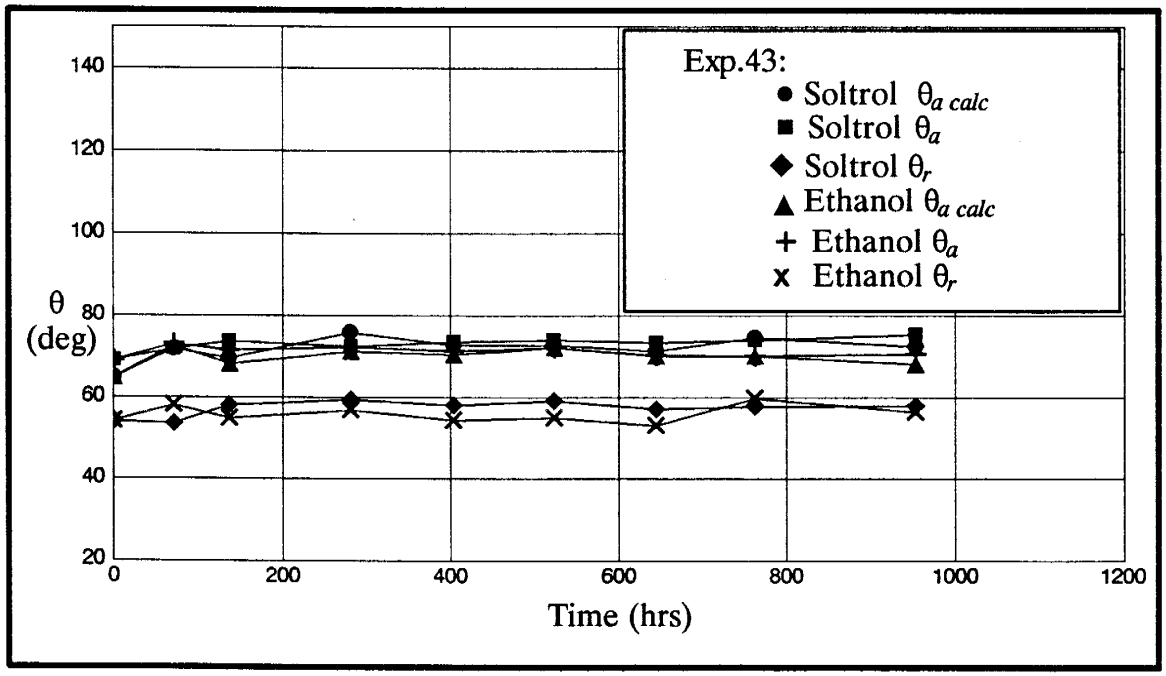

Figure 3.14. Stability of tBDP–treated slides stored in Soltrol and in ethanol.

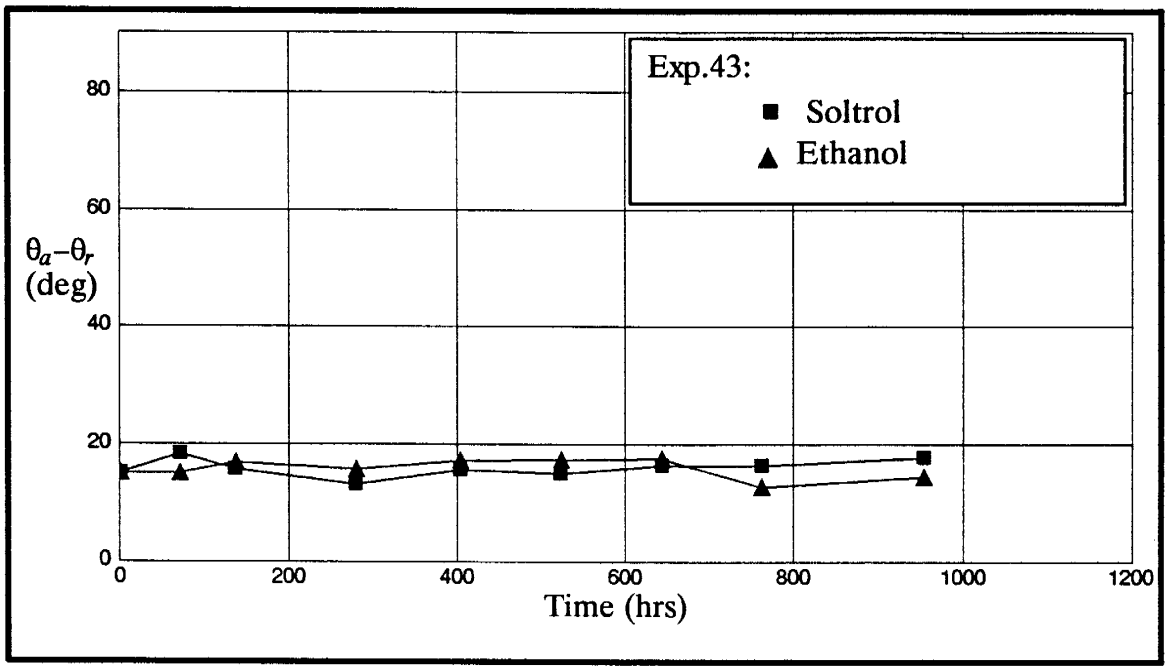

Figure 3.15. Contact angle hysteresis for tBDP–treated slides stored in Soltrol and ethanol.

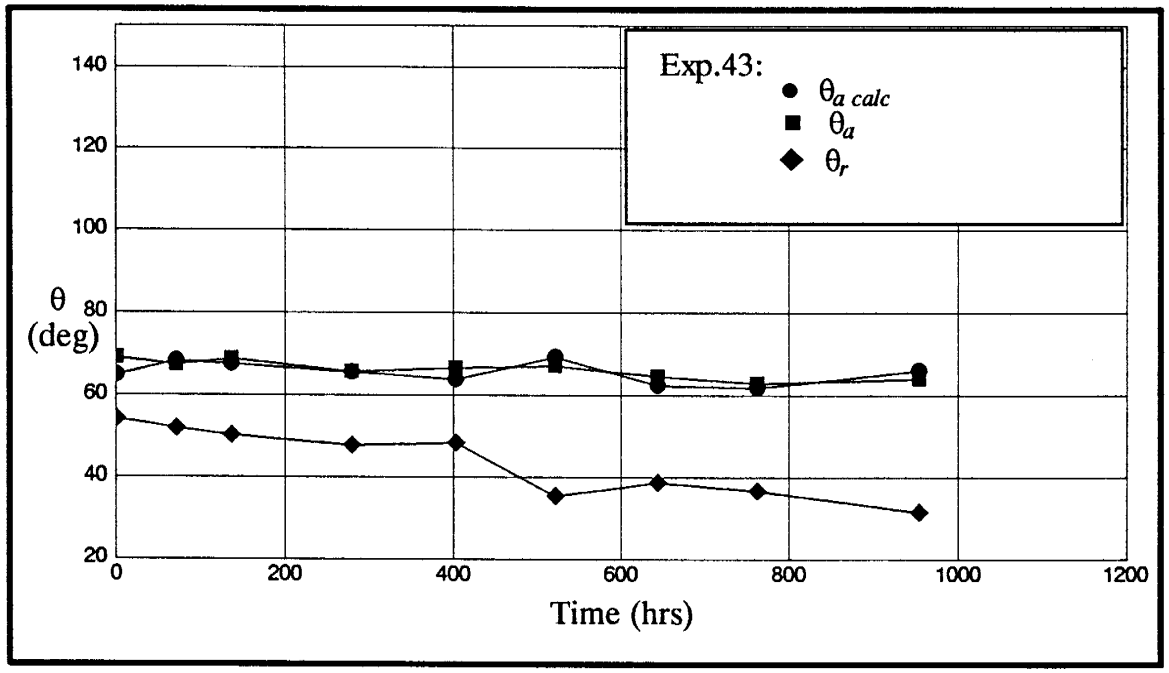

Figure 3.16. Stability of tBDP–treated slides coated in Soltrol and stored in deionized water.

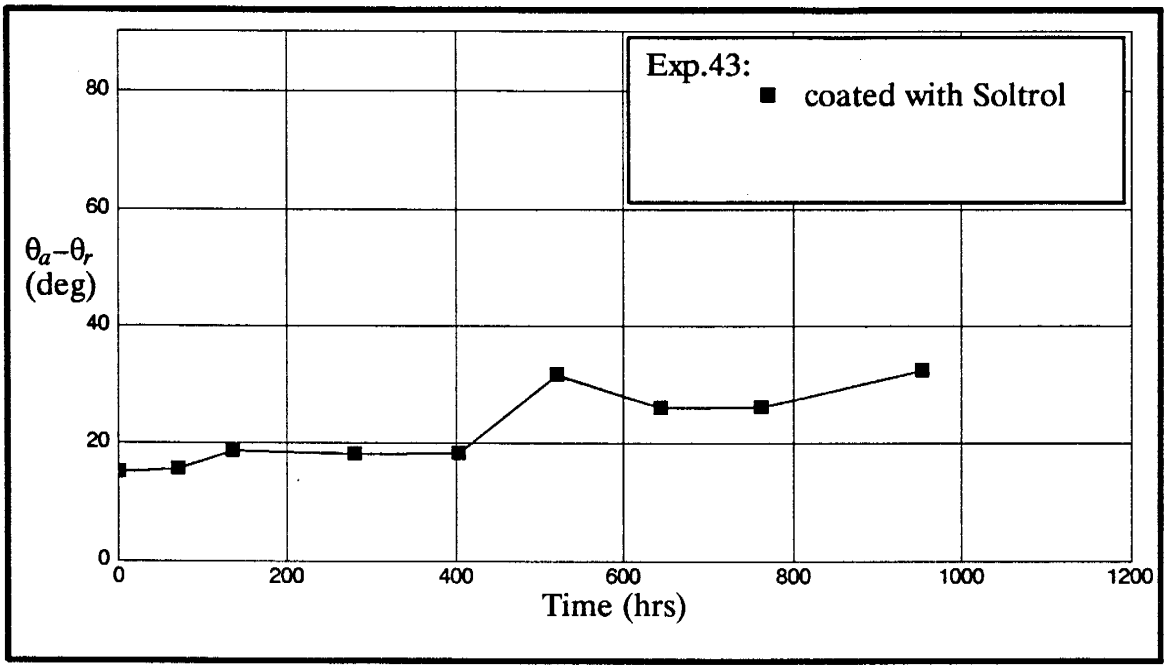

Figure 3.17. Contact angle hysteresis for tBDP–treated slides coated in Soltrol and stored in deionized water.

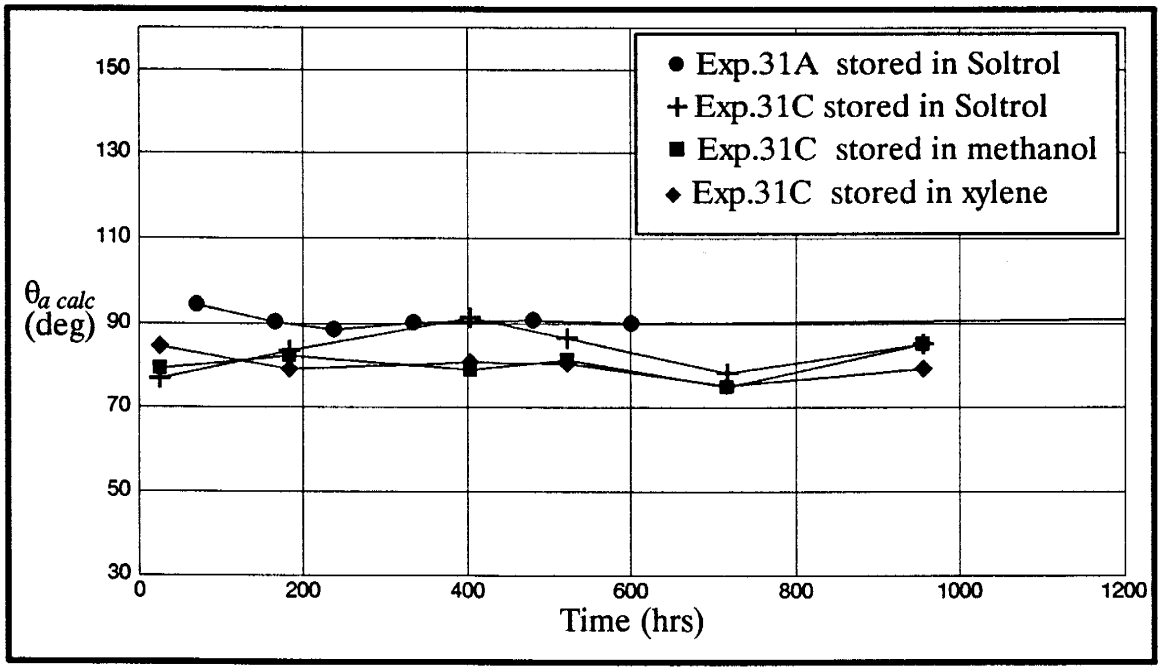

Figure 3.18. Stability of GC18–treated slides stored in Soltrol, methanol, and xylene.

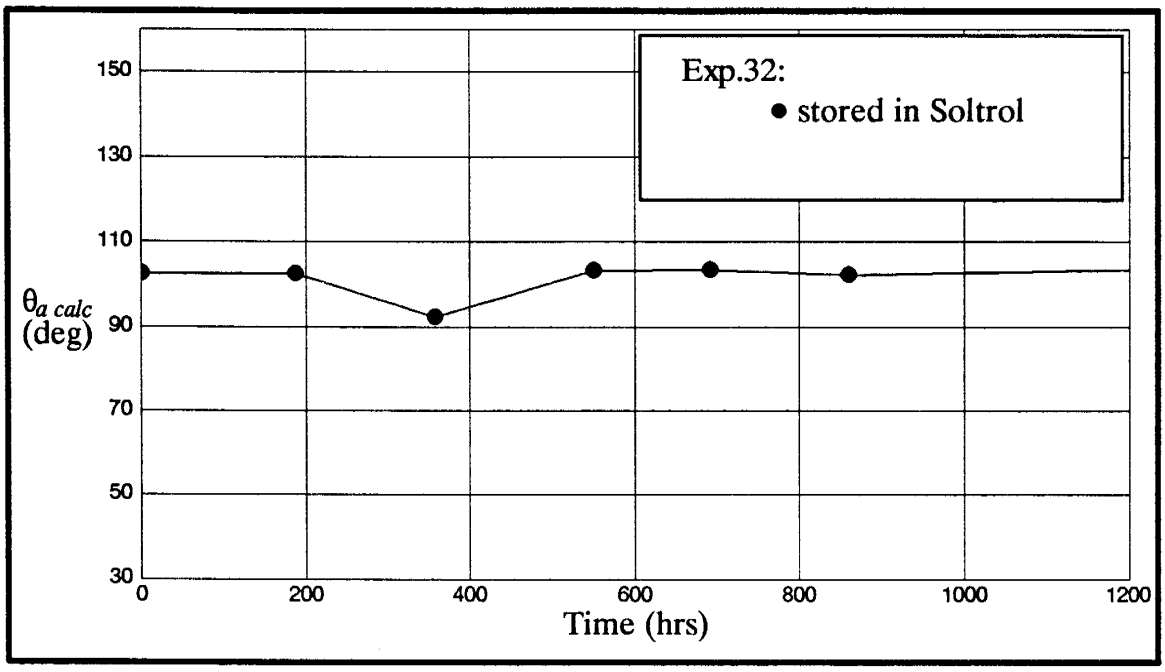

Figure 3.19. Stability of OtS–treated slides coated with Soltrol and stored in deionized water.

Stability of the treated slides stored in organic liquid was similar to those stored in air. The advancing contact angle, for all silanes used, remained essentially constant over a period of up to 1000 hours (Figures 3.9, 3.10, 3.14, and 3.18). Although receding angles were not measured in all experiments, receding angles in experiments 42 and 43 with tBDM– and tBDP–treated slides remained constant (Figures 3.10 and 3.14); contact angle hysteresis also did not change with time (Figures 3.11 and 3.15).

In some experiments with tBDM (experiment 42), tBDP (experiment 43), and OtS (experiment 32), treated slides were coated with Soltrol®130 and stored in deionized water to check if water could affect the treated slide surface after Soltrol® had first coated the surface (Figures 3.12, 3.16, and 3.19). For tBDM– and tBDP–treated slides, breakdown was indicated by a constantly decreasing receding angle and increasing contact angle hysteresis with time (Figures 3.12, 3.13, 3.16, and 3.17). Decrease in the advancing angle for tBDM– and tBDP–treated slides was very minor (Figures 3.12 and

3.16). The advancing angle for OtS–treated slides remained constant over time suggesting that no breakdown had occurred (Figure 3.19). Unfortunately, the receding angle was not measured. No data was gathered for GC18–treated slides but its stability in water (section 3.2.3) suggested that the surface was quite stable even in the absence of an oil film. Once stability in organic liquids was known for organochlorosilane–treated slides in early experiments, it was not studied in detail in later experiments with OtS–treated slides especially since stability for slides coated in Soltrol® became evident.

3.2.3 Stability in water

Stability of treated slides stored in water was of critical importance because treated porous media in later experiments would be carried out under initially water–saturated conditions. In the beginning, slides were stored in deionized water. Later on, slides were also stored in 3000mg/L $CaCl_2$ solution and 1000mg/L NaN_3 solution to see if solutes in the water affected stability. The $CaCl_2$ solution is a standard aqueous solution for our lab. The NaN_3 solution minimized bacterial growth in the water. Results of stability in water are plotted in Figures 3.20 to 3.38 and tabulated in Appendix B. In the figures, D&D, D&D&NaN_3, and D&D&$CaCl_2$ represent deionized water, deionized water with 1000mg/L NaN_3, and deionized water with 3000mg/L $CaCl_2$, respectively. In every case, the contact angle decreased with time. Results for each silane are presented in the following sections.

3.2.3.1 Stability of TMS–treated slides

Figure 3.20 shows the advancing angle decreased 10° within the first 100 hours for TMS–treated slides. In experiment 13, the silane added was only one–tenth that of the other experiments (Table 3.1). However, there appeared to be little difference except that the decrease in contact angle in experiment 13 may have occurred slightly earlier.

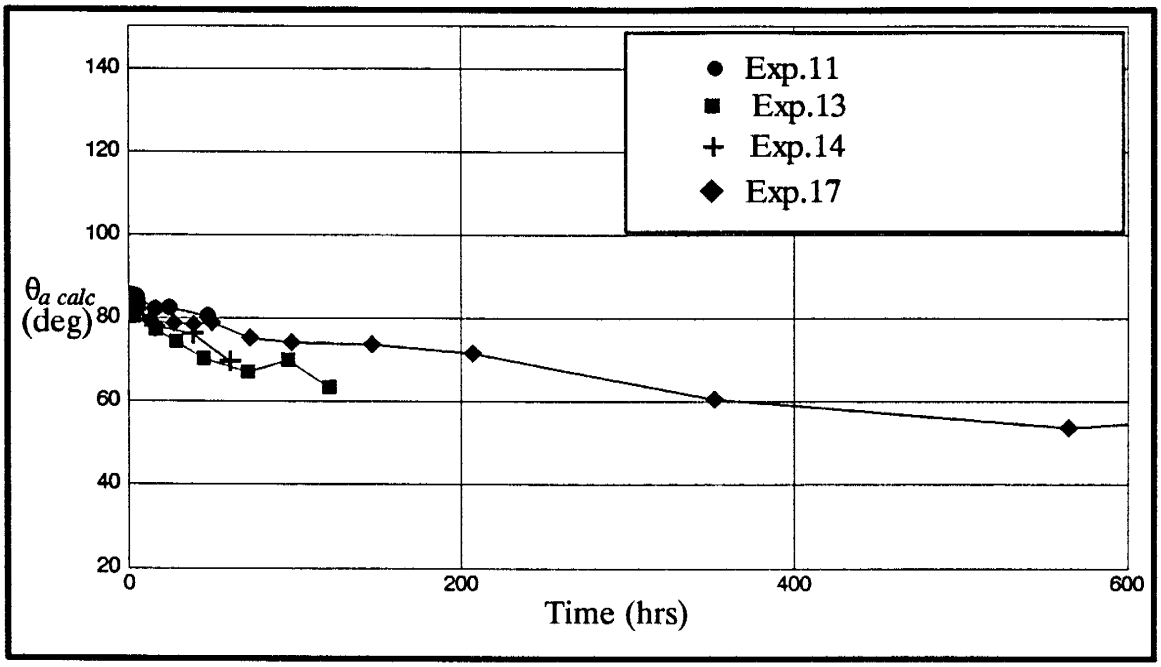

Figure 3.20. Stability of TMS–treated slides stored in deionized water.

In experiment 17, measurements were extended to 690 hours. A significant decrease in the contact angle was observed from 83.8° at the start to 57.1° after 690 hours, a difference of 26.7°. The decrease in contact angle implied that the treated surface was gradually breaking down when stored in water.

3.2.3.1.1 Effect of different substrates on stability

Since the contact angle for TMS–treated slides decreased within the first 100 hours, an experiment with TMS treatment of quartz and fused silica slides was performed to determine if purer, siliceous substrates would enhance stability in water. A more suitable substrate would yield a constant contact angle even though the contact angle of the treated sodalime glass slide decreased. Results of experiment 37 plotted in Figure 3.21 shows that quartz and fused silica slides did not significantly enhance stability in water. The advancing angle for treated quartz and silica slides decreased similarly to that of treated sodalime slides. The sodalime glass even seemed to maintain a higher contact angle throughout the first 400 hours than either the quartz or silica slides.

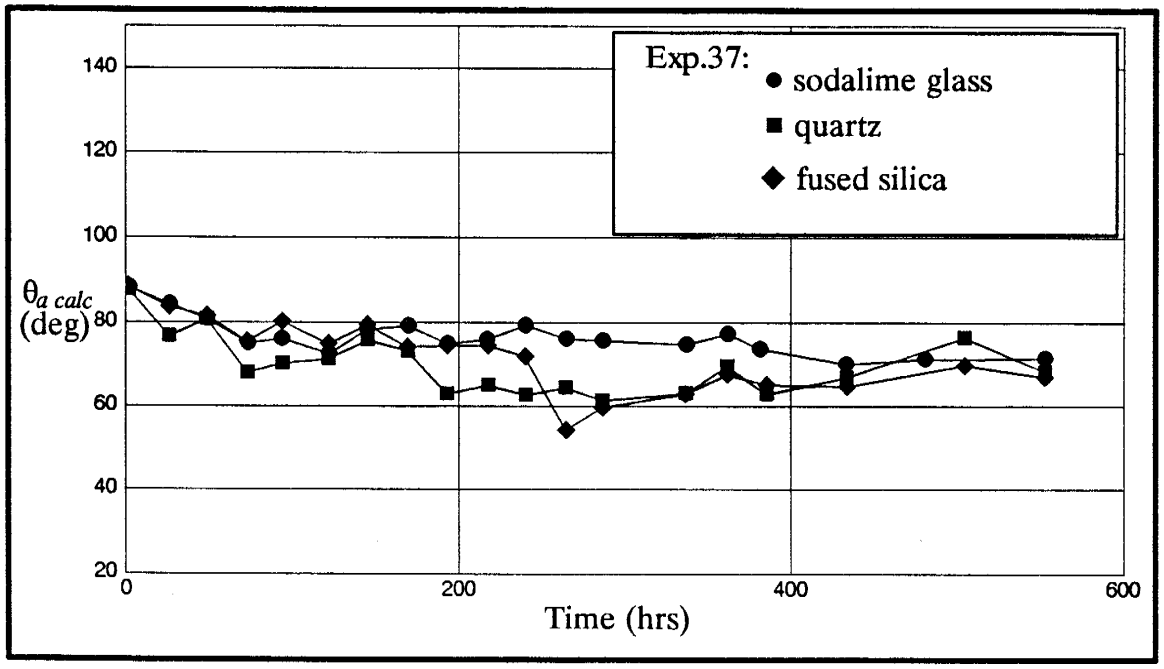

Figure 3.21. Effect of different substrates on the stability of TMS–treated slides stored in deionized water.

3.2.3.2 Stability of tBDM–treated slides

Results of advancing contact angles calculated from the static sessile drop method are shown in Figure 3.22. Advancing and receding angles from the dynamic sessile drop method and contact angle hysteresis are shown in Figures 3.23 and 3.24. The advancing angle uniformly decreased 15° to 20° over 1000 hours. The receding angle in experiment 42 decreased about 30° over the same period. Most of the decrease, however, occurred within the first 100 hours. The interface of the dynamic sessile drops tended to remain immobile and not recede when the sessile drops were drawn up the buret after the slide was stored in water for more than one day (Appendix B). The drops became pinned and eventually snapped off from the buret. The receding angles measured were the angles of the interface just prior to snap–off and as such, were difficult to define. There was negligible difference in stability for slides stored in deionized water or water with 1000mg/L NaN_3 bacteriacide. Contact angle hysteresis increased from about 15° at the beginning to about 35° after 1000 hours. Most

of the hysteresis developed within the first 100 hours when the receding angle decreased rapidly. After 100 hours, hysteresis increased gradually as the receding angle decreased at only a slightly faster rate than the advancing angle.

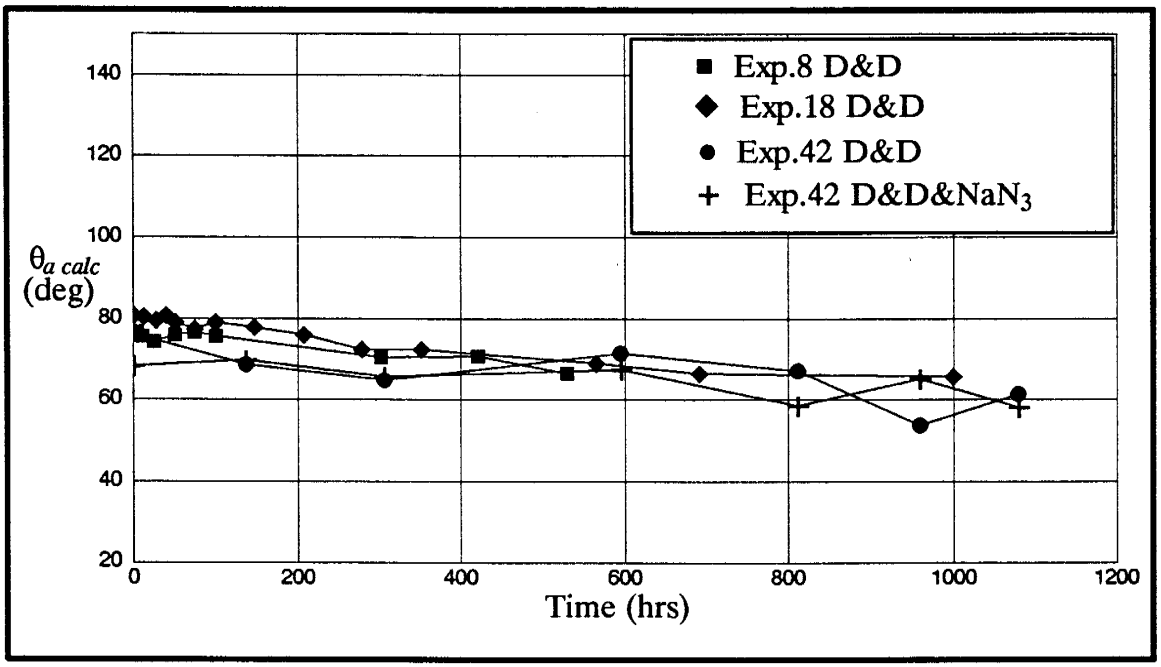

Figure 3.22. Stability of tBDM–treated glass slides stored in deionized water.

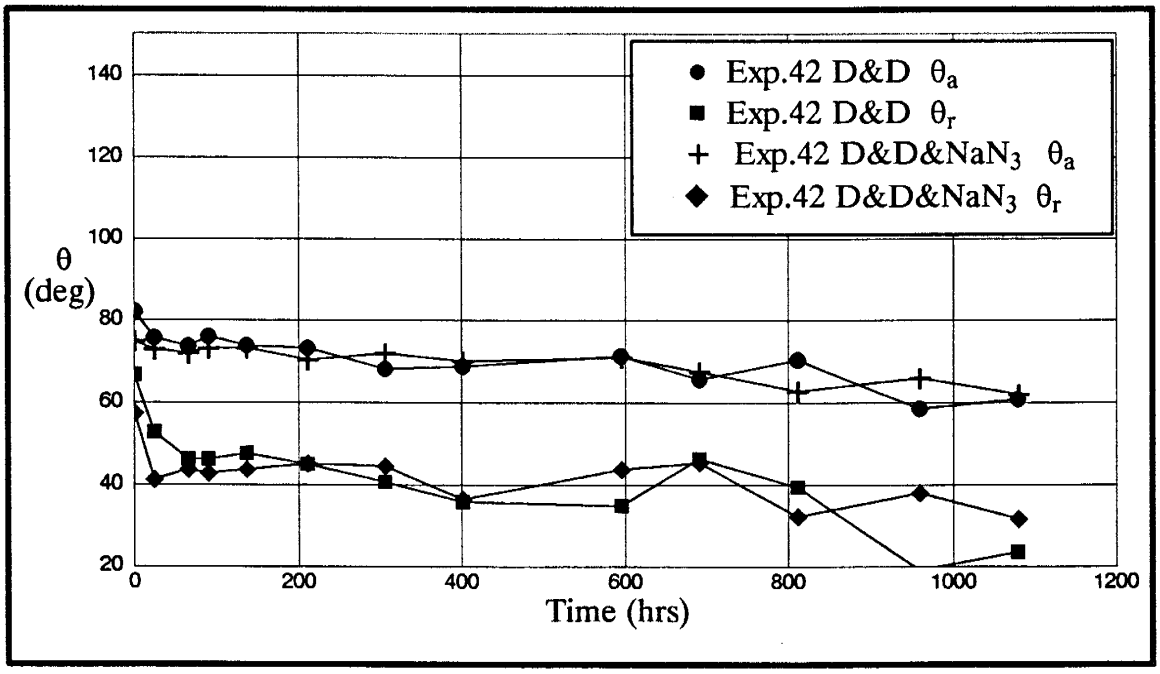

Figure 3.23. Stability of tBDM–treated glass slides stored in water.

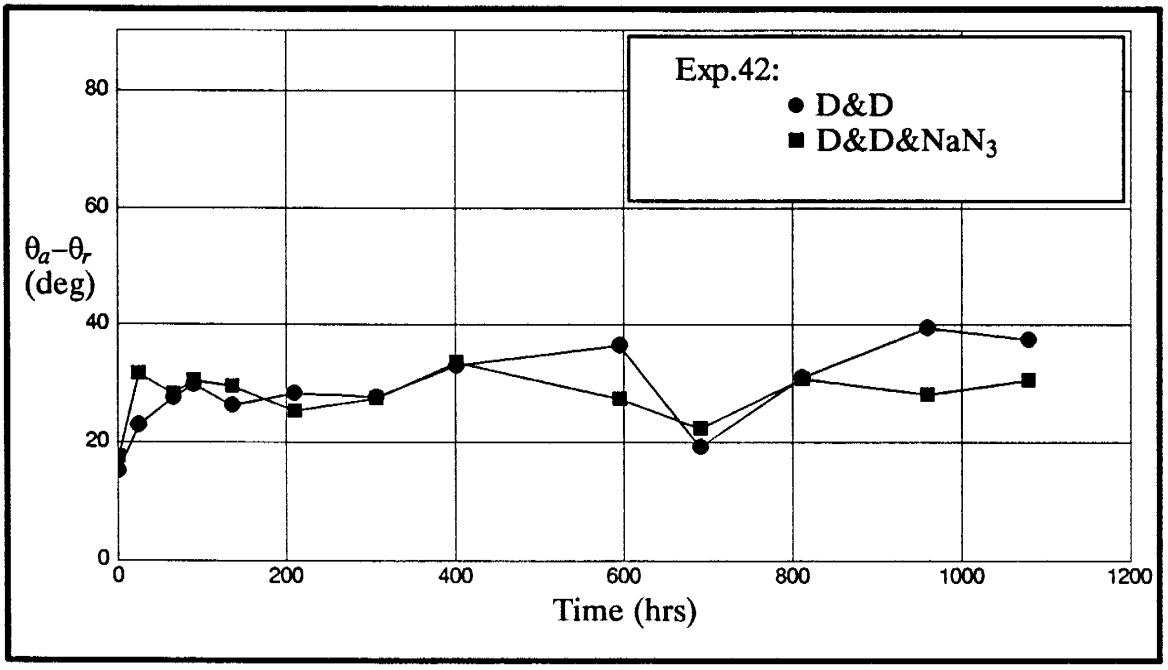

Figure 3.24. Contact angle hysteresis for tBDM–treated slides stored in water.

3.2.3.3 Stability of tBDP–treated slides

Results for tBDP–treated slides are shown in Figures 3.25 and 3.26. The advancing angle decreased continuously with time (20° to 25° over 950 hours). The receding angle decreased about 25° to 30° over the same period. After about 400 hours, the receding interface remained immobile when the dynamic water drop was drawn up the buret (Appendix B). As in experiment 42, the receding angle was defined as the angle measured through the water before the drop snapped off from the buret. The contact angles for slides stored in water and for slides stored in water with NaN_3 were similar. Contact angle hysteresis increased from about 15° to 35° for slides stored in water. For slides stored in water with NaN_3, contact angle hysteresis increased to just beyond 20° after about 100 hours and remained essentially constant thereafter. The constant hysteresis after 100 hours for slides stored in water with NaN_3 was because both the advancing and receding angles decreased at the same rate.

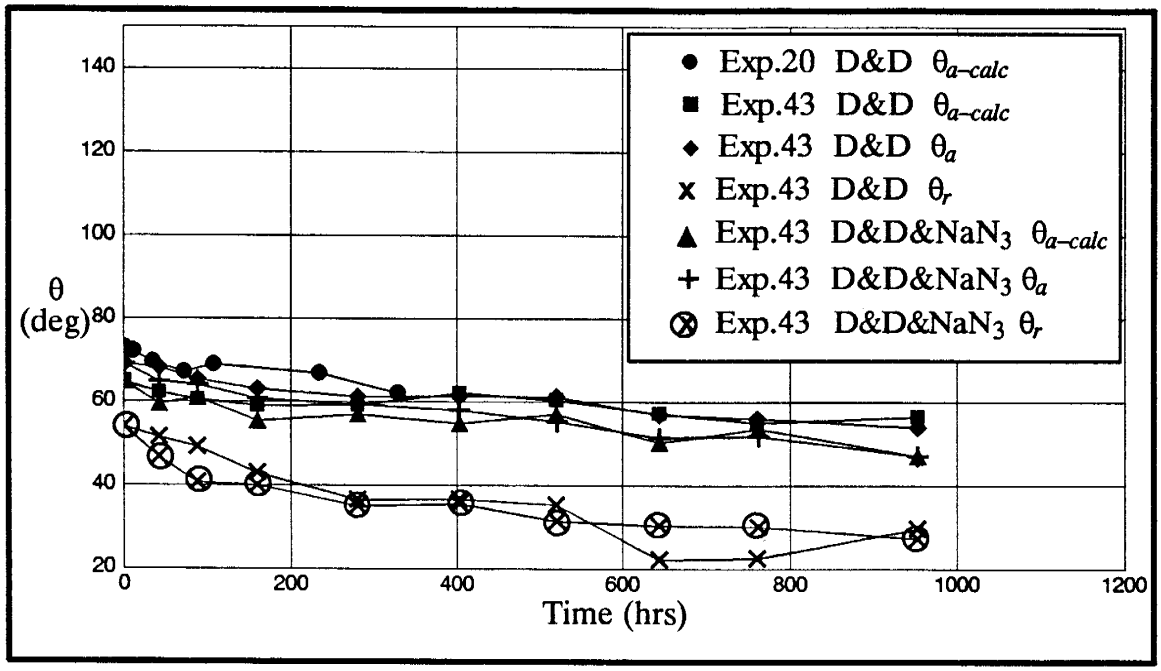

Figure 3.25. Stability of tBDP-treated glass slides stored in water.

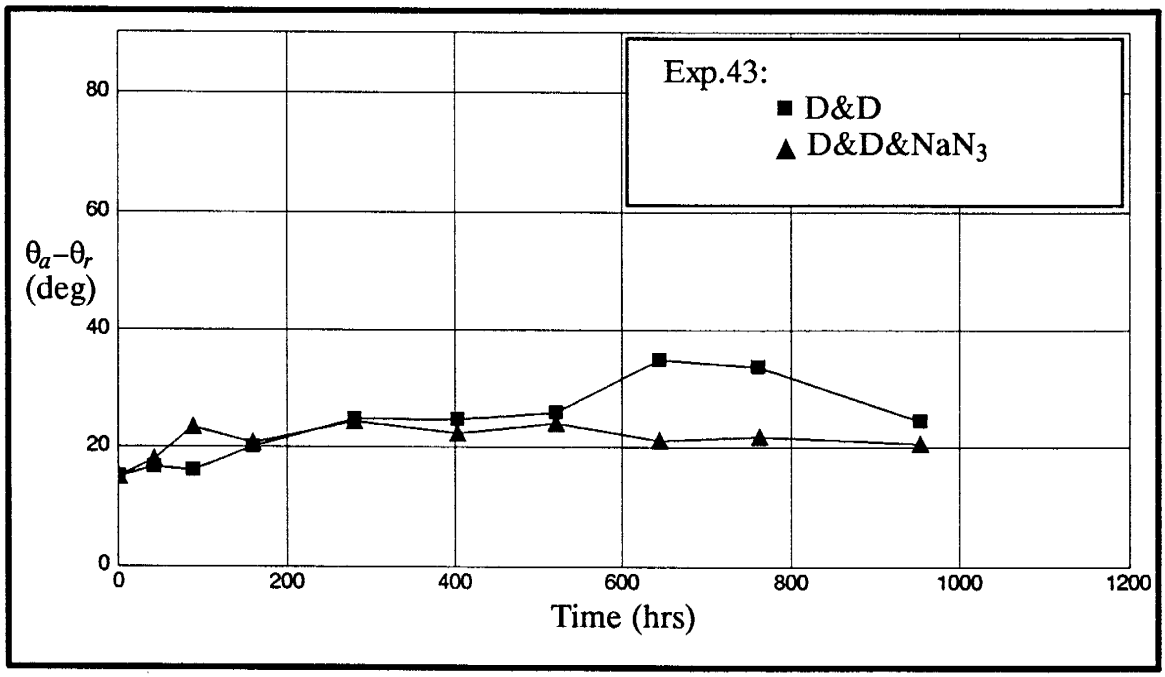

Figure 3.26. Contact angle hysteresis for tBDP-treated slides stored in water.

3.2.3.4 Stability of GC18–treated slides

Advancing contact angles on GC18–treated slides stored in deionized water or water with 1000mg/L NaN_3 decreased less than 10° over 1000 hours (Figures 3.27, 3.28, 3.30, and Appendix B). Stability appeared to be very similar between slides stored in deionized water and NaN_3 water. The behavior was reproducible (see Figures 3.27 and 3.30). On the other hand, slides stored in 3000mg/L $CaCl_2$ solution showed a markedly different trend in the advancing angle (Figure 3.29). After 3 to 4 days, the advancing angle decreased about 20° and then remained relatively constant for the remainder of the experiment. Unfortunately, the instability of GC18–treated slides stored in $CaCl_2$ solution was not duplicated experimentally. The receding angle decreased about 25° over 1000 hours (Figure 3.31). This rate was greater than for the advancing angle and resulted in a constant increase in contact angle hysteresis with time (Figure 3.32).

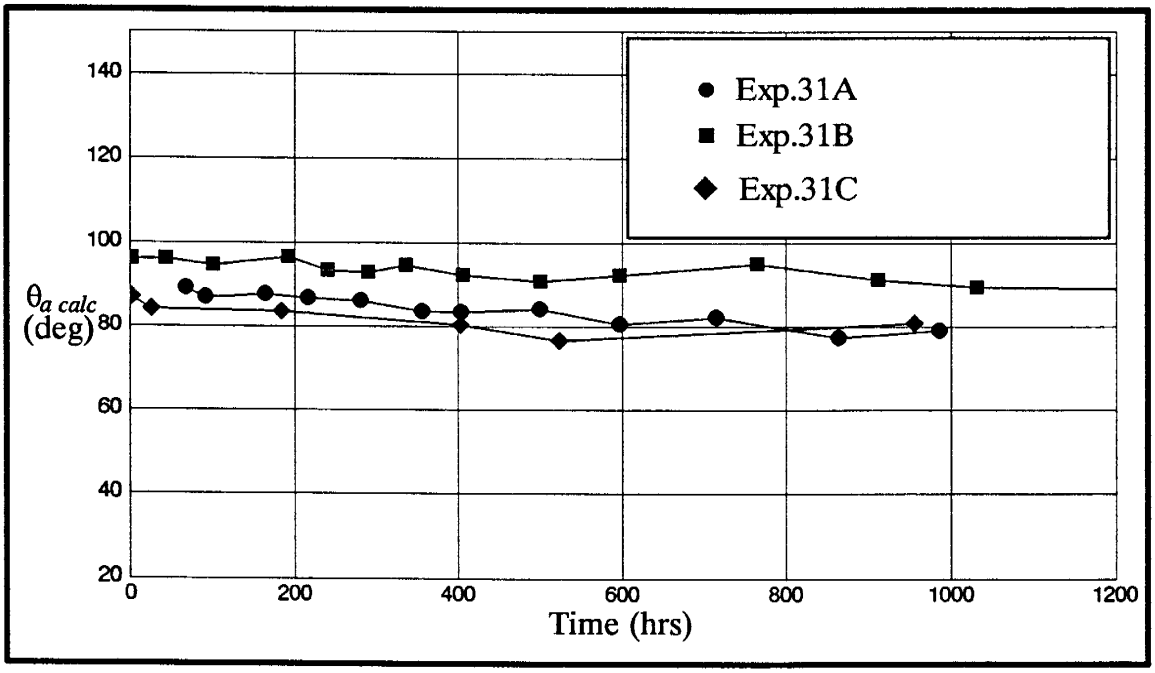

Figure 3.27. Stability of GC18–treated slides stored in deionized water.

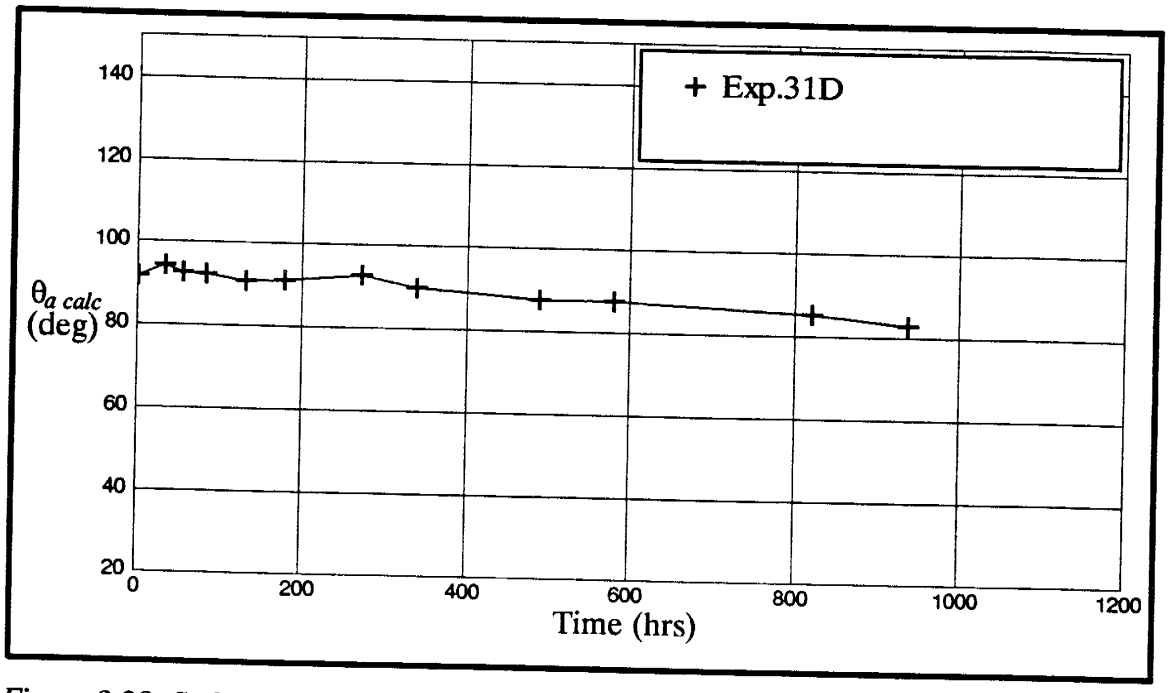

Figure 3.28. Stability of GC18–treated slides stored in NaN_3 water.

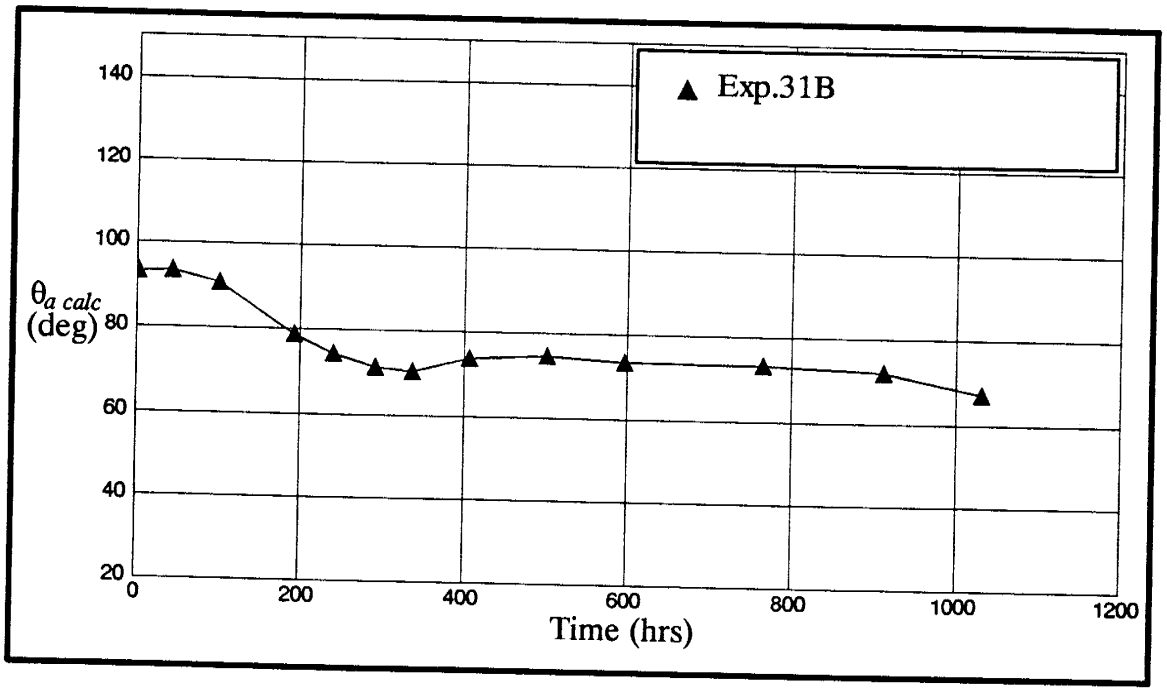

Figure 3.29. Stability of GC18 treated slides stored in $CaCl_2$ water.

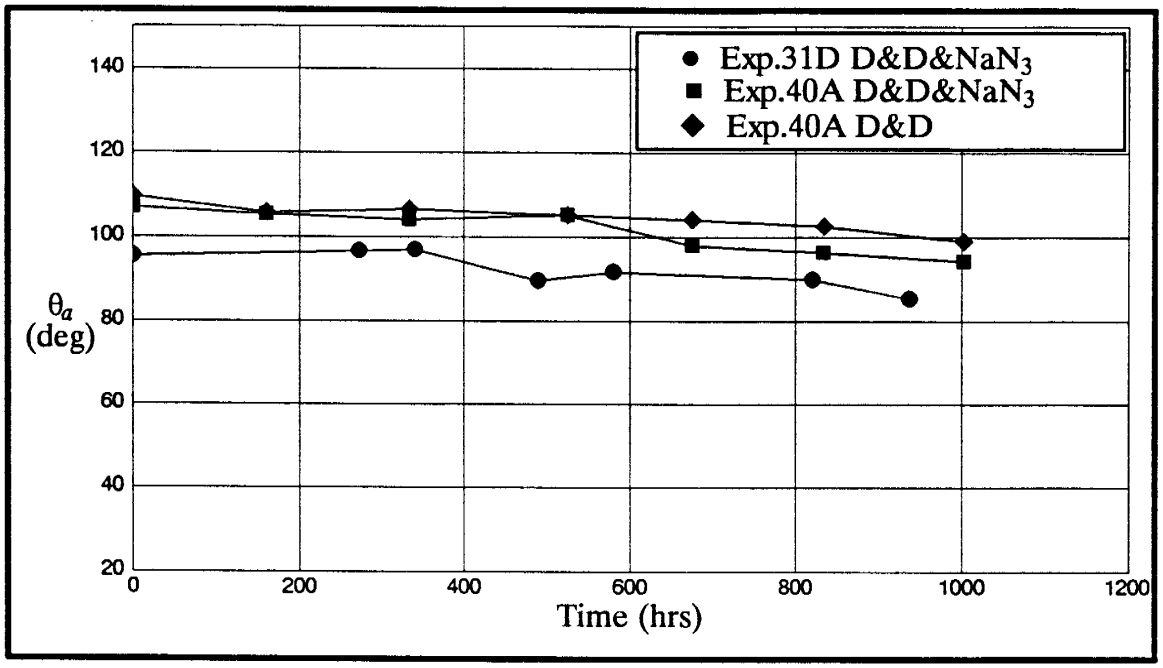

Figure 3.30. Advancing contact angle as a function of time for GC18–treated slides stored in water.

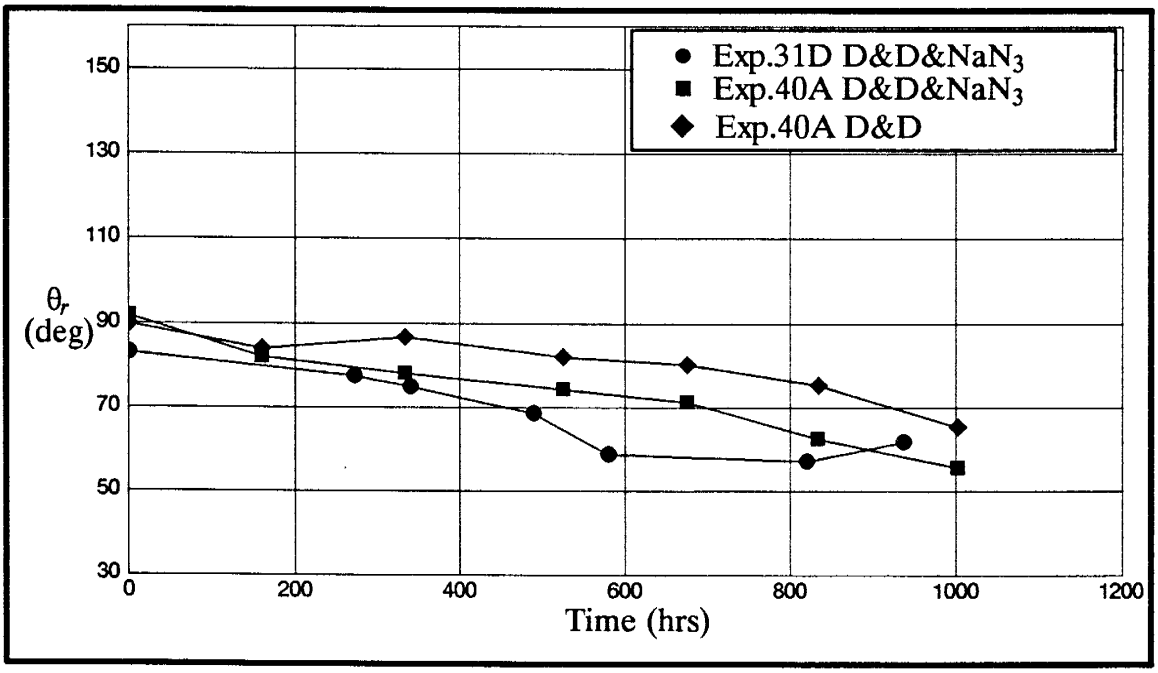

Figure 3.31. Receding contact angle as a function of time for GC18–treated slides stored in water.

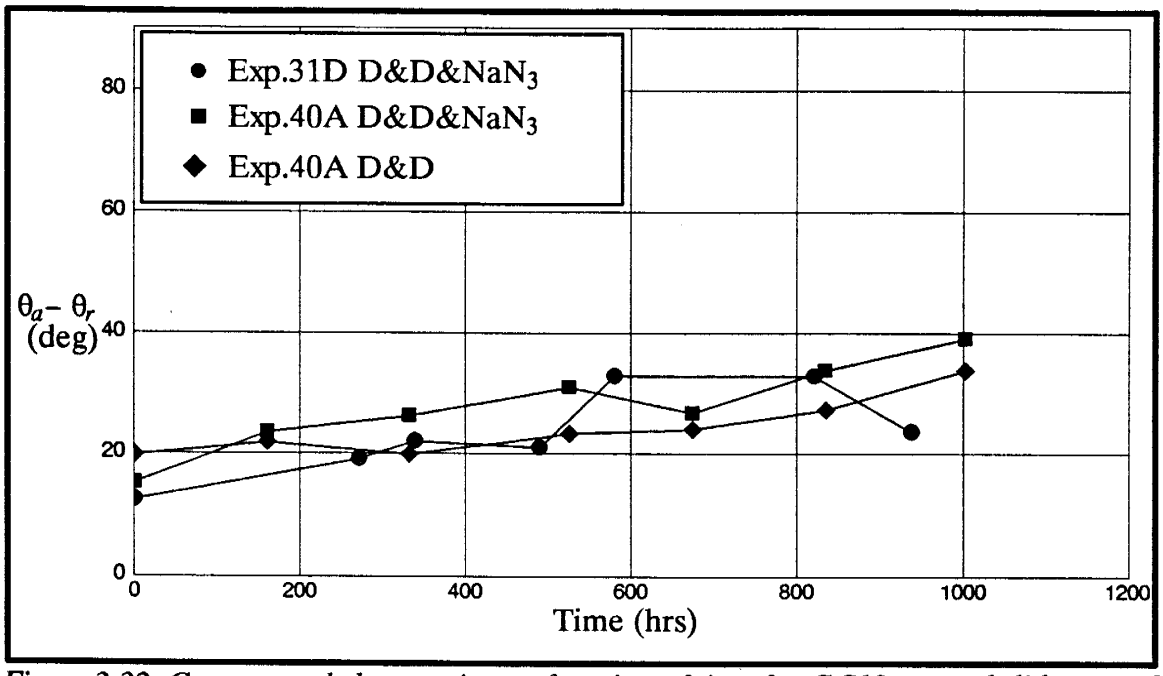

Figure 3.32. Contact angle hysteresis as a function of time for GC18-treated slides stored in water.

3.2.3.5 Stability of OtS-treated slides

Contact angles for OtS-treated slides stored in water also decreased over time. The results were, however, more variable than for the other silanes (Figures 3.33 to 3.41 and Appendix B). In experiments 32, 34, and 38, the initial advancing angle was between 100° and 120° (Figures 3.33, 3.34, and 3.35). In experiment 39, the initial advancing angle measured with the dynamic method was about 150°, significantly higher than in the previous three experiments. Advancing angles calculated from the static method decreased up to 40° over 1000 hours. Advancing angles decreased up to 50° for the dynamic method over the same period of time.

In experiment 39, the receding angles also decreased about 40° to 50° over the 1000 hours from initial values of 70° to 90° (Figure 3.37). A decrease of about 25° to 30° occurred within the first few days alone. The extremely high value of the advancing angle resulted in very large hysteresis. Contact angle hysteresis increased steadily with time. Hysteresis increased to 80° to 90° within the first few days as the receding

angle dropped sharply. Thereafter, contact angle hysteresis actually decreased slightly with time as the advancing angle decreased at a greater rate than the receding angle (Figure 3.38).

3.2.3.6 Water–Soltrol® contact angles

Water–Soltrol® contact angles were also measured for tBDM–, tBDP–, and GC18–treated slides stored in water. Measurements were taken at the end of the experiments. These final angles were compared with the initial water–Soltrol® contact angles to ascertain changes in wettability of the actual water/Soltrol®/glass system after prolonged exposure to water. Unfortunately, final water–Soltrol® contact angles were not measured for OtS–treated slides. Initial and final water–Soltrol® contact angles are shown in Table 3.5. Only the average contact angles are shown. Since water–Soltrol® contact angles were only measured on a few slides, standard deviations were not included. Also shown in Table 3.5 are the absolute values of the difference between the cosine of the initial and final angles. This difference provides a measure of the wettability change. The symbols, $\theta_{initial}$ and θ_{final}, represent the initial and final water–Soltrol® angles.

Table 3.5. Change in water–Soltrol contact angle for treated slides stored in water.

Silane	$\theta_{w-o\ a}$ *(deg.)*		$\theta_{w-o\ r}$ *(deg.)*		$\lvert cos\ \theta_{initial} - cos\ \theta_{final} \rvert$	
	initial	*final*	*initial*	*final*	$\theta_{w/o\ a}$	$\theta_{w/o\ r}$
tBDM	108.0	94.2	81.8	37.2	0.24	0.65
tBDP	98.1	80.2	81.3	29.3	0.31	0.72
GC18	151.4	120.9	119.8	78.7	0.36	0.69

Water–Soltrol® contact angles decreased for tBDM–, tBDP–, and GC18–treated slides stored in water. For tBDM–treated slides, the advancing angle decreased from an initial value of 108.0° to 94.2° at the end of the experiment (1080 hours) indicating that the tBDM–treated surface had degraded slightly when stored in water. The receding angle decreased from an initial value of 81.8° to 37.2° over the same period. Most

of the decrease probably occurred within the first 100 hours following the behavior observed with the receding water–air contact angles in Figure 3.23. The final receding angle represented the angle of the drop where the interface remained immobile. The treated surface at the end of the experiment was still intermediate–wet when water advanced against Soltrol® but was strongly water–wet when water receded against Soltrol® (refer to Table 1.1). The advancing water–Soltrol® angle for tBDP–treated slides decreased from 98.1° to 80.2° over 950 hours for slides stored in water. The receding angle decreased from 81.3° to 29.3° over the same period. As in experiment 42, the final receding angle represented the angle of an immobile interface. The surface was intermediate–wet for water advancing against Soltrol® and strongly water–wet for water receding against Soltrol® (Table 1.1). The water–Soltrol® advancing angle for GC18–treated slides also decreased with time. Initially, the contact angle was 151.4°. After prolonged storage in water, the water–Soltrol® advancing angle decreased to 120.9°. This final value indicates that the treated surface was still oil–wet (Table 1.1). The receding angle after 1000 hours was 78.7°, indicative of an intermediate–wet surface.

The decrease for the cosine of the receding angles was twice as great as for the cosine of the advancing angles. This was deduced from the difference in the cosine of the initial and final angles for the advancing and receding angles (Table 3.5). Interestingly, the overall decrease in the cosine of both the advancing and receding angles were similar between tBDM–, tBDP–, and GC18–treated slides stored in water. Although the decrease in the cosine of the receding angles were similar, the initial receding angle for tBDM– and tBDP–treated slides was low enough that the decrease shifted the wettability from intermediate–wet to water–wet. The initial receding angle for GC18–treated slides was higher by comparison. Consequently, the same amount of decrease did not drastically alter the wetting behavior; the GC18–treated slides re-

mained intermediate–wet when water receded against Soltrol® even after prolonged storage in water.

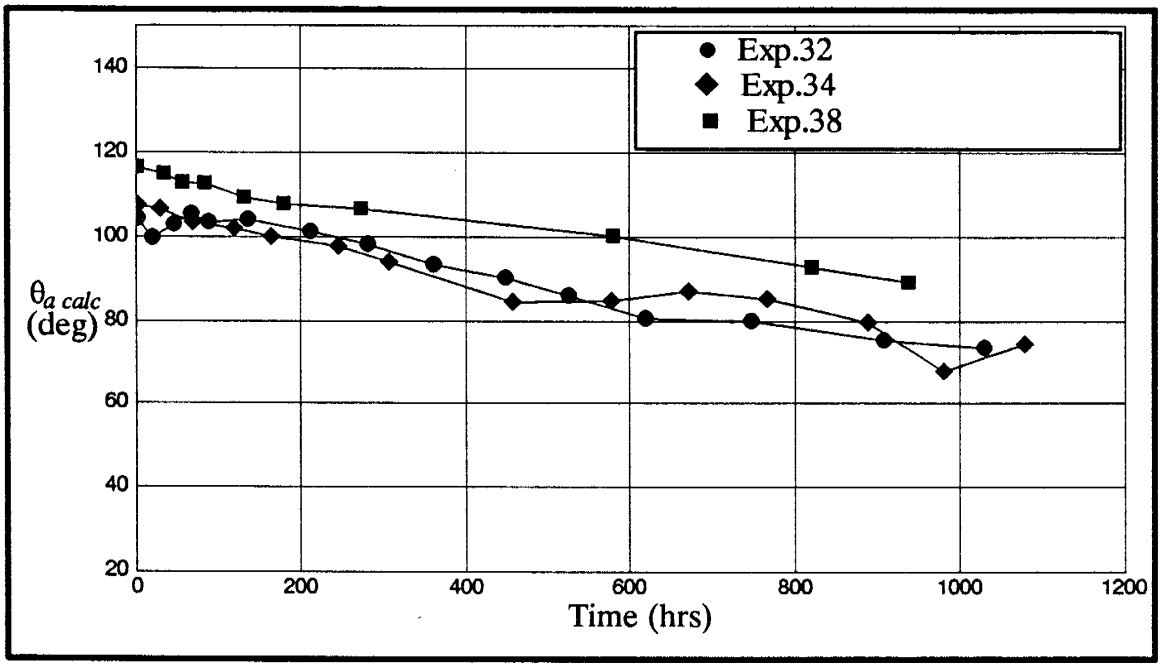

Figure 3.33. Stability of OtS–treated slides stored in deionized water.

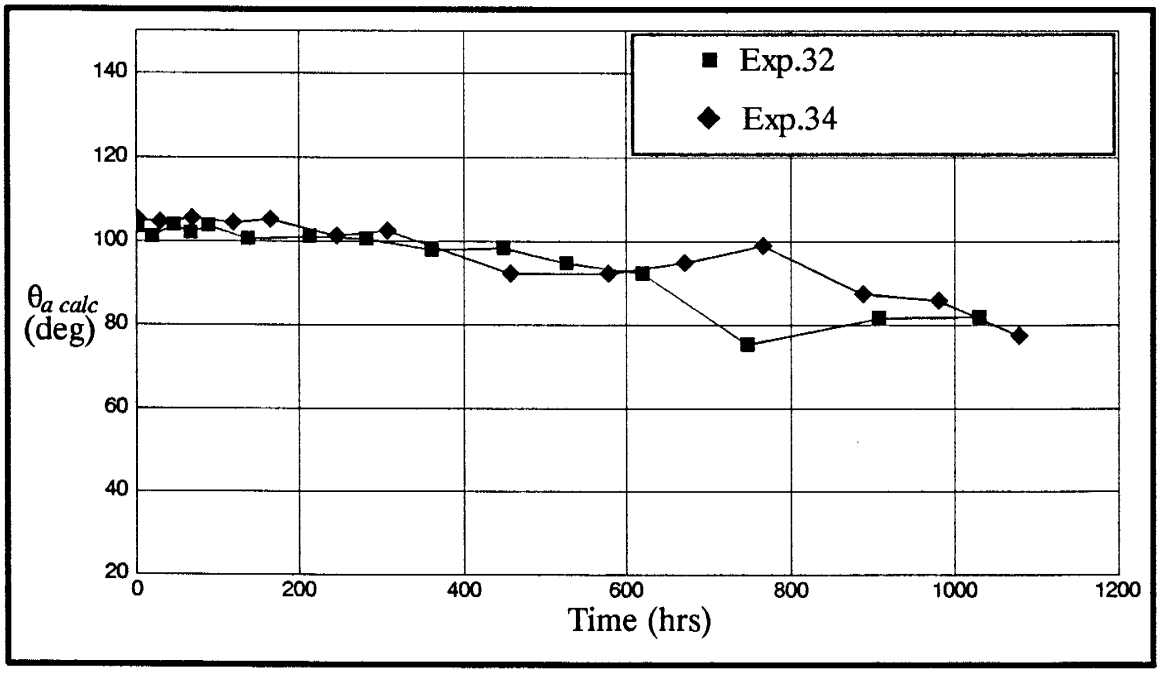

Figure 3.34. Stability of OtS–treated slides stored in $CaCl_2$ water.

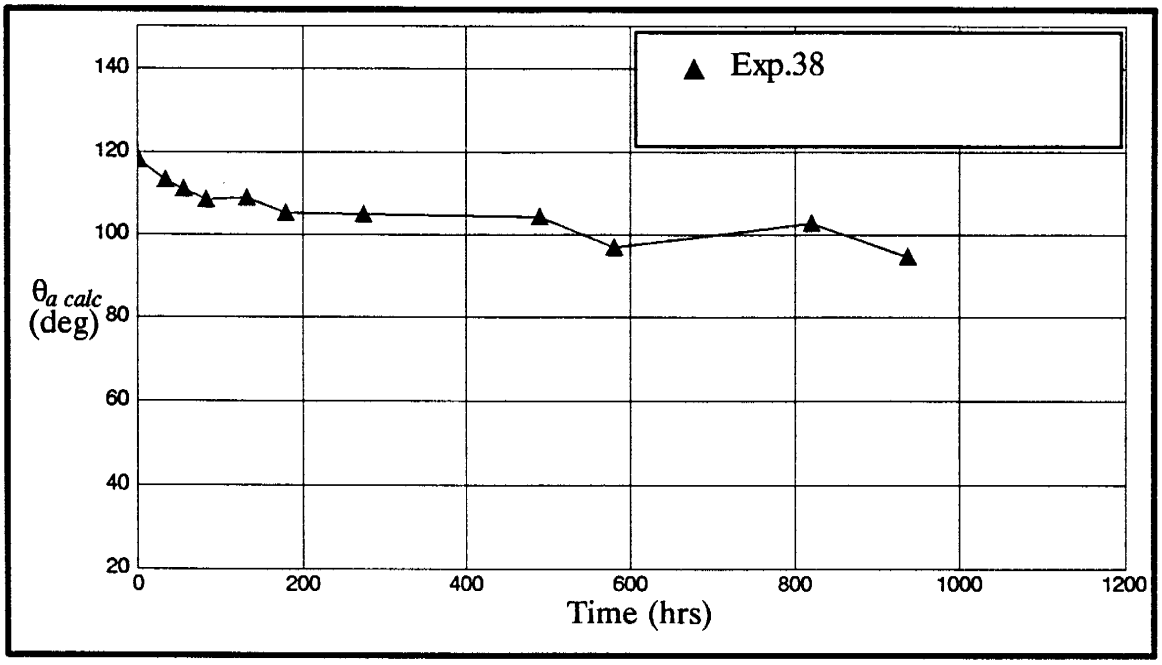

Figure 3.35. Stability of OtS–treated slides stored in NaN_3 water.

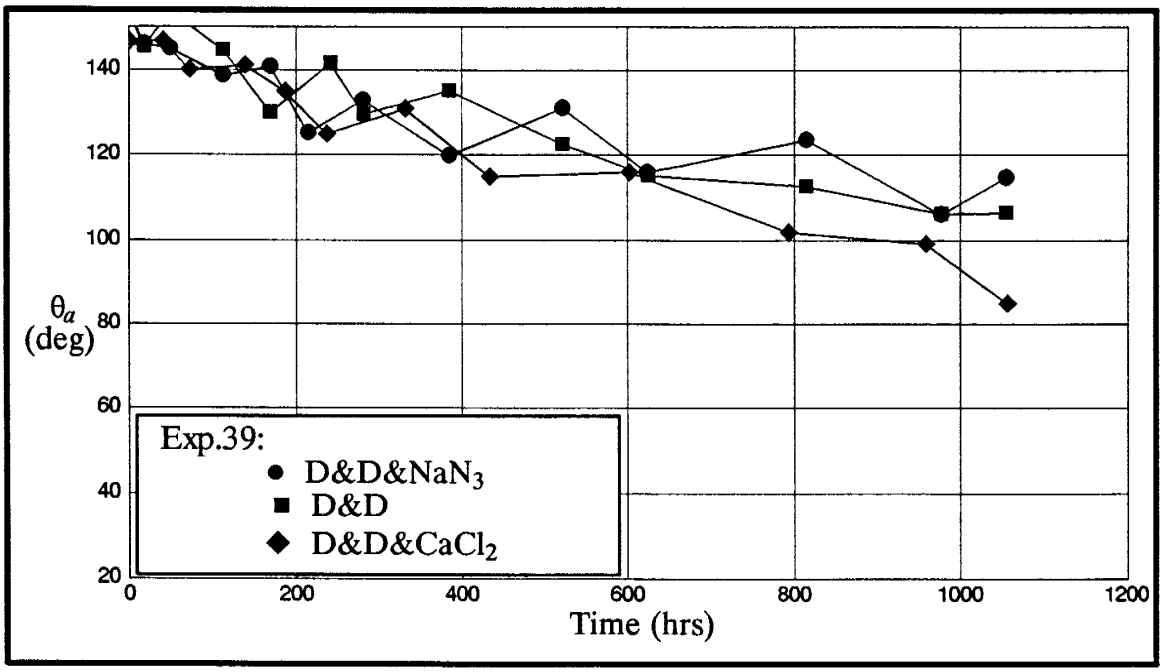

Figure 3.36. Advancing contact angle as a function of time for OtS–treated slides stored in water.

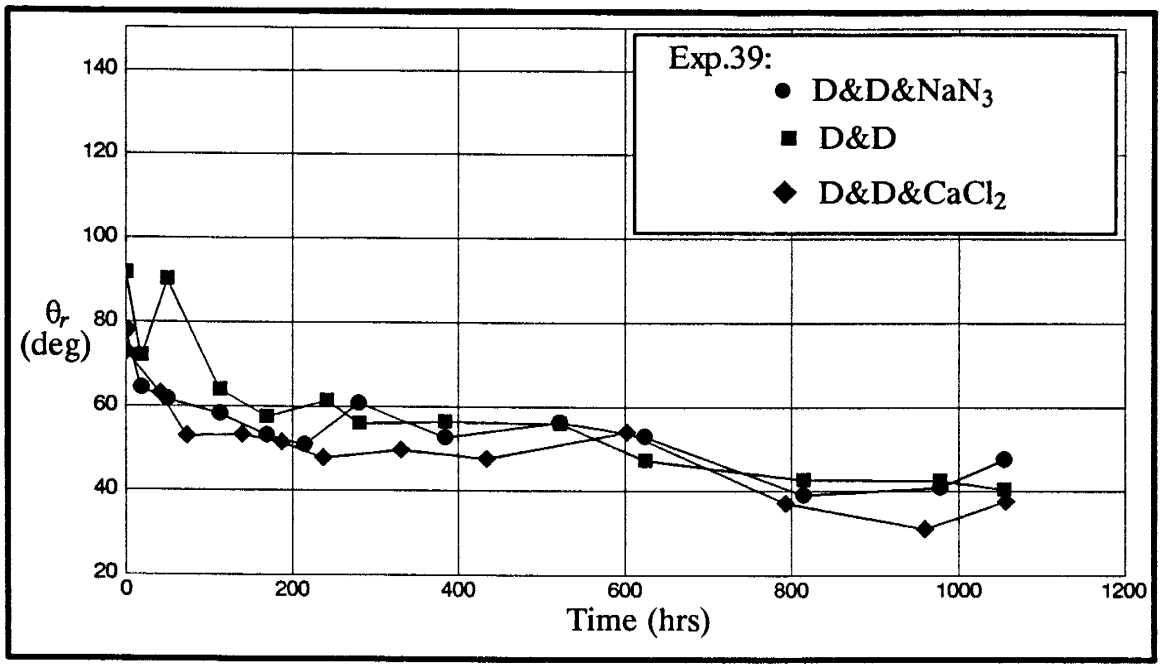

Figure 3.37. Receding contact angle as a function of time for OtS–treated slides stored in water.

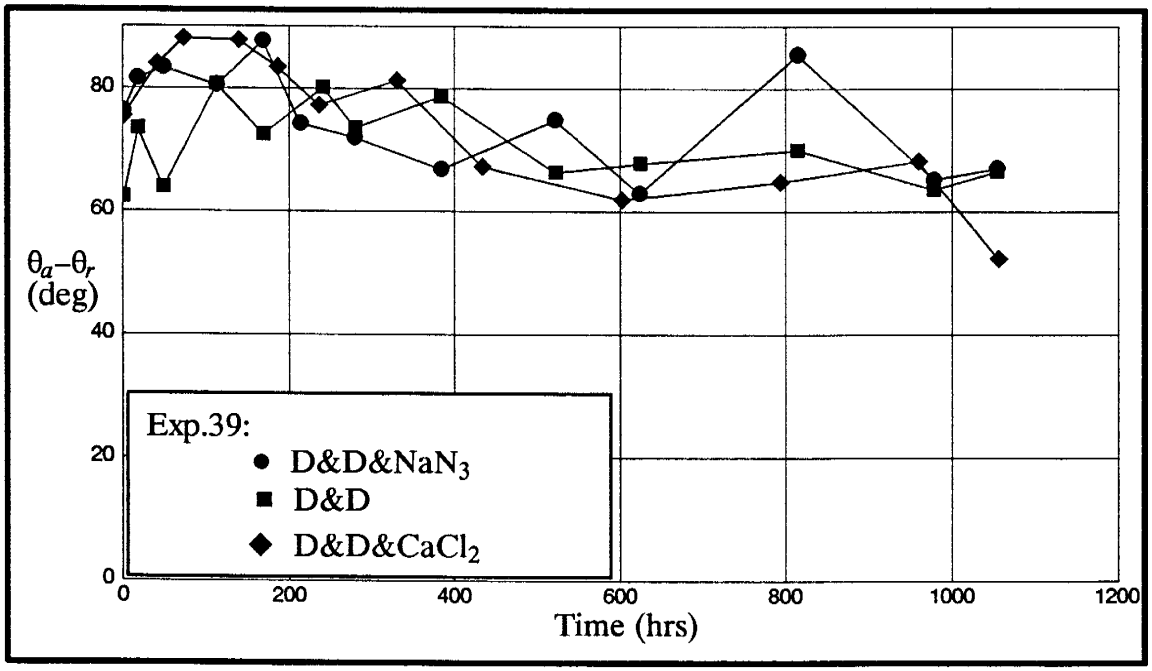

Figure 3.38. Contact angle hysteresis as a function of time for OtS–treated slides stored in water.

3.2.3.7 Presence of bacteria

At the conclusion of experiments 31A, 31B, and 38, slides stored in deionized water and $CaCl_2$ water were checked under a microscope for the presence of bacteria. Significant amounts of bacteria were present in all slides stored in water. However, bacteria were only reversibly (weakly) attached to the slides stored in deionized water from experiments 31A and 31B (GC18). Most of the bacteria could be removed by rinsing the slides with water. The advancing angle for these slides also did not decrease significantly with time (Figure 3.25). Bacteria were irreversibly (strongly) attached to OtS–treated slides stored in deionized water from experiment 38 and GC18–treated slides stored in $CaCl_2$ water from experiment 31B. Irreversibly attached bacteria could not be removed by rinsing with water. In both cases, a significant decrease in the advancing angle was observed over time (Figures 3.29 and 3.33).

After the presence of bacteria was known, treated slides were also stored in water with 1000mg/L NaN_3 as bacteriacide (see Brock, 1978) in later experiments to investigate the effect of the bacteria on stability.

3.3. Characterizing wettability with a homologous series of liquids – Zisman plots

Fox and Zisman (1950), in characterizing the wettability of polytetrafluoroethylene (Teflon®), proposed that the cosine of the advancing contact angle varied monotonically with the surface tension, σ, for a homologous series of liquids. In theory, the general relationship between the contact angle and surface tension is:

$$\cos \theta_a = 1 - \beta (\sigma - \sigma_c) \qquad (3.1)$$

where σ_c is the critical surface tension and β is a proportionality constant. Critical surface tension is, by definition, the minimum surface tension of the advancing liquid which does not spread and cosine $\theta_a = 1$. A liquid with surface tension less than σ_c will spread on the surface. A liquid with surface tension greater than σ_c will not spread and the fluid/liquid interface at the solid surface will exhibit a finite contact angle.

Critical surface tension is a direct measure of the *surface energy* of the solid surface. The greater the value of σ_c, the higher the surface energy. Teflon®, with a σ_c of 18 dynes/cm, has a low energy surface. Glass on the other hand, with a σ_c of 78 dynes/cm, has a high energy surface. The β is a measure of how much the contact angle increases for a given increase in surface tension. Both σ_c and β are unique for any given solid surface and together define the hydrophobicity of the solid. Equation 3.1 describes a straight line with a negative slope. This linear relationship applies to pure systems of fluid/liquid/solid where there is no chemical interaction between the liquid and the solid. As the surface tension increases, the cosine of the advancing angle decreases (advancing angle increases). For solids defined by equation 3.1, the hydrophobicity represented by the water–air contact angle increases for lower values of σ_c and higher values of β. Conversely, in this study where deterioration of the surface is of interest, a decrease in hydrophobicity should be evident by an increase in σ_c and possibly a decrease in β over time.

In our study, a mixture of methanol and ethanol in water was used to decrease the surface tension of the liquid. The cosine of the advancing angles measured with these liquids were plotted against surface tension from which the following could be investigated:

- the critical surface tension, σ_c, which is a parameter used universally to compare surface energies (wettability) of different solid surfaces

- how the advancing contact angle varies with the surface energy of the liquid and how wettability could be scaled. For example, in an air/liquid/Teflon® system, the liquid is the non–wetting phase if pure water is used. If, however, a water:ethanol mixture or pure ethanol was used instead of water, the air/liquid/Teflon®

system would be intermediate wetting to the liquid for the water–ethanol mixture and wetting to the liquid for pure ethanol

- chemical interaction between the liquid and the solid surface may be evident in deviation from the linearity of equation 3.1.
- changes in wettability over time for slides stored in water or air. A decrease in hydrophobicity of the surface (or increase in surface energy) shifts the plot to the right.

3.3.1. Results of Zisman plots for tBDM–, tBDP–, GC18–, and OtS–treated slides

The homologous liquids consisted of deionized water (0% alcohol), 7% methanol:93% water, 25% methanol:75% water, 50% methanol:50% water, and 50% ethanol: 50% water. Surface tension of the liquids was measured with a Fisher 20 tensiometer and shown in Table 3.6.

Table 3.6. Surface tensions for alcohol:water mixtures.

Liquid	*Surface tension (dynes/cm)*
deionized water	74
7% methanol : 93% water	62
25% methanol : 75% water	47
50% methanol : 50% water	37
50% ethanol : 50% water	31

Advancing angles were measured using the static sessile drop method (section 2.6). Measurements were made after silylation and at the end of the experiment after the slides had been stored in water or air. In experiments 31D and 38, measurements were also taken midway through the experiments. Results of the Zisman plots for treated slides before storage in water or air are plotted in Figures 3.39 to 3.43 and summarized in Table 3.7. The data in the figures have been connected with straight lines. Data for Teflon® from Fox and Zisman (1950) have been included in Table 3.7 for comparison.

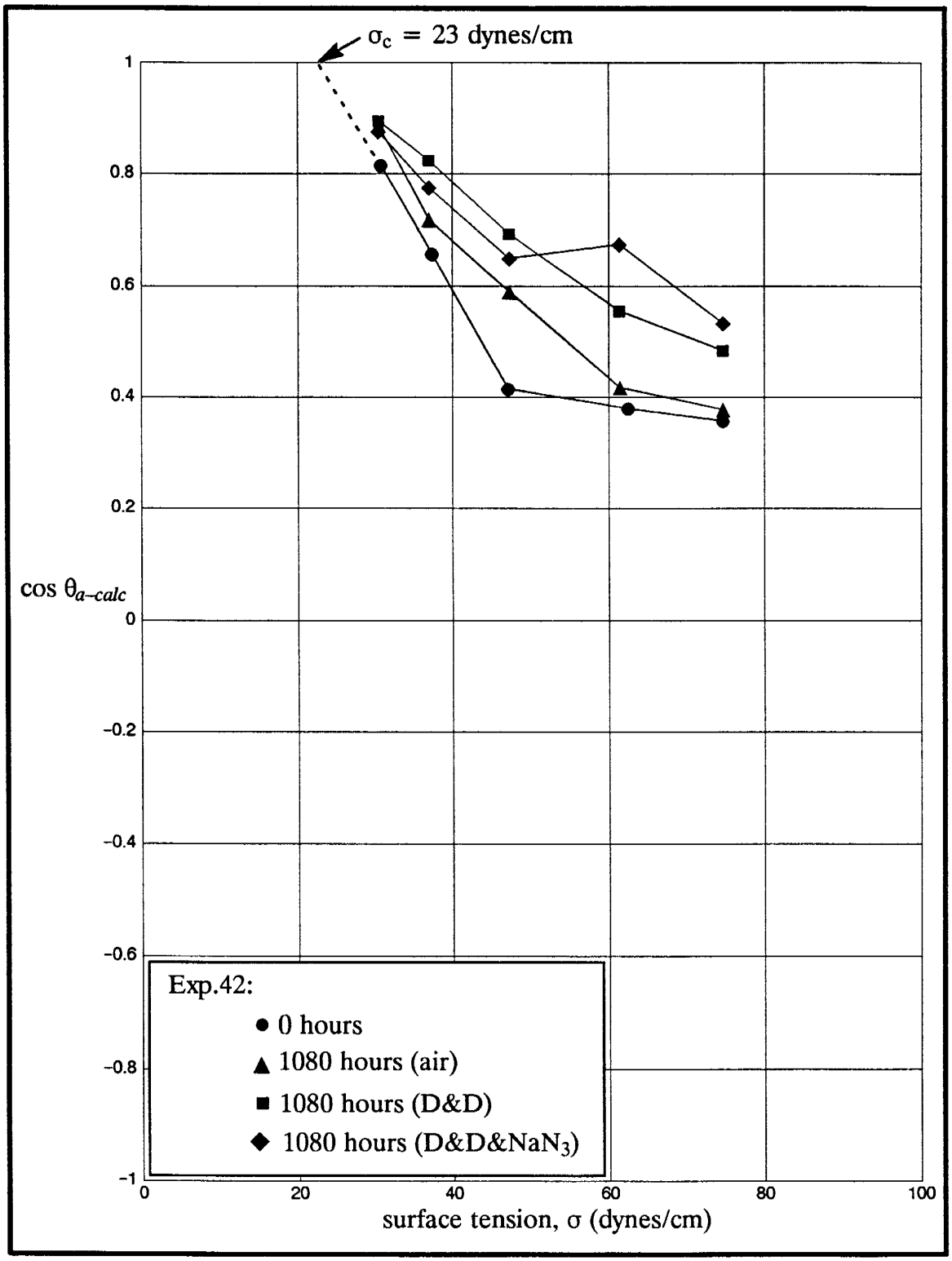

Figure 3.39. Zisman plots for tBDM–treated slides stored in air and water with 1000mg/L NaN_3.

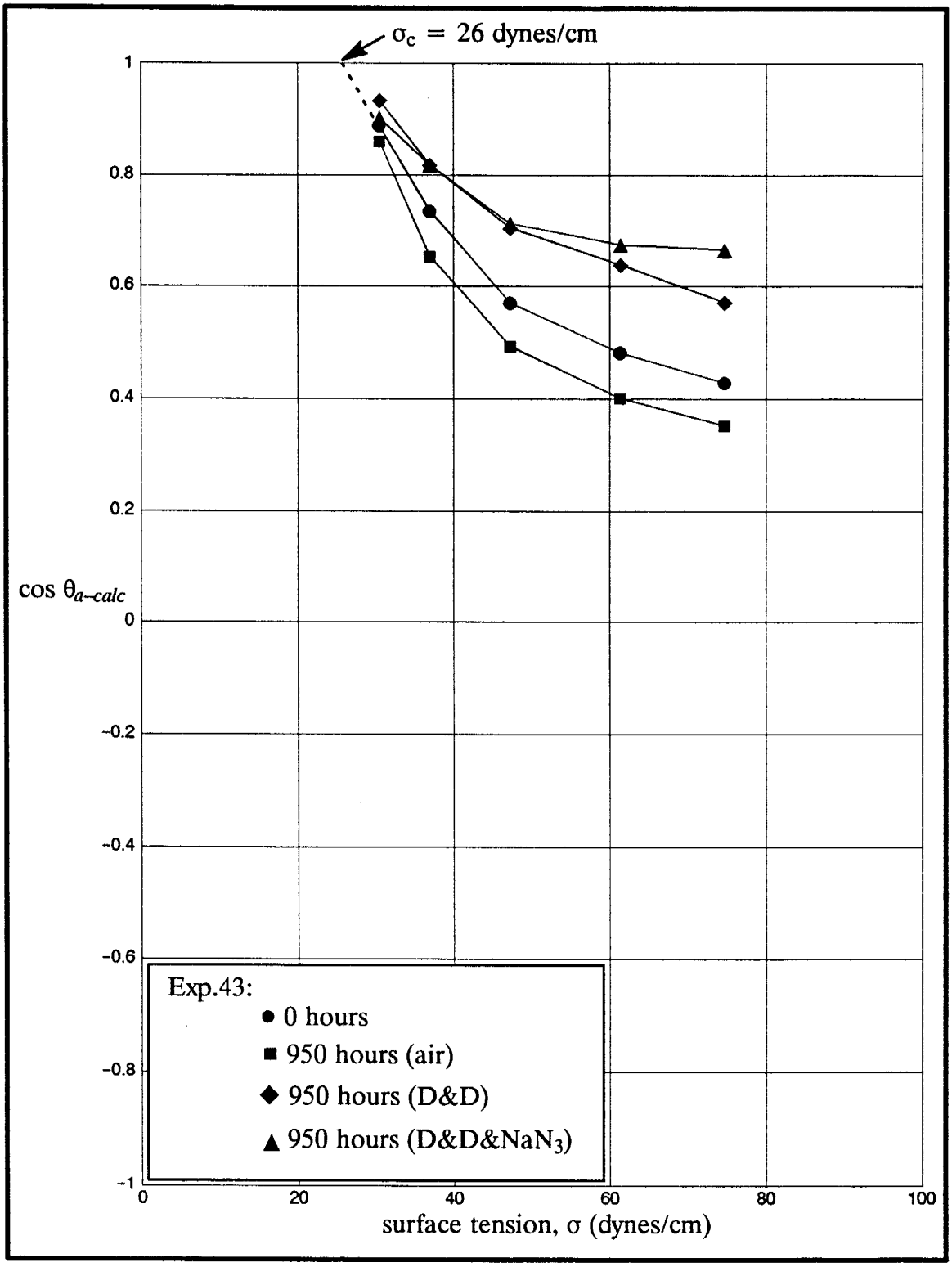

Figure 3.40. Zisman plots for tBDP–treated slides stored in air and water with 1000mg/L NaN_3.

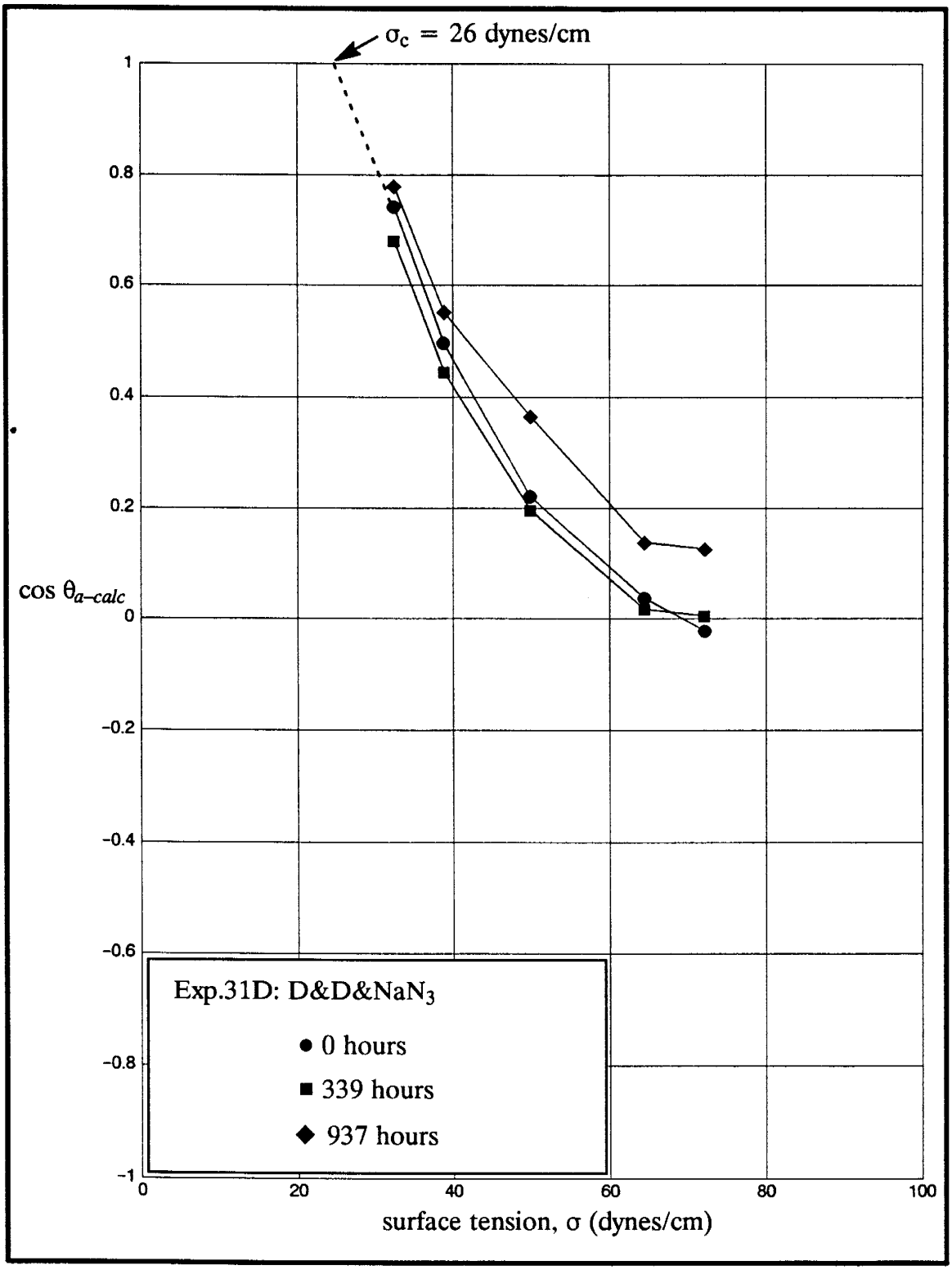

Figure 3.41. Zisman plots of GC18–treated slides stored in water with 1000mg/L NaN_3.

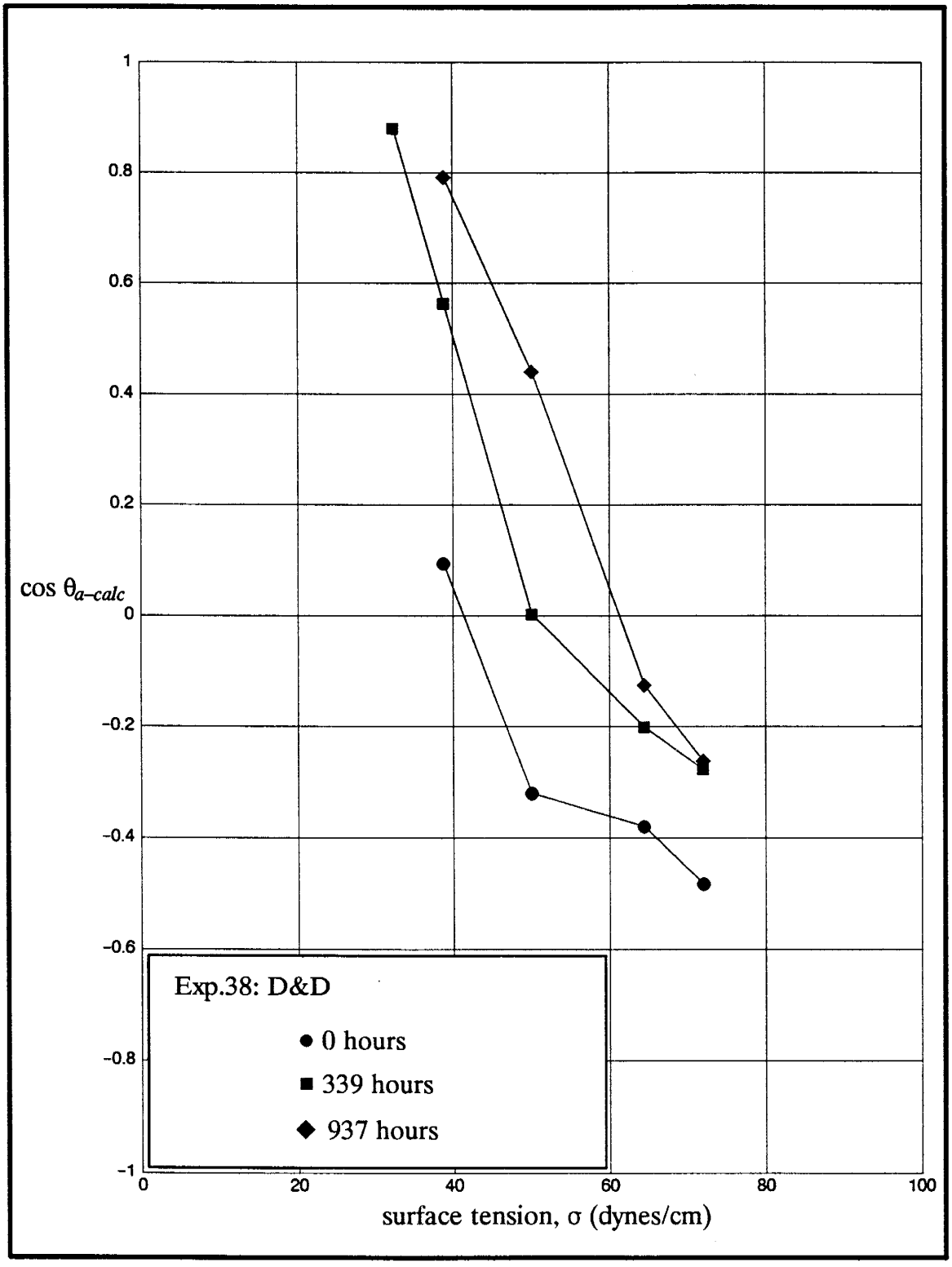

Figure 3.42. Zisman plots for OtS–treated slides stored in deionized water.

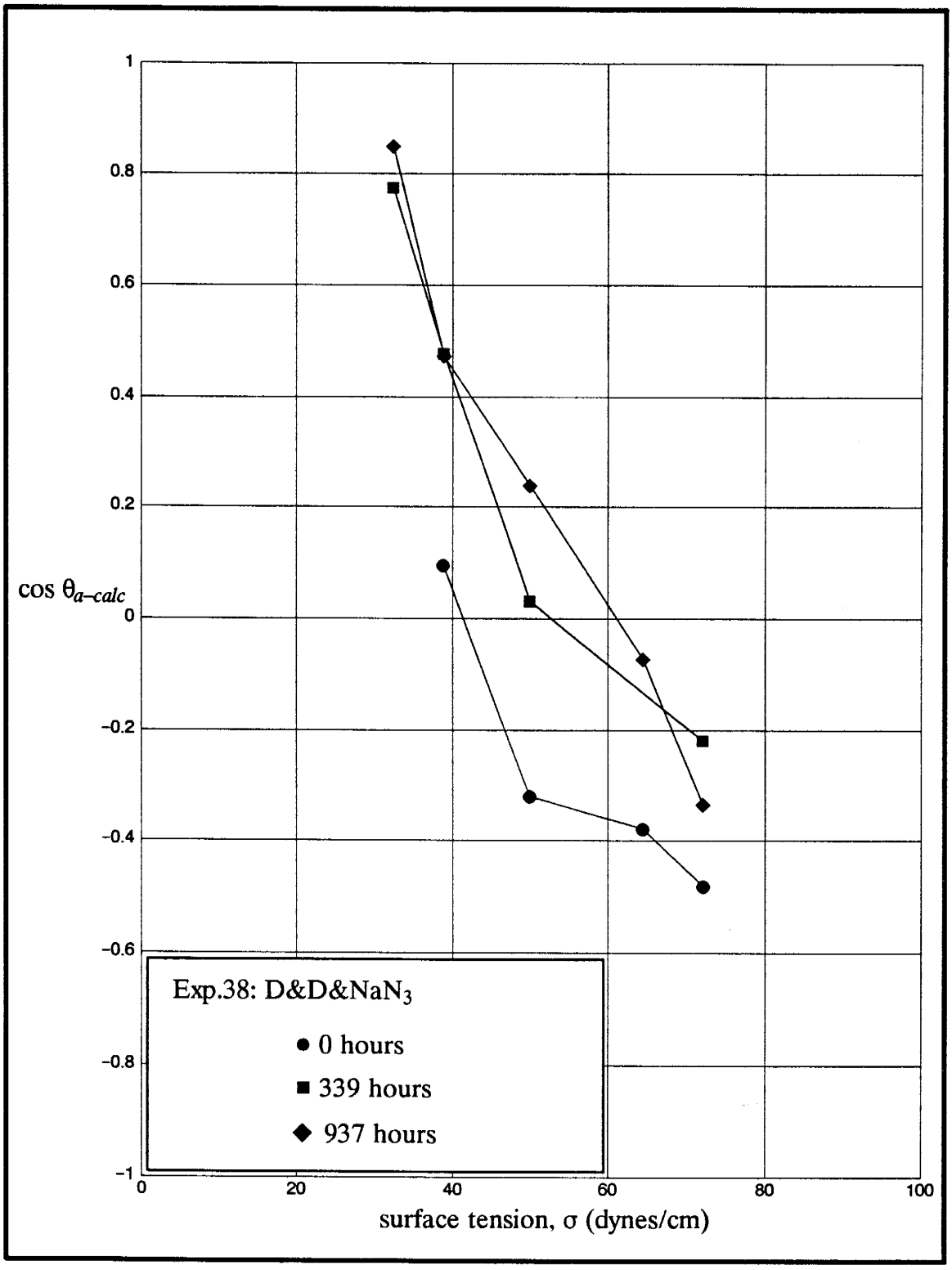

Figure 3.43. Zisman plots for OtS–treated slides stored in water with 1000mg/L NaN_3.

Figures 3.39 to 3.43 show that none of the plots are linear as described by equation 3.1. Generally, the slope of the line appeared to be quite straight for low surface tensions up to 40 – 50 dynes/cm. However, as surface tension increased to above 40 – 50 dynes/cm (more than 50 – 75% water in the water:alcohol mixture), the slope of the line decreased. The slope of the initial straight line segment (β) was greatest for OtS–treated slides and least for tBDM– and tBDP–treated slides. This trend resulted in the OtS–treated slides having the greatest water–air advancing angles and tBDM– and tBDP–treated slides having the lowest water–air advancing angles (see Table 3.2).

Table 3.7. Zisman plot analyses.

Exp.	*Silane*	σ_c *(dynes/cm)*	$\sigma_{\theta=45°}$ *(dynes/cm)*	$\sigma_{\theta=90°}$ *(dynes/cm)*	*Comments*
42	tBDM	23	34	N/A	nonlinear plot
43	tBDP	26	39	N/A	nonlinear plot
31D	GC18	26	33	70	nonlinear plot
38	OtS	15–30	32	41	nonlinear plot
–	Teflon®	18	27[3]	48[4]	nonlinear plot
–	untreated glass	78[5]			

3. From n–alkanes liquids (Fox and Zisman, 1950).
4. From ethylene glycol (Fox and Zisman, 1950).
5. From Petrarch Systems Silanes & Silicones (1987)

The critical surface tension for freshly treated slides was estimated by extrapolating the closest straight line segment back to where cosine $\theta_a = 1$. Critical surface tension for OtS–treated could not be estimated as accurately as the other silanes because the closest data point required greater extrapolation. Critical surface tension for tBDM–, tBDP–, and GC18–treated slides were remarkably similar (Table 3.7). Values ranged only from 23 dynes/cm for tBDM to 26 dynes/cm for tBDP and GC18. Critical surface tension for OtS–treated slides appear to fall somewhere between 15 and 30 dynes/cm. This was derived by linearly extrapolating the closest data point for 0 hours and 339 hours. Critical surface tension for Teflon® is 18 dynes/cm. It is usually presumed that the lower the critical surface energy, the more hydrophobic the surface is.

This is not always true. Even though the critical surface tension for tBDP– and GC18–treated surfaces was similar, wetting characteristics of both surfaces were different at higher surface tensions (Table 3.7). For example, the water–air contact angle was greater for GC18–treated than tBDP–treated slides even though the critical surface tension was similar. Hydrophobicity was governed not only by the intercept of the line at cosine $\theta_a = 1$ (σ_c) but by the slope of the line itself, β.

Zisman plots of advancing angles at the end of the experiments were also constructed (Figures 3.39 to 3.43). In all cases, for slides stored in water, the plots at the end of the experiment was to the right of the initial plot. In the latter plots, the critical surface tension was generally very close to, but slightly greater than, the original value; the overall slopes in the latter plots were also less. The critical surface tension appeared to have increased only slightly with time. The increase in σ_c for tBDM–, tBDP–, and GC18–treated slides stored in water appeared to be less than 5 dynes/cm after 1000 hours. The increase in σ_c for OtS–treated slides stored in water was difficult to evaluate.

The Zisman plots show that the hydrophobicity of the treated glass stored in water decreased (surface energy increases) with time. This was indicated by an increase in the value of the intercept and by the decrease in the overall slope of the curve. The change in surface energy also seems to have the greatest affect on the advancing liquid–air contact angle of liquids with moderate to high surface tension. In experiments 31D and 38, Zisman plots were also constructed for treated slides after 339 hours of storage in water (Figures 3.41, 3.42, and 3.43). For the GC18–treated slides in experiment, the Zisman plot at 339 hours was almost coincident with the original plot confirming that wettability had not changed after 339 hours of storage in NaN_3 water. This supports the data shown in Figures 3.27, 3.28, and 3.30 where changes in the advancing water–air angle were negligible after 300 to 400 hours. The plot for 339 hours was actually located very slightly to the left of the original plot but this was likely due to

variability in the contact angle measurements (Figure 3.41). Zisman plots for OtS–treated slides stored in water in experiment 38 was located to the right of the original plot (Figures 3.42 and 3.43). Data show that the degree of hydrophobicity of the treated slides had decreased after 339 hours of storage in water. The change in wettability for slides stored in deionized water and NaN_3 water was almost identical after 339 hours. Similar behavior was observed in the advancing water–air angle, which had decreased after 300 hours (Figures 3.33 and 3.35). Figures 3.39 and 3.40 indicate changes in wettability were negligible for tBDM– and tBDP–treated slides stored in air. This was consistent with the results in Figures 3.2 and 3.4 where the water–air contact angle did not change with time for tBDM– and tBDP–treated slides stored in air.

3.4 Discussion of results

The initial water–air advancing angles for tBDM– and tBDP–treated slides were very similar to the maximum angles at high silane concentrations reported by Menawat et al (1984) in their study. Differences, in degrees, were within the standard deviations reported in Table 3.2. Receding angles did not agree nearly as well. Significant contact angle hysteresis for tBDM–treated slides was observed by Menawat et al (1984) only at very low silane concentrations. This does not agree with the hysteresis of 17.9° measured in this work. Initial receding angles for tBDP–treated slides were similar to those obtained at low concentrations in Menawat et al (1984). One explanation for the discrepancy the in the receding angles is that contact angle measurements are subjective and depend on the observer. Differences of up to 10° are not uncommon. Another explanation is that treatment conditions can never be exactly duplicated. Adsorbed water on the glass surface, which is very difficult to detect, causes early deposition of silanes. The effective concentration or amount (actual number of active silane molecules capable of reacting with the glass in any given solution) was impossible to quantify.

Published values of water–air advancing angles for OtS–treated slides were also available for comparison (Spitze and Richards, 1947). Initial advancing angles were also very similar and within standard measurement variations. Although the standard deviation in contact angle measurements for OtS–treated slides were similar to that of other silanes, the average value of the contact angle between experiments was more variable. An apparent discrepancy in the advancing water–air contact angle exists between experiment 39 and experiments 32, 34, and 38 (compare Figures 3.36 and 3.33). This may be explained by the trifunctional character of the OtS silane. With three hydrolyzeable chlorine groups, OtS can form multimolecular layers on the glass. A thicker molecular layer could very well increase the hydrophobicity (and stability) of the glass. This may have occurred in experiment 39. The thickness can not be controlled however and varies between reactions. That was the primary reason why manufacturers used dimethyloctadecylchlorosilane (DMOS) instead of OtS to treat HPLC columns. DMOS is a monofunctional chlorosilane. Monofunctional silanes form monomolecular layers resulting in a more consistent, uniform treatment. Published values for receding angles on OtS–treated slides were not found. Published values of contact angles were also unavailable for GC18.

Contact angles in Tables 3.3 and 3.4 showed that wettability also depends on the type of immiscible fluids present in the porous media (see section 1.3.2). The untreated glass was more strongly wetting to water in the presence of air ($\theta_{w\text{-}a\ a} < 25°$) than in the presence of Soltrol® ($\theta_{w\text{-}o\ a} = 68.8°$). Similarly, the treated slides showed greater affinity for water in the presence of air than in the presence of Soltrol® ($\theta_{w\text{-}a} < \theta_{w\text{-}o}$).

Contact angle hysteresis observed in silane–treated slides did not appear to be caused solely by surface roughness or surface heterogeneity (see section 1). Surface roughness could be one factor because contact angle hysteresis was observed on the untreated glass slides (Table 3.4). Any effects of surface roughness on contact angle

hysteresis should be relatively constant for all slides and not systematic as observed for particular silane–treated slides. Surface heterogeneity was unlikely because repeated sessile drops in the same location on the slides gave the same advancing and receding angles each time. This contradicted the theory that contact angle hysteresis was caused by a temporary coating which dissolved upon first contact with water. Surface immobility on a macromolecular scale, however, could not be dismissed. Drag forces developed at the organic layer on the treated glass because of chemical interaction could hinder movement of the water/air interface and prevent the contact angle from reaching equilibrium. Non–linearity of the Zisman plots support the theory of chemical interaction between the liquid drop and the treated surface, especially for water for which hysteresis was observed. Contact angle hysteresis could also have been caused by surface roughness on a molecular scale. Differences in the size, length, area density, and chemical characteristics of the silanes could conceivably affect the advancing and receding angles. However, we could only speculate on the cause of hysteresis for silane–treated slides.

The critical surface tension estimated for the four silanes were all greater than the value for Teflon® ($\sigma_c = 18$ dynes/cm–Table 3.7). The published value of σ_c for GC18–treated glass was 31 dynes/cm by Petrarch Systems and Silanes (1987). This was higher than the value of 26 dynes/cm estimated from data in Table 3.7. One explanation could be that the glass slides in our experiments were put through repeated treatments. In the first few treatments, the water–air advancing angle increased steadily until a maximum value was reached. This likely reflected more and more complete coverage of the slides with each treatment. The value reported by Petrarch Systems Silanes & Silicones (1987) probably reflects only a one–time treatment. Critical surface tension for tBDM, tBDP, and OtS were not reported by Petrarch Systems Silanes & Silicones (1987) and therefore a comparison with our results was not possible.

Reporting only the critical surface tension as an index for wettability can be misleading. For example, σ_c for GC18 and tBDP–treated slides were similar but the advancing water–air contact angle was greater for GC18–treated slides than tBDP–treated slides (see Table 3.7 and Figures 3.40 and 3.41). If σ_c and β were reported together or if the contact angle at various surface tensions were tabulated for comparison as in Table 3.7, the wetting properties of the solid surface would be much less ambiguous.

All the Zisman plots constructed for the silane–treated slides in this study were nonlinear (Table 3.7 and Figures 3.39 to 3.43). At low surface tensions, the plots could be described as somewhat linear. At higher surface tensions however, the plots deviated from a straight line. The greatest deviation occurred for water:alcohol mixtures of greater than 50% water and could very well be attributed to hydrogen bonding between the liquid and the treated surface at high surface tensions. A different plot could result if non–polar liquids, such as n–alkanes, had been used as the test liquid instead of water–alcohol mixtures. However, the surface tension of n–alkanes only covers a very limited range of surface tensions (16–28 dynes/cm) while the range for water–alcohol is greater (24–72 dynes/cm). The effect of different test liquids on the linearity of the plot is a practical limitation of the Zisman plots.

The following trends reflect deterioration of silane–treated glass surfaces:

- decrease in advancing and receding contact angles
- increase in contact angle hysteresis
- increase in variability of contact angle measurements
- increase in critical surface tension and decrease in the slope of the Zisman plots.

Decrease in the advancing and receding angles with time reflected the breakdown of the treated surface. However, the receding angle was a more sensitive indicator of

deterioration. This was evident from Table 3.5 where the difference between the cosine of the initial and final water–Soltrol® angle was greater for the receding angles than the advancing angles. Also in experiments 31D and 40A with GC18, even though the advancing water–air contact angle seemed to indicate a stable surface, the receding angle revealed that the surface was gradually breaking down when stored in water (Figures 3.30 and 3.31). The presence of Soltrol® coating the tBDM– and tBDP–treated slides stored in water seemed too slow the rate of surface deterioration only slightly (compare Figures 3.12 and 3.16 to 3.23 and 3.25). The receding angle still decreased over time. The coating of Soltrol® appeared more effective on OtS–treated slides stored in water (compare Figures 3.19 and 3.33). Decrease in the advancing angle did not occur for the slides coated with Soltrol® while decrease in the advancing angle over time was evident for the uncoated slides. Unfortunately, only the advancing angles could be compared in this case. The effectiveness of the organic phase as a protective layer for the silane–treated surface immersed in water may depend on the degree of hydrophobicity of the surface.

Increase in contact angle hysteresis was an effective indicator of deterioration of the silane–treated slides. For example, in experiment 42, even though the advancing angle for tBDM–treated slides coated in Soltrol® and stored in deionized water (Figure 3.12) did not change significantly, the increase in contact angle hysteresis (and decrease in the receding angle) with time showed that wettability was changing and that breakdown of the treated surface was occurring. Breakdown of the treated surface reflected in increasing hysteresis was also reported by Takach et al (1989). Unfortunately, it was not possible to compare the results of Tackach et al (1989) with the results here because the methods of stability analysis were different. Tackach et al (1989) did not use contact angles but the difference in the force required to push and pull a treated slide across a liquid–air interface in their stability analysis. An anomaly was found in experiment 39 where contact angle hysteresis actually decreased after reach-

ing a maximum value after 150 hours (Figure 3.38). This was because the rate of decrease of the exceptionally high advancing angle was slightly greater than that for the receding angle. Deterioration was still reflected by the initial increase in hysteresis in the first 150 hours of storage in water.

Deterioration of the treated surface was also reflected in increased variability of the contact angle measurements (Figure 3.8) and placement of non-spherical sessile drops (part of the drop would spread and other parts would not). This showed that the wettability characteristics of the surface generally became more inconsistent as the surface deteriorated. Variability was not a very sensitive indicator because the variability in measurement and variability caused by surface deterioration were often not distinguishable.

The change in critical surface tension of the treated slides was also not a very sensitive indicator of surface deterioration. Critical surface tensions for tBDM-, tBDP-, and GC18-treated slides only appeared to increase slightly after 1000 hours of storage in water (see Figures 3.39 to 3.43). This change may be further obscured by the fact that low contact angles are very difficult to measure. On the other hand, the decrease in the slope of the Zisman plots for the treated slides stored in water was much more evident. This suggests that any changes in wettability could be more easily detected by contact angle measurements with a high surface tension liquid than a low surface tension liquid.

The cause of instability of treated slides stored in water cannot as yet to be pinpointed. Experiment 37 showed that different siliceous substrates did not affect the initial advancing contact angle nor the stability of TMS-treated surface in water (Figure 3.21). Spitze and Richards (1947) also showed that there was almost no difference in the initial advancing contact angle between sodalime glass, Pyrex® glass, and E-glass silylated with OtS at temperatures below 100°C.

The presence of irreversibly (strongly) attached bacteria on the treated slides stored in water implied that bacteria could be a cause of instability. However, the fact that the advancing angle decreased and contact angle hysteresis increased with time for treated slides stored in water containing bacteriacide (NaN_3) for all the silanes (experiments 31D, 39, 40A, 42, and 43) complicates this argument. The NaN_3 in the water could have also promoted deterioration of the treated surfaces somehow. These two factors could not be evaluated independently. The role of bacteria in the stability of treated slides stored in water remains inconclusive.

Menawat et al (1984) presented two other reasons for why the contact angle decreased with time: hydrolysis and desorption of weakly adsorbed silane molecules. Hydrophobicity of the treated surface could decrease if the silanes were not covalently bonded but only weakly adsorbed onto the glass surface. The silanes could then gradually desorb over time leaving less and less silanes on the treated surface. This appeared unlikely in our case because deterioration of the treated surface occurred only in water but not in air or organic liquid. Furthermore, the decrease in contact angle did not change even after the silylation procedure was refined to improve reaction. If desorption was the major reason, stability should have increased noticeably with improved silylation procedures.

Hydrolysis could occur in the presence of moisture as follows:

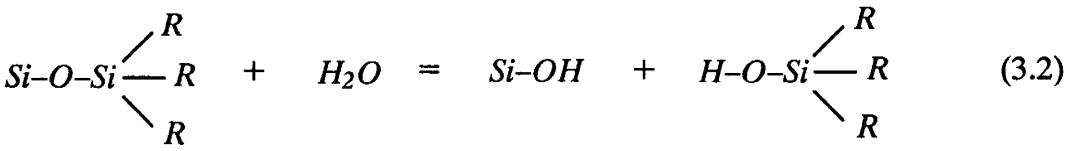

(3.2)

This process of hydrolysis would affect treated slides stored in water and, to a lesser extent, air. Slides treated with smaller, lighter silane molecules, such as TMS, would be more susceptible to hydrolysis because water could penetrate past the smaller silane molecules more easily. This trend was observed. TMS–treated slides deteriorated very rapidly (within 100 hours–see Figure 3.20) in water while slides treated with larger

silanes such as tBDM and tBDP remained more stable. If hydrolysis caused the breakdown, deterioration should be minimized if all the silanol sites on the glass surface were reacted with the silane. This implies that achieving different degrees of wetting by varying the concentration or amount of silane in the reaction may not be as feasible as was believed especially if long–term stability is critical as was the case here. Treatment with lesser amounts of silane than required for complete coverage would leave areas of unreacted silanol sites and a discontinuous molecular layer. Water could then penetrate the glass surface in these uncovered areas and attack the silanes to more easily break down the surface.

The amount of chlorosilanes used in the experiments was determined empirically (refer to Table 3.1). Although in theory, excess chlorosilane would be unnecessary for treating the slides, in practice, this is not so. Chlorosilanes may be used up in reaction with the Mason jar in which the reaction occurred and with any glassware during solution preparation. Bulk early deposition of the chlorosilanes also occurs in the presence of any water, which can never be completely eliminated, during solution preparation. Deposition may also occur in the storage bottles if any moisture is present. Consequently, an excess of chlorosilane was necessary for reaction with the slides themselves. The amount excess for each chlorosilane in Table 3.1 was what yielded uniform, maximum advancing angles for that particular silane under existing laboratory conditions.

There is a false notion that hydrophobicity is proportional to the number of carbon atoms in the silane or the silane's molecular weight. Figure 3.44 shows that the relationship between hydrophobicity (represented by σ_c) and molecular weight is much more complex. The graph was compiled from data published in Petrarch Systems Silanes & Silicones (1987). Figures 3.41 and 3.42 offer another example of why wettability and molecular weight of the silane are not necessarily related. Although GC18 and OtS are both C_{18} silanes, their wettability behavior for the whole spectrum of water:al-

cohol liquids were markedly different. The difference in wettability behavior in this case may be more a reflection of the reaction mechanism and molecular structure than molecular weight.

Table 3.3 showed that advancing angles measured with the dynamic sessile method gave consistently higher values than the static sessile method. This difference was especially pronounced for OtS–treated slides. Theoretically, both methods should yield identical results. It was possible that the method of placing the static sessile drop by lowering the lab jack (section 2.6) did not always result in a fully advancing angle but an angle a few degrees lower. Lowering of the lab jack also changed the angle of view of the sessile drop through the microscope which could have affected the measured dimensions of the drop used to calculate the advancing angle. Light reflecting off the top of the static drop could also cause the height of the drop to be underestimated resulting in a lower calculated angle. Finally, gravity affects could cause angles calculated from larger static drops to be lower than they actually are. The relative importance of these factors have not been differentiated and remain practical limitations of the static method.

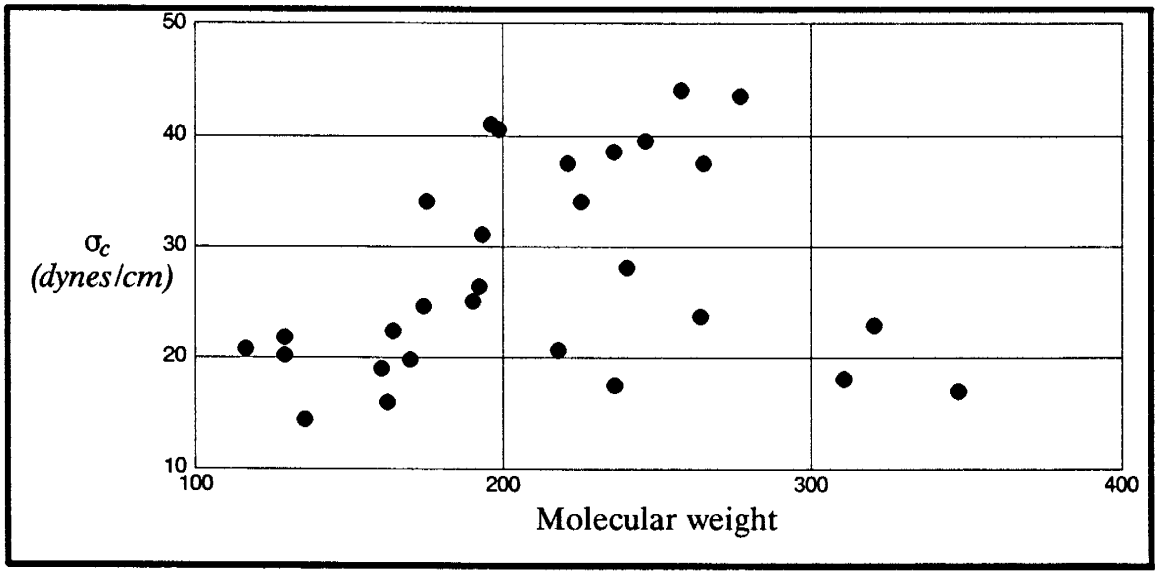

Figure 3.44. Critical surface tension as a function of molecular weight of silane.

It is evident from Tables 3.1 and 3.2 that silylation and measurement procedures were still being developed in the early experiments (refer to Table 3.2). The addition of pyridine to the chlorosilane reaction and the methanol rinse after the reaction were not implemented until experiment 34. Long-term measurement of stability in water was not standardized until experiment 31A. Receding angles could not be measured until experiment 31D when the goniometer was available. Hence, the main reason for experiments 42 and 43 was to gather data for receding angles and contact angle hysteresis for tBDM- and tBDP-treated slides, which were not obtainable in earlier experiments (experiments 8, 18, and 20), to complete the characterization of the treated slides. This was not done for TMS because it was obvious this silane would not be used for treating porous media. Much more attention was focused on stability in water than stability in air or organic liquids (Table 3.2). Once stability in organic liquid and air was established early on for some of the silanes, most of the contact angle measurements in subsequent experiments with other silanes were restricted to slides stored in water where deterioration of the surface was observed. Instability of the treated slides stored in water forced us to examine different silanes and refine our procedures for silylation and storage to improve stability. Most of the refinements were implemented in the later experiments where stability in air and organic liquids were ignored. The refinements in procedure did not have significant affects on the results on the contact angle and stability (Figures 3.22 (tBDM), 3.27 and 3.28 (GC18), and 3.33 (OtS) for example).

3.5 Suitable silanes for treating porous media

Table 3.5 shows that the magnitude of deterioration ($\cos\theta_{initial} - \cos\theta_{final}$) for slides stored in water was about the same for all three silanes. However, deterioration in the tBDM- and tBDP-treated slides caused wetting behavior to change from intermediate-wet to water-wet when water receded against Soltrol®. Deterioration in the GC18-treated slides did not drastically change wetting behavior as the surface re-

mained intermediate-wet when water receded against Soltrol®. Experiments with the treated slides coated with Soltrol® and stored in water suggest that deterioration of the treated surface in water with Soltrol® present will be even slower. Deterioration would also be limited by the duration of the short column experiments which normally take about 2 to 3 weeks to complete (300 to 500 hours). Results of the silylation experiments show that tBDM, tBDP, and GC18 would yield hydrophobic glass surfaces that will remain sufficiently stable in air, organic liquids, and water for short column and micromodel experiments.

GC18 can be used to treat glass beads and micromodels to render them oil-wet; tBDM can be used to achieve intermediate wettability. The tBDM was chosen instead of the tBDP because it showed greater contact angle hysteresis. Hysteresis developed within the first few days after exposure to water and remained constant up to 800 hours. Hysteresis in tBDP-treated slides developed gradually. The effect of hysteresis on fate and transport of immiscible liquids would be an additional focus in the study. OtS was not chosen even though it created extremely oil-wet surfaces because it was less stable and more variable than GC18 (see for example, Figures 3.41 and 3.43). TMS was also not chosen because it remained stable in water for only a few days, not long enough for short column experiments (Figures 3.20 and 3.21).

4. Short column results and discussions

Two–phase water–Soltrol® displacement experiments were conducted in short columns to measure saturations and capillary pressures in uniform glass beads. Experimental methods were presented in section 2. Soltrol® was introduced into an initially water–saturated column packed with glass beads to displace water until irreducible water saturation (IWS) was reached. Soltrol® displacement by water then ensued until residual oil saturation (ROS) was reached. This sequence of liquid displacement simulated contamination of the aquifer by NAPL followed by flushing and partial removal of the contaminants by ambient groundwater flow. In some experiments, water displacement by Soltrol® was repeated (secondary displacement).

Wettability conditions were varied in the experiments in order to investigate the influence of wettability on residual saturations and capillary pressures. Identical size glass beads were treated with silanes to achieve non–water–wet conditions. Three wettability conditions were investigated. GC18 was used to achieve oil–wet conditions and tBDM was used to achieve intermediate–wet conditions. These silanes were found to remain relatively stable in water and had different wettability characteristics (see section 3). For the water–wet case, beads were cleaned but left untreated.

4.1 Residual saturations

Results of residual saturations (IWS and ROS) for the experiments are summarized in Tables 4.1, 4.2, 4.3, and 4.4 and Appendix C. The ΔT in the tables represents the recorded temperature variation in the constant temperature cabinet during the period of the experiments. The other abbreviations in the tables have been previously defined in section 2. Averaged values for ROS (reported in percent Soltrol®), IWS, bulk density (ρ_b), and porosity (n) are included in the last row of each table.

Table 4.1. Short column experiments with untreated beads.

Exp. No.	V_{ce} *(cc)*	*PV (cc)*	ρ_b *(g/cc)*	*n (–)*	*IWS (%)*	*ROS (%)*	ΔT *(°C)*
MW13	115.48	40.60	1.595	0.352	5.1	17.5	1.6
MW14	90.13	32.18	1.582	0.357	7.4	17.2	1.8
MW17	103.80	36.54	1.594	0.352	5.8	18.8	0.8
MW18	110.71	39.24	1.588	0.354	9.5	18.7	1.0
MW19	112.05	40.11	1.579	0.358	7.1	19.1	1.2
MW21	103.33	36.33	1.595	0.352	6.7	16.5	1.6
MW22	107.87	38.15	1.590	0.354	7.7	17.2	0.3
MW23	103.08	37.35	1.569	0.362	7.2	17.9	0.1
MW24	110.42	39.41	1.582	0.357	6.2	18.6	1.3
MW25	103.47	36.79	1.585	0.356	6.1	16.8	4.8
MWO15	82.99	30.22	1.571	0.364	10.9	20.2	4.8
MWO30	91.76	33.98	1.555	0.370	10.5	12.9	4.9
Average	–	–	1.586 ± 0.008	0.355 ± 0.003	7.5 ± 2.0	17.6 ± 1.8	–

Table 4.2. Conventional short column experiments with GC18–treated beads.

Exp. No.	V_{ce} *(cc)*	*PV (cc)*	ρ_b *(g/cc)*	*n (–)*	*IWS (%)*	*ROS (%)*	ΔT *(°C)*
MWO7	113.47	37.95	1.637	0.334	10.4	32.2	–
MWO8	103.48	35.60	1.614	0.344	4.0	29.9	2.9
MWO9	111.03	37.86	1.621	0.341	3.1	31.1	2.9
MWO10	107.88	37.37	1.608	0.346	11.4	31.2	–
MWO11	106.09	35.23	1.643	0.332	8.9	33.7	–
Average	–	–	1.625 ± 0.015	0.339 ± 0.006	7.4 ± 4.0	31.6 ± 1.4	–

Table 4.3. Dual filter short column experiments with GC18–treated beads.

Exp. No.	V_{ce} *(cc)*	*PV (cc)*	ρ_b *(g/cc)*	*n (–)*	*IWS (%)*	*ROS (%)*	ΔT *(°C)*
MWO12	106.19	35.87	1.636	0.338	9.3	9.9	2.4
MWO13	90.35	31.69	1.604	0.351	3.7	10.4	9.6
MWO16	89.72	30.58	1.628	0.341	2.3	10.9	4.3
MWO32	92.08	31.92	1.614	0.347	11.3	9.1	5.5
Average	–	–	1.621 ± 0.014	0.344 ± 0.006	6.6 ± 4.3	10.1 ± 0.7	–

Table 4.4. Summary of short column experiments with tBDM–treated beads.

Exp. No.	V_{ce} *(cc)*	*PV (cc)*	ρ_b *(g/cc)*	*n (–)*	*IWS (%)*	*ROS (%)*	ΔT *(°C)*
MWO21	83.20	30.36	1.569	0.365	76.1	9.6	3.5
MWO22	88.81	32.50	1.566	0.366	12.2	17.9	4.5
MWO26	112.77	40.26	1.588	0.357	6.3	18.9	4.1
MWO29	84.39	30.92	1.565	0.366	22.5	23.2	4.4
MWO40	114.17	41.36	1.575	0.362	11.4	N/A	3.2
Average	–	–	1.573 ± 0.009	0.363 ± 0.004	10.1 ± 3.3[1]	18.4[2]	–

1. Based on MWO22, 26, and 40.
2. Based on MWO22 and MWO26.

4.1.1 Untreated glass beads

The IWS and ROS, based on 12 trials, were $7.5 \pm 2.0\%$ and $17.6 \pm 1.8\%$ respectively (Table 4.1). In experiments MW13, 14, 25, and MWO30, the displacements were incremental, allowing construction of S_w–ψ curves (Appendix C). Capillary pressure head was measured after each incremental displacement had stabilized. In the other columns, displacement was carried out continuously until residual saturation was reached. Displacement of Soltrol® by water was typically controlled at 0.3 mL/min with a syringe pump. There was no difference in the values of residual saturations obtained from incremental and continuous displacements. The latter method was used only to determine the residual saturations without measuring capillary pressures.

Experiments MWO15 and MWO30 were performed using the dual filter column set–up. The values of IWS (10.7%) and ROS (16.6%) averaged from those two experiments were similar to the values measured with the conventional columns. The value of IWS from the dual filter columns was slightly higher than IWS values from the conventional columns (Table 4.1). The ROS value of 12.9% from MWO30 and 20.2% from MWO15 were the lowest and highest values of ROS measured in the untreated beads. These differences in residual saturations will be discussed in section 4.4.

4.1.2 GC18–treated glass beads

GC18–treated beads were initially packed in conventional columns. In these experiments, Soltrol® displacement by water was controlled with a syringe pump.Values for IWS and final ROS from these experiments, based on five trials, were 7.4 ± 4.0% and 31.6 ± 1.4%, respectively (Table 4.2). At the normal water flood rate of 0.3 mL/min, water broke through the top endcap after only a couple of mL of water had been flooded through. Most of the Soltrol® in the column was by–passed leaving a very large amount of residual Soltrol® (Figure 4.1). The flow rate of the water flood was progressively increased to 60 mL/min, the maximum for the syringe pump, to displace the Soltrol® out of the column. Even at the highest flow rate, premature breakthrough of water was still observed although more and more Soltrol® in the column was being displaced. For example, in experiment MWO10, the flow rate was systematically increased from 0.3 mL/min to 60 mL/min after every 50 mL of water ($\sim$ 1.4 *PV*) was flushed through the column. The ROS decreased after each increase in flow rate (Figure 4.1). Although the decrease in ROS appeared to be leveling off at the rate of 60 mL/min, an equilibrium value of ROS was not completely achieved. ROS at flooding rates greater than 60 mL/min could not be measured.

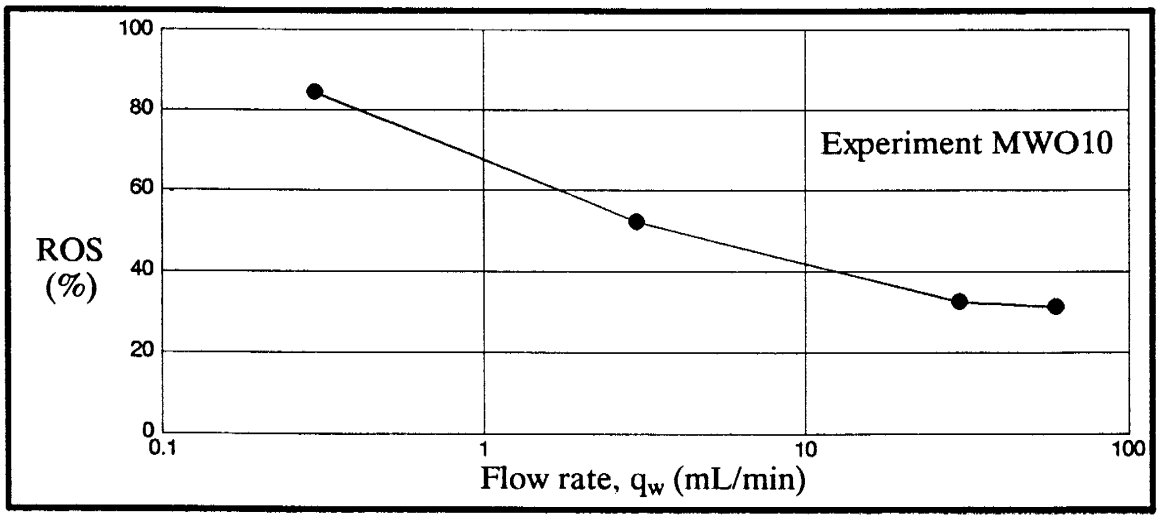

Figure 4.1 ROS as a function of water flood rate for GC18–treated bead packs.

In contrast, the average values of IWS and ROS, based on four trials with the dual filter columns, were $6.6 \pm 4.3\%$ and $10.1 \pm 0.7\%$, respectively (Table 4.3). The IWS was similar to the value determined for the water–wet case. The ROS, however, was almost half of that measured for the untreated case and three times lower than for the same GC18–treated beads measured with the conventional columns. Displacement in all of the four columns occurred incrementally and capillary pressures were measured.

4.1.3 tBDM–treated glass beads

Measurements for IWS and ROS for tBDM–treated bead packs were variable. Limited results were obtained from only three columns. Most of the experiments attempted with the dual filter column would not drain completely (see eg. MWO21 and MWO29 in Table 4.4). The average value of IWS from the three columns that did fully drain was $10.1 \pm 3.3\%$. This was slightly greater than the values of IWS measured in the columns for the other wettability cases and may reflect the difficulty in draining these columns (compare IWS values in Tables 4.1, 4.2, 4.3, and 4.4). Two of the successful experiments were conducted with conventional columns (MWO26 and MWO40). The average value of ROS from MWO22 and MWO26 was 18.4%. Although this value was almost identical to the value of ROS for the untreated case, the results should be viewed with skepticism.

4.2 Capillary pressures during water–Soltrol® displacements

Water saturation–capillary pressure head (S_w–ψ) data for the short column experiments are plotted in Figures 4.2 to 4.11 and tabulated in Appendix C. As mentioned in section 2, each data point on the plots was measured after the liquid levels in the burets had stabilized at the end of each incremental displacement step. Time for stabilization depended on the liquid saturation in the column and the capillary pressure head. Figure 4.12 shows typical water level equilibration curves for untreated (MWO30) and GC18–treated beads (MWO32) in the dual filter columns. Measure-

ments from both experiments were during secondary displacement of water by Soltrol® near $S_w \sim 50\%$ where significant displacement occurred. The data represent the increase in volume of water in the buret during the incremental displacement step. Measurements were from a few minutes after displacement began to just before the next incremental displacement step. Stabilization was typically approached within hundreds of minutes after the incremental displacement began (Figure 4.12).

4.2.1 Fitting van Genuchten's model to the S_w–ψ data

It was difficult to compare S_w–ψ data from different experiments in Figures 4.2 to 4.11 because the paucity of data points did not define completely the saturation–capillary pressure relationship. Before the data was analyzed, the van Genuchten least square fit program was used to fit van Genuchten's (1980) analytical function to the data. This provided a consistent basis from which to present and interpret results from the S_w–ψ measurements.

Van Genuchten (1980) adopted the following analytical function to describe the saturation–capillary pressure head relationship of soils:

$$(\theta - \theta_r) /(\theta_{max} - \theta_r) = [1 + (\alpha h)^n]^{-m} \qquad (4.1)$$

where θ is the volumetric soil water content, the subscripts r and max represent the residual and maximum soil water contents respectively, and h is the capillary pressure head. The symbols h and ψ represent the same thing, capillary pressure head. By convention, capillary pressure head in the aqueous phase (or the water tension) is denoted as positive. Water not under tension has a negative capillary pressure head. The superscripts n and m are fitting parameters. The term, $(\theta - \theta_r) /(\theta_{max} - \theta_r)$, normalizes the moisture content to between 0 and 1. The function can also be written as:

$$S_w = [1 + (\alpha\psi)^n]^{-1+1/n} \qquad (4.2)$$

where S_w is the water saturation and $-1 + 1/n$ is a specific expression for m that allows Mualem's (1976) model to be used to calculate unsaturated hydraulic conductivity

from the S_w–ψ data. The S_w in equation 4.2 effectively normalizes the moisture content between 0 and 1 just as the term, $(\theta - \theta_r) /(\theta_{max} - \theta_r)$, did in equation 4.1. The only difference is that S_w does not equal zero at θ_r if θ_r is not zero. The use of S_w was chosen here. The α largely affects the function by shifting it along the capillary pressure axis; the smaller the α, the more the function is shifted up the capillary pressure axis. The n affects the slope and S–shape of the function. The larger the n, the flatter the slope and the sharper the S–shape curve.

Although the parameters α and n are fitting parameters, they have some physical meaning. The α appears to be inversely proportional to the entry capillary pressure head and the n appears to reflect the pore size distribution. For example, a well sorted, fine sand will result in a fit with a small α value and a large n value. A well sorted, very coarse sand will have a similar n value but a larger α value. Finally, a silty clay will have a very small α and small n values.

4.2.1.1 General curve fitting procedures

The van Genuchten least square fit is a 7 parameter optimization process based on Marquardt's maximum neighborhood method. The parameters are: θ_r (or S_w at IWS), θ_{max} (or S_{sat} or S_w at ROS if the data for the Soltrol® displacement by water is to be fitted), α, n, m ($= 1–1/n$), l, and K_{sat}. The l is another fitting parameter that relates water saturation to unsaturated hydraulic conductivity and K_{sat} is the measured or calculated saturated hydraulic conductivity. K_{sat} was calculated for the glass beads from the Kozeny–Carman equation (see Freeze and Cherry, 1979). The parameters K_{sat} and l were of lesser importance here since we were interested only in fitting the model to the water saturation–capillary pressure data.

The model was fitted to the data by letting α, n, m, and l vary during the iterations. Values for S_w at IWS, S_{max} or S_w at ROS, and K_{sat} were assigned. Assigning fixed values

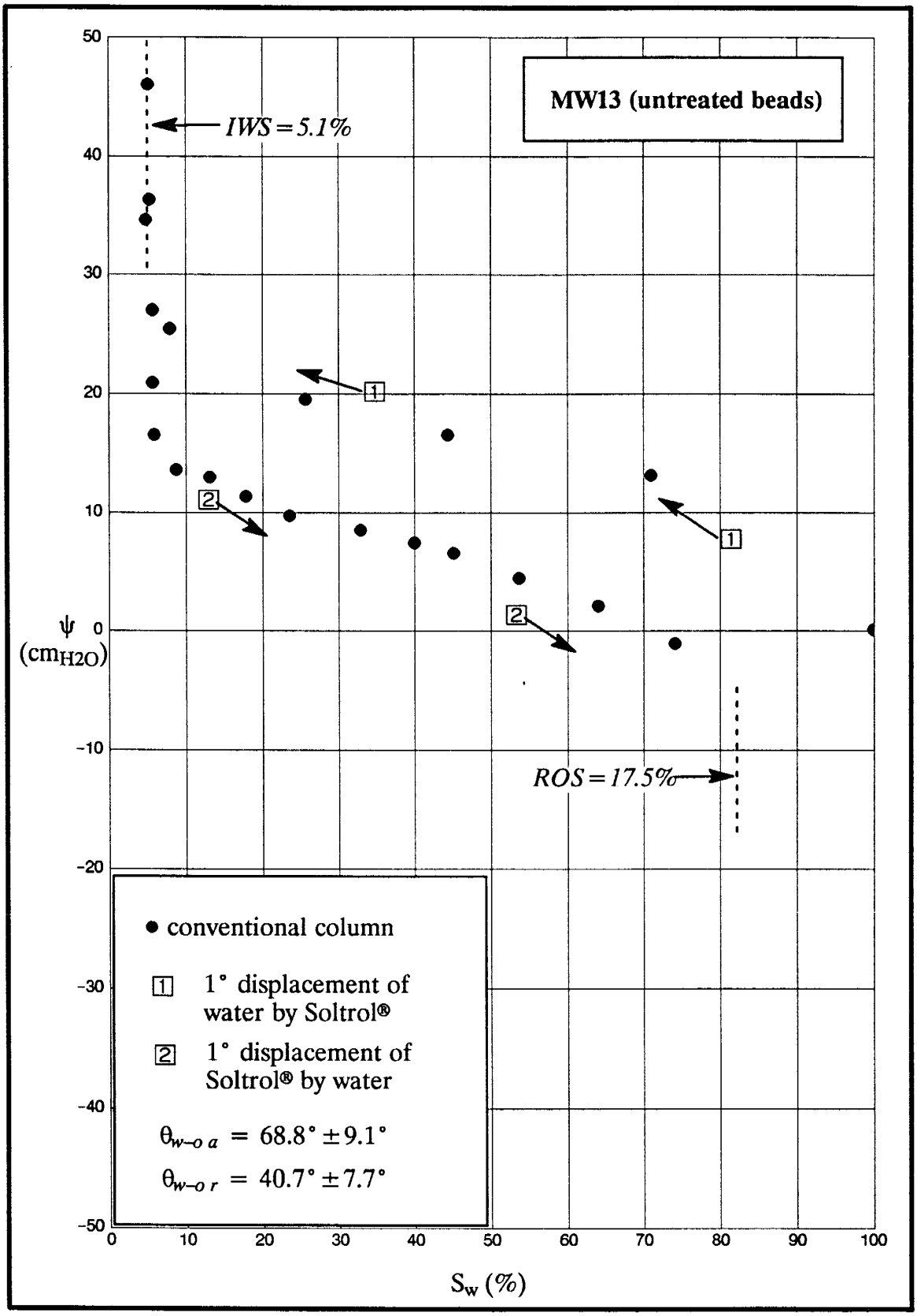

Figure 4.2. Water saturation vs capillary pressure head for MW13.

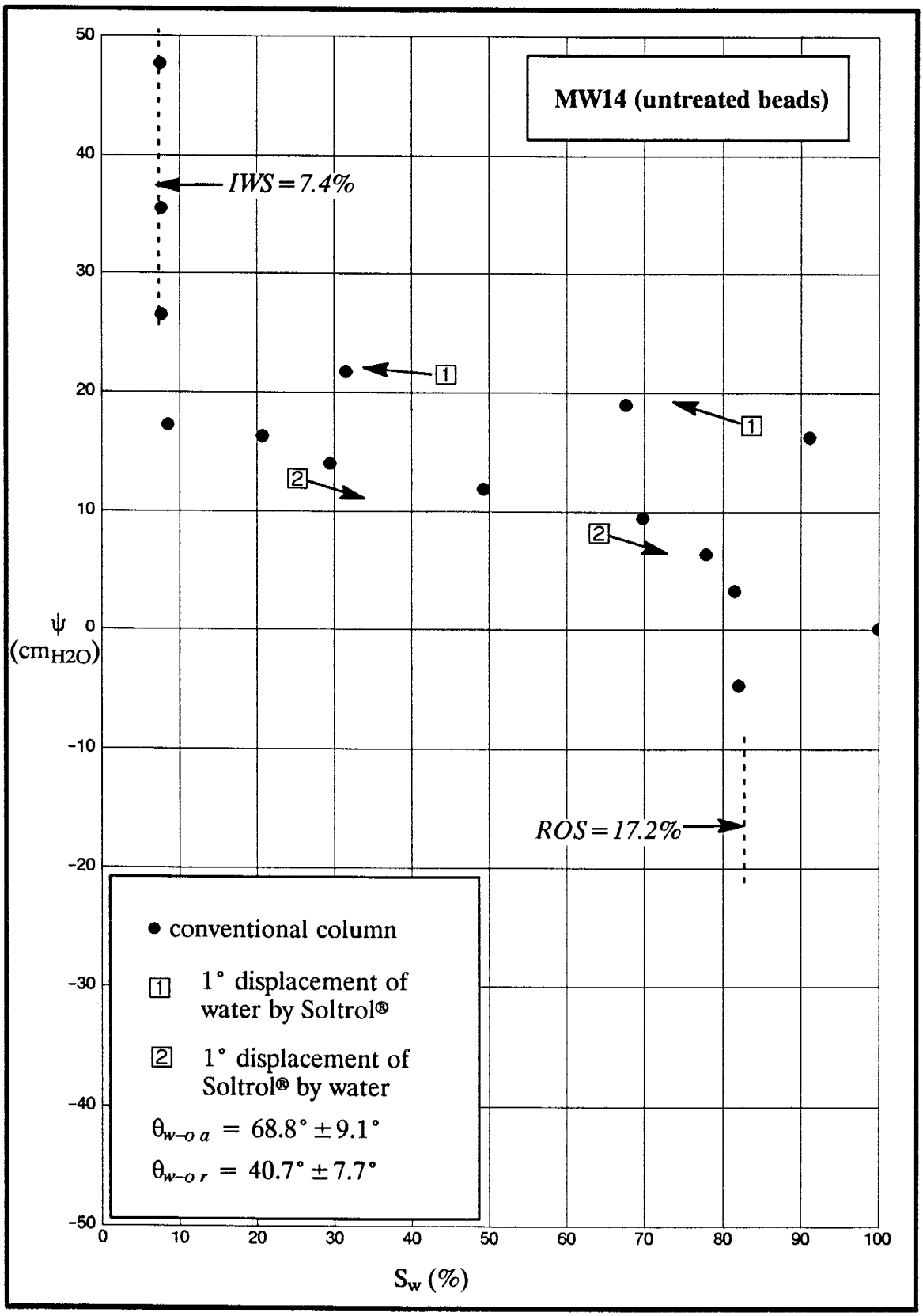

Figure 4.3. Water saturation vs capillary pressure head for MW14.

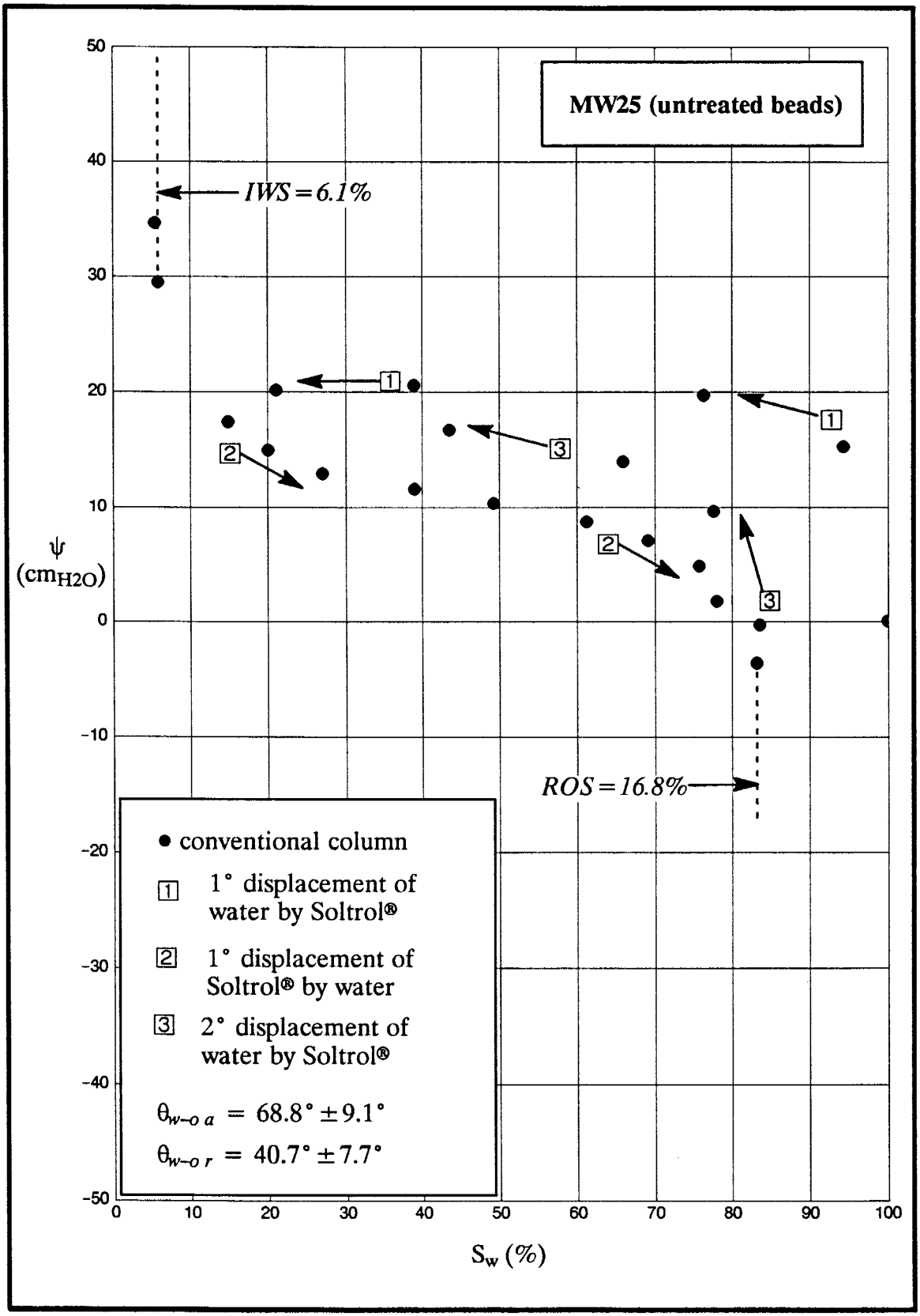

Figure 4.4. Water saturation vs capillary pressure head for MW25.

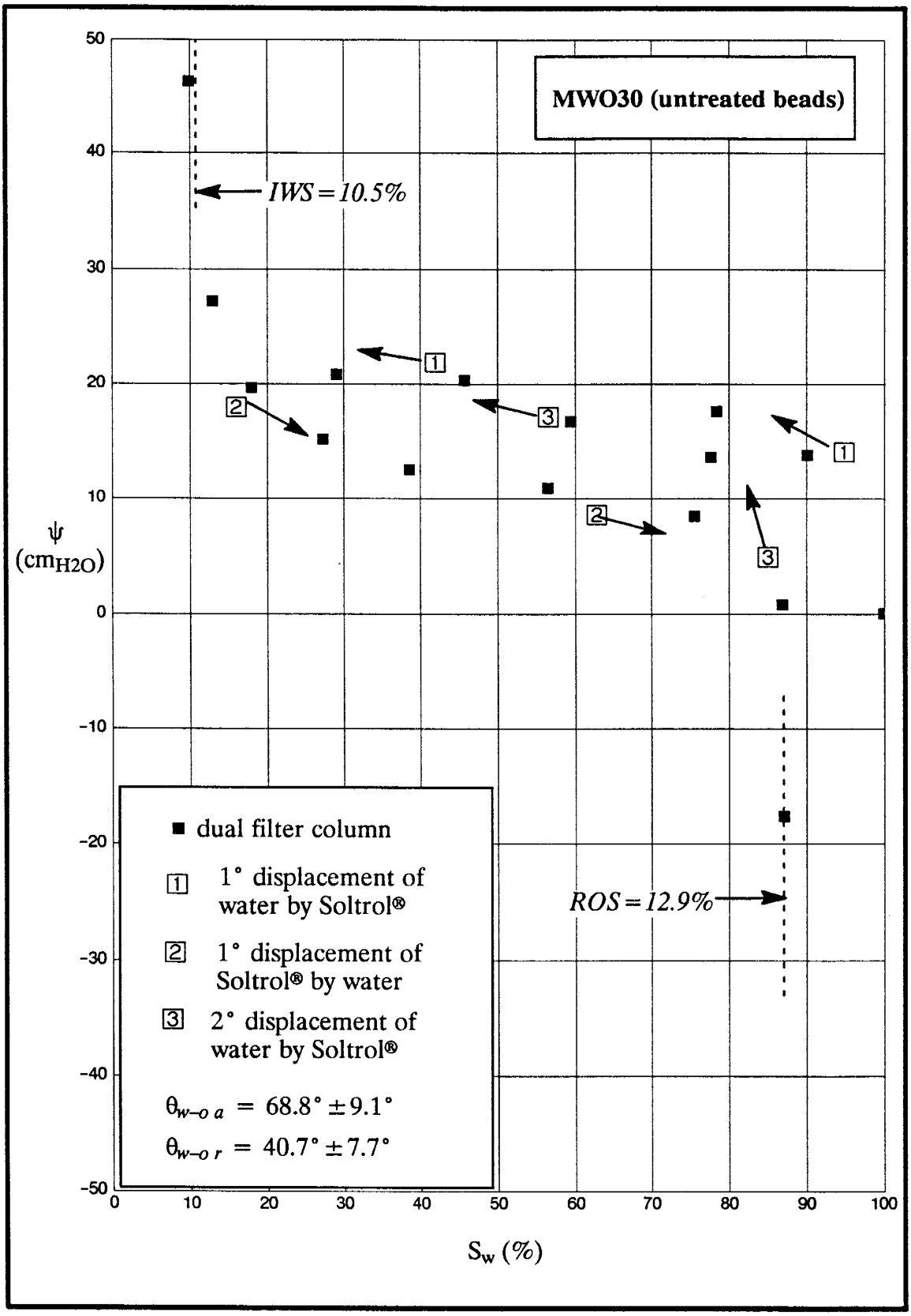

Figure 4.5. Water saturation vs capillary pressure head for MWO30.

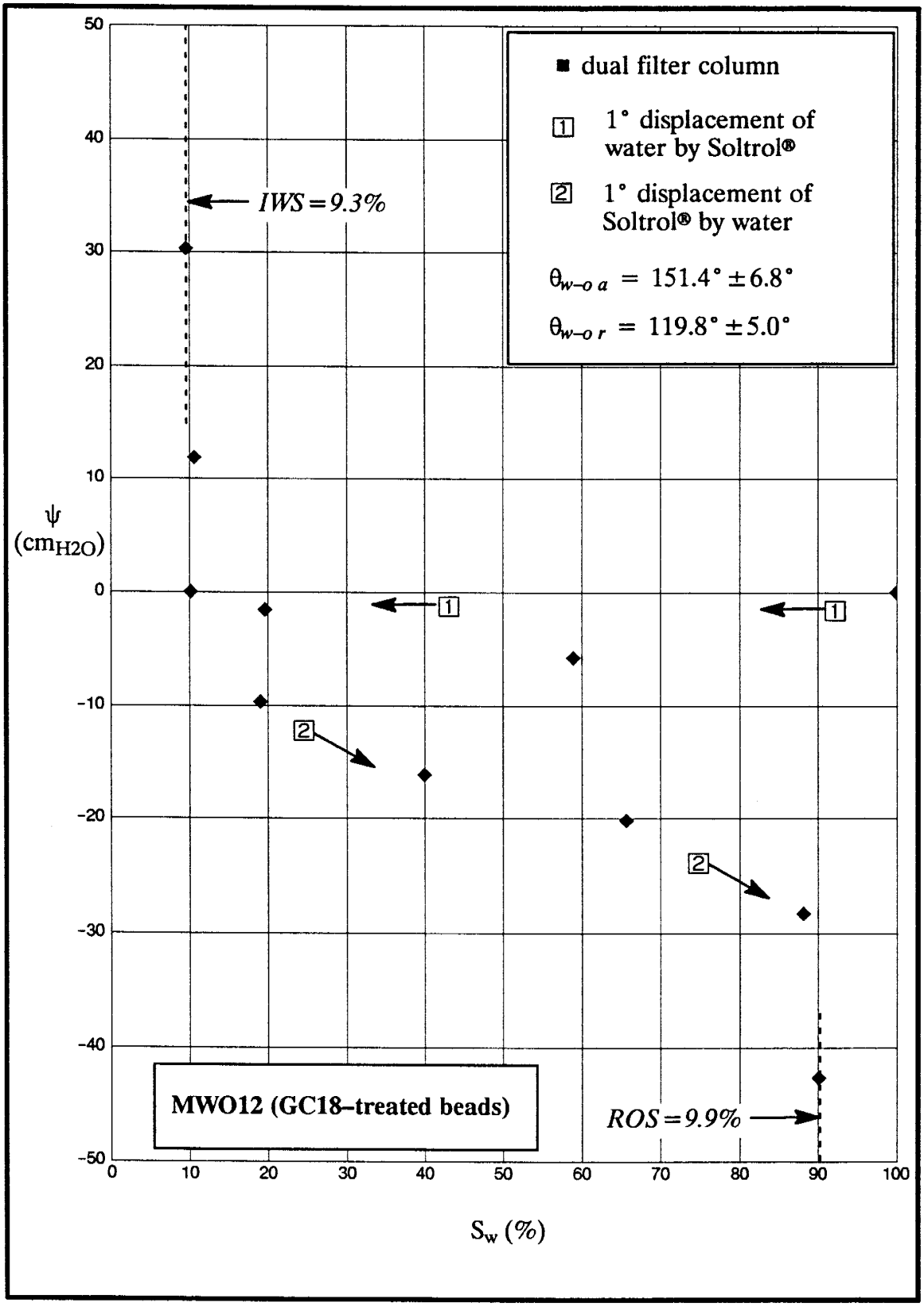

Figure 4.6. Water saturation vs capillary pressure head for MWO12.

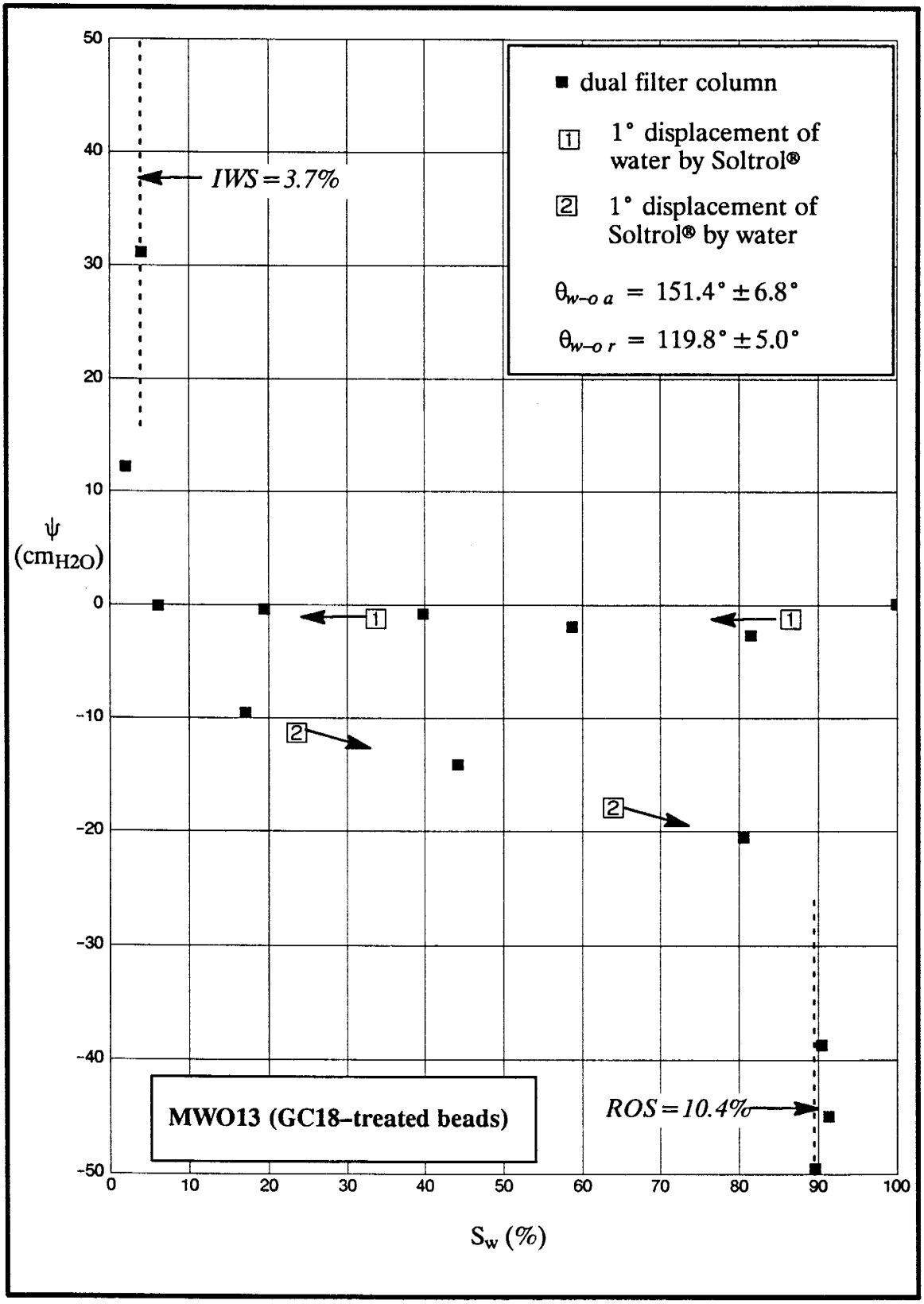

Figure 4.7. Water saturation vs capillary pressure head for MWO13.

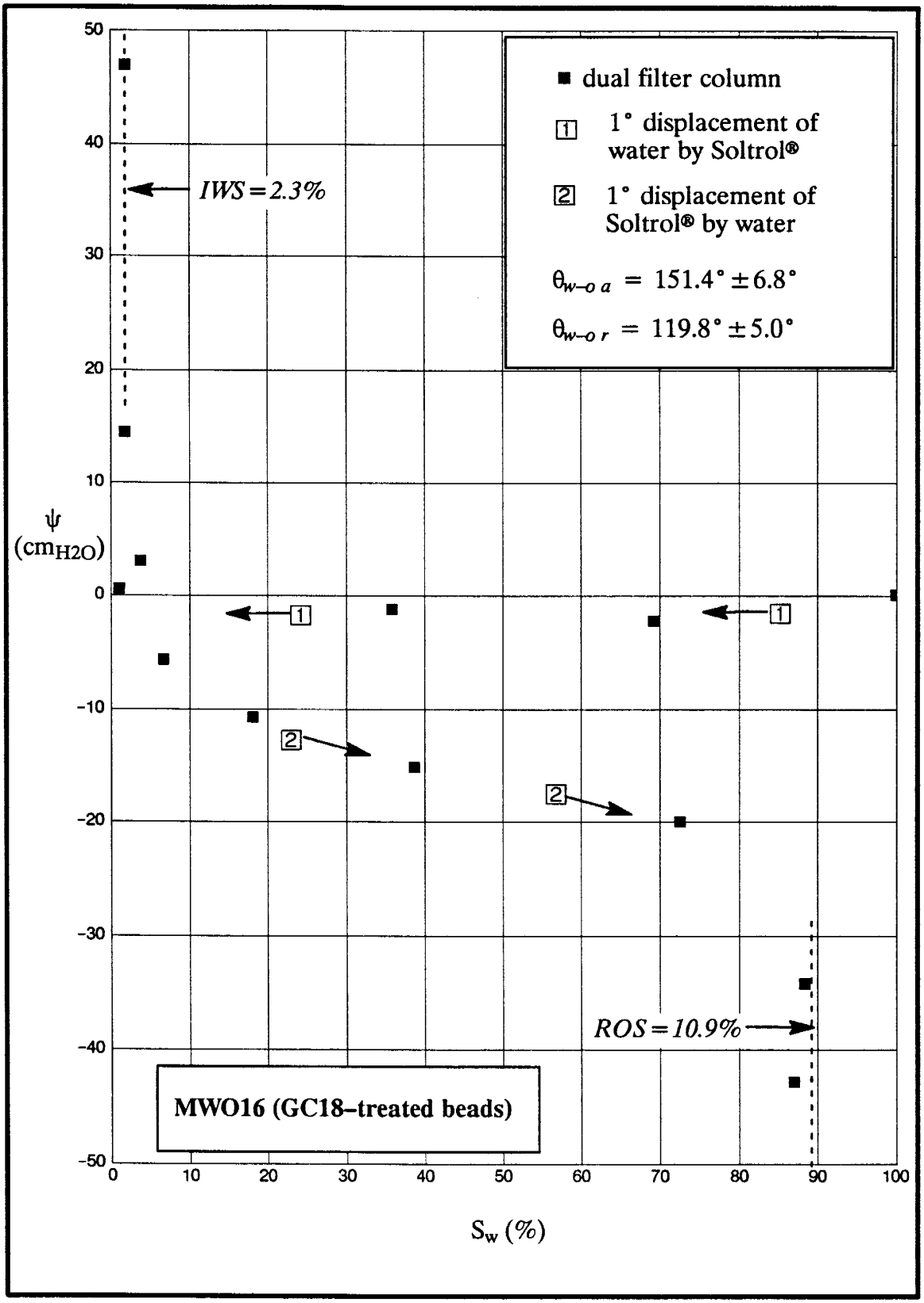

Figure 4.8. Water saturation vs capillary pressure head for MWO16.

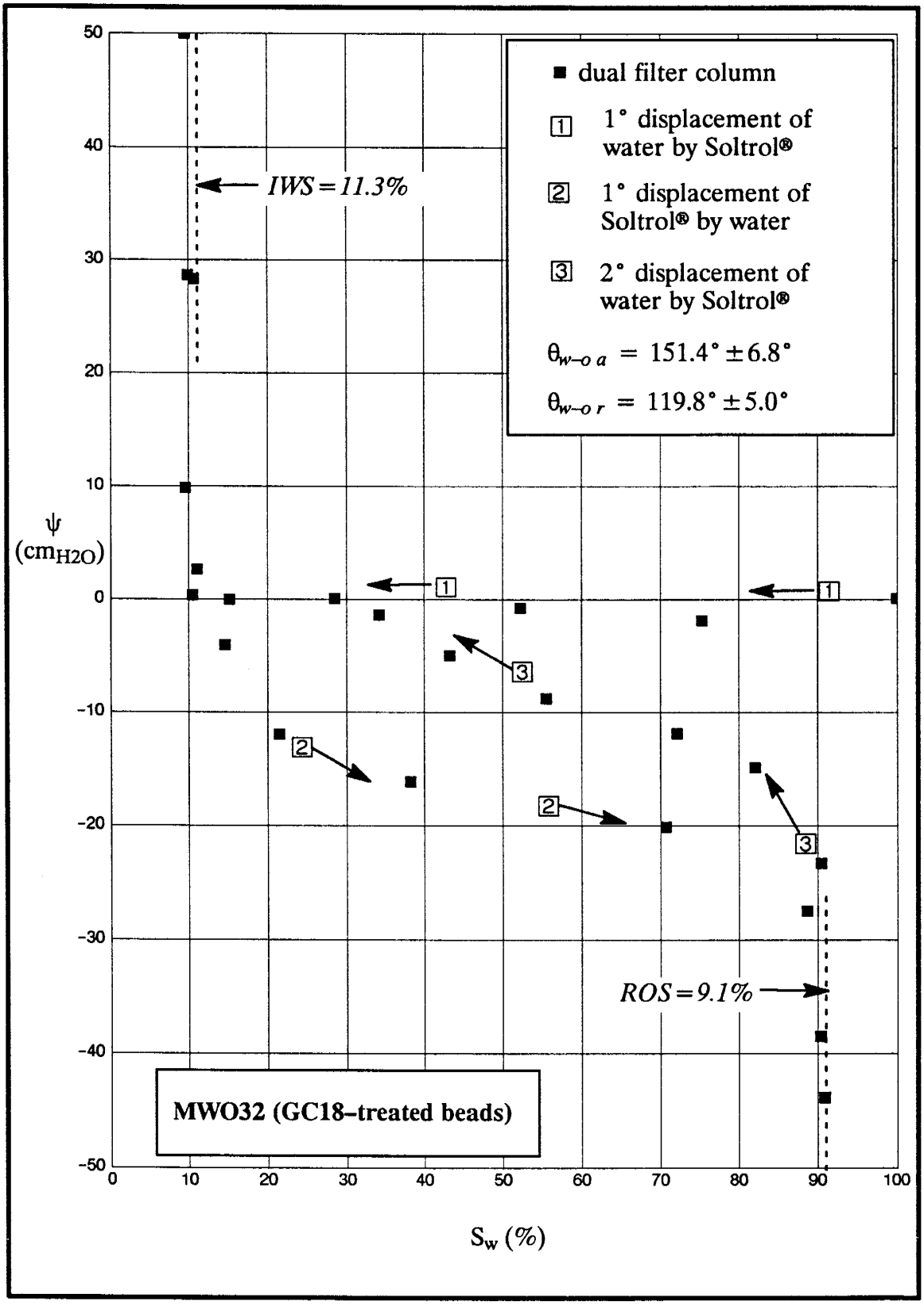

Figure 4.9. Water saturation vs capillary pressure head for MWO32.

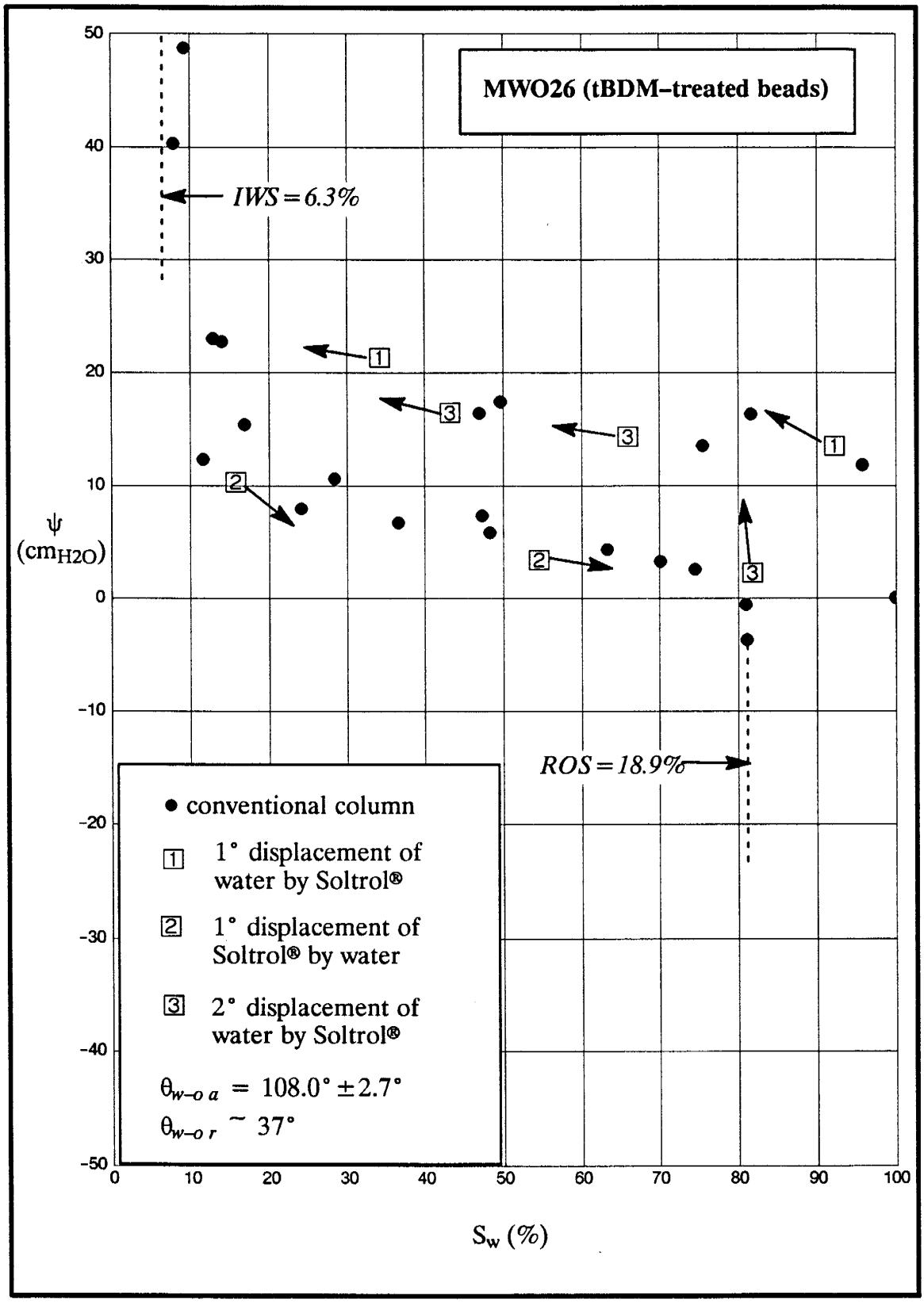

Figure 4.10. water saturation vs capillary pressure head for MWO26.

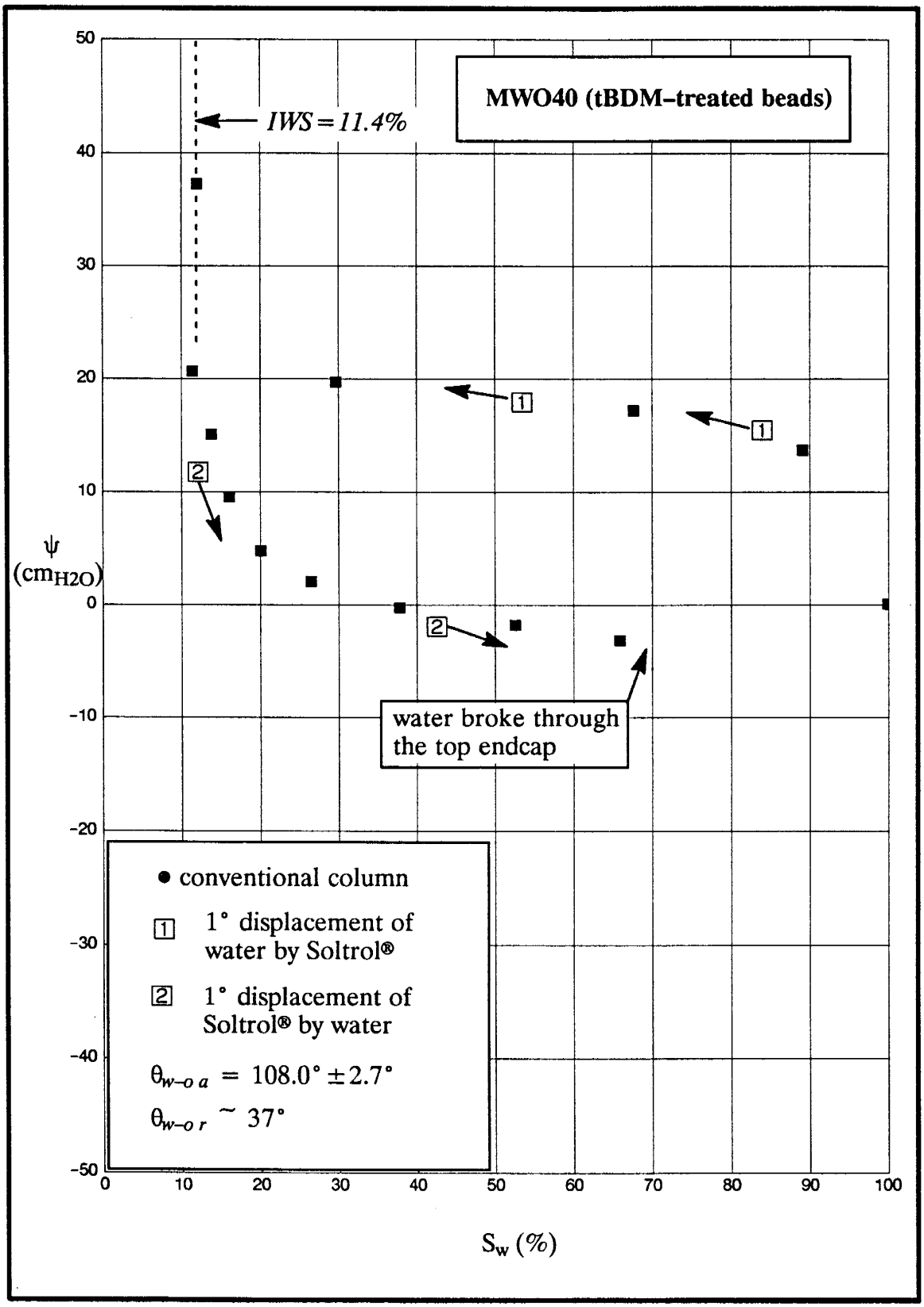

Figure 4.11. Water saturation vs capillary pressure head for MWO40.

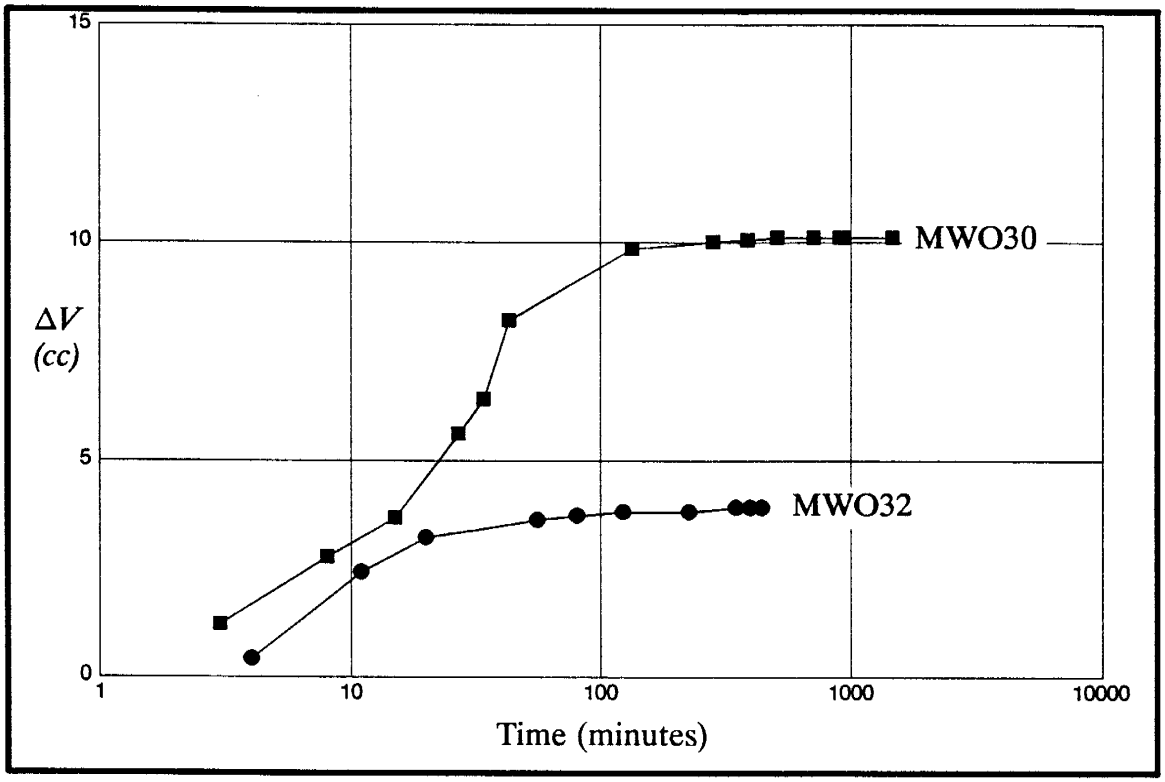

Figure 4.12. Typical equilibration curves for untreated (MWO30) and GC18-treated (MWO32) beads.

for S_w at IWS and ROS appeared justified because the data showed well defined residual saturations (Figures 4.2 to 4.11). Each experiment involved a primary displacement of water by Soltrol® and primary displacement of Soltrol® by water. In some experiments, secondary displacements were also conducted (MW25 and MWO26, 30, and 32–Figures 4.4, 4.5, 4.9, and 4.10). The van Genuchten program required data from each displacement process to be fitted separately. This sometimes resulted in the fitted curves from the different displacement sequences to cross over at water saturation values near IWS where the curves began to bend.

Data for GC18-treated beads contained negative capillary pressure values. Negative capillary pressures could not be fitted by the program. The negative values were eliminated by adding a constant value of 60 cm to all the data for GC18-treated beads to equally shift the data up into the positive capillary pressure region. This allowed

the transformed data to be fitted. Naturally, the α value obtained from these fits could not be compared with the α values from fits from the untransformed data. The fitted curves were then shifted back by subtracting the 60 cm from the fitted capillary pressures.

4.2.2 Results of the S_w–ψ data based on van Genuchten's model

The data, fitted by van Genuchten's program, are shown in Figures 4.13 to 4.15. Although the fitted curves facilitated visual comparisons between the experiments, a more quantitative analysis was desired for comparing the results. Capillary pressure head at strategic locations on the fitted curves, labelled A to H in Figure 4.16a, are summarized in Table 4.5 for this purpose. Point A is the original starting point where the beads were completely saturated with water. Point B corresponds to the Soltrol® entry pressure (defined in section 4.2.2.1). The capillary pressure head during primary displacement of water by Soltrol® at $S_w = 50\%$ is represented by C. Point D is the capillary pressure head where IWS occurred. At E, water began to displace Soltrol® in the column. Capillary pressure head during primary displacement of Soltrol® by water at $S_w = 50\%$ is represented by F. Point G is the capillary pressure head where ROS was reached. Finally, H and I correspond to capillary pressures during secondary displacements (Figure 4.16a). Point H is where secondary displacement of water by Soltrol® begins and I is defined by $S_w = 50\%$. The location of D, E, G, and H were determined by inspection because S_w at these points varied between experiments. Capillary pressure at the other points were determined graphically from Figures 4.13 to 4.15 because S_w was specified.

4.2.2.1 Untreated glass beads

In general, the S_w–ψ data for the columns packed with untreated glass beads were remarkably similar (compare Figures 4.13a, b, c, and d and capillary pressures at points A to H in Table 4.5). Soltrol® would not displace water in the column until a

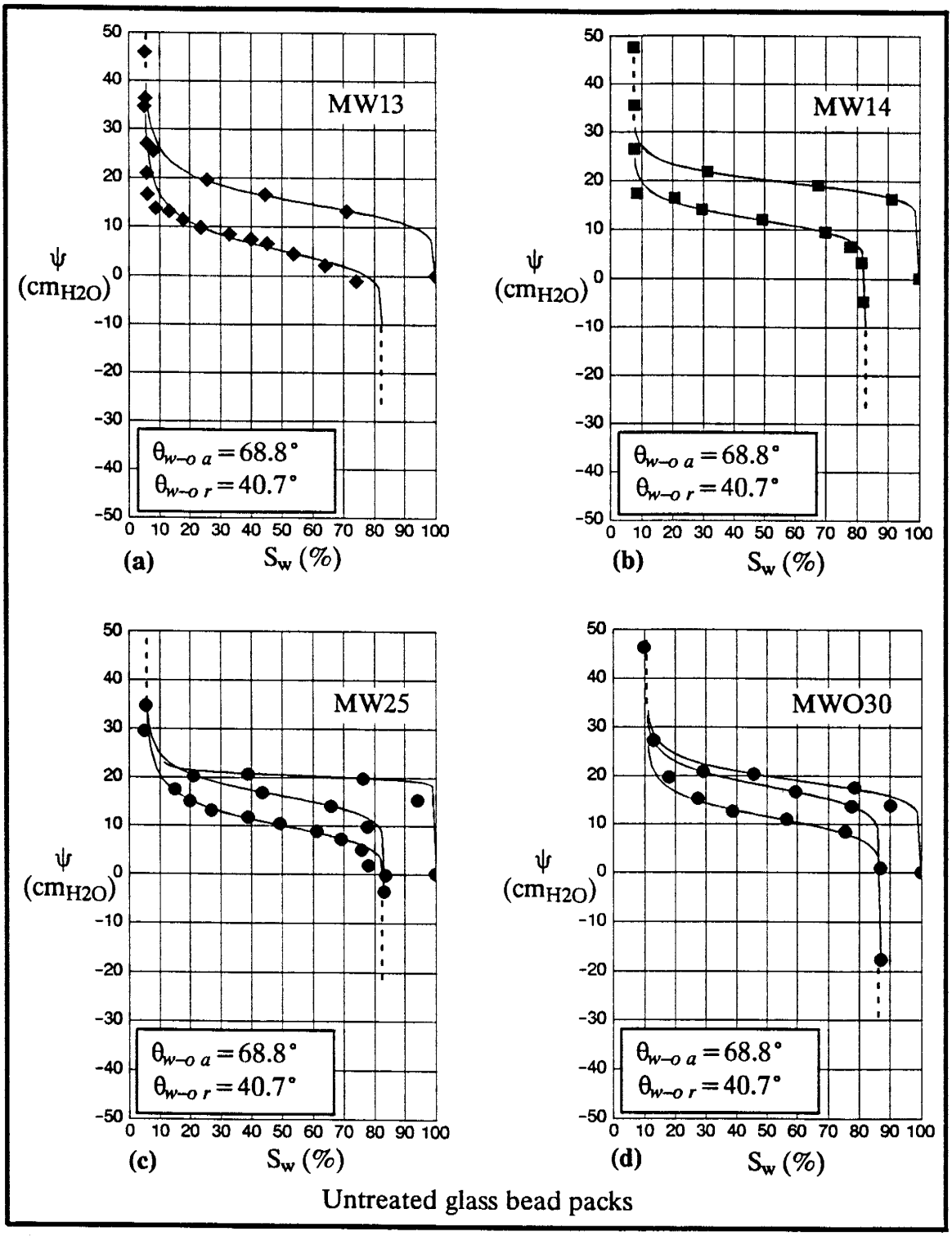

Figure 4.13. Van Genuchten fit to the water saturation–capillary pressure data.

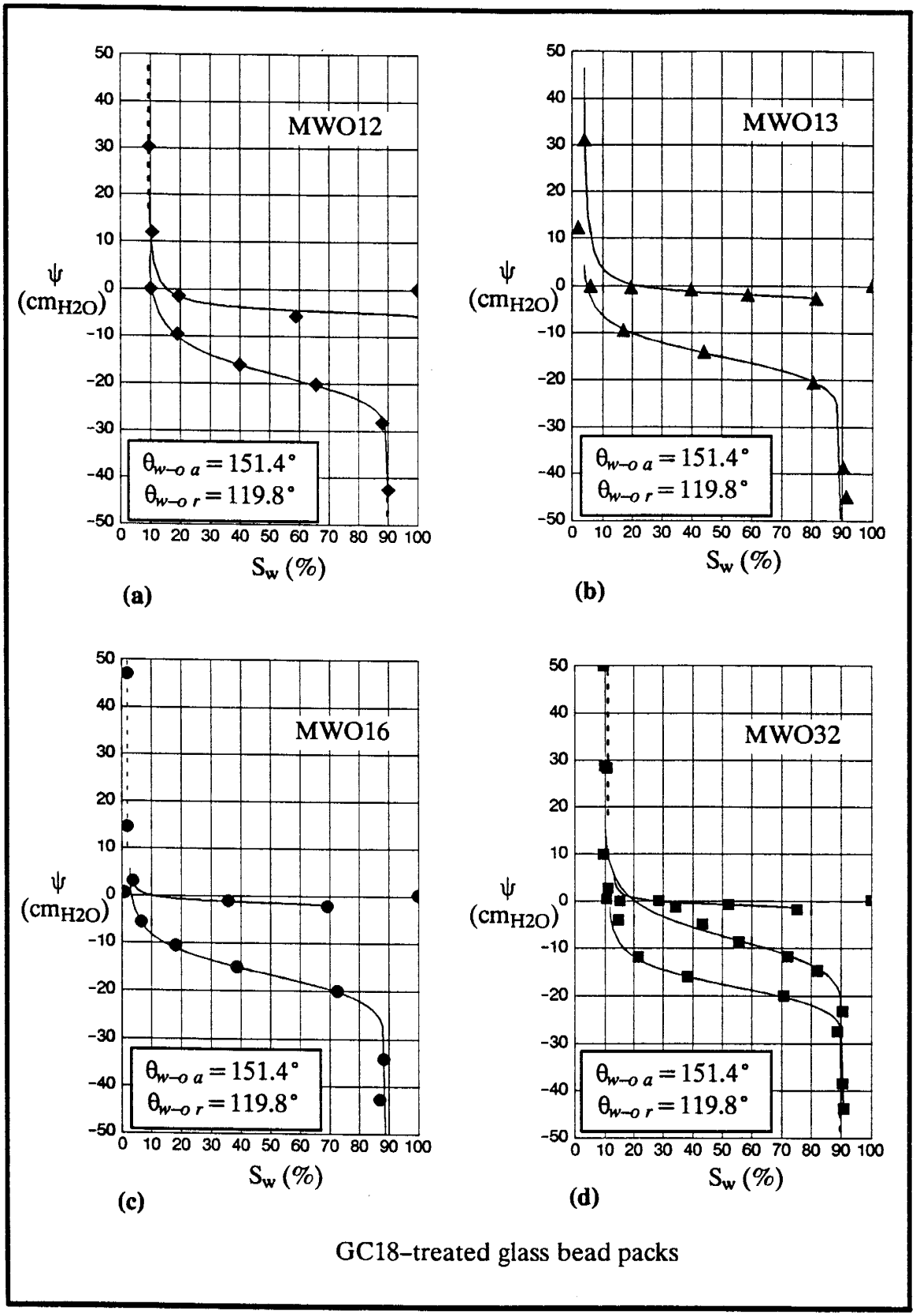

Figure 4.14. Van Genuchten fit to the water saturation–capillary pressure data.

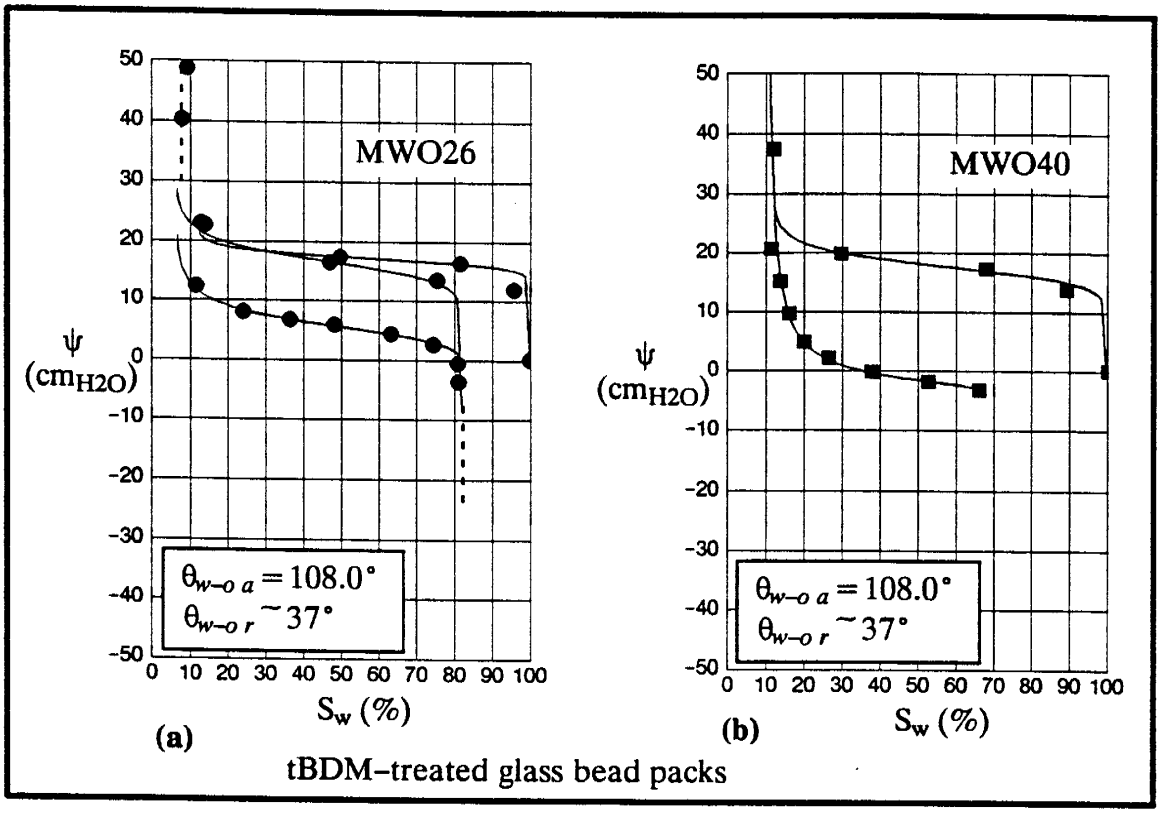

Figure 4.15. Van Genuchten fit to the water saturation–capillary pressure data.

Table 4.5. Comparison of capillary pressure head of different S_w–ψ curves.

Exp. No.	*B (cm)*	*C (cm)*	*D (cm)*	*E (cm)*	*F (cm)*	*G (cm)*	*H (cm)*	*I (cm)*
MW13	7.5	15.6	30	15	5.0	-2.8		
MW14	14.1	20.3	32	20	11.7	5.3		
MW25	18.4	20.3	29	23	9.9	3.1	8.4	15.8
MWO30	12.5	20.0	35	23	11.3	3.1	9.1	17.8
MWO12	0.0[2]	-4.22	10	-2	-18.0	-28.4		
MWO13	0.0[2]	-1.68	30	-3	-15.0	-25.2		
MWO16	0.0[2]	-1.53	10	-2	-16.7	-27.2		
MWO32	0.0[2]	-0.81	8	-5	-17.6	-26.6	-20.0	-7.8
MWO26	14.1	17.5	30	17	5.5	0.9	10.0	16.3
MWO40	12.2	18.1	30	9	-1.6	N/A		
Haines	23.7	26.7	41	25	17.2	12.7	19.3	
Haines[1]	18.4	20.7	32	19	13.3	9.9	15.0	

1. Corrected for Soltrol–water and glass bead diameter.
2. Assumed.

certain critical capillary pressure head was attained. The pressure at which Soltrol® began to displace the water, called the *Soltrol® entry pressure* (point B), was in the neighborhood of 13–18 cm of water (Table 4.5). Soltrol® then displaced water from the column to IWS where negligible amounts of water could be displaced from the column with increasing capillary pressure. The capillary pressure range over which most of the water was displaced was narrow: between the Soltrol® entry pressure and about 25 cm. Irreducible water saturation occurred at 30–35 cm (point D). At this pressure, most of the water remaining in the pores form pendular rings at the grain contacts (Haines, 1930) while Soltrol® occupied the larger cavities at the center of the pores. Displacement of Soltrol® by water began at pressures of between 20–25 cm (point E). The slope of the Soltrol® displacement by water curve was steeper than the slope for the water displacement by Soltrol® curve. ROS occurred at low positive capillary pressures (point G). The fact that Soltrol® was displaced by water at positive capillary pressures indicates that water spontaneously imbibed into the column to displace the Soltrol®.

Experiment MW13 deviated slightly from the behavior described above (compare Figures 4.13a to Figures 4.13b, c, and d). The entry pressure was slightly lower than in the other experiments. Displacement of water by Soltrol® and displacement of Soltrol® by water occurred at comparatively lower pressures (compare pressures at points C, D, E, F, and G in Table 4.5). Negative capillary pressure was required to displace the Soltrol® to ROS.

4.2.2.2 GC18–treated glass beads

Critical Soltrol® entry pressure did not exist during primary displacement of water by Soltrol® in the GC18–treated beads. In fact, the slightly negative capillary pressure values during this displacement suggest that Soltrol® spontaneously imbibed into the column to displace the water. IWS was usually reached at a capillary pressure well be-

low that observed in untreated beads (30 cm at point D). The high capillary pressure at point D for experiment MWO13 (30 cm at D) was an artifact of the curve fitted through a region where no measurements exist (see Figure 4.14b and Table 4.5). During displacement of Soltrol® by water, only a small amount of Soltrol® was displaced when 0 cm capillary pressure head was reached; water saturation at 0 cm was slightly greater than at IWS. Significant displacement of Soltrol® began, however, at about –2 to –5 cm (point E). ROS occurred at –25 to –30 cm capillary pressure head (point G). Lower capillary pressures were required to displace Soltrol® out of GC18–treated beads than untreated beads. Very little water imbibed into the column to displace Soltrol®. Forced imbibition of water at negative capillary pressure was necessary before Soltrol® displacement by water occurred.

4.2.2.3 tBDM–treated glass bead packs

The S_w–ψ curves for the tBDM–treated beads in experiments MWO26 and MWO40 differed (Figure 4.15). The curves for primary displacement of water by Soltrol® were very similar. The entry pressures were between 12 and 14 cm (point B), slightly less than for untreated beads (Table 4.5). The capillary pressures at which most displacement occurred were also about 2 cm less than for the untreated case (point C). IWS occurred at about 30 cm (point D). Pressures differed during primary displacement of Soltrol® by water between MWO26 and MWO40. Displacement occurred at positive capillary pressures for MWO26 indicating that water spontaneously imbibed into the column to displace Soltrol®. However, in MWO40, most of the displacement occurred at or slightly below zero capillary pressure.

4.3. Measurement of wettability index using USBM and Amott methods

The fitted curves were also used to determine the area under the curves for the USBM method (Cuiec, 1991; Morrow, 1990; Wilson et al, 1990; Anderson, 1987; Donaldson et al, 1969). The area corresponding to each displacement process is illus-

trated in Figure 4.16b. The method was developed by Donaldson et al (1969) based on earlier work by Gatenby and Marsden (1957) who compared areas under the displacement curves in describing wettability behavior of sintered Pyrex cores. The USBM method compares the area under the secondary displacement of water by Soltrol® curve, A_3, to the area under the primary displacement of Soltrol® by water curve, A_2 (Figure 4.16b). The USBM wettability index is the logarithm of the ratio of the area A_3 to A_2 ($\log A_3/A_2$). The actual number calculated for $\log(A_3/A_2)$ represents the order of magnitude difference between A_3 and A_2. A positive number means that $A_3 > A_2$. A negative number means that $A_3 < A_2$. The index ranges between positive numbers for water-wet porous media and negative numbers for extremely oil-wet porous media. The larger the absolute value of the wettability index, the stronger the

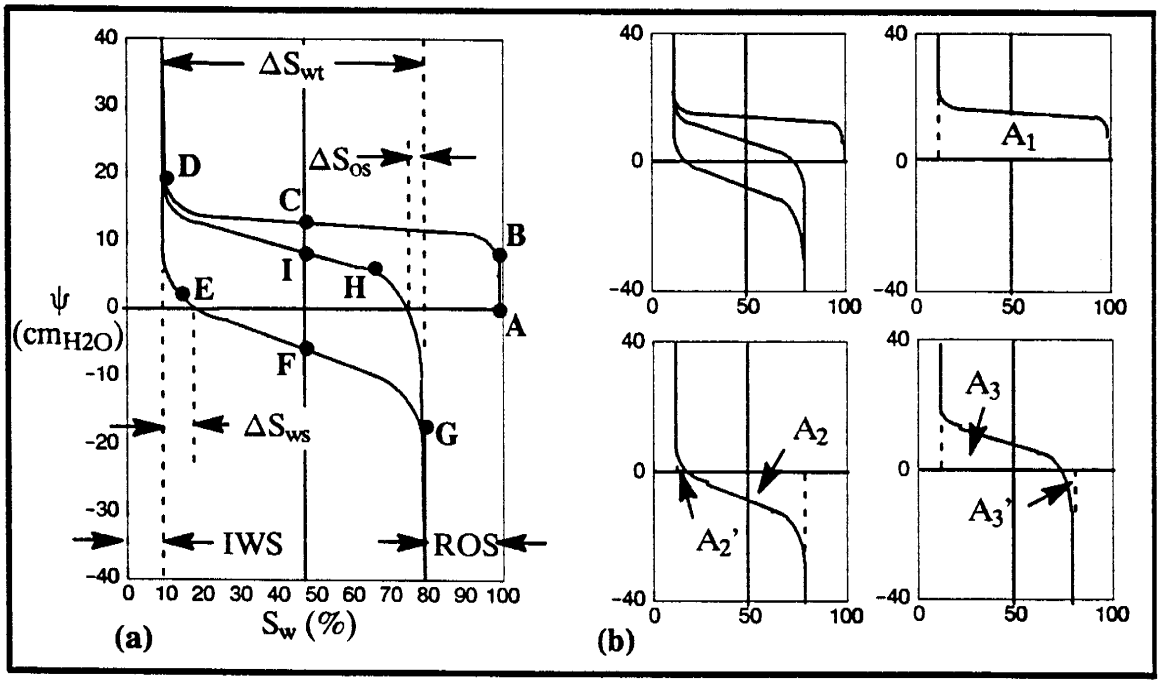

Figure 4.16. Schematic S_w–ψ curves with points A–H, areas A_1, A_2, A_2', A_3, and A_3', and volumes ΔS_{ws}, ΔS_{os}, and ΔS_{wt}.

wetting preference (Anderson, 1986b). The areas reflect the work done for one liquid to displace the other (see Morrow, 1990; Gatenby and Marsden, 1957; Haines, 1930). The relationship between area and work of displacement is not so direct, however,

because the effects of hysteresis are neglected (Morrow, 1990). The area A_3 rather than A_1 is used because both displacements from which areas are calculated begin at residual saturation of the displacing liquid (Figure 4.16b). This is conceptually more attractive than using A_1 in which displacement begins with no residual saturation. In practice, however, the value of residual saturation for water and oil are, in general, different anyway. The ratio of A_1/A_2 provides an alternative wettability index. In hydrology and soil science, secondary displacement curves are not usually measured. The logarithm of A_1/A_2 could be used to calculate a wettability index similar to the USBM index for experiments in which secondary displacement data were not measured (for example in MW13 and MWO13).

Recall in section 3 that wettability conditions depended on whether water was advancing or receding against Soltrol®. By comparing the areas under two different displacement curves, the USBM method implies that wettability conditions are the same during both displacement processes; contact angle hysteresis is ignored. Hysteresis in wetting behavior reported in section 3 provided motivation for modifying the USBM method to account for contact angle hysteresis. One method is to calculate separate wettability indexes from individual displacement curves. Wettability conditions when water recedes against Soltrol® and when water advances against Soltrol® could then be analyzed separately. Contact angle hysteresis would result in different wettability indexes calculated from each individual displacement curve. Wettability indexes for individual curves could be calculated, for example, by calculating the ratio of the area under the displacement curve with the complimentary area under the same displacement curve on the other side of the zero pressure axis (Figure 4.16b). For example, the index for primary displacement of Soltrol® by water would be the logarithm of A_2'/A_2. The index for secondary displacement of water by Soltrol® would be the logarithm of A_3/A_3'. The ratio was reversed in the latter case because the displacement liquid was reversed.

No thermodynamic explanation is given here for the alternate wettability indexes. The indexes should be considered empirical. It is sufficient to say that the complimentary area represents a spontaneous process and the area under the displacement curve represents a forced displacement process. As in the standard USBM method, positive values of log (A_2'/A_2) and log (A_3/A_3') indicate water–wet conditions; negative values indicate oil–wet conditions.

The areas, A_1, A_2, A_2', A_3, and A_3', in cm, and the logarithm of the ratio of areas are shown in Table 4.6. The cm unit represents the energy per unit weight of water. The areas were measured from the fitted curves with a planimeter. For untreated beads, A_1 was relatively large while A_2 was negligible (MW13, 14, 25, and MWO30). The area under the secondary displacement of water by Soltrol®, A_3, was slightly less than A_1. In contrast, areas for GC18–treated beads were opposite from the untreated beads. Area A_1 for GC18–treated beads was negligible and A_2 was relatively large (MWO12, 13, 16, 32). Area A_3 was smaller than A_1. For tBDM–treated beads, A_1 was slightly smaller than A_1 for untreated beads (compare A_1 for MW14 and MWO26 for example). Area A_2 was almost zero for experiment MWO26 but was >0.48 for MWO40. The total A_2 area for MWO40 could not be measured because water prematurely broke through the top endcap. Area A_3 was large, but smaller than A_1.

The Amott test is another semi–empirical wettability index (Cuiec, 1991; Morrow, 1990; Anderson, 1986b; Amott, 1959). This method is also restricted to the region between residual saturations. Unlike the standard USBM method however, separate indexes are calculated for each displacement curve. The ratio of the volume of Soltrol® spontaneously displaced by water, ΔS_{ws}, to the total volume of water displaced, ΔS_{wt}, is the index, I_w, for the primary displacement of Soltrol® by water (Figure 4.16a). The ratio of the volume of water spontaneously displaced by Soltrol®, ΔS_{os}, to the total volume is the index, I_o, for the secondary displacement of water by Soltrol®. The Amott–Harvey index, I_{A-H}, is the difference of the two indexes, $I_w - I_o$. The Amott

test can be very insensitive at moderate wettability and very sensitive at intermediate-wettability. Figures 4.17a and 4.17b show the primary displacement of Soltrol® by water for two soils of different wettability (soils A and B). Figure 4.17a shows that the I_w index calculated for soil A would be much smaller than the I_w index calculated for soil B, even though the displacement curves were nearly identical. Both soils are actually intermediate-wet, the only difference is that most displacement in soil A occurred on the other side of the zero capillary pressure axis. However, according to the Amott index, I_w, soil A was oil-wet and soil B was water-wet. Figure 4.17b shows water-wet conditions in soil B and less water-wet conditions in soil A. The Amott index, I_w, calculated for both soils were the same because displacement in both occurred almost entirely above zero capillary pressure. By using the zero capillary pressure axis as the dividing line to define spontaneous and forced imbibition, the difference between strongly and moderately wetted conditions may be obscured.

Table 4.6. Summary of areas and ratio of areas under the displacement curves.

Exp. No.	A_1 *(cm)*	A_2 *(cm)*	A_2' *(cm)*	A_3 *(cm)*	A_3' *(cm)*	*Log* (A_1/A_2)	*Log* (A_3/A_2)	*Log* (A_2'/A_2)	*Log* (A_3/A_3')
MW13	15.30	0.01	5.59			3.49		3.05	
MW14	18.84	<0.01	9.31			3.97		3.67	
MW25	20.19	<0.01	8.69	13.03	0.00	4.00	3.81	3.64	v. lg.
MWO30	17.71	<0.01	9.13	13.91	0.07	3.95	3.84	3.66	2.30
MWO12	0.91	14.06	0.22			-1.19		-1.81	
MWO13	1.42	12.67	0.04			-0.95		-2.53	
MWO16	0.18	13.91	0.11			-1.88		-2.10	
MWO32	0.55	13.95	0.11	0.44	6.24	-1.41	-1.50	-2.10	-1.15
MWO26	16.47	<0.01	4.71	12.82	0.07	3.92	3.81	3.37	2.26
MWO40	15.85	>0.48	1.35			<1.52		<0.45	

The volumes for the Amott test were measured graphically from the fitted curves and are shown in Table 4.7. The Amott method could only be used for those experiments in which secondary displacement of water by Soltrol® was performed. The in-

dexes, I_w, I_o, and I_{A-H} appear in the last three columns. The value of the indices range between −1 for very oil-wet beads to +1 for very water-wet beads. A value of 0 indicates intermediate-wettability.

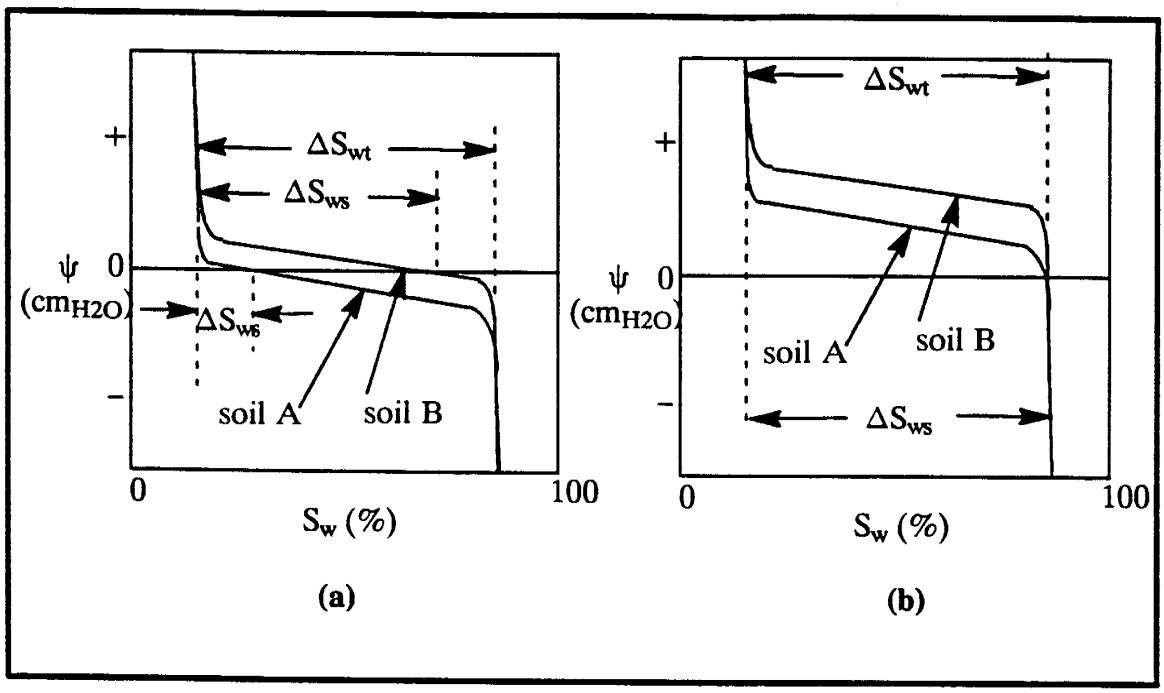

Figure 4.17. Hypothetical Soltrol displacement by water curves for 2 slightly different wettability soils.

Table 4.7. Summary of volumes displaced and Amott test.

Exp. No.	ΔS_{wt} *(%)*	ΔS_{ws} *(%)*	ΔS_{os} *(%)*	I_w	I_o	I_{A-H}
MW25	77.00	76.42	0.29	0.993	0.004	0.989
MWO30	76.30	75.34	0.77	0.987	0.010	0.977
MWO32	79.60	0.38	70.56	0.005	0.887	-0.882
MWO26	75.80	74.92	0.38	0.988	0.005	0.983

The total volume of water displaced between IWS and ROS ranged between 75–80% of the pore volume for all three wettability cases. Spontaneous water imbibition was significant during Soltrol® displacement by water for the untreated beads and

for tBDM–treated beads in experiment MWO26; spontaneous Soltrol® imbibition during water displacement by Soltrol® was very minor. The reverse was observed for GC18–treated beads. Spontaneous water imbibition during Soltrol® displacement by water was minor and spontaneous Soltrol® imbibition during water displacement by Soltrol® was significant. Amott indexes could not be calculated from experiment MWO40 because the S_w–ψ data were incomplete.

4.4. Discussion of the short column results

In analyzing the short column data for different wettability cases, one would expect the receding water–Soltrol® contact angle to prevail during water displacement by Soltrol® (water receding against Soltrol®). During Soltrol® displacement by water, the advancing water–Soltrol® contact angle should prevail (water advancing against Soltrol®). Advancing and receding water–Soltrol® contact angles for untreated, GC18–treated, and tBDM–treated beads are included in Figures 4.13, 4.14, and 4.15, respectively. Recall that the receding angle for tBDM–treated slides decreased very quickly from 81.8° to 37° after several days exposure to water. The value of 37° should apply because the tBDM–treated beads were flushed with water for several days after packing to remove the ethanol. The applicability of the advancing and receding angles measured on glass slides in section 3 to the analysis of S_w–ψ data in short columns are addressed later on in the discussion.

The values of IWS in the three wettability cases were similar. There was no statistically significant difference between the average value of IWS for the untreated and GC18–treated beads and only a very small statistical difference between the IWS of the tBDM–treated and untreated beads (Appendix D1). The slightly higher values of IWS for tBDM–treated beads may be due to experimental errors. Firstly, if trapped gas was present in the top endcap of the dual filter column (MWO22–Table 4.4), it could dissolve back into solution during the experiment. This would result in a higher

value of IWS and a lower value of ROS. Secondly, in calculating the effective volume of the conventional column, any space between the polypropylene filter and the top endcap created by the thickness of the epoxy was ignored. This space, however, could affect residual saturation measurements. At IWS, the space, initially filled with water, would be filled mostly with Soltrol®. The presence of Soltrol® occupying this space would result in a slight decrease in the mass of the column. This, in turn, would cause a lower IWS to be calculated in the conventional columns than in the dual filter columns. Any space between the Teflon® filter and the top endcap would always be filled by Soltrol®. A third explanation is that tBDM–treated beads had difficulty draining. The slightly higher value of 10% IWS for tBDM–treated beads may also reflect that these beads did not drain as completely as the untreated beads. These three reasons may help explain why the IWS for tBDM–treated beads were slightly higher than for untreated and GC18–treated beads.

Table 4.8. Values of residual saturations from other glass bead and sand columns.

Values from:	*IWS (%)*	*ROS[1] (%)*	*Comments*
Haines (1930)	8	12	water/air
Brooks and Corey (1964)	9.7	N/A	water/air
Topp and Miller (1966)	10	14	water/air
Morrow (1970)	7.5 ± 1.5	N/A	liquid/air
Laroussi and De Backer (1979)	9.7	~0	water/air
Morrow and Songkran (1981)	N/A	14.0	Soltrol®130/air
Kia (1988)	N/A	~12–13	calculated
Morrow et al (1988)	N/A	15.2 ± 0.6	brine/iso–octane
Mace (1990)	8.7 ± 2.1	16.9 ± 1.1	water/Soltrol®130[2]
Wei (this study)	7.5 ± 2.0	17.6 ± 1.8	water/Soltrol®130[3]

1. this includes residual non–wetting phase saturation such as air.
2. Sevietta sand with 0% clay fraction.
3. untreated beads.

The values of IWS agree qualitatively with the results of Morrow's (1970) who found experimentally that IWS for packed spherical beads was essentially constant at

$7.5 \pm 1.5\%$ for intrinsic contact angles ranging between 0° to 108° (Table 4.8). In this study the results apply for contact angles between 41° (untreated) and 120° (GC18–treated). The IWS measured here for untreated glass beads was slightly lower than the 12% residual wetting liquid saturation calculated by Kia (1988) for a porosity of 0.34 to 0.36. The value of $7.5 \pm 2.0\%$ for untreated beads also agreed well with other published results for glass beads (Table 4.8).

Although the average value of IWS was 6.6% for GC18–treated beads, some trials had values as low as 2% and as high as 11%. Some of this variability might have been caused by temperature variations during the experiments resulting in marked changes in liquid densities. However, high and low IWS values were also measured for experiments which did not experience large temperature variations such as MWO8, 9, and 10 (Table 4.2). Another explanation could be that the very low values of IWS reflect complete and very efficient displacement at neutral wettability; the receding water–Soltrol® angle measured on a freshly treated slide was $119.8° \pm 5.0°$. The higher IWS values may have reflected less complete (but equally efficient on a pore level) displacement with some by–passing.

The average value of ROS for untreated beads was higher (in percent Soltrol®) than the residual non–wetting phase saturation measured by Haines (1930), Topp and Miller (1966), and Morrow and Songkran (1981). To investigate this difference, some column experiments were run with Soltrol® dyed with Oil Red O (MW24, MWO7, and MWO10). The dye indicated that by–passing occurred along the top and bottom of the column where there was a flare in the column. This by–passing could be significant but its occurrence was irregular. The amount of non–wetting liquid by–passed could add up to a couple of percent of the total pore volume (Appendix E1). Another reason why the ROS was higher may be because there was less density difference between water and Soltrol® 130 in our experiments than between water and air in the experiments of Haines (1930) and Topp and Miller (1966) and between Soltrol® and air in

Morrow and Songkran (1981)'s experiments. This results in less buoyant forces for displacing Soltrol® than air. Experiments by Morrow et al (1988) showed that ROS was slightly higher in liquid/liquid displacements than in liquid /air displacements. The advancing contact angle in the water/Soltrol® system was also higher (68.8°) than in a water/air system ($<25°$). The higher contact angle operative in the water/Soltrol® system could decrease the importance of snap–off as a trapping mechanism. Other trapping mechanisms such as by–passing in the pores could have become more prevalent leading to a slightly greater residual non–wetting saturation. By–passing along the flare in the column, smaller density differences between the immiscible fluids, and the higher advancing contact angle in the water/Soltrol® system may account for the slightly higher values of ROS measured here.

Slight differences apparently exist between the IWS and ROS values obtained from the conventional and dual filter columns packed with untreated beads (compare MWO15 and MWO30 to the other columns in Table 4.1). The IWS from the dual filter columns were higher than the IWS from the conventional columns. The ROS measured from the two dual filter columns were the highest and lowest values obtained for untreated beads. These discrepancies could be due to slight differences in experimental procedures. The higher IWS in the dual filter columns could have been a result of trapped gas in the top endcap dissolving back into solution during the experiments. More pores could have been by–passed in the dual filter column than in the conventional column during water displacement by Soltrol® resulting in a higher value of IWS. Beads that were by–passed by Soltrol® would not contain any Soltrol® in the pores for the water to displace resulting in a lower value of ROS. The IWS from the conventional columns could also have been underestimated because Soltrol® would replace water in the space between the polypropylene filter and the top endcap at IWS. Higher values of IWS would also result if the pore volume calculated from the dummy endcap was larger than the actual pore volume. An over–estimate of the pore volume

in the dual filter column would also help explain the low ROS measured in MWO30 (the pore volume for both MWO15 and MWO30 were slightly greater than for the conventional columns). The value of 20.2% ROS from MWO15 could just reflect statistical sampling variation.

The IWS and ROS for untreated beads were very close to those measured by Mace (1990) for cleaned Sevietta sand with no clay fraction (Table 4.8). The comparison was useful because the short column procedures were almost identical, having been developed in the same laboratory. The median diameter for Sevietta sand and the glass beads used in this study were also about the same (0.3 mm diameter).

The ROS for GC18–treated beads in conventional columns was greater than for untreated beads. This was a result of wall effects in the column. In this case, the water was the non–wetting liquid and preferred to flow along the larger pore between the column and the hydrophobic beads (advancing water–Soltrol® angle was $151.4° \pm 6.8°$), resulting in an early breakthrough. The polypropylene scrim at the top endcap was not fine enough to prevent the water from breaking through. Had Soltrol® not been able to break through the top, preferential flow along the column wall would have ceased and the capillary pressure in the treated beads would have increased and forced water to flood through the beads themselves. Wall effects were negligible for untreated beads because water in that case was the wetting liquid. Although Figure 4.1 showed that ROS was decreasing more and more slowly with increasing flow rate, the value of ROS where it became independent of flow could not be predicted from the data. Although this column wall effect was an experimental issue, it also illustrated how heterogeneities, such as non–uniform pores, fractures, etc. in an otherwise homogeneous porous medium could promote preferential flow under oil–wet conditions. The column wall effect motivated the development of the dual filter column. The addition of a fine Teflon® filter at the top endcap prevented water breakthrough, caused the capillary pressure in the beads to increase, and water to flow through the glass

beads properly. The results of ROS and capillary pressure–saturation from the dual filter columns represented actual behavior of the homogeneous glass beads.

No published data of ROS for hydrophobic packed spherical beads could be found to compare with the value of ROS from the dual filter column experiments (MWO12, 13, 16, and 32). However, if wetting was reversed in the GC18–treated beads, the residual wetting liquid saturation for untreated and GC18–treated beads should be comparable. The value of IWS for untreated beads and ROS for GC18–treated beads were compared (Table 4.1 and 4.3). The average ROS value of $10.1 \pm 0.7\%$ for GC18–treated beads agreed well with the overall average IWS value of $7.5 \pm 2.0\%$ for untreated beads or the value of 10% for untreated beads in the two dual filter columns (MWO15 and 30). The difference between the values may be from slightly different initial non–wetting liquid saturations. No Soltrol® was present initially when Soltrol® (non–wetting) displaced water (wetting) in the untreated beads. However, residual water (non–wetting) was present when water displaced Soltrol® in the GC18–treated beads. Drainage of Soltrol® in GC18–treated beads was similar to drainage of water in untreated beads. In both cases, large pores drained first as the non–wetting liquid displaced the wetting liquid. Residual trapping in both cases occurred in smaller pores resulting in lower values of residual wetting liquid saturation. In addition, the residual wetting liquid could further drain by film flow. The larger ROS in the untreated beads could be explained by the fact that, during Soltrol® displacement by water, water (wetting) spontaneously imbibed into the smaller pores first to displace the Soltrol® there. This ultimately resulted in Soltrol® being trapped in the larger pores. The volume of Soltrol® in the large pores was responsible for the larger ROS in the untreated beads.

Measurements of ROS for tBDM–treated beads were inconclusive. The value of 18.4% averaged from two columns was unreliable especially when the capillary pressure data is taken into account (later in this section). Additional experiments are required to measure the ROS with more confidence for this treatment.

Wilson et al (1990) showed there was significant scatter in the ROS for temperature variations greater than 2°C in their short column experiments. The relatively large temperature variations in the later experiments (MWO13 to MWO40) were due mainly to sporadic increases in temperature when the constant temperature box was malfunctioning. Temperature variations were otherwise below 2–3°C most of the time.

Preliminary inspection of the S_w–ψ curves for the untreated beads shows they were strongly water–wet (MW14, MW25, and MWO30 in Figure 4.13). A critical entry capillary pressure was required to displace water out of the column during initial displacement of water by Soltrol®. During Soltrol® displacement by water, most of the Soltrol® was displaced before zero pressure was reached. The flat slope along the two primary displacement curves indicates a narrow pore size distribution as one would expect for a uniform bead size. The relationship between capillary pressure and water saturation were remarkably similar for MW14, MW25, and MWO30 (compare Figures 4.13b, c, and d). Results from the dual filter column also matched those from the conventional column for the untreated beads. Capillary pressures were slightly lower for MW13. This was probably not caused by differences in packing. The bulk density and porosity were similar to the other columns. Perhaps there was a difference in wettability. The lower positions of the displacement curves compared to those of MW14, MW25, and MWO30 indicate that the beads were less water–wet than the other untreated beads. It may be possible that the beads were not perfectly clean when they were packed in the column. The USBM and Amott–Harvey indexes calculated for MW13, MW25, and MWO30 indicate that the untreated beads were all strongly water–wet, however; the slight increase in hydrophobicity in MW13 was not detected (Tables 4.6 and 4.7).

The $S_{w-\psi}$ data for the untreated beads were analyzed by comparing with data from Haines (1930). The porosity of the packed glass bead column reported by Haines (1930) was between 0.36 and 0.37. This value was almost identical to ours ($\bar{n}$ =

0.355 ± 0.003) which was typical of a randomly packed sample. Although his experiment involved water and air and larger size beads (0.38mm diameter), the results were compared by scaling interfacial tensions and bead radii. Normalizing the capillary pressure by the interfacial tension is done in soil physics and petroleum engineering to compare capillary pressure–saturation data (see eg. Miller, 1980; Morrow and McCaffery, 1978; Morrow and Mungan, 1978; Elrick et al, 1959; Leverett, 1940; Haines, 1930). Lenhard and Parker (1987) and Parker et al (1987) used the method of scaling interfacial tensions to compare S_w–ψ data for air–water, air–oil, and oil–water data for the same soil. Demond and Roberts (in press) also used interfacial tension to scale S_w–ψ data for a sandy soil.

Capillary pressure head corresponding to water saturation at points A to H in Figure 4.16a for Haines' data were scaled by the ratio of the interfacial tensions and bead radii:

$$\psi_{corrected} = \psi_{Haines} \left(\sigma_{water\text{–}Soltrol} / \sigma_{water\text{–}air} \right) \left(r_{0.14mm} / r_{0.19mm} \right) \qquad (4.3)$$

where $\psi_{corrected}$ is the scaled value of capillary pressure head, ψ_{Haines} is the actual capillary pressure head measured in Haines' experiment, $\sigma_{water\text{–}Soltrol}$ is the interfacial tension between water and Soltrol®130, $\sigma_{water\text{–}air}$ is the surface tension of water, and $r_{0.14mm}$ and $r_{0.19mm}$ are the bead radii corresponding to our experiments and Haines' experiment. In scaling Haines' data, we assumed that the advancing and receding angles in his experiment were effectively zero. This assumption was not unreasonable because the advancing water–air contact angle measured on clean glass slides was $< 25°$ (Table 3.3). The data scaled from Haines (1930) are shown on the last row of Table 4.5. In comparing results, capillary pressures averaged from MW14, MW25, and MWO30 were used. Capillary pressures from MW13 were not used because they deviated from the other three columns. The average entry pressure for MW14, 25, and MWO30 (15.0 cm) was slightly lower than Haines' (18.4 cm). However, the average

capillary pressure head at points C (20.2 cm) and D (32 cm), where the funicular stage ends and IWS occurs, were very similar to Haines' (20.7 cm and 32 cm, respectively). Even if the receding water–Soltrol® contact angle measured on our clean slides (θ_{w-o} $_r = 40.7° \pm 7.7°$) differed from the receding angle in Haines' experiment, results from Morrow and McCaffery (1978) showed experimentally that effect of contact angle was relatively insensitive during drainage. For angles of less than about 60°, the porous medium in their experiments behaved as if the angles were effectively 0°. During imbibition, water displaced Soltrol® out of the column at slightly lower capillary pressures than in Haines' experiment (points F and G). Point E from Haines' data was from a scanning curve and hence had a slightly higher capillary pressure compared to our data. The lower capillary pressures of MW14, 25, and MWO30 to Haines' during water imbibition suggest that conditions were not completely water–wet when water advanced against Soltrol® in the untreated beads. The advancing water–Soltrol® contact angle for our clean glass ($\theta_{w-o\,a} = 68.8° \pm 9.1°$) was probably higher than the advancing contact angle for the *glistening dew* used in Haines' experiment. A higher advancing angle would cause displacement to occur at lower capillary pressures.

Figure 4.18 offers a visual comparison of Haines' scaled data to data from MW25. The match was very close for drainage but deviated for imbibition. The reason that the drainage curves matched may be because contact angle effects are less pronounced during drainage (Morrow and McCaffery, 1978). The imbibition curves, on the other hand, is more sensitive to the contact angle. Differences in contact angles between Haines' experiment and ours would be more evident in imbibition.

The S_w–ψ data for GC18–treated beads (MWO12, 13, 16, and 32) were different from the untreated beads. This difference could only have been imparted by wettability. The bead size and immiscible liquids were the same as for the untreated beads. During primary displacement of water by Soltrol®, most of the water was displaced under very low capillary pressures. This behavior, where very little pressure was re-

quired for one liquid to displace the other, reflected a condition of neutral or intermediate wettability. This agreed with receding angle measured on the GC18–treated slides. The receding water–Soltrol® contact angle on a freshly GC18–treated slide was 119.8° ±5.0°, representing intermediate to slightly oil–wet conditions (refer to Table 1.1). The receding angle may have also decreased slightly with time to a value close to 90° when the columns were being flushed with water for several days. The actual receding angle at the start of the experiment could not be pinpointed but should have been in the range of intermediate wettability.

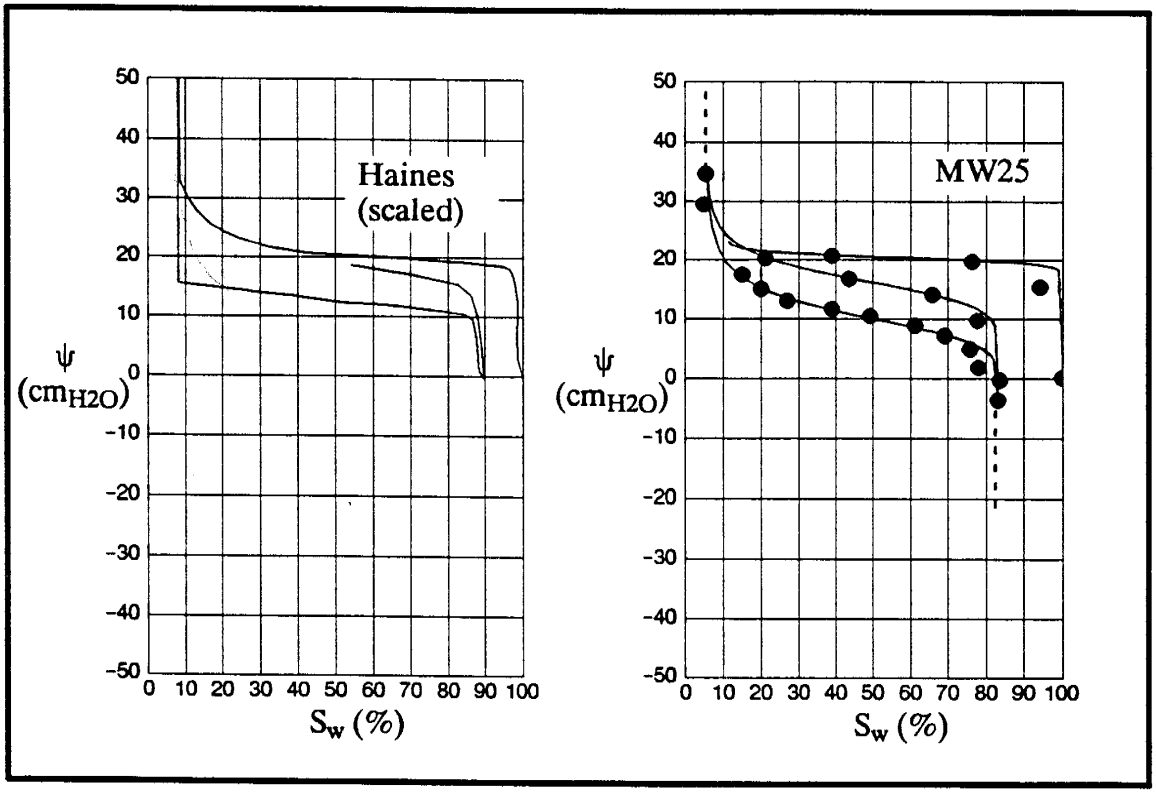

Figure 4.18. Comparison of Haines' scaled data and MW25.

During primary displacement of Soltrol® by water, negative capillary pressure was required to displace most of the water out of the column indicating that oil–wet conditions prevailed. The advancing water–Soltrol° contact angle of freshly treated slides

was 151.4° ± 6.8°. Results from section 3 showed that the deterioration of the advancing angle in water was minor.

No comparable results for the oil–wet data could be found. Bethel and Calhoun (1953) also used silane–treated glass beads but their columns were initially saturated with n–octane and so the saturation history was reversed from ours. They were also only able to measure the capillary pressure during the water flood. The capillary pressure–saturation curves from Killins et al (1953) and Donaldson et al (1969) were mostly from consolidated rock cores. Killins et al (1953) also used clean glass beads but initially saturated with oil. Morrow and M^{c}Caffery (1978) were able to measure drainage and imbibition capillary pressures in sintered Teflon® cores. However, they were not able to measure negative capillary pressures so their curves were incomplete.

Another way to assess the displacement curves for GC18–treated beads was to compare them with the results for the untreated beads. The results, of course, required scaling by a wettability factor such as the cosine of the appropriate contact angle (advancing or receding). Primary displacement of Soltrol® by water in GC18–treated beads was analogous to the secondary displacement of water by Soltrol® in untreated beads because in both cases, the non–wetting liquid was displacing the wetting liquid. Also, displacement in both cases began at residual non–wetting liquid saturation. By identical reasoning, the data from secondary displacement of water by Soltrol® for GC18–treated beads should be comparable to the data from the primary displacement of Soltrol® by water for untreated beads. In this case, however, the receding water–Soltrol® contact angle applies. The comparison was further complicated by the possibility that the untreated beads were not as completely water–wet during displacement of Soltrol® by water ($\theta_{w-o\,a} = 68.8°$).

A visual comparison between capillary pressures calculated from untreated beads and the measured pressures was done by fitting a curve using the van Genuchten pro-

gram to the data calculated from MW25 and then comparing it to the measured data points for the GC18–treated beads. The results of this exercise are shown in Figure 4.19. The data for water displacing Soltrol® were scaled by using either a contact angle value of 151.4° (Figure 4.19a) or 180° (Figure 4.19b). Data from the other displacement curves for MWO32 were excluded to improve clarity. Note that the saturation is in percent of the non–wetting liquid, S_{nw}. The assumption here that the contact angle during displacement of water by Soltrol® data in the untreated beads was zero seemed justified because drainage is relatively insensitive to contact angle effects (Morrow and McCaffery, 1978). The overall match was very close, especially for non–wetting liquid saturation between 30% and 75%. The pressures calculated with contact angle 180° seemed to fit the measured data slightly better. The match at residual wetting liquid saturation differed because ROS in the untreated beads was higher than IWS in the GC18–treated beads. The residual non–wetting liquid saturation agreed fairly well. That a contact angle value of 180° fitted the data better was not entirely surprising. Contact angle measurements are not exact. Table 3.4 showed that the contact angle could depend on the method of measurement. Water on GC18–treated slides was judged to be completely non–wetting with the static drop method but not with the dynamic method. Surface roughness and pore shape geometry also affect the contact angle (Morrow and McCaffery, 1978). The surface roughness of the beads was probably greater than the roughness of the glass slides. This, in effect, enhances wetting; an oil–wet surface would behave even more oil–wet.

Data from primary displacement of Soltrol® by water in MW25 were scaled by 119.8° and compared with the secondary displacement of water by Soltrol® data in MWO32 (Figure 4.19a). The scaled and measured data did not agree very well. Several reasons are offered here. Firstly, the assumption of 0° contact angle for MW25 was not entirely valid because the imbibition data differed from Haines' (Figure 4.18). The assumption was made, however, because the effective contact angle during imbibition

in MW25 could not be accurately estimated. Secondly, the contact angle may not be directly related to capillary pressure (Morrow and McCaffery, 1978). If the non-zero contact angle could be accounted for, the scaled curve would shift down closer to the measured data. Another possibility was that the measured data were from a scanning curve and therefore plotted below the primary displacement curve scaled from experiment MW25.

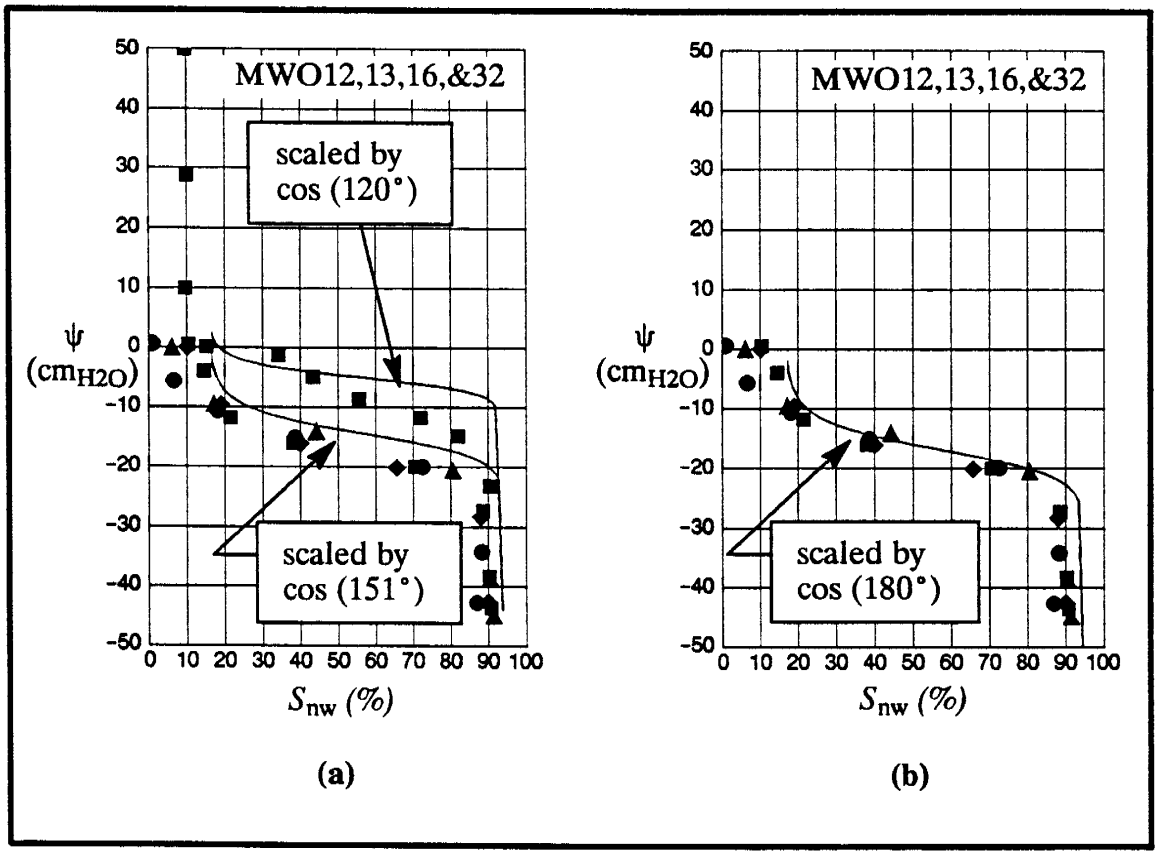

Figure 4.19. Scaling data from MW25(untreated beads) to measured data from MWO32 (GC18-treated beads).

The capillary pressure-saturation curves for MWO26 appeared water-wet (Figure 4.15a). This was unexpected. Based on the advancing and receding contact angles, the behavior was expected to be very much like that of MWO40. The low receding angle (~37°) should cause the beads to behave water-wet during primary displacement of water by Soltrol®. This was observed for both experiments. However, the intermediate

value of the advancing angle (108.0° ±2.7°) should have resulted in intermediate-wet behavior during Soltrol® displacement by water in which Soltrol® was displaced out of the column at or near zero capillary pressure. The Soltrol® displacement by water curve of MWO40 was anticipated but the curve for MWO26 was not. MWO26 was not completely water-wet but the capillary pressure-saturation curves resembled those of MW13. Wettability indexes calculated for MWO26 also indicated strongly water-wet conditions (Tables 4.6 and 4.7).

The limited S_w-ψ data for tBDM-treated beads were analyzed in a similar way. In experiments MWO26 and MWO40, the capillary pressures for Soltrol® displacing water was lower than those of Haines' or MW14, 25, and MWO30 (compare point C in Table 4.5). This indicates that conditions were not completely water-wetting. This is consistent with the cosine value of the receding water-Soltrol® angle measured on tBDM-treated slides aged in water (37°). The capillary pressures at which water displaced Soltrol® in MWO40 was consistent with pressures predicted by the advancing angle (108.0°). The capillary pressures in MWO26 during Soltrol® displacement by water were higher than predicted. The predicted capillary pressure at point F, using Haines' scaled data (assuming zero contact angle) was -4.1 cm. The measured data at F from MWO26 and MWO40 were 5.5 cm and -1.6 cm respectively (Table 4.5).

Scaled van Genuchten fitted curves for untreated beads were also compared to the tBDM-treated beads (Figure 4.20). The scaled data did not match the data for Soltrol® displacement by water in MWO26. The match was better for MWO40. The discrepancy in the calculated pressure and the measured pressure could not be pinpointed. The silane treatment may not have been as complete or may have deteriorated much more rapidly for glass beads than glass slides. Linear scaling of saturation-capillary pressure data in the neutral wettability range may also not be valid. Morrow and Mungan (1971) found that contact angles measured on a flat, smooth surface could not be used to predict capillary pressures in a sintered Teflon® core. Morrow

and McCaffery (1978) found that effective contact angles of roughened surfaces correlated much better with the capillary pressure–saturation results. Melrose (1965) found that correction factors for contact angles were necessary to predict capillarity behavior in sphere packs of differing wettability. Insufficient data prevent firm conclusions to be drawn.

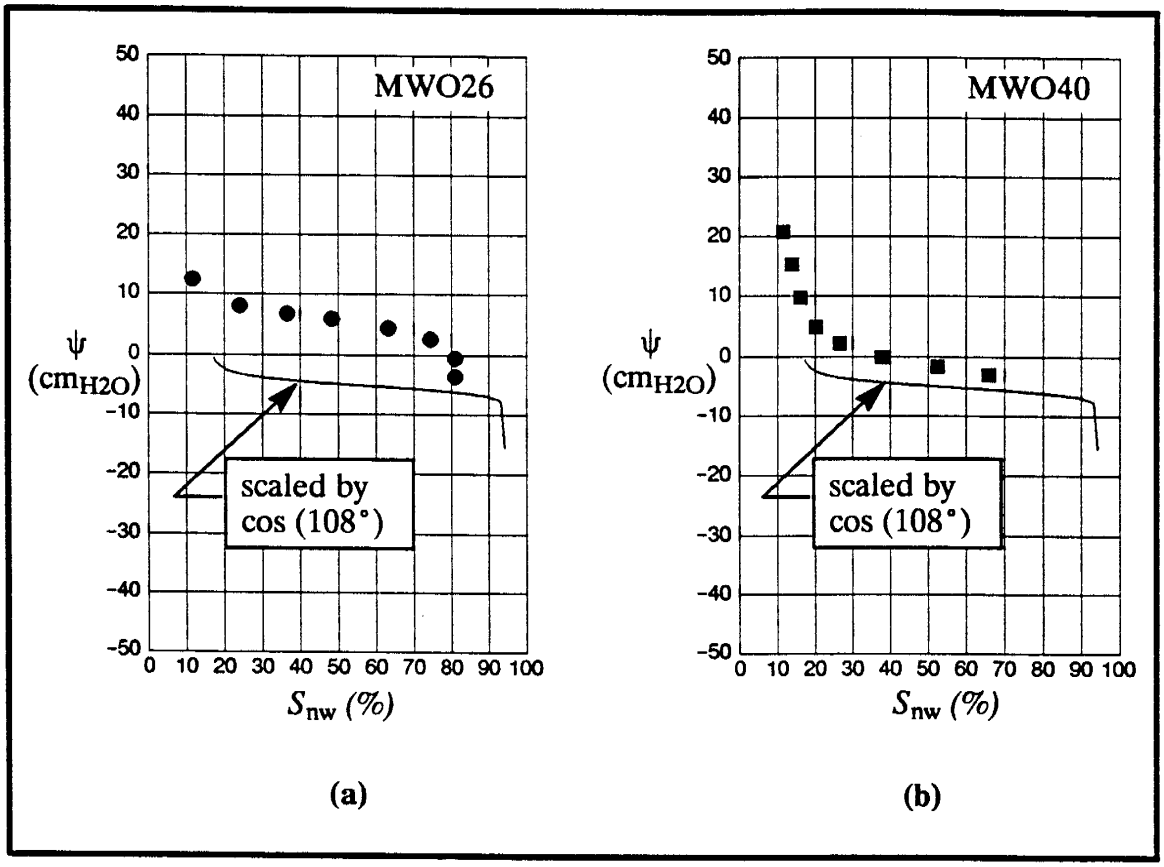

Figure 4.20. Scaling data from MW25 (untreated beads) to measured data from MWO26 and MWO40 (tBDM–treated beads).

Experiments MWO21 and MWO29 represent two of the many dual filter column experiments with tBDM–treated beads that did not fully drain during the primary displacement of water by Soltrol® (Table 4.4). The well defined IWS reflects non–equilibrium conditions during that part of the displacement (Morrow and Melrose, 1991). Although this condition was observed in all the experiments (well defined IWS), it was not reached until most of the water had been displaced out of the column. In experi-

ments MWO21 and MWO29, significant amounts of water remained in the beads when this non-equilibrium condition occurred. Morrow and Melrose (1991) gave two explanations for this phenomenon. First, during drainage, a fraction of the wetting liquid becomes disconnected and takes a very long time to drain. Second, during drainage, hydraulic contact between the membrane and the sample (beads) is lost. Regardless of the reason, anomalously high IWS was observed mostly in the tBDM-treated beads. Anomalously high IWS was never observed in the untreated beads. Interestingly, high ROS in the GC18-treated beads packed in the dual filter columns, from disconnection of Soltrol® (wetting liquid) was never observed either. Another possibility is clogging of the top endcap. This phenomenon remains a mystery.

Wettability indexes of reservoir rocks calculated by Donaldson et al (1969) ranged from -1.3 for oil-wet cores to 0.9 for water-wet cores. The wettability index for untreated and GC18-treated beads were 3.8 and -1.5, respectively. Both these values lie outside of the range of values reported by Donaldson et al (1969). The limited results of the glass beads showed extremely wetting behavior. Even the tBDM-treated beads from MWO26 was more water-wet (USBM wettability index of 3.81) than the water-wet cores tested by Donaldson (1969).

Results in Table 4.6 revealed very little difference between log (A_1/A_2) and the log (A_3/A_2) used to calculate the USBM index. This result may be fortuitous because the difference in water saturation at ROS and at complete saturation only caused A_3 to be slightly smaller than A_1. This difference may become greater in natural materials if more oil is trapped at ROS than in glass beads. The ratio, log (A_1/A_2) could still be a useful index for wettability, however, because many S_w-ψ experiments in soil physics and hydrology neglect measurement of secondary displacement. In those cases, the conventional USBM method could not be used. The logarithm of the ratio of A_1 to A_2 would give a similar indication of wettability as the conventional USBM method. The USBM method also appears to be insensitive to moderately wetted conditions

in which the displacement curves lie mostly on the same side of the zero pressure axis. For example, even though capillary pressures indicated that tBDM–treated beads in MWO26 were not as water–wet as the untreated beads in MWO30 during primary displacement of Soltrol® by water, the USBM wettability index calculated for both experiments was almost identical. The difference in wettability was indistinguishable because, in both cases, ROS occurred before zero capillary pressure was reached.

The USBM method also neglects contact angle hysteresis. It was clear from the S_w–ψ results for GC18–treated beads that wettability conditions for each displacement process was different and needed to be analyzed separately. The measurement of log (A_2'/A_2) and log (A_3/A_3') could be used as empirical indexes to help distinguish contact angle hysteresis and mixed wettability conditions. For example, the results in Table 4.6 showed that for MWO26, conditions during secondary displacement of water by Soltrol® was strongly water–wet (A_3/A_3') just like the untreated beads but conditions during primary displacement of Soltrol® by water were slightly less water–wet (A_2'/A_2) than the untreated beads (compare log (A_2'/A_2) of MWO26 and MW25, for example, in Table 4.6). Areas A_2' and A_3' could easily be obtained from S_w–ψ plots.

Figure 4.21 illustrates how the indexes, log (A_2'/A_2) and log (A_3/A_3'), can be useful. The figure shows S_w–ψ data from a water–Soltrol® displacement experiment for a hypothetical soil. In the figure, the areas A_3 and A_2 are equal, A_2' and A_3' are equal, and the residual saturations are equal. Furthermore, A_2' is 100 times smaller than A_2. The standard USBM wettability index calculated for this soil would equal zero suggesting that the soil was intermediate–wet. The S_w–ψ data show this is not the case. Actually, the soil behaved water–wet when Soltrol® displaced water and oil–wet when water displaced Soltrol®. Log (A_2'/A_2) and log (A_3/A_3') reveal the different wetting behavior in each displacement process. A value of +2 calculated for log (A_2'/A_2) indicates that the soil was water–wet when Soltrol® displaced water. Similarly, a value of –2 for log (A_3/A_3') indicates that the soil was oil–wet when water displaced Soltrol®. Intermedi-

ate wettability deduced from the USBM index was a result of the cancellation of extreme wetting conditions when the two areas, A_2 and A_3 were combined in the ratio.

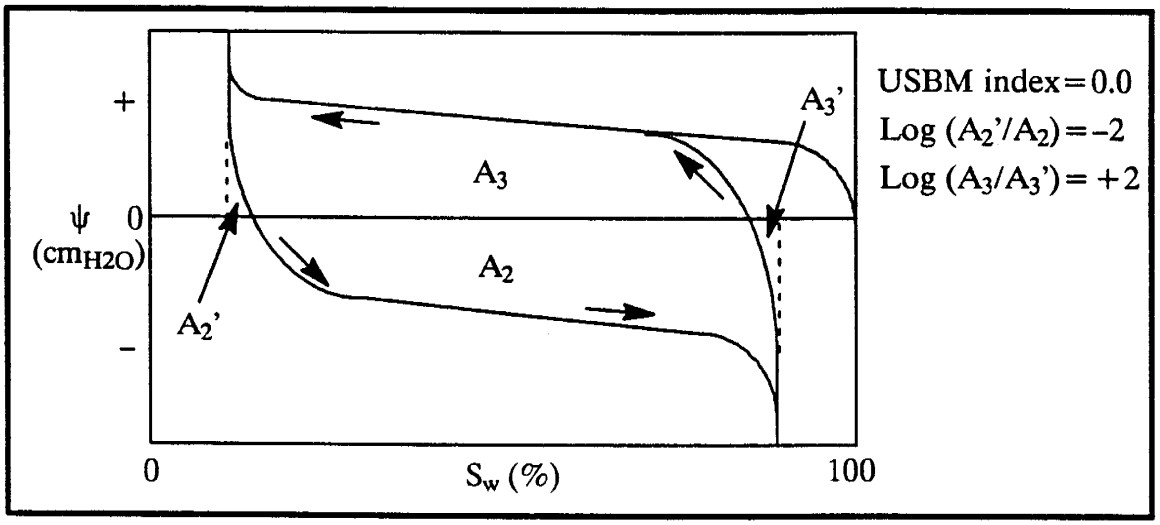

Figure 4.21. Wettability indexes for a hypothetical soil.

Limited results from the Amott wettability calculations also showed extreme wetting conditions for untreated and GC18–treated beads (Table 4.7). The indexes, I_w and I_o, for untreated and GC18–treated beads were very close to unity. The indexes, I_w and I_o, measured the wettability of each individual curve and could, therefore, distinguish conditions of mixed wettability. However, the Amott test could not distinguish between strongly and moderately wetted conditions as illustrated in Figure 4.17b. For example, the index, I_w for MWO26 (tBDM–treated beads) and MWO30 (untreated beads) were almost identical even though conditions were less water–wet in MWO26 than in MWO30.

5. Results of micromodel experiments

In this section, qualitative results of micromodel experiments are presented. The micromodel, H6C, has a homogeneous pore network (see Figure 2.21). Two–phase, water–Soltrol® experiments were run for the untreated (water–wet) model first. The model was then treated with GC18 and the same experiment was repeated for the oil–wet case. The GC18 treatment was removed by heating the model in the furnace after the experiment (see section 2.4.3). The model was then retreated with tBDM and the experiment was rerun. The displacement sequence remained the same for all three wettability cases with the model oriented vertically. Soltrol® was introduced from the top into the initially water–saturated model to displace the water (Soltrol® flood). After Soltrol® had broken through the bottom of the model, water was introduced from the bottom to displace the Soltrol® (water flood). The displacement sequence was analogous to that of the short column experiments. Micromodel experimental procedures were presented in section 2. In the experiments, the water was dyed blue and the Soltrol® was dyed red (section 2.15.1).

5.1 Untreated model

Soltrol® flood: the displacement front was very sharp and uniform as it moved down the model. Preferential flow of Soltrol® along the sides of the model was negligible. Capillary end effects, as the displacement front approached the bottom of the model, were minimized by the presence of the capillary barrier. Some end effects was still evident by the slightly greater amounts of water isolated in the lower quarter of the model after the Soltrol® initially broke through the capillary barrier. After the displacement, water was found in pore throats and pore bodies. Much of the residual water appeared isolated in irregularly shaped zones consisting of one or more pore bodies and adjacent pore throats.

Microscopic inspection at IWS showed that water completely wetted the model. Water adhered to the pore walls including the space along the wedges of the pore while Soltrol® occupied the center of the pores (Figure 5.1). Soltrol® was never seen in contact with the pore wall. The curvature of the water–Soltrol® interface was concave towards the water indicating that Soltrol® was the non–wetting liquid and water was the wetting liquid (Figures 5.1 and 5.2).

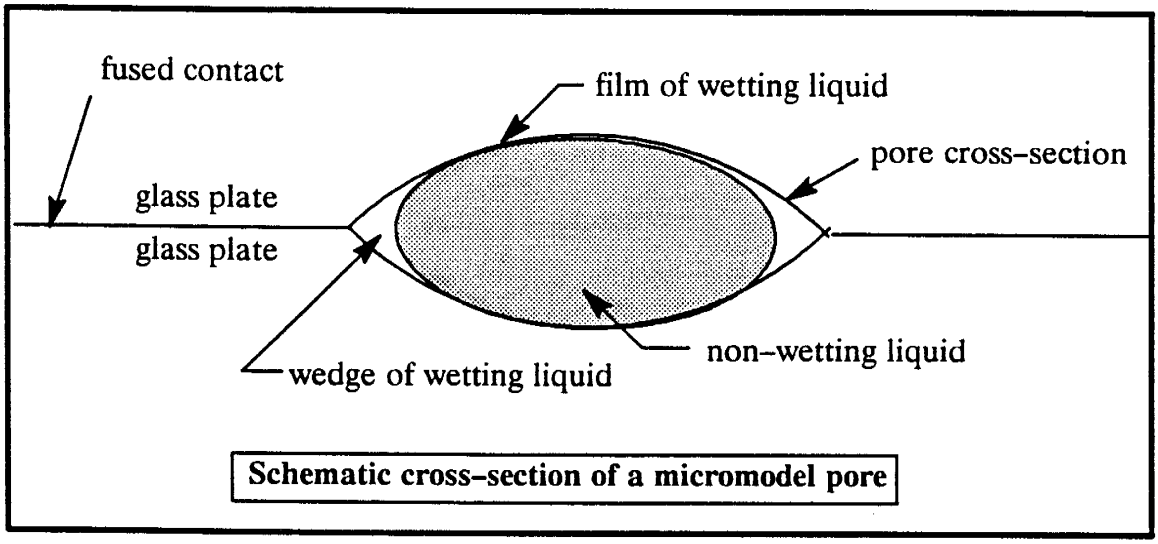

Figure 5.1. Location of the wetting and non–wetting liquids in a micromodel pore.

Figure 5.2, taken at the center of the model at IWS, shows that water frequently occupied the smaller pore throats. The residual water in the pore throats were still inter–connected by water in the wedges and possibly also by thin water films. Films were not visible through the microscope, however. Where water was trapped in the large pore bodies, it would also be trapped in the adjacent smaller pore throats. Water in pore bodies and adjacent pore throats took on a 'star' shape (lower left–Figure 5.2). The 'star' shapes form because Soltrol® commonly advanced into the pore throat and stopped before the pore throat became too narrow. The capillary pressure at the narrowest constriction was too great for the Soltrol® to break through. If the pore throat was wider and the capillary pressure there could be overcome, Soltrol® would natural-

ly advance past the narrowest constriction and enter into the larger pore body. Entry into the larger pore body would occur very quickly as a Haines jump. The characteristic 'star' shape of the water trapped in a pore node and adjacent pore throats, shown at the bottom left of Figure 5.2 for example, was a result of the Soltrol®, the non-wetting liquid, not being able to advance past the narrow constriction of the pore throats because the capillary pressure there was too great.

Figure 5.2. Water at IWS in an untreated micromodel. 12X magnification.

Water flood: the displacement front during water flood was also uniform but somewhat diffuse because of the presence of irreducible water. Some Soltrol® could still be displaced from the model after the first bit of water broke through at the top.

On the pore scale, much of the Soltrol® left in the model at ROS was trapped as ganglia and isolated zones (Figure 5.3). Some was trapped in pore nodes as singlets and doublets (center–Figure 5.3). Singlets, a consequence of trapping by snap–off in

an individual, water–wet pore, were not the most common feature. Soltrol® trapped as ganglia and groups of pores were much more prevalent. Soltrol® trapped in the pores did not take on the 'star' shape characteristic of the wetting liquid (water). The curvature of the water–Soltrol® interface was similar during both the Soltrol® flood and water flood. Strongly water–wet conditions prevailed during both Soltrol® and water flood. This was consistent with the water–Soltrol® contact angles measured for untreated glass ($\theta_{w-o\,r} = 40.7° \pm 7.7°$ and $\theta_{w-o\,a} = 68.8° \pm 9.1°$).

Figure 5.3. Trapped Soltrol at ROS in an untreated micromodel. Photo taken at the center–right area of the model. 12X magnification.

5.2 GC18–treated model

Soltrol® flood: in contrast with the untreated model, the displacement front was initially more uneven. As displacement progressed down the model however, the front evened out. Water appeared to be isolated in zones consisting of several pore bodies

as well as in single pore bodies. The amount of water isolated in large zones appeared to be less than for the untreated model. Pore throats located adjacent to water–filled pore bodies were not necessarily water–filled as in the untreated model.

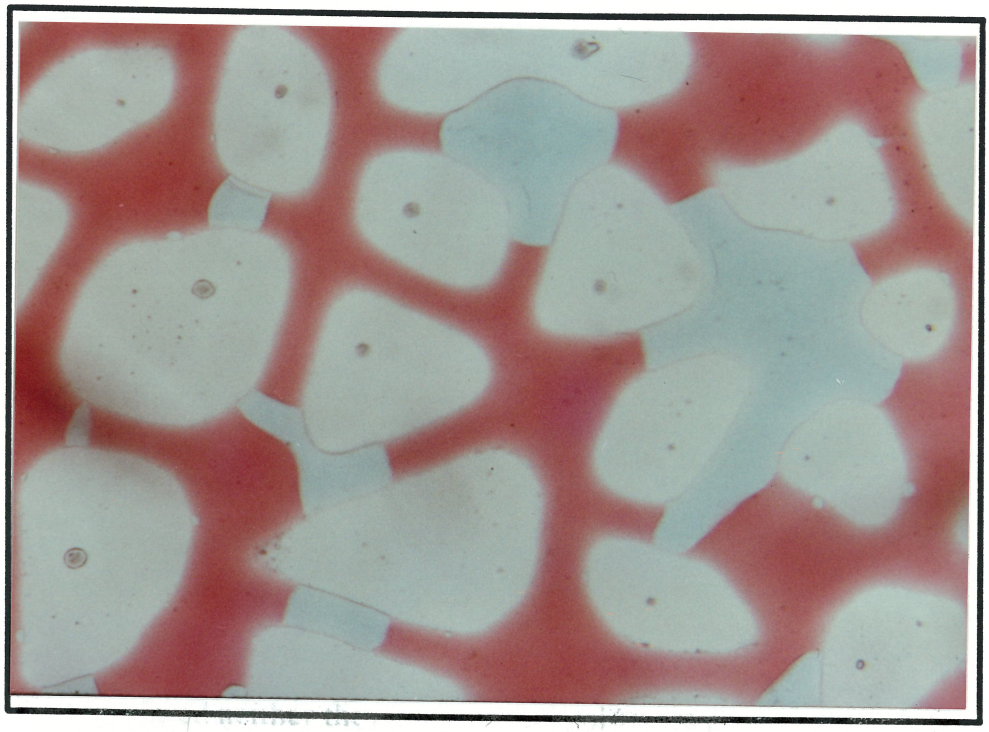

Figure 5.4. Trapped water at IWS in a GC18–treated micromodel. Photo taken near the center of the model. 20X magnification.

Microscopic inspection at IWS showed that the wettability of the system was intermediate to slightly oil–wet. There was no strong preference for either the Soltrol® nor the water to wet the pore walls; the Soltrol®–water interfaces were perpendicular to subperpendicular to the pore walls (Figure 5.4). Water was trapped in pore throats, pore bodies, and in parts of both. An example of the latter case could be seen in the water trapped at the left and right of center in Figure 5.4. The water did not appear to be connected to each other through wedges or thin films, as was the case in the untreated model. Whereas water at IWS in the untreated model usually occupied the fine

pore throats or in pore bodies isolated behind the fine pore throats, there appeared to be no characteristic locations in the pore system where the water was trapped in the GC18–treated model. Trapping did not seem to be capillary dominated but resulted simply from cut–off or isolation.

water flood: as in the untreated model, the displacement front during water flood was fairly uniform but diffuse. Water broke through at the top of the model while much of the top 20% of the model had still yet to be water flooded. Significant amounts of Soltrol® was displaced from this 20% zone after the initial breakthrough occurred. The shapes of the residual Soltrol® were very similar to the shapes of the water at IWS in the untreated model (Figure 5.5). Residual Soltrol® occupied the smaller pore throats. Soltrol® occupying pore bodies and adjacent pore throats took on characteristic 'star' shapes of the wetting liquid (lower left–Figure 5.5).

Microscopic inspection showed that the curvature of the interface during water flooding differed significantly from that during Soltrol® flood (compare interfacial curvatures in Figures 5.4 and 5.5). Soltrol® strongly wetted the pore walls whereas during the Soltrol® flood neither the water nor Soltrol® were preferentially wetting. Soltrol® in pore throats were commonly inter–connected by Soltrol® in the pore wedges and possibly in thin oil films (Figure 5.1). The preference for Soltrol® to wet the pore walls, although very strong, was not as complete as that for water in the untreated model.

The difference in the curvature of the liquid–liquid interface during Soltrol® flood and water flood indicated hysteretic behavior of wettability of the GC18–treated surface (lower left–Figure 5.5). During the initial Soltrol® flood, intermediate–wet conditions prevailed. During the subsequent water flood, oil–wet conditions prevailed. This was consistent with the water–Soltrol® contact angles in section 3 ($\theta_{w-o\ r} = 119.8° \pm 5.0°$; $\theta_{w-o\ a} = 151.4° \pm 6.8°$) The original water trapped in the pore throats

during Soltrol® flood could be easily distinguished from the more recent water introduced into the model during the water flood by the difference curvature of the Soltrol®–water interface. Evidence of contact angle hysteresis is clearly shown in the lower part of Figure 5.5. The water trapped in the pore throat to the left and right were there before the Soltrol® flood. The water occupying the vertical pore channel at the center for example was from the more recent water flood.

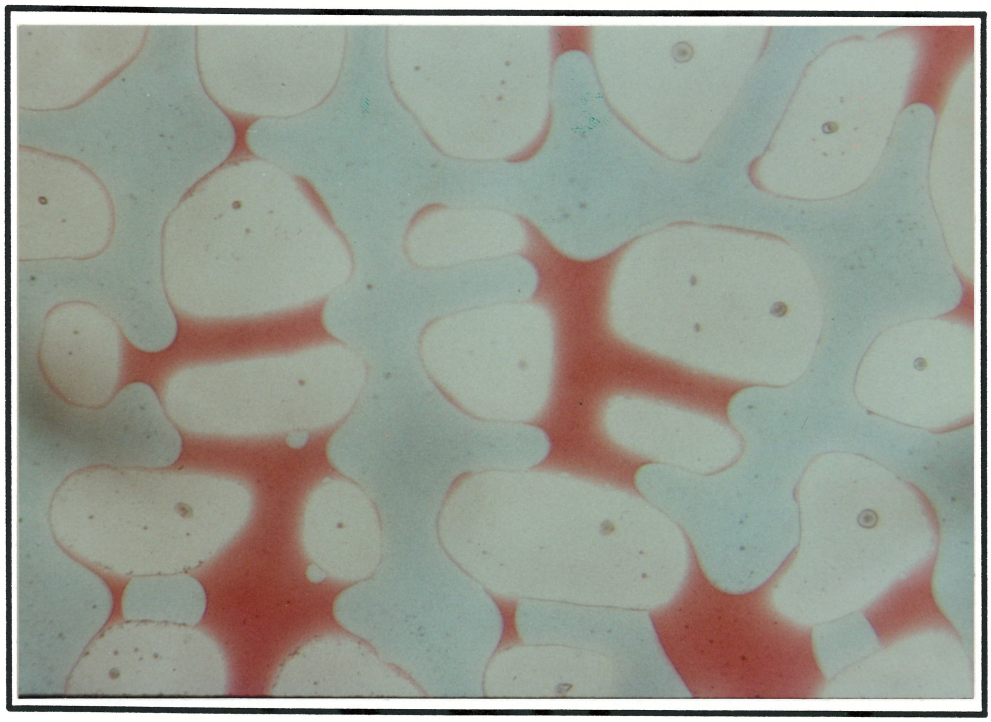

Figure 5.5. Soltrol at ROS in a GC18–treated micromodel. Photo taken at the center of the model. 20X magnification.

5.3 tBDM–treated model

Soltrol® flood: the displacement front was very uniform and sharp as it moved down the model. Residual water was very uniformly distributed throughout the model except at the very bottom where slightly more water was trapped at breakthrough because

of end effects. The characteristic locations of the residual water was very similar to that seen in the untreated (water–wet) model. Water was trapped in pore bodies and adjacent pore throats and in just the pore throats themselves. The tBDM–treated model had been flushed by circulating de–aired water through the model for 2 days. The prolonged flushing time was required to cause the receding angle to decrease. This simulated the conditions in the short columns packed with tBDM–treated beads (recall that the receding angle on tBDM–treated surfaces decreased from 81.8° to ~37° after a few days' exposure to water).

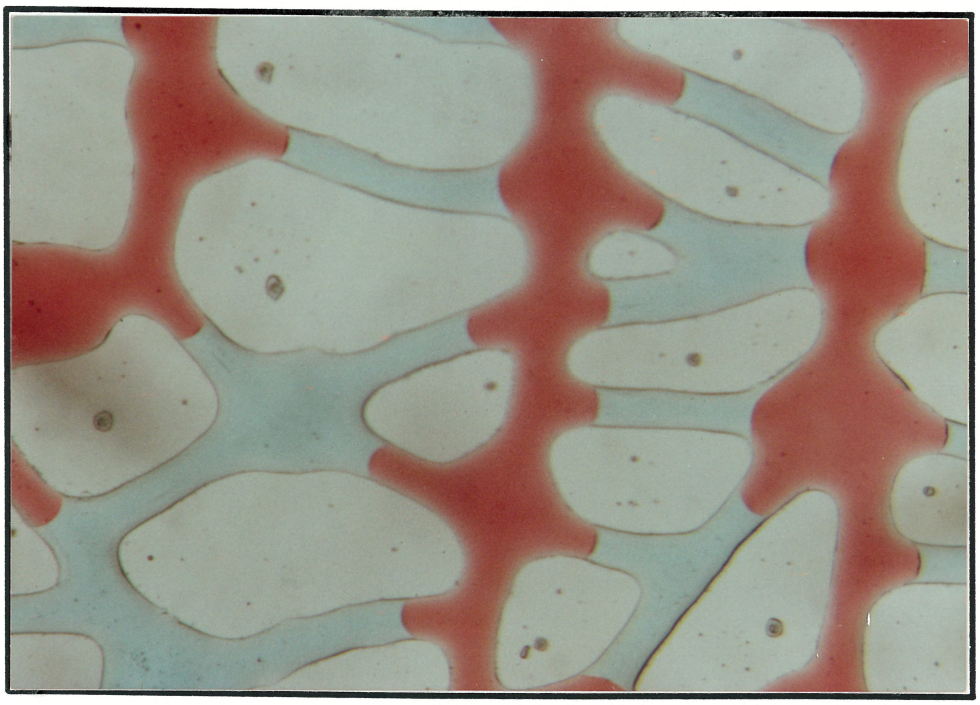

Figure 5.6. Water at IWS in a tBDM–treated homogeneous micromodel. Photo taken at the center–right area of the model. 12X magnification.

At the pore level, the curvature of the interface indicated that water was the wetting liquid and Soltrol® was the non–wetting liquid (Figure 5.6). However, wettability conditions appeared to vary from strongly water–wet in some places and weakly wa-

ter–wet in others. Water in wedges could be seen connecting water trapped in the horizontal pore throats at center–right in Figure 5.6. The most common condition was strongly water–wet but not completely water wetting. Under this wetting condition, trapped water appeared to be only locally interconnected.

Figure 5.7. Trapped Soltrol at ROS in a tBDM–treated homogeneous micromodel. Photo taken at the upper right area of the model. 2X magnification.

Water flood: the displacement front during water flood was again uniform but diffuse. Some Soltrol® still occupied the pores in the very top part of the model when water first broke through. This amount was less than in the GC18–treated model. Generally, areas occupied by Soltrol® and displaced by water were very cleanly displaced. Other areas were completely by–passed by the water including a large area at the bottom–center of the model.

At the pore level, much of the Soltrol® at ROS was not trapped in any characteristic locations (Figure 5.7). Soltrol® was trapped in pore throats, pore bodies, and frequent-

ly the same blob would be trapped in parts of both. Residual Soltrol® was not interconnected by wedges. Curvature of the water–Soltrol® interface showed that intermediate wettability conditions prevailed during water flood; interfacial curvatures were very slight. Contact angle hysteresis was evident from the difference in interfacial curvatures evident during Soltrol® flood and water flood (right side–Figure 5.7).

5.4 Discussion

The micromodel experiments were used only as a qualitative tool to observe interfacial curvatures, contact angle hysteresis, relative wetting and distribution of the liquids, and mechanisms of liquid trapping. No attempt was made to simulate the pore network geometry and pore aspect ratio of the glass beads in the micromodel. The lack of control of flow rates and the inability to measure capillary pressures preclude meaningful quantitative analysis of the micromodel experiments. Residual saturations and prevalence of certain trapping mechanisms observed in the micromodel experiments could not be reliably extrapolated to the short column experiments because of the variables mentioned above.

One of the most useful micromodel results was the visualization of interfacial curvatures in the micromodel. The observed curvatures, which reflect wettability, were consistent with the water–Soltrol® contact angles reported in section 3 (Table 3.4). Although the dyes in the water and in the Soltrol® decreased the interfacial tension between the liquids, they should not directly affect the interfacial curvature. Interfacial curvature is defined by:

$$J = P_c / \sigma = \sigma (1/r_1 + 1/r_2) / \sigma \qquad (5.1)$$

where J is the curvature (dimensionless) and the terms P_c, σ, r_1, and r_2 have been previously defined in section 1. A change in interfacial tension changes the capillary pressure but not the curvature because the interfacial tension in the numerator and denominator cancel each other out. A change in interfacial tension, however, may

indirectly affect the contact angle through equation 1.2 which in turn could affect the interfacial curvature. The significance of the dyes appeared to be minor because the interfacial curvatures were consistent with the contact angles in section 3.

By-passing appeared to be a more common mechanism of trapping than snap-off in the untreated model during water flood. The aspect ratio of the pore body to pore throat in the plane of the micromodel was sufficient (> 1.5) for snap-off to occur. By-passing of the non-wetting liquid usually occurs in porous media having a non-uniform pore size distribution. By-passing in the micromodel did not necessarily indicate that the pores were non-uniform or heterogeneous. As mentioned in section 2, the low aspect ratio of the pore body to pore throat perpendicular to the plane of the model may have caused the effective aspect ratio to become small enough so that snap-off became less prevalent. The relatively large advancing water-Soltrol® angle (68.8°) also could have prevented snap-off from being a major trapping mechanism (Wardlaw, 1982).

Soltrol® occupying the wedges at ROS in the GC18-treated case reflected a water-Soltrol® advancing contact angle of closer to 180° than the 151.4° measured on the GC18-treated glass slides. This greater oil wettability was probably caused by the surface roughness and pore shape irregularities such as the angular wedges at the edge of the pores. The corners at the edge of the pores were smaller than the radius of curvature of the water-Soltrol® interface (Figure 5.1). As a result, a wedge of Soltrol® remained in these corners which extended throughout the pore system. The wedges effectively enhanced oil wettability by increasing the affinity of the Soltrol® to adhere to the pore wall. Surface roughness of the pores should be greater than the glass slides and therefore also enhance wettability (see Figure 1.3 in section 1.3). This could explain why, in the short column experiments, the data from the untreated beads (MW25) scaled by 180° rather than the 151.4° measured on smooth, flat GC18-treated slides, fitted the measured data for GC18-treated beads (MWO32)

better. Similarly, conditions in the untreated micromodel appeared completely water-wet even though finite advancing and receding angles were measured on untreated slides (Table 3.4). This greater water wettability could be explained by pore shape irregularities (wedges) and surface roughness of the pores.

The experiment with the tBDM-treated model revealed that even if intermediate wettability conditions prevailed and displacement efficiency on a pore scale was high, by-passing and isolation of Soltrol® was observed during water flood. This may explain the unexpectedly high values of ROS in the tBDM-treated beads in experiments MWO22 and MWO26 (Table 4.4).

Interfacial curvature and location of the wetting and non-wetting liquids in the micromodel experiments could explain displacement behavior in the GC18-treated and untreated beads. If the wetting liquid displaces the non-wetting liquid (eg. water flood in the untreated model), the non-wetting liquid is displaced from the smaller pores first. Displacement progresses to the larger pores where the non-wetting liquid gets trapped by snap-off and by-passing. These mechanisms cause relatively large volumes of the non-wetting liquid to be trapped in the larger pores. Recall how Soltrol® occupied the larger pore bodies in the untreated model after water flood. This could explain the relatively large ROS (17.6%) in the untreated beads. Residual non-wetting liquid saturation was caused by entrapment of the non-wetting liquid. Trapped non-wetting liquid behind the displacement front formed discontinuous 'blobs' which were very hard to mobilize.

If the non-wetting liquid displaces the wetting liquid (eg. Soltrol® flood in the untreated model and water flood in the GC18-treated model), the process is reversed. Displacement initially occurs in the larger pores where it is easier for the non-wetting liquid to penetrate and progresses to the smaller pores. At the end of the displacement, the residual wetting liquid remains in the smaller pores while the non-wetting

liquid fills the larger pores. This could explain the relatively low IWS in the untreated (7.5%) and tBDM-treated beads (10.1%) in which water was the wetting liquid. This could also explain the relatively low ROS (10.1%) in the GC18-treated beads in which Soltrol® was the wetting liquid after wettability had essentially been reversed. In all these cases, the wetting liquid occupied the smaller pore throats in the micromodel. Residual wetting liquid saturation occurred, not by entrapment, but by drainage and isolation (Morrow, 1971). If the wetting liquid was completely wetting, residual wetting liquid behind the displacement front could continue to drain through film flow.

6. Summary discussion

Contact angle hysteresis should receive greater attention in wettability studies. All silane–treated surfaces where advancing and receding angles were measured displayed contact angle hysteresis (Tables 3.3 and 3.4). Hysteresis was large enough in the treated beads that different wettability conditions prevailed during water–Soltrol® displacements depending on whether water was advancing or receding against Soltrol®.

Development of the dual filter short column provided the breakthrough in measuring the saturation–capillary pressure (S_w–ψ) curves and ROS for GC18–treated beads. The dual filter column allowed saturations in the negative capillary pressure region to be measured. Similar dual filter cells were used by Gatenby and Marsden (1957) and Killins et al (1953) to measure capillary pressure–saturation relationships in silane–treated cores. Stonestrom and Rubin (1989) recently developed a dual filter cell for measuring S_w–ψ data in soils.

The close match between S_w–ψ data for untreated beads measured with the conventional and dual filter columns helped validate the dual filter column method and gave further support that the S_w–ψ results for untreated beads were intrinsically correct (Figure 4.13). This, in turn, provided greater confidence in interpreting the results for GC18–treated beads in the dual filter column. The S_w–ψ curves measured here for GC18–treated beads are believed to be the first ever done for unconsolidated, uniformly oil–wet spherical beads. No such published results appear to exist.

The large ROS (> 31.6%) in GC18–treated beads packed in the conventional columns was caused by wall effects. The space between the GC18–treated beads and the column wall acted as a large pore and caused water to preferentially flow along the column wall and prematurely breakthrough the top endcap. The value of 10.1% ROS for GC18–treated beads packed in the dual filter column more closely reflected resid-

ual Soltrol® saturation in an actual homogeneous, oil–wet system. Although the ROS was significantly less than in the untreated beads (ROS = 17.6%), Soltrol® was displaced out of the GC18–treated beads at lower capillary pressures.

The use of interfacial tension, σ, and grain size, r, to scale Haines' water–air data to our water–Soltrol® data appeared valid because the scaled data and the measured data were consistent (Figure 4.18). Using cosine θ to scale data for strongly wetted (water–wet and oil–wet) conditions also appeared valid because the scaled and measured data gave good agreement (Figure 4.19). The close match between the measured oil–wet data and the scaled water–wet data may also be facilitated by the fact that S_w–ψ behavior is less sensitive when the non–wetting phase is displacing the wetting phase (during drainage). This was experimentally demonstrated by Morrow and M^{c}Caffery (1978). Scaling by cosine θ in homogeneous porous media appeared to work for strongly wetted conditions perhaps because there is less propensity for the interface to be located at the corner of the pores where it can take on various curvatures (Anderson, 1987). The use of cosine θ to scale data not under strongly wetted conditions could not be determined based on our experiments with the tBDM–treated beads. Results from Morrow and Mungan (1971) indicated that this method of direct scaling with the contact angle measured on a smooth, flat surface did not work. Morrow and M^{c}Caffery (1978) showed that contact angles could be correlated with capillary pressure–saturation results if the roughness and irregularities of the porous medium were taken into account.

An important result of this study was that caution must be exercised when comparing and interpreting results measured by different experimental methods. For example, the advancing contact angles measured with the dynamic and static sessile drop methods differed. The static method gave slightly lower values except under strongly oil–wet conditions. The lower values were probably due to the pull on the drop as it was being snapped–off the buret causing the contact angle to be slightly less than the

true maximum angle. Advancing angles measured with the dynamic method may, therefore, more truly represent the advancing angle. The ROS in GC18-treated beads measured from the conventional and dual filter columns also could not be compared. Discretion must be used when comparing ROS values obtained from water flooding and from capillary pressure-saturation data especially for non water-wet porous media.

Results from this study indicated that wettability could have implications in the investigation of NAPL contaminated sites and in subsequent remediation design. For example, the amount of residual NAPL would be less in a uniformly oil-wet, homogeneous aquifer than in a uniformly water-wet, homogeneous aquifer. The distribution of NAPL in the pores would also be different between the water-wet and oil-wet cases. The distribution of water and NAPL in the pores caused by wettability alteration could affect the choice of remedial action. For example, trapped NAPL blobs in water-wet aquifer materials could, at least in theory, be mobilized by hydraulic sweeps. In practice, this may only be possible in very permeable aquifer zones (Mercer and Cohen, 1990; Wilson and Conrad, 1984). On the other hand, NAPL films adhering to pore walls in very permeable oil-wet aquifer materials would remain even after hydraulic sweeps and become a prolong source of contamination via dissolution.

The wall effect in the conventional column packed with GC18-treated beads illustrate how non-uniform pore sizes (heterogeneities) could increase ROS in uniformly oil-wet systems. Greater ROS should be expected in a heterogeneous, uniformly oil-wet system than in a homogeneous, uniformly oil-wet system. In a heterogeneous aquifer rendered uniformly oil-wet by NAPL contaminants, most of the NAPL should be trapped in the finer sediments. This is contrary to the water-wet situation where more NAPL are typically trapped in the coarser sediments (Wilson et al, 1990). If the aquifer was uniformly intermediate-wet, observations from experiments with the

tBDM–treated micromodel suggest that there should be no preferred or characteristic location as to where most of the NAPL would be trapped.

The difference in values between water–air and water–Soltrol® contact angles on the untreated glass slides (Tables 3.3 and 3.4) imply that wettability alteration does not depend only on the decrease of the surface energy or critical surface tension of the aquifer grains due to adsorption of polar organic compounds from NAPL. Wettability alteration also depends on the type of NAPL present. For a given porous medium, different NAPLs result in different water–NAPL contact angles even if no adsorption occurred.

7. Conclusions

- Organosilanes were successfully used to alter wettability of glass beads and glass micromodels to simulate hydrophobic soils and aquifer materials.
- Silane treated surfaces were characterized on glass slides by contact angles. Contact angle hysteresis and stability were quantified for various fluids.
    1. All treated slides, where advancing and receding angles were measured, displayed contact angle hysteresis.
    2. The treated surfaces remained stable in air and in various organic liquids over an indefinite period of time.
    3. All treated surfaces deteriorated in water. Deterioration could usually be detected within the first few days.
    4. Deterioration was indicated by a decrease in the advancing and receding contact angles, increase in contact angle hysteresis, and increase in the critical surface tension. The receding angle and hysteresis were more sensitive indicators than the advancing angle or the critical surface tension.
    5. The GC18–treated surfaces remained the most stable in water over the 1000 hours of observation. The GC18–treated surfaces were intermediate–wet when water receded against Soltrol® ($\theta_{w-o_r} = 119.8°$) and oil–wet when water advanced against Soltrol® ($\theta_{w-o_a} = 151.4°$).
    6. The tBDM–treated surfaces also remained relatively stable in water. The tBDM–treated surfaces were initially intermediate–wet when

water receded against Soltrol® ($\theta_{w-o\,r} = 81.8°$) and when water advanced against Soltrol® ($\theta_{w-o\,a} = 108.0°$). Significant hysteresis did develop once the surface had been exposed to water for several days because the receding angle decreased rapidly (from 81.8° to 37.2°). The surface appeared to remain stable thereafter for up to 800 hours however.

7. Deterioration of the treated surface was probably due to hydrolysis. Although bacteria were present on some of the early treated slides stored in water, their role in the breakdown of the surface was unclear.

- Wettability affects capillary pressures, ROS, and fluid distribution in porous media.
- Average values of IWS for untreated, GC18-treated, and tBDM-treated beads were $7.5 \pm 2.0\%$, $6.6 \pm 4.3\%$ (from the dual filter columns only), and $10.1 \pm 3.3\%$, respectively. These values were similar and suggest that IWS was essentially independent of wettability from water-wet to intermediate-wet conditions ($41° < \theta < 120°$). The slightly higher IWS for tBDM-treated beads could indicate that the beads did not drain as fully as the untreated and GC18-treated beads.
- Average values of ROS for untreated and GC18-treated beads were $17.6 \pm 1.8\%$ and $10.1 \pm 0.7\%$ (from the dual filter columns), respectively. The ROS was significantly lower for GC18-treated beads. The ROS from two experiments with tBDM-treated beads averaged 18.4% but this value was unreliable.

- The high ROS (> 31.6%) for GC18-treated beads packed in the conventional column was caused by wall effects in the experiment. This wall effect caused greater trapping of Soltrol® in the GC18-treated beads.

- The capillary pressure-saturation data for untreated beads could be compared to Haines' data after scaling by the ratio of the interfacial tension and the grain size. The drainage data matched but the imbibition data did not agree as well. The discrepancy during imbibition was probably due to different contact angles operative in Haines' experiment and the experiments here with water and Soltrol®. This indicated that completely water-wet conditions did not prevail during imbibition when water displaced Soltrol®.

- The use of cosine θ to scale the strongly water-wet data to the oil-wet data appeared valid. The use of cosine θ to scale data to not strongly wetted conditions could not be evaluated based on our results for tBDM-treated beads.

- Development of the dual filter short column was a breakthrough that allowed capillary pressure-saturation data for GC18-treated beads to be measured. The capillary pressure-saturation relationship for GC18-treated beads is believed to be the first one measured for uniformly oil-wet, unconsolidated spherical beads. The good agreement in the capillary pressure-saturation results for untreated beads in the conventional and dual filter columns strengthened the validity of the dual filter column method.

- The USBM and Amott-Harvey wettability indexes indicated very water-wet conditions for untreated beads and oil-wet conditions for GC18-treated beads. Both indexes combined the wettability behavior

of the drainage and imbibition processes and therefore implicitly ignored contact angle hysteresis.

- The results (ROS and wettability indexes) were inconclusive for tBDM-treated beads. Only three columns drained properly and the capillary pressure-saturation data during Soltrol® displacement by water did not match for two of the columns.

- Wettability conditions inferred from the interfacial curvatures in the untreated, GC18-treated, and tBDM-treated micromodel were consistent with the receding and advancing water-Soltrol® contact angles measured on similarly treated slides. The receding angle corresponded to the Soltrol® flood and the advancing angle corresponded to the water flood.

- In the untreated micromodel, residual Soltrol® was most commonly trapped during water flood in zones that were by-passed and became disconnected with the bulk Soltrol® phase. Soltrol® trapped in singlets and doublets from snap-off also occurred but was less common. The effective aspect ratio of the pore body to pore throat may not have been large enough for snap-off to have become a dominant trapping mechanism in the micromodel. The relatively high advancing water-Soltrol® contact angle (68.8°) also would not promote snap-off to occur.

- Residual Soltrol® after water flood in the GC18-treated model occurred mostly in the smaller pore throats, in the pore bodies and adjacent pore throats, and in wedges and possibly thin films along the pore walls. The curvature of the interface and the wettability were reversed from the untreated case. Contact angle hysteresis was evident from the

difference in interfacial curvature during Soltrol® flood and during water flood.

- The low ROS (10.1%) in GC18–treated beads packed in the dual filter column could be explained by the fact that Soltrol®, being the wetting liquid, occupied the smaller pores and pore throats, and in the small wedges along the pore walls in a GC18–treated porous medium. The presence of a thin film of Soltrol® along the pore wall also would allow Soltrol® trapped behind the displacement front to continue to drain. The higher ROS (17.6%) in the untreated beads was caused by Soltrol® being trapped in the larger pore bodies as the non–wetting liquid.
- Soltrol® in the tBDM–treated micromodel was not trapped in any characteristic locations at ROS. Residual Soltrol® trapped behind the displacement front were disconnected from the bulk Soltrol® phase and became immobilized. Contact angle hysteresis was evident from the difference in interfacial curvature after Soltrol® flood and after water flood.

8. Recommendations for future research

- Contact angle measurements should always include advancing and receding angles. Receding angles should also be included in the Zisman plots to see how the receding angle and contact angle hysteresis changes with surface tension. This would provide a more complete understanding of the wettability of the treated surface.

- If the silanes used in this study are to be exposed to other fluids not investigated here, the stability of the treated surface in those fluids should be adequately quantified.

- Consider finding another silane to use instead of the tBDM for intermediate wettability studies. Experience shows that a silane treatment involving water or alcohol may result in a more successful treatment especially if repeated treatments can be done easily.

- Perform dual filter short column experiments with Teflon® beads to further validate the oil-wet results.

- In future wettability experiments where capillary pressure-saturation data are measured, include measurement of the secondary displacements. This allows the USBM and Amott wettability indexes to be calculated.

- Continue indefinitely, the MWO32 experiment to see if and when wettability changes in the treated beads will occur. Longevity of silane-treated porous media under actual operation has never been measured before. If the long-term stability of the GC18-treated beads can be demonstrated, GC18 will be an extremely useful treatment for 2-phase wettability studies in hydrology and petroleum engineering.

- Dual filter columns should continue for tBDM–treated beads to confirm the capillary pressure–saturation relationship and ROS. One or two layers of finer, untreated glass beads between the tBDM–treated beads and the filter on the bottom endcap may enhance drainage. Alternatively, dual filter experiments for GC18–treated beads with water and air instead of water and Soltrol® should be considered to obtain data for intermediate–wet systems.

- Perform some dual filter column experiments for OtS–treated beads. Significant contact angle hysteresis should develop during flushing of the column. The resulting capillary pressure–saturation curve should show water–wet behavior during water displacement by Soltrol® and oil–wet behavior during Soltrol® displacement by water. The possibility of scaling the curves with cosine θ can be investigated. Deterioration of the treated surface should be retarded by the presence of Soltrol®.

- Conducting short column experiments with initially Soltrol®–saturated instead of water–saturated beads should be considered. The silane–treated surface may not deteriorate as much if the beads are exposed to Soltrol® first instead of water. Residual saturations and USBM and Amott wettability indexes can still be calculated if secondary displacements are performed.

- Repeat the micromodel experiments on micromodel H6C using a high pressure pump to control flow rates and video–tape the displacement on a pore level scale to better understand the displacement and trapping mechanisms operative for different wettabilities. Use an image processing system to quantify residual saturations.

- Develop a treatment to achieve mixed and fractional wettability and run short column experiments to measure residual saturations and capillary pressure–saturation relationships. Use micromodels to visualize fluid distribution.
- Measure the residual saturations in heterogeneous beads with uniform wettability. Mix beads of (two or more) different sizes and run short column experiments to determine IWS and ROS. Measure the relationship between sorting, such as the coefficient of curvature or coefficient of uniformity (see Craig, 1978 for example) and ROS. Use micromodels to visualize displacement and trapping.
- Perform vadose zone short column experiments for untreated and treated glass beads. Perform 3–phase micromodel experiments as analogues to the short columns. Investigate the propensity of preferential flow induced by wettability alteration.
- Develop a way to measure the pH of the pore water in the short columns. In the present study, we have ignored the sensitivity of the treated surface to any changes in the pH of the water.
- Confirm the existence of wettability alteration by NAPL contaminants in the field. Determine the mechanisms of wettability alteration.

9. References

Adamson, A. W. 1982. *Physical Chemistry of Surfaces*. 4th ed., John Wiley & Sons, New York, NY.

American Society of Testing Materials. 1986. *Standard test method for hydrophobic contamination on glass by contact angle measurement.* ASTM, Philadelphia, pp. 339–341.

Amott, E. 1959. Observations Relating to the Wettability of Porous Rocks. *Trans.* AIME, 216, pp. 156–162.

Anderson, W. G. 1986a. Wettability Literature Survey–Part 1: Rock/Oil/Brine Interactions and the Effects of Core Handling on Wettability. *JPT* (Oct. 1986), pp. 1125–1144.

Anderson, W. G. 1986b. Wettability Literature Survey–Part 2: Wettability Measurement. *JPT* (Nov. 1986), pp. 1246–1262.

Anderson, W. G. 1987. Wettability Literature Survey–Part 4: Effects of Wettability on Capillary Pressure. *JPT* (Oct. 1987), pp. 1283–1300.

Arkles, B. 1987. Silane Coupling Agent Chemistry. In *Silicon Compounds Register and Review.* Petrarch Systems Silanes & Silicones, Bristol, PA, pp. 54–59.

Bear, J. 1972. *Dynamics of Fluids in Porous Media*. Dover Publications, Inc., New York, 764 pp.

Berendsen, G. E., K. A. Pikaart, and L. de Galan. 1980. Preparation of various bonded phases for HPLC using monochlorosilanes. *J. Liquid Chromatogr.*, 3, no. 3, pp. 1437–1464.

Berendsen, G. E., and L. de Galan. 1978. Preparation and chromatographic properties of some chemically bonded phases for reversed-phase liquid chromatography. *J. Liquid Chromatogr.*, 1, no. 5, pp. 561–586.

Bethel, F. T., and J. C. Calhoun. 1953. Capillary desaturation in unconsolidated beads. *Trans.* AIME, 198, pp. 197–202.

Bowman, R. S. and J. L. Wilson. 1988. The Effects of Wetting on Transport of Organics. Unpublished research proposal to USGS.

Brock, T. D. 1978. The poisoned control in biogeochemical investigations. In *Environmental biogeochemistry and geomicrobiology,* ed. W. E. Krumbein. Ann Arbor, pp. 717–725.

Brooks, R. H. and A. T. Corey. 1964. Hydraulic Properties of Porous Media. Hydrology Papers, Colorado State University, Fort Collins, CO.

Buckley, J. S. 1991. Multiphase Displacements in Micromodels. *Interfacial Phenomena in Petroleum Engineering*, ed. N. R. Morrow. Marcel Dekker, Inc., New York, NY, pp. 157–189.

Chatzis, I. and F. A. L. Dullien. 1983. Dynamic Immiscible Displacement Mechanisms in Pore Doublets. *J. Colloid Interface Sci*, 91, no. 1, pp. 199–222.

Coley, F. H., S. S. Marsden, and J. C. Calhoun. 1956. A Study of the Effect of Wettability on the Behavior of Fluids in Synthetic Porous Media. *Producers Monthly,* 20, no. 8, pp. 29–45.

Craig, R. F. 1978. *Soil mechanics.* 2nd ed., Van Nostrand Reinhold Company, New York, NY.

Cuiec, L. E. 1991. Evaluation of Reservoir Wettability and Its Effect on Oil Recovery. *Interfacial Phenomena in Petroleum Engineering*, ed. N. R. Morrow. Marcel Dekker, Inc., New York, NY, pp. 319–375.

DeBano, L. F. and J. Letey, eds.. 1969. Water–Repellent Soils. *Proceedings of the Symposium on Water–Repellent Soils*. University of California, Riverside, CA, 354 pp.

Demond, A. H. 1988. Capillarity in Two-Phase Liquid Flow of Organic Contaminants in Groundwater. Unpublished PhD dissertation, Stanford University.

Demond, A. H. and P. V. Roberts. In press. The Effect of Interfacial Forces on the Capillary Pressure of Organic Liquid-Water Systems in Unconsolidated Sand. *Water Resources Res.*, 27.

Donaldson, E. C., R. D. Thomas, and P. B. Lorenz. 1969. Wettability Determination and Its Effect on Recovery Efficiency. *SPEJ* (March 1969), pp. 13-20.

Elrick, D. E., J. H. Scandrett, and E. E. Miller. 1959. Tests of Capillary Flow Scaling. *Soil Sci. Soc. Amer. Proc.*, 23, no. 5, pp. 329-332.

Fox, H. W., and W. A. Zisman. 1950. The spreading of liquids on low energy surfaces. I. Polytetrafluoroethylene. *J. Colloid Sci.*, 5, pp. 514-531.

Freeze, R. A. and J. A. Cherry. 1979. *Groundwater*. Prentice-Hall, Inc., Englewood Cliffs, NJ.

Gatenby, W. A., and S. S. Marsden. 1957. Some wettability characteristics of synthetic porous media. *Producers Monthly,* 22, no. 1, pp. 5-12.

Hagan, E. 1989. A Quantitative Experimental Investigation of the Physical Processes Responsible for Determining Residual Organic Liquid Saturations in Porous Media. Open file report H 89-4, New Mexico Institute of Mining and Technology.

Haines, W. B. 1930. Studies in the Physical Properties of Soil. V. The Hysteresis Effect in Capillary Properties, and the Modes of Moisture Distribution Associated Therewith. *J. Agri. Sci.* 20, pp. 97-116.

Hillel, D. 1980. *Fundamentals of Soil Physics*. Academic Press, New York, NY.

Jennings, H. Y. 1957. Surface Properties of Natural and Synthetic Porous Media. *Producers Monthly,* 21, no. 5, pp. 20-24.

Johnson, R. E. and R. H. Dettre. 1969. Wettability and Contact Angles. In *Surface and Colloid Science*, ed. E. Matijevic, 2, pp. 85–153.

Kennedy, H. T., E. O. Burja, and R. S. Boykin. 1955. An Investigation of the Effects of Wettability on the Recovery of Oil by Water Flooding. *J. Phys. Chem.* (Sept. 1955), 59, pp. 867–869.

Kia, S. F. 1988. Modeling of the retention of organic contaminants in porous media of uniform spherical particles. *Water Res.*, 22, no. 10, pp. 1301–1309.

Killins, C. R., R. F. Nielson, and J. C. Calhoun. 1953. Capillary Desaturation and Imbibition in Porous Rocks. *Producers Monthly*, 18, no. 2, pp. 30–39.

Lambe, T. W. 1951. Soil Testing for Engineers. John Wiley & Sons, New York, NY.

Laroussi, Ch. and L. W. De Backer. Relations Between Geometrical Properties of Glass Beads Media and Their Main $\psi(\theta)$ Hysteresis Loops. *Soil Sci. Soc. Am. J.*, 43, pp. 646–650.

Lenhard, R. J. and J. C. Parker. 1987. Measurement and Prediction of Saturation–Pressure Relationships in Three Phase Porous Media Systems. *J. Contam. Hydrol.* 4, pp. 407–424.

Letey, J., J. F. Osborn, and N. Valoras. 1975. Soil Water Repellency and the Use of Nonionic Surfactants. Dept. of Soil Science and Agricultural Engineering, University of California, Riverside, CA, 85 pp.

Leverett, M. C. 1941. Capillary Behavior in Porous Solids. *Trans.* AMIE, 142, pp. 152–169.

Mace, R. E. 1990. The Effect of the Fine Fraction on the Residual Trapping of Non-aqueous Organic Liquids in Unconsolidated Porous Media in the Saturated Zone. Open file report, H 90–6, New Mexico Institute of Mining and Technology.

Mason, W. R. 1989. Micromodel Study of Organic Liquid Advance into a Soil. Unpublished independent study, New Mexico Institute of Mining and Technology.

Mattax, C. C. and J. R. Kyte. 1961. Ever see a water flood? *The Oil and Gas Journal* (October, 1961), 59, pp. 115–128.

Melrose, J. C. 1965. Wettability as Related to Capillary Action in Porous Media. *SPEJ* (Sept. 1965), pp. 259–271.

Menawat, A., J. Henry, and R. Siriwardane. 1984. Control of Surface Energy of Glass by Surface Reactions: Contact Angle and Stability. *J. Colloid Interface Sci,* 101, no. 1, pp. 110–119.

Mercer, J. W. and R. M. Cohen. 1990. A Review of Immiscible Fluids in the Subsurface: Properties, Models, Characterization and Remediation. *J. Contam. Hydrol.* 6, pp. 107–163.

Miller, E. E. 1980. Similitude and Scaling of Soil–Water Phenomena. In: Hillel, D. *Applications of Soil Physics*, Academic Press, New York, NY.

Morrow, N. R., ed. 1991. *Interfacial Phenomena in Petroleum Recovery*. Marcel Dekker, Inc., New York, NY.

Morrow, N. R. 1990. Wettability and Its Effect on Oil Recovery. *JPT* (Dec. 1990), pp. 1476–1484.

Morrow, N. R. 1970. Irreducible wetting–phase saturations in porous media. *Chemical Engineering,* 25, pp. 1799–1815.

Morrow, N. R. and J. C. Melrose. 1991. Application of Capillary Pressure Measurements to the Determination of Connate Water Saturation. *Interfacial Phenomena in Petroleum Engineering*, ed. N. R. Morrow. Marcel Dekker, Inc., New York, NY, pp. 257–287.

Morrow, N. R., I. Chatzis, and J. J. Taber. 1988. Entrapment and Mobilization of Residual Oil in Bead Packs. *SPERE* (Aug. 1988), pp. 927–934.

Morrow, N. R., and B. Songkran. 1981. Effect of Viscous and buoyancy forces on nonwetting phase trapping in porous media. In *Surface phenomena in enhanced oil recovery,* ed. D. O. Shah, pp. 387–411.

Morrow, N. R. and F. G. McCaffery. 1978. Displacement Studies in Uniformly Wetted Porous Media. *Wetting, Spreading, and Adhesion*. ed. G. F. Padday, Academic Press, New York, NY, pp. 289–319.

Morrow, N. R. and N. Mungan. 1971 Wettability and Capillarity in Porous Media. Report RR–7, Petroleum Recovery Research Inst., Calgary, Alta.

Mualem, Y. 1976. A New Model for Predicting the Hydraulic Conductivity of Unsaturated Porous Media. *Water Resources Res.*, 12, no. 3, pp. 513–521.

Mungan, N. 1981. Enhanced Oil Recovery Using Water as a Driving Fluid: Part 2–Interfacial Phenomena and Oil Recovery: Wettability. *World Oil* (March, 1981), 192, no. 4, pp. 77–83.

Newcombe, J., J. McGhee, and M. J. Rzasa. 1955. Wettability versus displacement in water flooding in unconsolidated sand columns. *Trans.* AIME, 204, pp. 227–232.

Petrarch Systems Silanes & Silicones 1987. *Silicone Compounds Register and Review.* Bristol, PA.

Parker, J. C., R. J. Lenhard, and T. Kuppusamy. 1987. A Parametric Model for Constitutive Properties Governing Multiphase Flow in Porous Media. *Water Resources Res.*, 23, no. 4, pp. 618–624.

Stonestrom, D. A. and J. Rubin. 1989. Water Content Dependence of Trapped Air in Two Soils. *Water Resources Res.*, 25, no. 9, pp. 1947–1958.

Singhal, A. K., and P. M. Dranchuk. 1973. Wettability Control of Glass Beads. *Cdn. J. Chem. Eng.*, 53, pp. 3–8.

Spitze, L. A., and D. O. Richards. 1947. Surface Studies of Glass. Part I. Contact Angles. *J. Applied Physics.* 18, pp. 904–911.

Szecsody, J., and R. C. Bales. 1988. Sorption kinetics of low–molecular–weight hydrophobic organic compounds on surface–modified silica. *J. Contaminant Hydrology*, in press.

Takach, N. E., L. B. Bennett, C. B. Douglas, M. A. Andersen, and D. C. Thomas. 1989. Generation of Oil–Wet Model Sandstone Surfaces. *SPE Intern. Symp. on Oilfield Chemistry.* Houston, pp. 85–90.

Takach, N. E., L. B. Bennett, C. B. Douglas, M. A. Andersen, and D. C. Thomas. 1988. Wettability Alteration of Model Sandstone Surfaces by Vapor–Phase treatment with Organosilanes. *Preprints, American Chemical Soc.*, 33, pp. 525–529.

Topp, G. C. and E. E. Miller. 1966. Hysteretic Moisture Characteristics and Hydraulic Conductivities for Glass–Bead Media. *Soil Sci. Soc. Amer. Proc.*, 30, pp. 156–162.

Treiber, L. E., D. L. Archer, and W. W. Owens. 1972. A Laboratory Evaluation of the Wettability of Fifty Oil Producing Reservoirs. *SPEJ* 12, pp. 531–540.

van Genuchten, M. Th. 1980. A Closed–form Equation for Predicting the Hydraulic Conductivity of Unsaturated Soils. *Soil Sci. Soc. Am. J.*, 44, pp. 892–898.

Wan, J. and J. L. Wilson. 1990. Preliminary Study of Particle Transport During Single and Two Phase Fluid Flow in Pores and Fractures. Poster, *Manteo III–Concepts in Manipulating Groundwater Colloids for Environmental Restoration*, Manteo, NC.

Wardlaw, N. C. 1982. The Effect of Geometry, Wettability, Viscosity, and Interfacial Tension on Trapping in Single Pore–throat Pairs. *J. Cdn. Pet. Tech.* 21, no. 3, pp. 21–27.

Wilson, J. L. 1988. The Need for Research: Physical Processes–Land, The Role of Wetting in Environmental Problems. *Proc. Conf. on Fundamental Research Needs in Envr. Engineering,* eds. R. G. Luthy and M. J. Small, Assoc. Environ. Engr. Professors, Washington, DC,

Wilson, J. L. and S. H. Conrad. 1984. Is Physical Displacement of Residual Hydrocarbons a Realistic Possibility in Aquifer Restoration? *Proc. Petroleum Hydrocarbons and Organic Chemicals in Ground Water*, NWWA, Houston, TX, pp. 107–133.

Wilson, J. L., S. H. Conrad, W. R. Mason, W. P. Peplinski, and E. Hagan. 1990. Laboratory Investigation of Residual Liquid Organics from Spills, Leaks, and the Disposal of Hazardous Wastes in Groundwater. EPA report: EPA/600/6–90/004, 267 pp.

Zisman, W. A. 1964. Relation of Equilibrium Contact Angle to Liquid and Solid Constitution. *Contact Angle, Wettability and Adhesion,* Advances in Chemistry Series 43, American Chemical Soc., Washington, pp. 1–51.

Appendixes

Appendix A1. Chemical composition of glass substrates

Component	Corning slides	Quartz slides[1]	Silica slides[1]	Willard mirrors	Cataphote beads
SiO_2	72.1%			73.1%	71–74%
Fe_2O_3	0.045%	0.8ppm	0.2ppm		0–Tr.
Al_2O_3	1.80%	10–50ppm	0.1ppm		0.2–1.5%
CaO	7.30%	0.8–3ppm	0.1	8.9%	8.0–10.0%
MgO	3.80%	0.2ppm	0–0.1ppm	3.9%	1.5–3.8%
K_2O	0.15%	0.8ppm	0–0.001ppm		0–0.2%
Na_2O	14.0%	1ppm	0.04ppm	13.7%	12.0–15.0%
SO_3	0.30%				

1. impurities reported as ppm by weight for the element. eg. Na_2O ⧫ Na.

Appendix A2. Effect of heating on GC18–treated surfaces

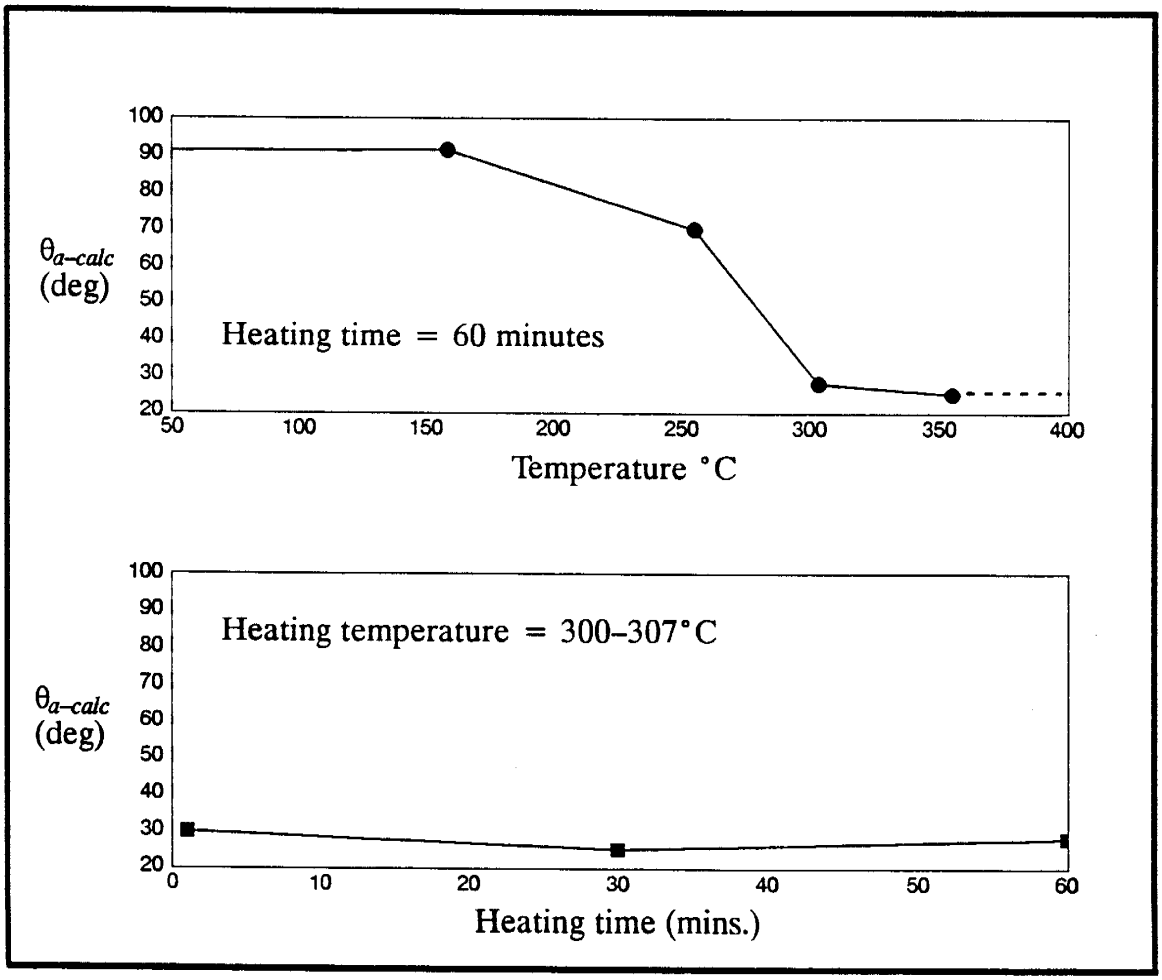

Appendix B1. Average water–air contact angles for tBDM–treated glass slides

Exp: 8	*Date: 5/89*		*Moles: 5.81e–2 moles*		*Med: deionized water*
Elapsed time (hrs)	$\theta_{a\text{–}calc}$ *(deg)*	θ_a *(deg)*	θ_r *(deg)*	$\theta_a - \theta_r$ *(deg)*	*Comments*
2.4	76.4				
4.3	76.5				
10.2	75.4				
24.6	74.1				
49.9	75.8				
73.3	76.4				
99.4	75.5				
302.9	70.1				
421.4	70.5				
530.0	66.2				

Appendix B2. Average water–air contact angles for TMS–treated glass slides

Exp: 11	*Date: 5/89*		*Moles: 2.44e–1*		*Med: air*
Elapsed time (hrs)	$\theta_{a\text{–}calc}$ *(deg)*	θ_a *(deg)*	θ_r *(deg)*	$\theta_a - \theta_r$ *(deg)*	*Comments*
0.2	76.5				
1.5	78.6				
4.2	77.3				
15.3	77.7				
24.0	74.7				
47.4	71.4				
74.2	70.4				

Appendix B3. Average water–air contact angles for TMS–treated glass slides

Exp: 11	*Date: 5/89*		*Moles: 2.44e–1*		*Med: deionized water*
Elapsed time (hrs)	$\theta_{a\text{–}calc}$ *(deg)*	θ_a *(deg)*	θ_r *(deg)*	$\theta_a - \theta_r$ *(deg)*	*Comments*
1.9	85.4				
4.4	85.1				
15.6	82.0				
24.1	82.4				
47.9	80.4				

Appendix B4. Average water–air contact angles for TMS–treated glass slides

Exp: 11	*Date: 5/89*		*Moles: 2.44e–1*		*Med: xylene*
Elapsed time (hrs)	θ_{a-calc} *(deg)*	θ_a *(deg)*	θ_r *(deg)*	$\theta_a - \theta_r$ *(deg)*	*Comments*
2.0	77.0				
4.5	79.2				
15.7	79.7				
24.2	77.6				
47.8	77.3				

Appendix B5. Average water–air contact angles for TMS–treated glass slides

Exp: 13	*Date: 5/89*		*Moles: 2.7e–2*		*Med: air*
Elapsed time (hrs)	θ_{a-calc} *(deg)*	θ_a *(deg)*	θ_r *(deg)*	$\theta_a - \theta_r$ *(deg)*	*Comments*
0.1	73.8				
2.5	74.1				
5.6	75.6				
16.9	76.7				
28.2	73.0				
44.9	73.5				
72.0	74.5				
96.3	74.7				

Appendix B6. Average water–air contact angles for TMS–treated glass slides

Exp: 13	*Date: 5/89*		*Moles: 2.7e–2*		*Med: deionized water*
Elapsed time (hrs)	θ_{a-calc} *(deg)*	θ_a *(deg)*	θ_r *(deg)*	$\theta_a - \theta_r$ *(deg)*	*Comments*
2.7	80.2				
5.7	83.0				
16.0	77.2				
28.5	74.3				
45.1	70.3				
72.1	67.0				
96.4	69.9				
121.0	63.3				

Appendix B7. Average water–air contact angles for TMS–treated glass slides

Exp: 13	*Date: 5/89*		*Moles: 2.7e–2*		*Med: xylene*
Elapsed time (hrs)	θ_{a-calc} *(deg)*	θ_a *(deg)*	θ_r *(deg)*	$\theta_a - \theta_r$ *(deg)*	*Comments*
2.8	74.8				
5.8	79.0				
17.2	78.3				
28.6	76.8				
45.2	73.8				
72.3	78.4				
96.6	74.2				

Appendix B8. Average water–air contact angles for TMS–treated glass slides

Exp: 14	*Date: 6/89*		*Moles: 2.4e–1*		*Med: air*
Elapsed time (hrs)	θ_{a-calc} *(deg)*	θ_a *(deg)*	θ_r *(deg)*	$\theta_a - \theta_r$ *(deg)*	*Comments*
0.4	80.5				
3.5	80.0				
14.9	76.2				
38.2	78.2				
60.9	77.2				

Appendix B9. Average water–air contact angles for TMS–treated glass slides

Exp: 14	*Date: 6/89*		*Moles: 2.4e–1*		*Med: deionized water*
Elapsed time (hrs)	θ_{a-calc} *(deg)*	θ_a *(deg)*	θ_r *(deg)*	$\theta_a - \theta_r$ *(deg)*	*Comments*
3.6	82.1				
15.1	77.9				
38.5	76.3				
61.1	69.6				

Appendix B10. Average water–air contact angles for TMS–treated glass slides

Exp: 14	*Date: 6/89*		*Moles: 2.4e–1*		*Med: xylene*
Elapsed time (hrs)	θ_{a-calc} *(deg)*	θ_a *(deg)*	θ_r *(deg)*	$\theta_a - \theta_r$ *(deg)*	*Comments*
3.7	81.2				
15.2	80.3				
38.6	78.6				
61.2	79.0				

Appendix B11. Average water–air contact angles for TMS–treated glass slides

Exp: 17	*Date: 6/89*		*Moles: 2.53e–1*		*Med: air*
Elapsed time (hrs)	$\theta_{a\text{–}calc}$ *(deg)*	θ_a *(deg)*	θ_r *(deg)*	$\theta_a - \theta_r$ *(deg)*	*Comments*
0.3	75.0				
12.2	73.6				
26.7	75.4				
109.2	74.8				
277.9	71.6				
878.7	70.7				

Appendix B12. Average water–air contact angles for TMS–treated glass slides

Exp: 17	*Date: 6.89*		*Moles: 2.53e–1*		*Med: deionized water*
Elapsed time (hrs)	$\theta_{a\text{–}calc}$ *(deg)*	θ_a *(deg)*	θ_r *(deg)*	$\theta_a - \theta_r$ *(deg)*	*Comments*
0.7	83.8				
12.3	79.3				
26.8	78.7				
38.9	78.4				
50.1	78.8				
73.2	75.2				
98.3	74.2				
146.8	73.7				
206.9	71.6				
352.6	60.6				
565.0	53.6				
691.8	57.1				

Appendix B13. Average water–air contact angles for tBDM–treated glass slides

Exp: 18	*Date: 6/89*		*Moles: 4.86e–2*		*Med: air*
Elapsed time (hrs)	$\theta_{a\text{–}calc}$ *(deg)*	θ_a *(deg)*	θ_r *(deg)*	$\theta_a - \theta_r$ *(deg)*	*Comments*
0.2	75.2				
12.1	72.3				
26.6	75.0				
109.1	72.1				
277.8	72.3				
878.6	71.5				

Appendix B14. Average water–air contact angles for tBDM–treated glass slides

Exp: 18	*Date: 6/89*		*Moles: 4.86e–2*		*Med: deionized water*
Elapsed time (hrs)	$\theta_{a\text{–}calc}$ *(deg)*	θ_a *(deg)*	θ_r *(deg)*	$\theta_a - \theta_r$ *(deg)*	*Comments*
0.6	80.6				
12.4	80.2				
26.9	79.3				
38.8	80.6				
50.0	78.9				
73.1	77.1				
98.2	78.8				
146.4	77.6				
206.8	75.7				
278.2	72.2				
352.4	72.1				
565.0	68.8				
691.6	66.2				
999.4	65.5				

Appendix B15. Average water–air contact angles for tBDP–treated glass slides

Exp: 20	*Date: 7/89*		*Moles: 3e–3*		*Med: air*
Elapsed time (hrs)	$\theta_{a\text{–}calc}$ *(deg)*	θ_a *(deg)*	θ_r *(deg)*	$\theta_a - \theta_r$ *(deg)*	*Comments*
0.4	59.5				
33.9	58.5				
233.9	57.1				

Appendix B16. Average water–air contact angles for tBDP–treated glass slides

Exp: 20	*Date: 7/89*		*Moles: 3e–3*		*Med: deionized water*
Elapsed time (hrs)	$\theta_{a\text{–}calc}$ *(deg)*	θ_a *(deg)*	θ_r *(deg)*	$\theta_a - \theta_r$ *(deg)*	*Comments*
0.5	73.0				
11.3	72.1				
34.0	69.5				
72.0	67.0				
107.8	68.8				
234.0	66.8				
328.9	62.0				

Appendix B17. Average water–air contact angles for tBDP–treated glass slides

Exp: 20	*Date: 7/89*		*Moles: 3e–3*		*Med: 3000mg/L $CaCl_2$*
Elapsed time (hrs)	θ_{a-calc} *(deg)*	θ_a *(deg)*	θ_r *(deg)*	$\theta_a - \theta_r$ *(deg)*	*Comments*
0.6	72.8				
11.4	69.9				
34.1	67.8				
72.1	68.0				
107.9	66.0				
234.3	63.2				
329.0	56.6				

Appendix B18. Average water–air contact angles for GC18–treated glass slides

Exp: 31A	*Date: 8/89*		*Moles:*		*Med: air*
Elapsed time (hrs)	θ_{a-calc} *(deg)*	θ_a *(deg)*	θ_r *(deg)*	$\theta_a - \theta_r$ *(deg)*	*Comments*
0.3	89.7				
67.0	92.5				
163.5	86.9				
356.6	87.5				
714.6	91.5				
986.0	90.3				

Appendix B19. Average water–air contact angles for GC18–treated glass slides

Exp: 31A	*Date: 8/89*		*Moles:*		*Med: deionized water*
Elapsed time (hrs)	θ_{a-calc} *(deg)*	θ_a *(deg)*	θ_r *(deg)*	$\theta_a - \theta_r$ *(deg)*	*Comments*
67.0	89.1				
91.1	86.9				
163.6	87.7				
216.6	86.6				
281.6	86.1				
356.7	83.6				
403.5	83.4				
499.5	84.2				
596.7	80.5				
714.7	82.2				
863.4	77.3				
986.0	79.0				

Appendix B20. Average water–air contact angles for GC18–treated glass slides

Exp: 31A	*Date: 8/89*		*Moles:*		*Med: Soltrol*
Elapsed time (hrs)	$\theta_{a\text{-}calc}$ *(deg)*	θ_a *(deg)*	θ_r *(deg)*	$\theta_a - \theta_r$ *(deg)*	*Comments*
70.1	94.3				
165.9	90.2				
237.2	88.5				
334.2	90.1				
480.6	90.7				
600.4	89.9				
1257.1	91.2				

Appendix B21. Average water–air contact angles for GC18–treated glass slides

Exp: 31B	*Date: 9/89*		*Moles:*		*Med: deionized water*
Elapsed time (hrs)	$\theta_{a\text{-}calc}$ *(deg)*	θ_a *(deg)*	θ_r *(deg)*	$\theta_a - \theta_r$ *(deg)*	*Comments*
1.0	96.0				
42.8	96.1				
100.8	94.6				
192.4	96.6				
240.6	93.4				
291.1	92.9				
336.9	94.6				
405.6	92.4				
500.9	90.9				
596.7	92.3				
765.3	95.1				
911.5	91.3				
1031.2	89.4				
1688.1	88.0				
1781.9	89.4				

Appendix B22. Average water–air contact angles for GC18–treated glass slides

Exp: 31B	*Date: 9/89*		*Moles:*		*Med: 3000mg/L $CaCl_2$*
Elapsed time (hrs)	$\theta_{a\text{–}calc}$ *(deg)*	θ_a *(deg)*	θ_r *(deg)*	$\theta_a - \theta_r$ *(deg)*	*Comments*
1.1	93.1				
42.8	93.4				
100.8	90.7				
192.5	78.7				
240.6	74.2				
291.2	71.2				
336.9	70.3				
405.7	73.7				
501.0	74.5				
596.7	73.3				
765.3	73.2				
911.5	72.0				
1031.3	67.1				

Appendix B23. Average water–air contact angles for GC18–treated glass slides

Exp: 31C	*Date: 10/89*		*Moles:*		*Med: CCl_4*
Elapsed time (hrs)	$\theta_{a\text{–}calc}$ *(deg)*	θ_a *(deg)*	θ_r *(deg)*	$\theta_a - \theta_r$ *(deg)*	*Comments*
24.9	82.4				
183.4	83.2				
402.7	83.1				
522.6	83.9				
716.8	74.8				
954.9	80.9				

Appendix B24. Average water–air contact angles for GC18–treated glass slides

Exp: 31C	*Date: 10/89*		*Moles:*		*Med: deionized water*
Elapsed time (hrs)	$\theta_{a\text{–}calc}$ *(deg)*	θ_a *(deg)*	θ_r *(deg)*	$\theta_a - \theta_r$ *(deg)*	*Comments*
0.8	87.1				
25.0	84.2				
183.6	83.6				
402.9	80.4				
522.9	76.6				
955.1	80.9				

Appendix B25. Average water–air contact angles for GC18–treated glass slides

Exp: 31C	*Date: 10/89*		*Moles:*		*Med: methanol*
Elapsed time (hrs)	θ_{a-calc} *(deg)*	θ_a *(deg)*	θ_r *(deg)*	$\theta_a - \theta_r$ *(deg)*	*Comments*
24.8	79.2				
183.4	82.3				
402.7	79.0				
522.8	81.4				
716.7	74.8				
954.8	85.1				

Appendix B26. Average water–air contact angles for GC18–treated glass slides

Exp: 31C	*Date: 10/89*		*Moles:*		*Med: hexane*
Elapsed time (hrs)	θ_{a-calc} *(deg)*	θ_a *(deg)*	θ_r *(deg)*	$\theta_a - \theta_r$ *(deg)*	*Comments*
24.7	82.0				
183.3	85.6				
402.7	85.7				
522.7	79.3				
717.1	75.0				
954.9	82.1				

Appendix B27. Average water–air contact angles for GC18–treated glass slides

Exp: 31C	*Date: 10/89*		*Moles:*		*Med: xylene*
Elapsed time (hrs)	θ_{a-calc} *(deg)*	θ_a *(deg)*	θ_r *(deg)*	$\theta_a - \theta_r$ *(deg)*	*Comments*
24.9	84.5				
183.3	79.1				
402.6	80.7				
522.7	80.4				
716.7	75.1				
955.0	79.3				

Appendix B28. Average water–air contact angles for GC18–treated glass slides

Exp: 31C	*Date: 10/89*		*Moles:*		*Med: Soltrol*
Elapsed time (hrs)	θ_{a-calc} *(deg)*	θ_a *(deg)*	θ_r *(deg)*	$\theta_a - \theta_r$ *(deg)*	*Comments*
24.8	76.9				
183.5	83.5				
402.8	91.3				
522.8	86.5				
717.0	78.2				
955.0	85.1				

Appendix B29. Average water–air contact angles for GC18–treated glass slides

Exp: 31D	*Date: 11/89*		*Moles:*		*Med: 1000mg/L NaN_3*
Elapsed time (hrs)	θ_{a-calc} *(deg)*	θ_a *(deg)*	θ_r *(deg)*	$\theta_a - \theta_r$ *(deg)*	*Comments*
0.0	91.7	95.4	83.0	12.4	
33.3	94.2				
55.4	92.5				
82.9	92.2				
131.5	90.7				
179.1	91.0				
272.2	92.5	96.6	77.5	19.1	
339.2	89.8	96.8	74.8	22.0	
489.3	87.5	89.4	68.5	20.9	
580.4	87.6	91.6	58.8	32.8	
820.1	85.3	89.8	57.0	32.8	
936.9	82.8	85.3	61.8	23.5	

Appendix B30. Average water–air contact angles for OtS–treated glass slides

Exp: 32	*Date: 8/89*		*Moles: 9.8e–3*		*Med: air*
Elapsed time (hrs)	θ_{a-calc} *(deg)*	θ_a *(deg)*	θ_r *(deg)*	$\theta_a - \theta_r$ *(deg)*	*Comments*
1.3	103.6				
45.7	101.2				
161.3	101.5				
336.0	102.2				
526.0	102.5				
907.1	103.4				
1030.4	103.6				

Appendix B31. Average water–air contact angles for OtS–treated glass slides

Exp: 32	*Date: 8/89*		*Moles: 9.8e–3*		*Med: deionized water*
Elapsed time (hrs)	$\theta_{a\text{–}calc}$ *(deg)*	θ_a *(deg)*	θ_r *(deg)*	$\theta_a - \theta_r$ *(deg)*	*Comments*
1.4	104.4				
19.3	99.7				
45.7	102.9				
66.4	105.5				
87.8	103.4				
136.4	104.1				
212.6	101.2				
281.9	98.2				
360.7	93.3				
448.2	90.2				
526.1	86.0				
620.5	80.5				
747.8	80.0				
907.3	75.2				
1030.5	73.4				

Appendix B32. Average water–air contact angles for OtS–treated glass slides

Exp: 32	*Date: 8/89*		*Moles: 9.8e–3*		*Med: 1000mg/L $CaCl_2$*
Elapsed time (hrs)	$\theta_{a\text{–}calc}$ *(deg)*	θ_a *(deg)*	θ_r *(deg)*	$\theta_a - \theta_r$ *(deg)*	*Comments*
1.5	103.3				
19.4	101.0				
45.8	103.8				
66.4	101.9				
87.9	103.7				
136.9	100.5				
212.7	101.1				
282.0	100.5				
360.7	97.8				
448.3	98.3				
526.3	94.6				
620.6	92.3				
747.9	75.3				
907.4	81.6				
1030.6	81.9				

Appendix B33. Average water–air contact angles for OtS–treated glass slides

Exp: 32	*Date: 8/89*		*Moles: 9.8e–3*		*Med: Soltrol coat*
Elapsed time (hrs)	θ_{a-calc} *(deg)*	θ_a *(deg)*	θ_r *(deg)*	$\theta_a - \theta_r$ *(deg)*	*Comments*
0.0	102.4				
187.6	102.4				
357.3	92.3				
550.6	103.2				
691.2	103.3				
860.4	102.1				
1028.8	97.7				
1223.6	103.4				

Appendix B34. Average water–air contact angles for OtS–treated glass slides

Exp: 34	*Date: 9/89*		*Moles: 2.45e–2*		*Med: air*
Elapsed time (hrs)	θ_{a-calc} *(deg)*	θ_a *(deg)*	θ_r *(deg)*	$\theta_a - \theta_r$ *(deg)*	*Comments*
0.7	105.4				
28.4	102.9				
307.1	101.5				
671.5	105.7				
1079.5	98.3				

Appendix B35. Average water–air contact angles for OtS–treated glass slides

Exp: 34	*Date: 9/89*		*Moles: 2.45e–2*		*Med: deionized water*
Elapsed time (hrs)	θ_{a-calc} *(deg)*	θ_a *(deg)*	θ_r *(deg)*	$\theta_a - \theta_r$ *(deg)*	*Comments*
0.8	107.6				
28.5	106.7				
67.9	103.4				
118.8	102.0				
163.9	100.0				
246.0	97.7				
307.2	94.0				
457.4	84.5				
577.7	84.8				
671.5	87.0				
766.5	85.2				
887.8	79.6				
980.3	67.7				
1079.6	74.4				

Appendix B36. Average water–air contact angles for OtS–treated glass slides

Exp: 34	*Date: 9/89*		*Moles: 2.45e–2*		*Med: 1000mg/L $CaCl_2$*
Elapsed time (hrs)	$\theta_{a\text{–}calc}$ *(deg)*	θ_a *(deg)*	θ_r *(deg)*	$\theta_a - \theta_r$ *(deg)*	*Comments*
0.9	105.2				
28.5	104.6				
68.0	105.4				
118.9	104.4				
164.0	105.2				
246.0	101.2				
307.2	102.4				
457.5	92.2				
577.8	92.3				
671.6	94.8				
766.5	99.0				
887.9	87.3				
980.2	85.9				
1079.7	77.4				

Appendix B37. Average water–air contact angles for TMS–treated glass slides

Exp: 37	*Date: 10/89*		*Moles: 1.58e–1*		*Med: deionized water*
Elapsed time (hrs)	$\theta_{a\text{–}calc}$ *(deg)*	θ_a *(deg)*	θ_r *(deg)*	$\theta_a - \theta_r$ *(deg)*	*Comments*
2.0	88.1				
26.4	82.3				
48.8	80.7				
73.8	75.0				
93.9	76.0				
121.9	72.4				
144.5	78.3				
169.8	79.0				
193.6	77.1				
217.6	75.9				
241.2	79.2				
265.9	76.0				
288.0	75.6				
337.4	74.7				
362.4	77.3				
381.8	73.6				
433.5	70.0				

481.4	71.2				
553.4	71.4				

Appendix B38. Average water–air contact angles for TMS–treated quartz slides

Exp: 37	***Date: 10/89***		***Moles: 1.58e–1***		***Med: deionized water***
Elapsed time (hrs)	$\theta_{a\text{–}calc}$ ***(deg)***	θ_a ***(deg)***	θ_r ***(deg)***	$\theta_a - \theta_r$ ***(deg)***	***Comments***
1.7	87.7				
26.1	76.6				
49.1	80.7				
73.3	68.0				
94.2	70.2				
121.5	71.3				
145.0	75.7				
169.3	73.1				
193.1	62.9				
218.0	65.0				
240.9	62.5				
265.6	64.4				
287.6	61.2				
337.0	63.0				
362.1	69.6				
385.5	62.8				
434.0	66.9				
505.2	76.4				
553.1	68.3				

Appendix B39. Average water–air contact angles for TMS–treated fused silica slides

Exp: 37	***Date: 10/89***		***Moles: 1.58e–1***		***Med: deionized water***
Elapsed time (hrs)	$\theta_{a\text{–}calc}$ ***(deg)***	θ_a ***(deg)***	θ_r ***(deg)***	$\theta_a - \theta_r$ ***(deg)***	***Comments***
1.5	88.4				
26.0	83.5				
49.0	81.4				
73.1	75.4				
94.1	81.1				
121.3	74.8				
144.8	79.3				
169.1	73.6				
193.0	74.4				

217.9	66.3				
240.8	71.9				
265.5	54.2				
287.4	59.5				
336.9	62.8				
362.0	67.6				
385.4	65.1				
433.8	64.6				
505.1	70.8				
553.0	66.9				

Appendix B40. Average water–air contact angles for OtS–treated glass slides

Exp: 38	***Date: 11/89***		***Moles: 2.45e–2***		***Med: 1000mg/L NaN_3***
Elapsed time (hrs)	θ_{a-calc} ***(deg)***	θ_a ***(deg)***	θ_r ***(deg)***	$\theta_a - \theta_r$ ***(deg)***	***Comments***
0.0	118.3				
33.1	113.2				
55.5	111.0				
82.7	108.4				
131.6	108.9				
179.2	105.2				
273.6	105.0				
489.9	104.3				
580.5	96.9				
820.2	102.8				
937.1	94.6				

Appendix B41. Average water–air contact angles for OtS–treated glass slides

Exp: 38	*Date: 11/89*		*Moles: 2.45e–2*		*Med: deionized water*
Elapsed time (hrs)	θ_{a-calc} *(deg)*	θ_a *(deg)*	θ_r *(deg)*	$\theta_a - \theta_r$ *(deg)*	*Comments*
0.0	116.5				
33.2	114.9				
55.5	112.8				
82.8	112.7				
131.8	109.3				
179.9	107.8				
273.5	106.7				
580.7	100.1				
820.4	92.8				
937.4	89.1				

Appendix B42. Average water–air contact angles for OtS–treated glass slides

Exp: 39	*Date: 1/90*		*Moles: 2.45e–2*		*Med: 1000mg/L NaN_3*
Elapsed time (hrs)	θ_{a-calc} *(deg)*	θ_a *(deg)*	θ_r *(deg)*	$\theta_a - \theta_r$ *(deg)*	*Comments*
0.0		154.1	77.9	76.2	
17.8		146.0	64.4	81.6	
48.7		144.9	61.7	83.3	
112.5		138.6	58.2	80.5	
168.7		140.8	53.1	87.7	
214.1		125.1	50.9	74.2	
280.3		132.8	60.8	71.9	
384.5		119.7	52.7	66.9	
522.0		131.0	56.2	74.8	
624.1		115.8	52.9	62.9	
814.6		123.5	38.0	85.5	
978.2		106.0	40.8	65.2	
1055.0		114.6	47.5	67.1	

Appendix B43. Average water–air contact angles for OtS–treated glass slides

Exp: 39	*Date: 1/90*		*Moles: 2.45e–2*		*Med: 1000mg/L NaN_3*
Elapsed time (hrs)	θ_{a-calc} *(deg)*	θ_a *(deg)*	θ_r *(deg)*	$\theta_a - \theta_r$ *(deg)*	*Comments*
0.0		146.6	72.9	75.4	
40.7		146.8	63.0	83.9	
72.2		140.0	52.9	88.1	
138.8		141.0	53.3	87.8	
186.2		134.9	51.5	83.4	
236.5		124.9	47.7	77.2	
330.7		130.8	49.6	81.3	
433.8		114.8	47.6	67.3	
602.1		115.9	54.0	61.9	
793.3		101.8	37.0	64.8	
959.1		99.1	30.9	68.2	
1056.3		84.8	37.5	52.3	

Appendix B44. Average water–air contact angles for OtS–treated glass slides

Exp: 39	*Date: 1/90*		*Moles: 2.45e–2*		*Med: deionized water*
Elapsed time (hrs)	θ_{a-calc} *(deg)*	θ_a *(deg)*	θ_r *(deg)*	$\theta_a - \theta_r$ *(deg)*	*Comments*
0.0		153.8	91.5	62.3	
17.9		145.4	72.0	73.4	
48.8		154.0	90.1	63.9	
112.6		144.6	63.9	80.6	
168.9		130.0	57.5	72.5	
214.2		141.5	61.4	80.1	
280.5		129.5	56.0	73.5	
384.6		135.1	56.4	78.7	
522.2		122.4	56.0	66.4	
624.7		115.1	47.3	67.8	
814.7		112.5	42.6	70.0	
978.0		106.1	42.5	63.6	
1054.9		106.4	40.4	66.5	

Appendix B45. Average water–air contact angles for GC18–treated glass slides

Exp: 40A	*Date: 3/90*		*Moles:*		*Med: 1000mg/L NaN_3*
Elapsed time (hrs)	$\theta_{a\text{-}calc}$ *(deg)*	θ_a *(deg)*	θ_r *(deg)*	$\theta_a - \theta_r$ *(deg)*	*Comments*
0.0		107.0	91.8	15.1	
160.2		105.3	81.9	23.4	
332.9		104.1	78.0	26.1	
525.1		105.1	74.2	30.9	
674.7		97.9	71.2	26.7	
834.1		96.2	62.5	33.7	
1002.4		94.1	55.5	39.0	

Appendix B46. Average water–air contact angles for GC18–treated glass slides

Exp: 40A	*Date: 3/90*		*Moles:*		*Med: deionized water*
Elapsed time (hrs)	$\theta_{a\text{-}calc}$ *(deg)*	θ_a *(deg)*	θ_r *(deg)*	$\theta_a - \theta_r$ *(deg)*	*Comments*
0.0		109.5	89.8	19.7	
160.3		105.7	83.9	21.8	
333.0		106.5	86.7	19.8	
525.2		105.1	81.9	23.2	
674.8		104.1	80.1	24.0	
834.2		102.5	75.3	27.2	
1002.6		99.0	65.3	33.7	

Appendix B47. Average water–air contact angles for tBDM–treated glass slides

Exp: 42	*Date: 6/90*		*Moles:5.72e–2*		*Med: air*
Elapsed time (hrs)	$\theta_{a\text{-}calc}$ *(deg)*	θ_a *(deg)*	θ_r *(deg)*	$\theta_a - \theta_r$ *(deg)*	*Comments*
0.0	69.1	75.3	57.4	17.9	
135.7	64.7	68.6	51.6	17.0	
401.2	65.0	70.9	54.9	16.0	
595.0	66.9	71.7	54.9	16.8	
1079.7	67.9	69.8	52.8	17.0	

Appendix B48. Average water–air contact angles for tBDM–treated glass slides

Exp: 42	*Date: 6/90*		*Moles:5.72e–2*		*Med: deionized water*
Elapsed time (hrs)	θ_{a-calc} *(deg)*	θ_a *(deg)*	θ_r *(deg)*	$\theta_a - \theta_r$ *(deg)*	*Comments*
0.0	75.9	81.8	66.8	15.1	
24.0		75.4	52.6	22.8	
65.0		73.4	46.0	27.4	
89.3		75.7	46.0	29.7	
135.9	68.4	73.6	47.5	26.1	
210.5		72.9	44.8	28.2	interface did not recede
306.7	64.5	67.9	40.4	27.5	interface did not recede
401.5		68.6	35.7	32.9	interface did not recede
595.2	71.3	71.1	34.7	36.4	interface did not recede
691.3		65.5	46.2	19.2	interface did not recede
811.5	66.9	70.1	39.2	30.9	interface did not recede
959.5	53.5	58.3	18.9	39.4	interface did not recede
1079.8	61.2	60.7	23.4	37.3	interface did not recede

Appendix B49. Average water–air contact angles for tBDM–treated glass slides

Exp: 42	*Date: 6/90*		*Moles:5.72e–2*		*Med: 1000mg/L NaN_3*
Elapsed time (hrs)	θ_{a-calc} *(deg)*	θ_a *(deg)*	θ_r *(deg)*	$\theta_a - \theta_r$ *(deg)*	*Comments*
0.0	68.2	74.6	57.2	17.4	
24.1		72.6	41.1	31.5	interface did not recede
65.1		71.7	43.6	28.1	interface did not recede
89.5		73.0	42.6	30.4	interface did not recede
136.0	69.6	73.0	43.6	29.4	interface did not recede
210.5		70.2	45.0	25.2	interface did not recede
307.0	65.5	71.7	44.4	27.3	interface did not recede
401.6		69.8	36.3	33.5	interface did not recede
595.5	67.2	70.8	43.6	27.2	
691.4		67.4	45.2	22.3	interface did not recede
812.0	58.3	62.7	32.0	30.7	interface did not recede
959.6	64.9	65.8	37.8	28.0	interface did not recede
1080.0	57.9	61.9	31.5	30.4	interface did not recede

Appendix B50. Average water–air contact angles for tBDM–treated glass slides

Exp: 42	*Date: 6/90*		*Moles:5.72e–2*		*Med: Soltrol coat*
Elapsed time (hrs)	θ_{a-calc} *(deg)*	θ_a *(deg)*	θ_r *(deg)*	$\theta_a - \theta_r$ *(deg)*	*Comments*
0.0	65.3	74.0	55.7	18.3	
65.2		76.0	50.2	25.8	
136.2	73.9	75.9	54.0	22.0	
307.2	75.2	75.5	38.9	36.7	interface did not recede
595.6	72.8	74.6	34.2	40.4	interface did not recede
766.0	71.6	70.0	35.3	34.6	interface did not recede
883.0	67.4	66.7	31.6	35.1	interface did not recede
1054.0	73.8	68.6	24.8	43.8	interface did not recede

Appendix B51. Average water–air contact angles for tBDM–treated glass slides

Exp: 42	*Date: 6/90*		*Moles:5.72e–2*		*Med: Soltrol*
Elapsed time (hrs)	θ_{a-calc} *(deg)*	θ_a *(deg)*	θ_r *(deg)*	$\theta_a - \theta_r$ *(deg)*	*Comments*
0.0	67.1	72.3	53.1	19.2	
65.3		77.3	55.0	22.3	
136.4	73.4	79.4	58.7	20.7	
307.4	73.1	79.8	49.9	29.9	
595.8	77.0	77.8	49.3	28.5	
766.5	74.8	80.7	56.6	24.1	
883.1	76.7	78.6	54.8	23.8	
1054.5	77.8	77.8	62.6	17.6	

Appendix B52. Average water–air contact angles for tBDM–treated glass slides

Exp: 42	*Date: 6/90*		*Moles:5.72e–2*		*Med: ethanol*
Elapsed time (hrs)	θ_{a-calc} *(deg)*	θ_a *(deg)*	θ_r *(deg)*	$\theta_a - \theta_r$ *(deg)*	*Comments*
0.0	69.2	74.0	54.3	19.7	
24.2		79.0	52.8	26.2	
65.4		79.2	57.0	22.2	
136.5	73.7	80.9	61.6	19.4	
307.5	73.2	79.8	58.6	21.2	
596.0	74.1	79.6	56.6	23.0	
766.5	77.6	80.1	58.7	21.4	
883.3	74.8	76.1	63.9	12.2	
1054.7	73.1	75.6	58.9	16.7	

Appendix B53. Average water–air contact angles for tBDP–treated glass slides

Exp: 43	*Date: 8/90*		*Moles:4e–3*		*Med: air*
Elapsed time (hrs)	θ_{a-calc} *(deg)*	θ_a *(deg)*	θ_r *(deg)*	$\theta_a - \theta_r$ *(deg)*	*Comments*
0.0	64.7	69.0	54.0	15.0	
42.1	67.9	69.9	58.8	11.1	
88.6	67.4	69.2	57.5	11.8	
160.0	70.5	72.8	59.6	13.2	
280.3	69.1	71.2	57.5	12.5	
403.2	70.0	71.6	56.4	15.2	
521.0	69.0	69.3	55.6	13.7	
644.0	73.2	72.5	61.6	11.0	
761.2	69.8	69.8	56.8	13.0	
952.7	68.4	70.5	59.3	11.3	

Appendix B54. Average water–air contact angles for tBDP–treated glass slides

Exp: 43	*Date: 8/90*		*Moles:4e–3*		*Med: with 1000mg/L NaN_3*
Elapsed time (hrs)	θ_{a-calc} *(deg)*	θ_a *(deg)*	θ_r *(deg)*	$\theta_a - \theta_r$ *(deg)*	*Comments*
0.0	64.7	69.0	54.0	15.0	
42.2	62.2	68.1	51.5	16.6	
88.6	60.5	65.3	49.2	16.1	
160.1	59.0	62.9	42.9	20.0	
280.4	59.2	61.2	36.4	24.8	
403.3	62.1	61.3	36.6	24.6	
521.1	60.4	61.1	35.3	25.8	interface did not recede
644.2	57.2	56.9	22.0	34.9	interface did not recede
761.3	55.0	56.0	22.3	33.7	interface did not recede
952.9	56.5	53.9	29.5	24.4	interface did not recede

Appendix B55. Average water–air contact angles for tBDP–treated glass slides

Exp: 43	*Date: 8/90*		*Moles:4e–3*		*Med: deionized water*
Elapsed time (hrs)	$\theta_{a\text{–}calc}$ *(deg)*	θ_a *(deg)*	θ_r *(deg)*	$\theta_a - \theta_r$ *(deg)*	*Comments*
0.0	64.7	69.0	54.0	15.0	
42.3	59.5	64.7	46.7	17.9	
88.7	61.0	64.0	40.7	23.4	
160.2	55.4	60.7	40.0	20.7	
280.5	56.9	59.3	35.0	24.3	
403.4	54.7	57.9	35.6	22.3	
521.2	57.1	55.3	31.3	24.0	interface did not recede
644.5	50.3	51.4	30.3	21.1	interface did not recede
762.4	53.5	51.8	30.0	21.7	interface did not recede
953.0	47.1	47.6	27.0	20.6	interface did not recede

Appendix B56. Average water–air contact angles for tBDP–treated glass slides

Exp: 43	*Date: 8/90*		*Moles:4e–3*		*Med: Soltrol coat*
Elapsed time (hrs)	$\theta_{a\text{–}calc}$ *(deg)*	θ_a *(deg)*	θ_r *(deg)*	$\theta_a - \theta_r$ *(deg)*	*Comments*
0.0	64.7	69.0	54.0	15.0	
70.5	68.2	67.2	51.8	15.5	
136.4	67.4	68.6	50.0	18.6	
280.6	65.3	65.6	47.5	18.1	
403.5	63.7	66.4	48.2	18.2	
521.3	69.1	66.9	35.3	31.6	
644.5	62.2	64.5	38.5	26.0	
762.5	61.7	62.8	36.5	26.2	interface did not recede
953.0	65.9	63.8	31.4	32.4	interface did not recede

Appendix B57. Average water–air contact angles for tBDP–treated glass slides

Exp: 43	*Date: 8/90*		*Moles:4e–3*		*Med: Soltrol*
Elapsed time (hrs)	$\theta_{a\text{–}calc}$ *(deg)*	θ_a *(deg)*	θ_r *(deg)*	$\theta_a - \theta_r$ *(deg)*	*Comments*
0.0	64.7	69.0	54.0	15.0	
70.6	72.5	71.8	53.5	18.3	
136.5	69.4	73.6	58.0	15.6	
280.7	75.8	72.4	59.3	13.1	
403.6	72.7	73.5	58.0	15.5	
523.2	72.7	73.9	59.0	14.9	
644.6	71.2	73.3	57.0	16.3	
762.6	74.5	73.9	57.6	16.3	
953.1	72.4	75.3	57.7	17.7	

Appendix B58. Average water–air contact angles for tBDP–treated glass slides

Exp: 43	*Date: 8/90*		*Moles:4e–3*		*Med: ethanol*
Elapsed time (hrs)	$\theta_{a\text{–}calc}$ *(deg)*	θ_a *(deg)*	θ_r *(deg)*	$\theta_a - \theta_r$ *(deg)*	*Comments*
0.0	64.7	69.0	54.0	15.0	
70.7	72.5	73.0	58.0	15.0	
136.5	68.0	71.5	54.7	16.8	
280.4	71.1	72.2	56.7	15.6	
403.7	70.4	71.2	54.8	17.2	
523.4	72.0	72.1	54.8	17.2	
644.2	70.1	70.2	52.9	17.4	
762.7	70.0	72.2	59.6	12.6	
953.2	68.0	70.5	56.2	14.3	

Appendix C1. Summary of short column experiments for untreated glass beads.

Exp.No.	*Date start (d/m/yr)*	M_{dry} *(g)*	M_{sat} *(g)*	V_{gr} *(cc)*	M_{glue} *(g)*	M_s *(g)*	L_c *(cm)*	C_f *(%)*	M_{start} *(g)*	M_{IWS} *(g)*	M_{ROS} *(g)*	*Comments*
MW13	4/2/90	913.13	1028.08	0.51	0.15	184.21	+3.86	1.3	1147.68	1138.03	1145.93	1; S_w–ψ
MW14	9/2/90	890.52	980.42	0.51	0.16	142.55	+3.18	1.6	1070.62	1063.13	1069.25	1; S_w–ψ
MW17	24/2/90	923.99	1028.22	0.37	0.16	165.48	+1.25	1.0	1131.63	1123.04	1129.93	1
MW18	5/3/90	922.35	1033.43	0.35	0.15	175.82	+1.33	0.9	1140.89	1132.03	1139.08	1
MW19	13/3/90	921.28	1033.64	0.38	0.19	176.07	+1.62	0.9	1142.60	1133.31	1140.71	1
MW21	17/3/90	916.54	1020.03	0.38	0.14	164.82	+1.86	1.0	1121.74	1113.28	1120.26	1
MW22	16/3/90	910.23	1018.23	0.51	0.14	171.50	+2.25	1.3	1124.36	1115.54	1122.74	1
MW23	3/4/90	923.83	1027.86	0.37	0.11	161.71	-0.10	1.0	1127.97	1119.32	1126.32	1
MW24	3/4/90	925.33	1036.82	0.35	0.13	174.70	-0.37	0.9	1144.05	1134.83	1142.24	2
MW25	19/6/90	914.94	1019.46	0.38	0.16	164.04	-0.20	1.0	1122.69	1114.07	1121.16	1; S_w–ψ
MWO15	30/8/90	760.25	844.38	0.15	0.11	130.35	-0.11	–	1037.09	1030.44	1035.58	2
MWO30	14/10/90	780.10	871.52	0.15	0.13	142.72	+2.50	–	1076.14	1068.65	1075.06	2; S_w–ψ

1. conventional column. 2. dual filter column. 3. dyed Soltrol with Oil Red O.

Appendix C2. Summary of conventional short column experiments for GC18–treated glass beads.

Exp.No.	*Date start (d/m/yr)*	M_{dry} (g)	M_{sat} (g)	V_{gr} (cc)	M_{glue} (g)	M_s (g)	L_c (cm)	C_f (%)	M_{start} (g)	M_{IWS} (g)	M_{ROS} (g)	*Comments*
MWO7	23/6/90	920.69	1034.68	0.38	0.15	185.78	+1.35	1.0	1149.73	1141.24	1146.71	1; 3
MWO8	27/6/90	925.29	1030.11	0.37	0.14	166.98	-1.00	1.0	1133.62	1125.09	1130.99	1
MWO9	27/6/90	924.60	1037.27	0.35	0.16	179.97	-1.68	0.9	1147.85	1138.71	1144.94	1
MWO10	17/7/90	914.07	1022.38	0.51	0.15	173.45	+1.23	1.3	1129.24	1120.93	1126.36	1;3
MWO11	17/7/90	924.62	1031.77	0.35	0.12	174.33	-0.37	1.0	1140.45	1132.44	1137.52	1

1. conventional column. 2. dual filter column. 3. dyed Soltrol with Oil Red O.

Appendix C3. Summary of dual filter short column experiments for GC18–treated glass beads.

Exp.No.	*Date start (d/m/yr)*	M_{dry} (g)	M_{sat} (g)	V_{gr} (cc)	M_{glue} (g)	M_s (g)	L_c (cm)	C_f (%)	M_{start} (g)	M_{IWS} (g)	M_{ROS} (g)	*Comments*
MWO12	14/8/90	788.14	894.78	0.37	-	173.67	+0.78	-	1113.37	1105.33	1112.49	2; S_w-ψ
MWO13	19/8/90	789.27	875.57	0.15	0.14	144.89	-0.55	-	1082.04	1074.50	1081.23	2; S_w-ψ
MWO16	30/8/90	906.99	997.17	0.35	0.12	146.08	+1.05	-	1082.25	1074.87	1081.43	2; S_w-ψ
MWO32	15/10/90	777.50	870.50	0.15	0.12	148.60	-0.53	-	1075.33	1068.34	1074.61	2; S_w-ψ

1. conventional column. 2. dual filter column. 3. dyed Soltrol with Oil Red O.

Appendix C4. Summary of short column experiments for tBDM–treated glass beads.

Exp.No.	*Date start (d/m/yr)*	M_{dry} *(g)*	M_{sat} *(g)*	V_{gr} *(cc)*	M_{glue} *(g)*	M_s *(g)*	L_c *(cm)*	C_f *(%)*	M_{start} *(g)*	M_{IWS} *(g)*	M_{ROS} *(g)*	*Comments*
MWO21	8/9/90	876.93	959.36	0.24	0.12	130.50	+3.70	–	1049.15	1047.36	1048.43	2; S_w–ψ
MWO22	20/9/90	882.17	971.26	0.49	0.11	139.07	+1.78	–	1067.68	1060.63	1066.24	2; S_w–ψ
MWO26	9/10/90	925.11	1038.25	0.35	0.14	179.11	+1.32	0.9	1150.05	1140.63	1148.17	1; S_w–ψ
MWO29	5/10/90	862.48	946.75	0.49	0.14	132.07	+2.80	–	1039.39	1033.47	1035.82	2; S_w–ψ
MWO40	25/10/90	918.18	1032.64	0.37	0.15	179.84	+1.55	0.9	1144.32	1135.22	N/A	1; S_w–ψ

1. conventional column. 2. dual filter column. 3. dyed Soltrol with Oil Red O.

Appendix C5. S_w–ψ data for experiment MW13

Time & date	*T(°C)*	*ψ(cm)*	*Mc(g)*	*S_w(%)*	*Comments*
19:19 4/2/90	24.7	0.00	1147.68	100.0	Soltrol® flood
23:27 5/2/90	24.6	13.13	1144.64	71.0	
0:05 7/2/90	25.3	16.54	1141.97	44.4	
19:40 7/2/90	24.8	19.48	1140.09	25.6	
15:38 8/2/90	25.2	25.42	1138.31	7.9	
15:23 9/2/90	24.7	34.56	1138.00	4.8	
14:54 10/2/90	24.5	46.05	1138.03	5.1	
14:26 11/2/90	25.2	51.05	1138.03	5.1	IWS, water flood
13:07 12/2/90	24.7	36.28	1138.05	5.3	
14:45 13/2/90	24.9	26.98	1138.09	5.7	
14:00 14/2/90	24.6	20.88	1138.09	5.7	
17:03 15/2/90	24.8	16.51	1138.11	5.9	
16:52 16/2/90	23.8	13.58	1138.39	8.7	
15:05 17/2/90	25.0	12.97	1138.84	13.1	
18:02 18/2/90	25.0	11.34	1139.31	17.8	
15:05 19/2/90	25.1	9.67	1139.88	23.5	
13:31 21/2/90	25.2	8.42	1140.82	32.9	
16:44 22/2/90	24.8	7.34	1141.53	40.0	
17:15 23/2/90	24.8	6.45	1142.04	45.1	
16:03 24/2/90	24.4	4.38	1142.90	53.6	
17:07 25/2/90	25.3	2.04	1143.94	64.0	
10:08 27/2/90	24.5	-1.17	1144.95	74.1	
10:22 28/2/90	25.3	–	1145.88	82.1	Water breakthrough
28/2/90	–	–	1145.93	82.6	ROS = 16.5%[1]

1. After additional waterflood at 0.3 mL/min for 120 mL.

Appendix C6. S_w–ψ *data for experiment MW14*

Time & date	*T(°C)*	*ψ(cm)*	*Mc(g)*	*S_w(%)*	*Comments*
15:21 9/2/90	24.7	0.00	1070.62	100.0	Soltrol® flood
14:59 10/2/90	24.6	16.22	1069.79	91.2	
14:32 11/2/90	25.3	18.95	1067.92	67.6	
13:04 12/2/90	24.6	21.69	1065.05	31.5	
14:58 13/2/90	25.4	35.48	1063.15	7.6	
14:06 14/2/90	24.7	47.65	1063.14	7.5	
16:59 15/2/90	24.8	52.00	1063.13	7.4	IWS, water flood
17:05 16/2/90	24.2	26.43	1063.15	7.6	
15:16 17/2/90	24.9	17.21	1063.22	8.5	
18:12 18/2/90	25.0	16.29	1064.19	20.7	
15:20 19/2/90	25.3	14.00	1064.89	29.5	
13:46 21/2/90	25.3	11.88	1066.46	49.3	
16:49 22/2/90	25.1	9.41	1068.09	69.8	
17:05 23/2/90	24.5	6.36	1068.73	77.8	
16:11 24/2/90	24.6	3.23	1069.02	81.5	
17:03 25/2/90	25.3	–	1069.19	82.0	Water breakthrough
			1069.25	82.8	ROS = 17.2%[1]

1. After additional waterflooding at 0.3 mL/min for 120 mL.

Appendix C7. S_w–ψ *data for experiment MW25*

Time & date	*T(°C)*	*ψ(cm)*	*Mc(g)*	S_w*(%)*	*Comments*
10:13 19/6/90	25.4	0.00	1122.69	100.0	Soltrol® flood
9:00 20/6/90	24.5	15.24	1122.17	94.3	
13:43 21/6/90	23.6	19.64	1120.54	76.3	
9:03 22/6/90	24.9	20.53	1117.14	38.9	
9:33 23/6/90	24.9	29.42	1114.04	5.8	
13:48 24/6/90	23.5	55.40	1114.07	6.2	IWS, water flood
10:18 25/6/90	24.7	17.35	1114.86	14.9	
8:36 26/6/90	24.2	14.91	1115.33	20.0	
9:04 27/6/90	25.1	12.91	1115.96	27.0	
8:35 28/6/90	23.6	11.54	1117.05	39.0	
9:50 29/6/90	24.8	10.29	1117.99	49.3	
11:24 30/6/90	24.1	8.68	1119.07	61.2	
10:15 1/7/90	23.7	7.06	1119.79	69.1	
9:10 2/7/90	25.9	4.80	1120.39	75.7	
11:10 3/7/90	25.0	1.70	1120.60	78.0	
9:10 4/7/90	23.7	0.88	1121.11	83.6	
10:15 5/7/90	24.5	–3.69	1121.16	83.2	ROS, Soltrol® flood
9:00 6/7/90	24.1	9.61	1120.56	77.6	
11:30 7/7/90	24.6	13.92	1119.50	65.9	
2:05 8/7/90	25.3	16.65	1117.46	43.5	
10:15 9/7/90	24.4	20.09	1115.44	21.1	
8:37 10/7/90	24.6	34.64	1114.00	5.4	
9:50 11/7/90	26.2	50.84	1114.00	5.4	IWS, water flood
9:10 12/7/90	26.6	16.36	1114.92	15.5	
8:04 13/7/90	23.9	11.70	1116.07	28.2	
10:30 14/7/90	23.5	10.38	1116.87	37.0	
10:45 16/7/90	24.1	9.27	1117.60	45.0	
8:34 17/7/90	24.1	8.29	1118.20	51.6	
10:20 18/7/90	24.8	7.45	1118.69	57.0	
8:51 19/7/90	25.2	6.63	1119.54	66.4	
8:30 20/7/90	24.4	3.68	1120.04	71.9	

9:10 21/7/90	25.1	2.47	1120.31	74.8	
13:10 22/7/90	23.4	0.68	1120.87	81.0	
10:00 23/7/90	25.1	-	1120.88	81.9	ROS

Appendix C8. S_w–ψ *data for experiment MWO8.*

Time & date	*T(°C)*	*ψ(cm)*	*Mc(g)*	*S_w(%)*	*Comments*
23:25 1/7/90	26.4	0.00	1133.62	100.0	Soltrol® flood
8:50 2/7/90	25.1	-0.35	1133.58	100.0	
0:35 3/7/90	25.5	-0.63	1131.67	78.8	
11:10 3/7/90	25.1	-1.27	1128.49	42.6	
20:50 3/7/90	24.5	4.78	1125.46	8.2	
9:15 4/7/90	24.0	25.27	1125.30	6.4	
16:45 4/7/90	24.9	43.56	1125.19	5.1	
0:20 5/7/90	24.0	53.40	1125.16	4.8	
20:25 5/7/90	25.2	56.82	1125.16	4.0	IWS

Appendix C9. S_w–ψ *data for experiment MWO9.*

Time & date	*T(°C)*	*ψ(cm)*	*Mc(g)*	*S_w(%)*	*Comments*
23:25 1/7/90	26.4	0.00	1147.85	100.0	Soltrol® (dyed) flood
8:50 2/7/90	25.1	0.59	1147.76	100.0	
0:40 3/7/90	25.5	0.48	1146.54	86.9	
11:15 3/7/90	25.1	-0.11	1144.35	63.5	
20:50 3/7/90	24.5	-0.37	1140.03	17.3	
9:20 4/7/90	24.2	20.80	1138.89	5.1	
16:45 4/7/90	24.9	43.10	1138.80	4.2	
0:20 5/7/90	24.0	52.23	1138.75	3.6	
20:25 5/7/90	25.2	56.31	1138.71	3.2	IWS

Appendix C10. S_w–ψ *data for experiment MWO12.*

Time & date	*T(°C)*	*ψ(cm)*	*Mc(g)*	*S_w(%)*	*Comments*
9:00 14/8/90	24.6	0.00	1113.37	100.0	Soltrol® flood
17:00 14/8/90	24.5	-5.73	1109.73	58.9	
23:57 14/8/90	23.7	-1.58	1106.24	19.6	
8:09 15/8/90	25.1	11.82	1105.45	10.6	
16:05 15/8/90	24.7	30.26	1105.35	9.5	
23:57 15/8/90	23.8	51.58	1105.33	9.3	IWS, water flood
8:28 16/8/90	24.2	-0.04	1105.40	10.1	
16:05 16/8/90	23.7	-9.68	1106.19	19.0	
23:57 16/8/90	25.1	-16.12	1108.04	39.9	
8:21 17/8/90	25.0	-20.23	1110.32	65.6	
15:58 17/8/90	26.1	-28.32	1112.23	87.1	
0:22 18/8/90	25.9	-42.64	1112.49	9.9	ROS

Appendix C11. S_w–ψ *data for experiment MWO13.*

Time & date	*T(°C)*	*ψ(cm)*	*Mc(g)*	*S_w(%)*	*Comments*
8:23 19/8/90	25.6	0.00	1082.04	100.0	Soltrol® flood
16:14 19/8/90	26.9	-2.73	1080.59	81.5	
0:15 20/8/90	27.4	-1.99	1078.81	58.7	
7:50 20/8/90	25.9	-0.87	1077.33	39.8	
15:47 20/8/90	27.4	-0.46	1075.74	19.5	
0:10 21/8/90	31.4	12.15	1074.37	2.0	
8:05 21/8/90	26.7	31.07	1074.53	4.0	
8:09 22/8/90	23.4	50.66	1074.50	3.6	IWS, water flood
16:45 22/8/90	24.4	-0.15	1074.69	6.1	
0:10 22/8/90	24.0	-9.62	1075.55	17.1	
9:12 23/8/90	22.3	-14.16	1077.67	44.2	
16:17 23/8/90	25.7	-20.62	1080.52	80.6	
0:10 24/8/90	23.3	-38.75	1081.30	90.5	
8:12 24/8/90	21.8	-45.00	1081.37	91.4	
16:27 24/8/90	28.1	-49.59	1081.23	89.6	ROS

Appendix C12. S_w–ψ *data for experiment MWO16.*

Time & date	*T(°C)*	*ψ(cm)*	*Mc(g)*	*S_w(%)*	*Comments*
9:00 30/8/90	24.0	0.00	1082.25	100.0	Soltrol® flood
16:14 30/8/90	28.3	–2.27	1079.92	69.2	
0:11 31/8/90	25.3	–1.26	1077.40	35.8	
8:25 31/8/90	24.0	2.94	1074.97	3.7	
16:22 31/8/90	27.1	14.45	1074.83	1.7	
0:26 1/9/90	25.6	46.93	1074.83	1.8	
8:17 1/9/90	24.0	53.16	1074.87	2.4	IWS, water flood
16:24 1/9/90	26.9	0.51	1074.77	1.0	
0:08 2/9/90	26.8	–5.73	1075.19	6.6	
8:13 2/9/90	24.2	–10.77	1076.06	18.1	
16:12 2/9/90	27.5	–15.21	1077.62	38.7	
0:20 3/9/90	26.0	–20.03	1080.17	72.5	
8:30 3/9/90	24.7	–34.23	1081.37	88.4	
16:11 3/9/90	24.4	–42.90	1081.27	87.0	
0:05 4/9/90	25.0	–49.63	1081.39	88.6	
8:27 4/9/90	24.0	–57.49	1081.43	89.2	ROS

Appendix C13. S_w–ψ *data for experiment MWO21.*

Time & date	*T(°C)*	*ψ(cm)*	*Mc(g)*	*S_w(%)*	*Comments*
8:29 12/9/90	24.5	0.00	1049.15	100.0	Soltrol® flood
16:13 12/9/90	26.0	4.42	1048.72	94.3	
0:21 13/9/90	24.2	7.45	1048.08	85.7	
8:12 13/9/90	22.8	13.67	1047.41	76.8	
16:14 13/9/90	25.8	21.72	1047.35	76.0	
0:15 14/9/90	24.0	37.66	1047.37	76.3	
8:30 14/9/90	22.5	65.62	1047.43	77.1	IWS, water flood
16:59 14/9/90	25.9	–0.73	1047.36	76.1	
0:30 15/9/90	23.5	–10.72	1048.32	88.9	
8:27 15/9/90	22.5	–21.54	1048.34	89.2	
15:56 15/9/90	24.5	–31.74	1048.31	88.8	
23:58 15/9/90	22.4	–39.89	1048.41	90.1	
9:07 16/9/90	23.6	–50.92	1048.43	90.4	ROS

Appendix C14. S_w–ψ *data for experiment MWO26.*

Time & date	*T(°C)*	*ψ(cm)*	*Mc(g)*	*S_w(%)*	*Comments*
16:07 9/10/90	22.3	0.00	1150.05	100.0	Soltrol® flood
0:14 10/10/90	22.5	11.78	1149.53	95.7	
8:57 10/10/90	21.8	16.25	1148.12	80.5	
16:22 10/10/90	23.3	17.37	1144.95	49.6	
0:21 11/10/90	23.5	22.63	1141.40	13.9	
8:58 11/10/90	22.8	40.24	1140.79	7.8	
16:15 11/10/90	25.0	51.39	1140.63	6.2	IWS, water flood
9:47 12/10/90	23.8	12.27	1141.46	11.5	
16:26 12/10/90	24.3	7.92	1142.40	24.0	
23:32 12/10/90	24.5	6.67	1143.65	36.5	
16:07 13/10/90	25.4	5.81	1146.30	48.2	
0:21 14/10/90	25.5	4.26	1146.30	63.2	
10:45 14/10/90	24.0	2.49	1147.41	74.4	
23:29 14/10/90	22.9	–0.65	1148.06	80.9	
10:11 15/10/90	24.3	–3.78	1148.17	82.0	ROS, Soltrol® flood
23:40 15/10/90	25.0	13.45	1147.51	75.4	
8:47 16/10/90	22.0	16.35	1144.68	46.9	
15:57 16/10/90	24.5	22.93	1141.29	12.8	
0:15 17/10/90	23.0	48.74	1140.93	9.2	IWS, water flood
8:40 17/10/90	22.8	15.35	1141.69	16.8	
15:58 17/10/90	23.8	10.58	1142.83	28.3	
0:23 18/10/90	22.8	7.28	1144.71	47.2	
8:33 18/10/90	21.6	3.23	1146.98	70.0	

Appendix C15. S_w–ψ *data for experiment MWO29.*

Time & date	*T(°C)*	*ψ(cm)*	*Mc(g)*	*S_w(%)*	*Comments*
15:57 9/10/90	22.0	0.00	1039.39	100.0	Soltrol® flood
0:05 10/10/90	22.6	10.70	1039.08	95.9	
8:47 10/10/90	21.8	14.42	1038.57	89.3	
16:12 10/10/90	23.0	15.90	1036.49	62.0	
0:10 11/10/90	23.4	18.29	1033.86	27.6	
1:35 12/10/90	23.8	55.53	1033.47	22.5	IWS, water flood
23:43 12/10/90	24.7	9.91	1033.61	24.3	
16:00 13/10/90	25.5	7.05	1034.01	29.6	
15:46 14/10/90	26.2	5.05	1034.63	37.7	
10:01 15/10/90	24.4	3.18	1035.84	53.5	
23:33 15/10/90	25.0	0.74	1037.01	68.8	
8:56 16/10/90	22.0	–4.97	1037.69	77.7	
16:06 16/10/90	24.8	–20.89	1037.62	76.8	ROS
0:06 17/10/90	22.9	11.22	1037.34	73.2	
8:47 17/10/90	22.8	17.46	1035.82	53.3	

Appendix C16. S_w-ψ *data for experiment MWO30.*

Time & date	*T(°C)*	*ψ(cm)*	*Mc(g)*	*S_w(%)*	*Comments*
16:06 14/10/90	26.2	0.00	1076.14	100.0	Soltrol® flood
16:38 15/10/90	26.5	13.73	1075.31	90.1	
15:49 16/10/90	24.6	17.53	1074.33	78.4	
15:45 17/10/90	23.8	20.29	1071.58	45.7	
16:07 18/10/90	23.0	27.18	1068.83	12.9	
12:13 19/10/90	23.0	46.36	1068.65	9.9	
12:05 20/10/90	22.5	52.60	1068.65	10.8	IWS, water flood
12:22 21/10/90	23.0	19.63	1069.26	18.0	
12:51 22/10/90	21.5	15.11	1070.04	27.3	
11:51 23/10/90	24.0	12.46	1070.99	38.6	
12:45 24/10/90	22.3	10.87	1072.49	56.5	
10:28 25/10/90	21.0	8.29	1074.09	75.6	
10:56 26/10/90	22.1	0.77	1075.04	86.9	
12:17 27/10/90	23.1	-17.69	1075.06	87.1	ROS, Soltrol® flood
10:36 28/10/90	23.7	13.55	1074.27	77.7	
8:44 29/10/90	21.6	16.69	1072.73	59.4	*1*
9:20 30/10/90	22.9	20.77	1070.19	29.1	
/10/90	24.5	22.93	1141.29	12.8	
/10/90	23.0	48.74	1140.93	9.2	IWS, water flood
/10/90	22.8	15.35	1141.69	16.8	
/10/90	23.8	10.58	1142.83	28.3	
/10/90	22.8	7.28	1144.71	47.2	
/10/90	21.6	3.23	1146.98	70.0	

1. Measured equilibration time.

Appendix C17. S_w–ψ *data for experiment MWO32.*

Time & date	*T(°C)*	*ψ(cm)*	*Mc(g)*	*S_w(%)*	*Comments*
16:34 15/10/90	26.6	0.00	1075.33	100.0	Soltrol® flood
23:46 15/10/90	25.0	–1.97	1073.38	75.3	
9:05 16/10/90	22.1	–0.87	1071.57	52.3	
16:13 16/10/90	24.8	–0.03	1069.69	28.5	
16:08 17/10/90	23.8	2.60	1068.32	11.1	
0:38 18/10/90	23.0	28.23	1068.29	10.7	
8:12 18/10/90	21.6	51.24	1068.34	11.3	IWS, water flood
16:36 18/10/90	23.7	0.29	1068.27	10.5	
0:15 19/10/90	21.8	–4.16	1068.60	14.6	
12:24 19/10/90	23.4	–12.01	1069.14	21.5	
23:49 19/10/90	22.7	–16:19	1070.46	38.2	
11:50 20/10/90	22.3	–20.15	1073.02	70.7	
23:55 20/10/90	23.7	–27.51	1074.44	88.7	
12:35 21/10/90	23.2	–38.54	1074.57	90.4	
20:25 21/10/90	22.8	–43.88	1074.61	90.9	ROS, Soltrol® flood
9:26 22/10/90	23.3	–23.34	1074.58	90.5	
16:38 22/10/90	22.7	–14.94	1073.92	82.1	
0:12 23/10/90	23.9	–11.93	1073.13	72.1	
9:33 23/10/90	23.7	–8.84	1071.83	55.6	*1*
17:06 23/10/90	24.1	–5.08	1070.86	43.3	
0:17 24/10/90	22.9	–1.48	1070.14	34.2	
10:25 24/10/90	22.0	0.11	1068.64	15.2	
0:12 25/10/90	22.0	9.79	1068.20	9.6	
10:19 25/10/90	21.1	28.59	1068.23	9.9	
16:05 25/10/90	23.0	49.96	1068.20	9.6	IWS, water flood
23:52 25/10/90	22.9	–0.01	1068.21	9.7	
10:45 26/10/90	22.0	–2.63	1068.90	18.4	
23:48 26/10/90	24.5	–8.34	1069.27	23.1	
12:06 27/10/90	23.0	–13.52	1069.93	31.5	
0:05 28/10/90	25.0	–16.90	1071.70	54.0	
10:28 28/10/90	23.7	–22.20	1073.65	78.7	

16:38 28/10/90	23.8	–31.89	1074.45	88.8	
23:42 28/10/90	23.0	–44.92	1074.52	89.7	ROS, Soltrol® flood

1. Measured equilibration time.

Appendix C18. S_w–ψ *data for experiment MWO40.*

Time & date	*T(°C)*	*ψ(cm)*	*Mc(g)*	*S_w(%)*	*Comments*
16:45 25/10/90	23.0	0.00	1144.32	100.0	Soltrol® flood
23:43 25/10/90	23.0	13.65	1143.11	89.1	
10:38 26/10/90	22.0	17.17	1140.92	67.6	
23:40 26/10/90	24.3	19.66	1137.05	29.7	
23:15 28/10/90	23.0	37.24	1135.24	12.0	
9:08 29/10/90	21.8	51.28	1135.22	11.8	IWS, water flood
17:12 29/10/90	23.8	20.58	1135.18	11.4	
17:16 30/10/90	23.7	15.06	1135.42	13.8	
9:34 31/10/90	23.4	9.55	1135.66	16.1	
23:00 31/10/90	24.3	4.72	1136.07	20.1	
22:47 1/11/90	25.0	2.02	1136.72	26.5	
11:49 2/11/90	23.8	–0.31	1137.87	37.8	
23:30 2/11/90	23.7	–1.86	1139.39	52.6	
10:56 3/11/90	23.5	–3.23	1140.74	65.9	

Appendix D1. Test concerning mean values of IWS and ROS.

The averaged values for IWS and ROS from the short column experiments were analyzed statistically using the standard test of hypothesis method (Walpole and Myers, 1978). We have the sample mean, $\overline{X}$, and standard deviation, S, for IWS and ROS for each wettability case. To determine whether the mean value of the IWS and ROS for the GC18–treated and tBDM–treated cases were statistically similar to the untreated case, the following formula was used:

$$T = (\overline{X}_{untreated} - \overline{X}_{treated}) - d_o \,/(S_p \,[(1/n_{untreated}) + (1/n_{treated})]^{1/2}) \qquad \text{(D–1)}$$

where T is the statistic that defines whether one mean may be considered similar to the compared mean, $\overline{X}_{untreated}$ is the mean residual saturation (IWS or ROS) for the untreated case, $\overline{X}_{treated}$ is the mean residual saturation for the treated case (GC18 or tBDM), d_o is the actual difference in the true mean, which was assumed to be zero, $n_{untreated}$ and $n_{treated}$ are the number of observations for the untreated and treated cases respectively, and S_p is:

$$S_p = \{[(n_{untreated} -1)S_{untreated}^2 + (n_{treated} -1)S_{treated}^2] / (n_{untreated} + n_{treated} -2)\}^{1/2} \text{(D–2)}$$

where $S_{untreated}$ and $S_{treated}$ are the sample standard deviation for the untreated and treated cases, respectively.

For a specified confidence interval and degree of freedom ($\gamma = n_{untreated} + n_{treated} -2$), the theoretical region for T for which the two means being compared would be considered similar was looked up from tabulated values of the t–Distribution. The actual T was then calculated from equations D–1 and D–2 and compared with the theoretical range of value of T. If the calculated T was within the theoretical region, then the two means were similar at that level of confidence. Otherwise, the two means were not similar.

Results of the statistical analysis is tabulated below for a 90% level of confidence:

Treatment	S_w	γ	S_p	*T region*	$T_{calc.}$	*Comments*
GC18[1]	IWS	15	2.68	$-1.753 < T < 1.753$	0.07	No difference
GC18[1]	ROS	15	1.70	$-1.753 < T < 1.753$	-15.47	Difference
GC18[2]	IWS	14	2.67	$-1.761 < T < 1.761$	0.584	No difference
GC18[2]	ROS	14	1.63	$-1.761 < T < 1.761$	7.97	Difference
tBDM	IWS	13	2.25	$-1.771 < T < 1.771$	-1.79	Slight difference
tBDM	ROS	-	-	-	-	Not analyzed

1. conventional column. 2. dual filter column.

Appendix E1. Estimating the amount of Soltrol® by-passed along the flare in the short columns during Soltrol® displacement by water.

The amount of by-passing was estimated by integrating the triangular area of the bottom flair around the vertical centerline axis of the column. The volume of revolution was then multiplied by the average porosity. The estimated percentage by-passed (in volume terms) was the effective pore volume of the flair divided by the average pore volume of the column.

The shape and approximate dimensions of the flair are shown below:

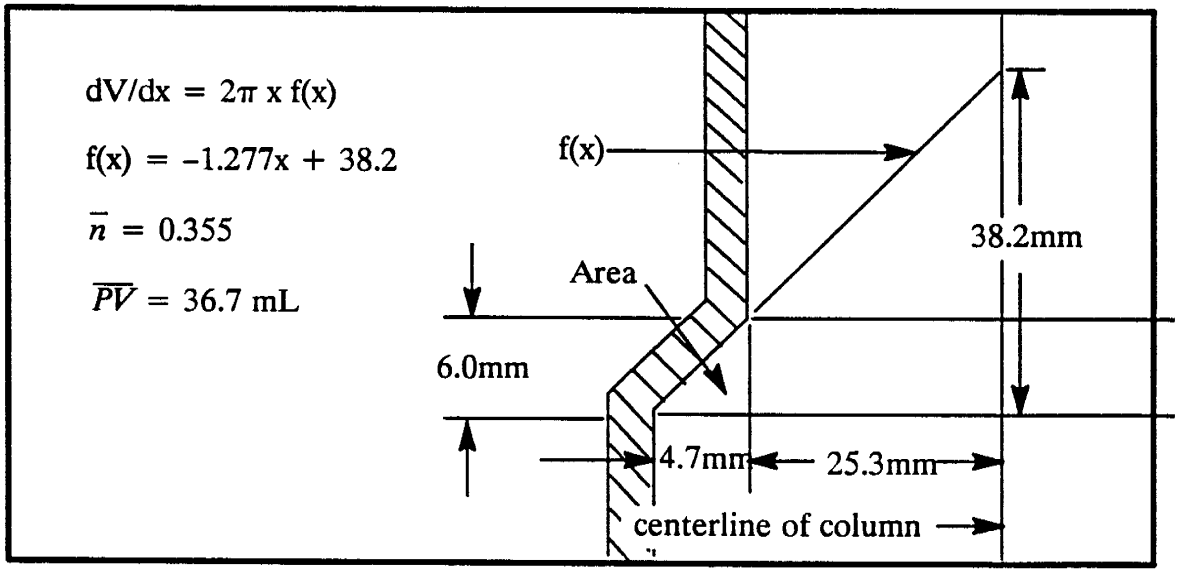

Upon integrating dV/dx, the total volume of the flair becomes:

$$V = 2\pi\,[\,-0.426x^3 + 19.12x^2\,] \qquad \text{(E-1)}$$

evaluated between x = 30.0mm and x = 25.3mm. The total volume was about 2.35 mL. The effective pore volume, multiplied by the average porosity of 0.355, was 0.83 mL. The volume percentage of Soltrol® by-passed during water flood was then estimated by dividing the effective pore volume by 36.7 mL, an average pore volume, or 2.3%.

The amount of by-passing would, undoubtedly, vary between experiments.

This thesis is accepted on behalf of the faculty of the Institute by the following committee:

Robert J Brown — 1 Feb 1991

Advisor — Date

John L Peters — 1 February 1991

Date

N R Morrow — 1 Feb 91

Date